N° d'ordre: 41048

PhD thesis presented under the co-tutorial agreement between the University of Lille 1, Sciences et Technologies and the Tokyo Metropolitan University

by

Damien Amédro

For obtaining the PhD degree in

"Engineering"

and

"Sciences de la Matière, du Rayonnement et de l'Environnement"

Atmospheric measurements of OH and HO_2 radicals using FAGE: Development and deployment on the field

December 17th 2012

Jury committee

Prof. Denis Petitprez **Université Lille 1, France**	**Jury president**
Dr. Christa Fittschen **Research Director CNRS, Université Lille 1, France**	**Thesis supervisor**
Prof. Yoshizumi Kajii, **Tokyo Metropolitan University, Japan**	**Thesis supervisor**
Dr. Lisa Whalley **Researcher, University of Leeds, UK**	**Referee**
Dr. Alexandre Kukui **Researcher, Laboratoire Atmosphères, Milieux, Observations Spatiales, France**	**Referee**
Dr. Shungo Kato **Tokyo Metropolitan University, Japan**	**Examiner**
Dr. Coralie Schoemaecker **Researcher, CNRS, Université Lille , France**	**Examiner**

Remerciements

Tout d’abord, je remercie mes deux directeurs de thèse, Dr. Christa Fittschen et Prof. Yoshizumi Kajii. Non seulement, ils ont été d’excellent directeurs de thèse mais ils m’ont permis de découvrir grâce à la mise en place de la co-tutelle deux points de vue de recherche et m’offrir une position unique.

Mes seconds remerciements vont aux deux rapporteurs, Dr. Lisa Whalley et Dr. Alexandre Kukui. Leurs remarques et commentaires ont ajoutés une valeur à mon manuscrit de thèse. De plus, je remercie Prof. Denis Petitprez pour avoir accepté de présider mon jury de thèse à la dernière minute ainsi qu’au Dr. Shungo Kato pour ses questions.

Merci à Alex, Chieb, Mike, Marion, Chaithania, Pranay, Pascale, Ida, Yoshi 2, Doi, Charlotte et Alisa pour les bons moments passés au laboratoire PC2A et à TMU.

Au PC2A, je remercie en premier lieu le directeur du laboratoire, Prof. Jean-François Pauwels. Le PC2A ne pourrai pas tourner aussi efficacement sans Béa, Jean-Jacques, Patrick, Sylvie et Valérie ainsi qu’aux autres membres du labo. Je n’oublie pas Séb et Pascal pour toute l’aide qu’ils ont apporté pour rendre la manip prête dans les temps. Merci pour votre bonne humeur.

Je remercie la Japan Society for The Promotion of Science, Eurochamp 2 et l’Université Metropolitaine de Tokyo pour avoir aidé aux financements de ma thèse.

Non, je n’ai pas oublié Coralie. Merci pour tout. Nous avons passé de nombreuses heures ensemble au fin fond de l’Allemagne à Goldlauter, à Palaiseau ou encore à Marseille. Je n’oublierai pas notre 14 Juillet 2011 à installer le FAGE dans le Collège Victor Hugo. Merci pour ton soutien et ta présence durant ces trois années. Je m’excuse pour les quelques compte-rendus que je n’ai pas rédigé.

Et bien sûr, ma famille.

Damien

Table of Contents

Chapter 1. HOx measurements in the troposphere

1. HOx radicals in the tropospheric chemistry 12
- 1.1. HOx chemistry 13
- 1.2. Comparison between measurements and models 18

2. Review of the techniques for HOx radicals measurement 19
- 2.1. Measurement techniques for OH 19
  - 2.1.1. DOAS 19
  - 2.1.2. CIMS 21
- 2.2. Measurement techniques for HO_2 22
  - 2.2.1. MIESR 23
  - 2.2.2. Selective PERCA/LIF 25
  - 2.2.3. CIMS methods for HO_2 measurements 26

3. Review of the FAGE instruments 29
- 3.1. First attempts to measure OH and HO_2 using LIF 29
- 3.2. Developments of the FAGE technique 32
- 3.3. Description of the different aspect of FAGE instruments 36
  - 3.3.1. Air sampling 35
  - 3.3.2. Type of cells 36
  - 3.3.3. High repetition rate lasers 36
  - 3.3.4. Fluorescence detection 37
  - 3.3.5. Reference cells 39
  - 3.3.6. Measurement sequence 40
  - 3.3.7. Deployment on field campaigns 40
  - 3.3.8. HO_2 measurement with FAGE 40
- 3.4. Type of calibrations 41
  - 3.4.1. Theoretical sensitivity 41
  - 3.4.2. Experimental calibrations 43
  - 3.4.3. H_2O dependence of the sensitivity 45
- 3.5. Interference for OH measurements 47
  - 3.5.1. Ozone interference 48
  - 3.5.2. Internal OH production 48
- 3.6. Interference for HO_2 measurements 51

4. Review of the OH reactivity techniques 55
- 4.1. Flow tube OH reactivity method 55
- 4.2. Flash photolysis OH reactivity method 57
- 4.3. Comparative Reactivity Method (CRM) 58

5. References 62

Chapter 2. Development of a FAGE instrument for the quantification of HOx radicals

1. Description of the UL-FAGE 76
1.1. OH excitation 77
1.1.1. Laser system 77
1.1.2. Optical train 78
1.1.3. Gas expansion 79
1.2. Multi-pass cells 80
1.3. OH fluorescence detection 81
1.4. Data acquisition 84
1.5. Reference cell 84
1.6. Ambient measurements 85
2. Calibration 87
2.1. Calibration source 89
2.2. Calibration procedure 91
2.3. Calibration uncertainty 92
2.4. Radical losses 93
2.5. H_2O quenching 94
2.6. NO conversion 99
2.7. Limits of detection 102
2.8. Future improvements for the calibration 103
3. Possible interferences 103
3.1. O_3 interference 104
3.2. Acetone interference 106
3.3. RO_2 interference 108
4. References 111

Chapter 3. Intercomparative measurement in the SAPHIR chamber

1. History of intercomparative measurement for OH and HO_2 118
1.1. Intercomparative measurements for OH 118
1.2. Intercomparative measurements for HO_2 119
2. Experimental details 129
2.1. SAPHIR chamber 130
2.2. FZJ-LIF 130
2.3. UL-FAGE 131
2.4. Measurement protocol 132
3. Results 133
3.1. H_2O interference tests 134
3.2. O_3 interference tests 137
3.2.1. Open chamber 137

3.2.2. Dark chamber 138
3.3. NOx interference test 140
3.4. CO experiments 141
3.5. Phenol experiments 144
3.6. Isoprene experiment 146
3.7. Calibration source exchange 148
3.8. Statistical analysis 149
3.8.1. Analysis of the all data set 150
3.8.2. Day by day analysis 151
3.8.3. Precision of the two instruments 154
4. Discussion 155
4.1. Intercomparison for OH 156
4.2. Intercomparison for HO_2 156
4.2.1. Impact of H_2O on HO_2 measurements 158
4.2.2. Impact of O_3 on HO_2 measurements 160
5. References 163

Chapter 4. Ambient HOx measurements: CompOH, SURFIN

1. CompOH 170
1.1. Experimental section 172
1.1.1. Site description 172
1.1.2. Ancillary measurements 172
1.2. Results and discussion 174
1.2.1. Intercomparative measurement 176
1.2.2. Nighttime measurement 179
1.2.3. Profile interpretation 181
1.2.4. HO_2/OH concentration ratio 185
1.3. Summary of the CompOH campaign 187
2. SURFIN 190
2.1. Instrumentation 190
2.2. Measurement protocol 191
2.3. Results and discussion 192
2.4. Summary of the SURFIN campaign 197
3. References 199

Chapter 5. OH reactivity set-up: Application to ambient and laboratory measurements

1. Development of the UL-OH reactivity system 208

2. Intercomparative measurements during CompOH 212

2.1. Experimental conditions 213

2.1.1. UL-OH reactivity 214

2.1.2. Measurement details 217

2.2. Results and discussion 218

2.2.1. Ambient measurements 219

2.2.2. Forced measurements 223

2.2.3. Correlation plots 225

3. Study of the reaction between NO_2* and H_2O 226

4. References 232

Introduction

HOx (=OH+HO_2) radicals play a key role in tropospheric chemistry. OH is the main oxidant and reacts with most of the trace gases that are emitted in the atmosphere. HO_2 radicals are mainly produced from the reaction of OH with CO and volatile organic compounds and play an important role in the formation of tropospheric ozone. To understand the impact of human activities on the atmospheric composition, atmospheric chemistry models are supported by laboratory and in-situ measurements.

The concentration of HOx radicals is very low with concentrations of less than 0.1 pptv and 10 pptv for OH and HO_2 respectively. Due to their very low concentrations, the selective detection of OH and HO_2 radicals was a challenge for experimentalists. Detection methods for OH and HO_2 radicals were developed since the 1980s. In Chapter 1, the summary of these different methods is presented. Special attention is given to the FAGE (Fluorescence Assay by Gas Expansion) technique since it is the one that was chosen at the University of Lille. In the end of the first chapter, the methods that measure OH reactivity are presented.

In Chapter 2, a detailed description of the different parts of UL-FAGE (University of Lille – FAGE) is given. The calibration procedure is presented. The sensitivity of UL-FAGE is shown to be adapted for ambient measurements. Different interference tests were conducted in order to check the selectivity of our instrument and are presented in the last part of the second chapter.

The UL-FAGE was deployed for the first time in different field campaigns during the course of this thesis. First, the UL-FAGE was intercompared with the FZJ-LIF in the SAPHIR chamber in April 2010. The results of each experiment are detailed in the Chapter 3. A statistical analysis of the data allowed the agreement between the two instruments and the impact of possible artefacts on the measurement of OH and HO_2 radicals to be verified.

In Chapter 4, the preliminary results of the CompOH and the SURFIN campaigns are given. The goal of the CompOH field measurement was to intercompare the UL-FAGE with the LATMOS-CIMS in ambient air for the measurement of OH. Similar to the Chapter 3, statistical analysis was made in order to understand the differences between the two instruments. The SURFIN campaign aimed at exploring the role of radicals in indoor chemistry. The first OH and HO_2 indoor measurements are reported. The photolysis rate intensities and the concentration of HONO were observed to be key parameters in the formation of OH radicals indoors.

The last chapter is dedicated to OH reactivity measurements. In the first part, a description of the UL-OH reactivity system is presented. Then, the results of the CompOH campaign in which the UL-OH reactivity system was intercompared with two other CRM instruments are detailed. Finally, the results of the study of the reaction between NO_2* and H_2O as a potential source of OH radicals are presented.

HOx measurements in the troposphere

Introduction

The hydroxyl radical, OH, is the main oxidant in the troposphere during daytime and a key intermediate in the formation of secondary pollutants in the troposphere such as ozone (O_3), nitric acid (HNO_3) and peroxyacetyl nitrate (PAN). Field measurements of OH, HO_2 concentrations and OH reactivity are used to validate atmospheric chemistry models that help to predict the evolution of the oxidising capacity of the atmosphere. The comparison between models and measurements in specific locations allows improvement of our knowledge on the fast photochemical processes occurring in the troposphere (Stone et al., 2012). Since the 1990s, over 60 field measurement campaigns were organized to observe OH and HO_2 in various environments (e.g. polar, mega-city, semi-polluted, polluted, marine, marine boundary layer, with biogenic emissions).

The first reliable measurements for OH (Campbell et al., 1986; Eisele and Tanner, 1991; Hard et al., 1992; Perner et al., 1976) and for HO_2 (Cantrell and Stedman, 1982; Hanke et al., 2002; Hornbrook et al., 2011; Mihelcic et al., 1985) confirmed earlier model studies (Crutzen, 1973, 1974; Levy, 1971) predicting concentrations in the range of 10^6 and 10^8 molecule cm^{-3} for OH and HO_2, respectively. OH and HO_2 concentrations are very low and highly variable with time and location. Hence, their detection requires techniques with high sensitivity, selectivity and time resolution. The development of such instruments was and still is a challenge for experimentalists over the last 30 years.

A review of the techniques for the measurement of OH and HO_2 will be given in the following paragraphs with attention drawn on the Fluorescence Assay by Gas Expansion (FAGE) technique as it is the one that was chosen for the presented work at the University of Lille. The last section concerns techniques that measure the OH reactivity.

1. HOx radicals in the tropospheric chemistry

Planet Earth is surrounded by a layer of solid, liquid and mainly gas constituents called the atmosphere. The atmosphere can be divided into layers namely troposphere, stratosphere, mesosphere, thermosphere and exosphere (not represented on Figure 1) characterized by a temperature inversion profile as can be seen on Figure 1.

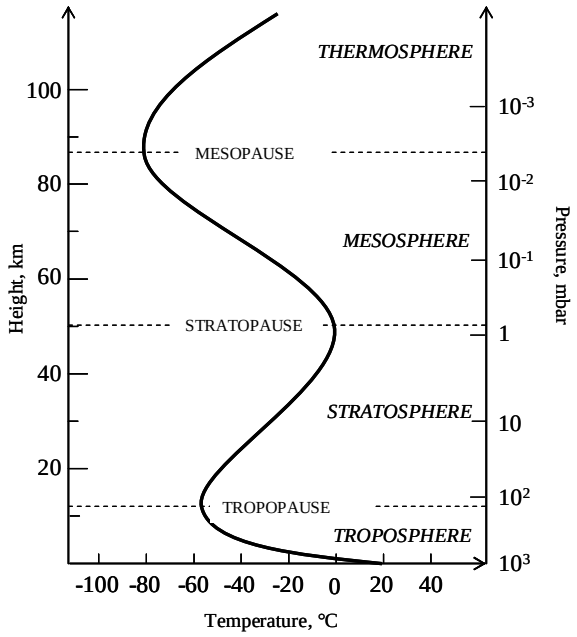

Figure 1. Temperature profile as a function of the height of the Earth's atmosphere (Seinfeld and Pandis, 1998)

The Earth atmosphere is composed of 78 % N_2, 20.9 % O_2, 1% Ar and 0.036 % of CO_2 (Seinfeld and Pandis, 1998). Water vapour is the next most ambient constituent with concentration that can vary up to 3 %. The remaining gas constituent is composed of a multitude of volatile components with concentrations below 10^{-6} mole fraction (i.e. 1 ppm, 1 part per million by volume) called trace gases.

Trace gases are either emitted from biogenic sources such as forest environments (so-called Biogenic Volatile Organic Compounds (BVOC), e.g isoprene, monoterpenes) or from oceans (halogenated hydrocarbons). Also, human activities release an important amount of trace gases called anthropogenic Volatile Organic Compounds (VOC) such as from car exhausts (e. g. aromatic compounds, CO_2, NO_x) or industries (e.g. CFC; ChloroFluoroCarbons). After being emitted in the atmosphere, these trace gases can go through different processes: (i) deposition (dry or wet), (ii) transport over long distances or (iii) chemical transformation.

Since about 90% of the total mass resides in the troposphere (Wayne, 2000), most of these different processes will occur in this lower part of the atmosphere.

As the major constituents of the atmosphere are not reactive, it was long thought that only slow chemical transformations were occurring in the atmosphere. One of the first hints that lead scientists to investigate the fate of the chemical species released in the troposphere in more details was the formation of photochemical smog on sunny days in Los Angeles in the 1940s (Haagen-Smit, 1952). The characteristics of photochemical smog days were: a decrease in visibility (due to particles), crop damage and eye irritation, due to the generation of highly oxidizing species. Soon it was recognized that the formation of pollutants such as O_3, HNO_3 and solid particles were linked to the combination of high VOC and NO_x concentrations in the presence of light

$$VOC + NO_x + h\nu \rightarrow O_3 + HNO_3 + ...+ \text{ particles} \qquad (R\ 1)$$

1.1. HOx chemistry

Levy (Levy, 1971) first hypothesized that OH radicals could play a central role in the degradation of VOC in the troposphere during day time which in the presence of NO_x could lead to the formation of photochemical smog. He developed a 15 reactions chemical model of the CH_4 and CO oxidation in which HO_x (= OH + HO_2) radicals species were at the centre of a chain reactions mechanism and were rapidly interconvert.

The main source of OH in the troposphere is via the photolysis of O_3 ($\lambda < 310$ nm) to form an electronically excited oxygen atom $O(^1D)$ that reacts with water vapour to form OH.

$$O_3 + h\nu\ (\lambda < 310\ nm) \rightarrow O(^1D) + O_2(^1\Delta_g) \qquad (R\ 2)$$
$$O(^1D) + H_2O \rightarrow 2\ OH \qquad (R\ 3)$$

The excited $O(^1D)$ can also be quenched (i.e. deactivation of the excited molecular entity by collision with other substituent though a non-radiative process (Nič et al., 2006) to from $O(^3P)$ that can react with O_2 to recycle O_3.

$$O(^1D) + O_2 \rightarrow O(^3P) + O_2 \qquad (R\ 4)$$
$$O(^1D) + N_2 \rightarrow O(^3P) + N_2 \qquad (R\ 5)$$
$$O(^3P) + O_2 + M \rightarrow O_3 + M \qquad (R\ 6)$$

The fraction of $O(^1D)$ atoms that forms OH is dependent on the H_2O concentration as can be seen from (R 3). For water mixing ratio equal to 1.5 %, 10 % of the $O(^1D)$ reacts with H_2O to form OH rather than being quenched by N_2 and O_2.

The primary source via the photolysis of O_3 [(R 2)-(R 3)] is defined as

$$P(\mathrm{OH}) = 2 \times f \times [\mathrm{O_3}] \times j(\mathrm{O^1D}) \qquad \text{Eq. 1}$$

where f is the fraction of $O(^1D)$ that reacts with H_2O to form OH rather than being quenched by N_2 and O_2 defined as

$$f = \frac{k_{\mathrm{O1D+H2O}}[\mathrm{H_2O}]}{k_{\mathrm{O1D+H2O}}[\mathrm{H_2O}] + k_{\mathrm{O1D+O2}}[\mathrm{O_2}] + k_{\mathrm{O1D+N2}}[\mathrm{N_2}]} \qquad \text{Eq. 2}$$

Other sources of OH radicals are the photolysis of HONO, H_2O_2 and the reaction of alkenes with O_3 (Monks, 2005).

The OH radical initiates the oxidation of hydrocarbons species (e.g CH_4) that leads to the formation of HO_2 [(R 7) to (R 10)]. In the presence of NO, HO_2 is quickly recycled back to OH and NO_2 [(R 11)] and so the hydrocarbon oxidation is enhanced by the HOx/NOx catalytic cycles. The photolysis of NO_2 is then leading to the formation of O_3 [(R 12)-(R 13)]. Under high NOx conditions, the oxidation of hydrocarbons leads to the formation of O_3. However, under very high NOx conditions the reaction between OH and NO_2 [(R 15)] dominates and can lead to a decrease in the O_3 concentration.

$OH + CH_4 \rightarrow CH_3 + H_2O$	(R 7)
$CH_3 + O_2 + M \rightarrow CH_3O_2 + M$	(R 8)
$CH_3O_2 + NO \rightarrow CH_3O + NO_2$	(R 9)
$CH_3O + O_2 \rightarrow HCHO + HO_2$	(R 10)
$HO_2 + NO \rightarrow OH + NO_2$	(R 11)
$2(NO_2 + h\nu\ (\lambda < 420\ nm) \rightarrow NO + O(^3P))$	(R 12)
$2(O(^3P) + O_2 + M \rightarrow O_3 + M)$	(R 13)
$CH_4 + 4O_2 + h\nu \rightarrow HCHO + H_2O + 2O_3$	(R 14)

$OH + NO_2 + M \rightarrow HNO_3 + M$	(R 15)

Two different regimes can be established: high NOx and low NOx conditions. As opposed to high NOx conditions, under low NOx conditions (typically NO concentration lower than 100 ppt), the main losses of HO_2 and methyl peroxy radicals CH_3O_2 are via self reaction or cross

reactions. Then, O_3 is mainly consumed by the reaction with HO_2 (R 21) and with OH (R 21). In addition, under very low NOx conditions, the photolysis of O_3 can be considered as a major ozone loss.

$CH_3O_2 + CH_3O_2 \rightarrow 2CH_3O$ + others products (R 16)
$CH_3O + O_2 \rightarrow HCHO + HO_2$ (R 17)
$HO_2 + HO_2 \rightarrow H_2O_2 + O_2$ (R 18)
$CH_3O_2 + HO_2 \rightarrow CH_3OOH + O_2$ (R 19)
$HO_2 + O_3 \rightarrow OH + 2O_2$ (R 20)
$OH + O_3 \rightarrow HO_2 + O_2$ (R 21)

Figure 2 is a simplified representation of the productions and losses of HOx radicals and their role in the oxidation of CH_4 and CO. OH is converted to HO_2 via propagation reactions with CH_4 and CO and HO_2 is recycled back to OH after its reaction with NO and O_3. An additional significant source of HO_2 is the photolysis of HCHO. OH radicals are removed from the HOx cycle with their reaction with NO_2 to produce HNO_3 (R 15). It is a termination reaction as it removes radicals from the gas phase.

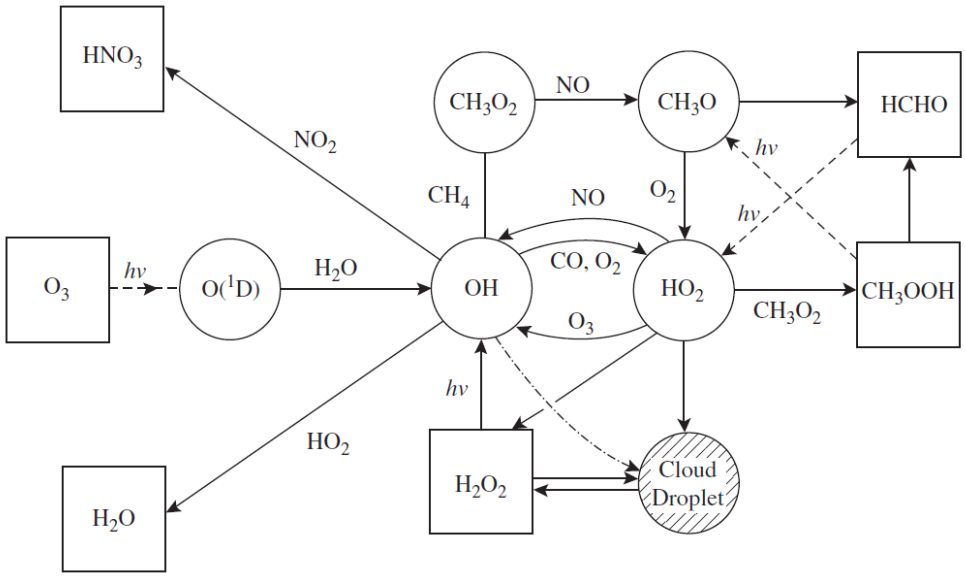

Figure 2. Oxidation of CH_4 and CO in the presence of NO. Implications of OH and HO_2. (Wayne, 2000)

As they are dependent on the chemical composition, the OH and HO_2 concentrations in the troposphere will vary greatly depending on the location as well as the meteorological conditions. The range of concentration for OH ranges from below 10^5 up to 10^7 molecule cm^{-3} and its lifetime from ms in polluted areas to 1 s in clean environments. For HO_2, the range of

concentration is from 10^7 to 10^8 molecule cm^{-3} and its lifetime as for OH varies from 10 s in polluted areas to 1 min in clean environments.

The OH concentration is the balance between the production and the loss.

$$\frac{d[\mathrm{OH}]}{dt} = P(\mathrm{OH}) + k_{\mathrm{HO2+O3}}[\mathrm{HO_2}][\mathrm{O_3}] + k_{\mathrm{NO+HO2}}[\mathrm{NO}][\mathrm{HO_2}] + \sum_i \nu_i j_i[\mathrm{i}] + P' - \sum_n k_{OH+X}[X][\mathrm{OH}] \qquad \text{Eq. 3}$$

The first four terms of the equation are for the production of OH, $\Sigma v_i j_i$[i] which is the sum of the photolytic source of OH (e.g HONO, H_2O_2, CH_3OOH) where v_i is the OH yield, j_i the photolysis frequency in s^{-1} and [i] the concentration in molecule cm^{-3} and *P'* which is the additional OH production from other processes such as ozonolysis of alkenes. The last terms encompass all the different losses of OH via reaction with NO_2 or VOC, it is the sum of the product of the bimolecular rate coefficient k_{OH+X} in cm^3 $molecule^{-1}$ s^{-1} and the concentration of the OH sinks, X and the OH concentration given in molecule cm^{-3}. Since the atmospheric lifetime of OH is less than 1 s, its concentration is not affected by transportation and a steady state is rapidly reached in the atmosphere. The approximation d[OH]/dt = 0 can be made so the OH concentration is given as the ratio between its sources and its sinks.

Intensive field campaigns were set on the ground or in an airplane accompanied by a large set of ancillary measurements in order to constrain the OH and HO_2 sources and sinks. The main interest of these measurements is to check our understanding of the fast photochemical reactions with the simulation of the measured OH and HO_2 concentrations using chemical models such as the Master Chemical Mechanism (MCM) (Jenkin et al., 2003; Saunders et al., 2003). If discrepancies appear between the model and the measurement, it helps to either improve the model by for example adding chemical mechanisms or point out potential measurement errors.

In order to improve tropospheric models the additional measurement of the total OH reactivity recently became of interest. The total OH reactivity is the rate at which the OH decays due to its reaction with mainly VOC, NOx and CO. Indeed, a high number of VOC are emitted in the troposphere from anthropogenic and biogenic sources and recent studies have shown that only a limited fraction are routinely measured using standard techniques (PTR-MS, GC) (Lewis et al., 2000) and the unmeasured VOC will affect the quality of the model as the OH losses are underestimated.

The total OH reactivity, *k'*, is the sum of the rate at which all individual species are reacting with OH, it is given as

$$k' = \sum k_{X+OH}[X] = k_{CO+OH}[CO] + k_{CH4+OH}[CH_4] + k_{O_3+OH}[O_3] + k_{NO+OH}[NO] + k_{NO_2+OH}[NO_2] + \sum_i k_{VOC_i+OH}[VOC_i] + \sum k_{others+OH}[others] \quad \text{Eq. 4}$$

where k_{X+OH} is the bimolecular rate coefficients of the reaction of X with OH, [X] is the concentration of each trace gas.

The measurement of ambient reactivity can be compared to calculated OH reactivity obtained from the individual reactivity of each measured trace gas knowing their concentrations and their bimolecular rate coefficients with OH. During field measurements, it was often observed that the measured total OH reactivity was greater than the calculated reactivity obtained from the measurement of the individual trace gas concentration indicating that a fraction of VOC was unmeasured (Carlo et al., 2004; Lee et al., 2009; Nölscher et al., 2012b; Yoshino et al., 2006).

As already mentioned previously, a large fraction of VOCs are not being measured (Lewis et al., 2000). Among VOCs, Oxygenated Volatile Organic Compounds (OVOC) (i.e. alcohols, aldehydes, ketones and acids), which are oxidation products from the reactions of hydrocarbon species with oxidant such as the OH radical, are found to be difficult to quantify with high accuracy (Apel et al., 2008). The gap between the measured and the calculated OH reactivity can be partly resolved by taking into account the portion of reactivity coming from unmeasured OVOC species. Chemical models such as the MCM can estimate the concentration of these species and from the bimolecular rate coefficient the reactivity of each individual species can be estimated. Lee et al. (Lee et al., 2009) using this method found that for their measurement at a coastal site in the United Kingdom, they could reduce the fraction of missing OH reactivity. During the entire campaign, they measured on average a OH reactivity of 4.9 s^{-1}. From the calculated OH reactivity which included 42 measured individual species, they found a missing OH reactivity of 37 %. Using the MCM model, which included ~ 800 species they were able to reduce the missing fraction down to 30 %. They observed that oxygenated species such as aldehydes or ketones were having the strongest impact on the missing fraction. However, a significant fraction of missing OH reactivity remains. In forest environments, the unexplained portion of measured reactivity was found to be even higher

(Carlo et al., 2004; Nölscher et al., 2012b). In these environments, it highly depends on environmental factors (e. g. temperature, type of trees, mechanical stress). Nölscher et al. (Nölscher et al., 2012b) found that in their conditions the missing OH reactivity would be explained if 780 to 3500 compounds with an average bimolecular rate coefficient of $k = 5 \times 10^{-11}$ cm^3/s were not detected. Questions remain in order to explain the missing OH sinks.

The experimental techniques allowing the quantification of HOx radicals and the OH reactivity are presented in the following sections.

1.2. Comparison between measurements and models

Field measurement of OH and HO_2 and models that try to reproduce their concentrations are intertwined as they both contribute to the improvement of our knowledge of the tropospheric chemistry. On one hand, measurements have demonstrated a certain lack in our understanding while models pointed out measurement errors. Sometimes, models and measurements agreed for the wrong reasons e.g. the underestimation or the overestimation of the OH sources and sinks could have lead to a fake agreement.

In a very recent review by Stone et al. (Stone et al., 2012), the comparison between the measurements and the models is summarized for the field campaigns where OH and HO_2 were measured over the last decade. The discrepancies observed between models and measurements differ depending on the environments. They can be attributed to a lack in the understanding of the fast tropospheric chemistry at the time when the model calculations were performed and/or the absence of supporting measurements (e.g. OVOC, halogen oxides, HONO,…) that help to constrain the models. However, from many field campaigns, new knowledge was brought up such as the role of halogen oxides in the marine boundary layer or the polar environment in the HOx chemistry. The predominance of HONO and carbonyl photolysis as well as the ozonolysis of alkenes in urban environments was highlighted.

In recent field campaigns in biogenic environments, the overestimation of the measurement over the models showed that the chemistry of peroxy radicals in very low NOx environments is not understood (Kubistin et al., 2010; Lu et al., 2012; Mao et al., 2012a; Whalley et al., 2011).

2. Review of the techniques for HO_x radicals measurement

The different measurement techniques for the quantification of OH and HO_2 were reviewed in details by Heard and Pilling (Heard and Pilling, 2003). In this section we shall discuss briefly the techniques other than the FAGE technique but with similar performances in term of sensitivity and time resolution. Attention will be focused on the FAGE technique in section 3.

2.1. Measurement techniques for OH

The DOAS (Differential Optical Absorption Spectroscopy) and the CIMS (Chemical Ionization Mass Spectrometry) techniques have a comparable time resolution and sensitivity to the FAGE for the measurement of tropospheric OH. They are fundamentally different from the FAGE technique in which OH is detected using Laser Induced Fluorescence (LIF). The DOAS technique is an absorption technique in which OH is detected over a very long path. It is an absolute technique and as such does not require any calibration. In the CIMS technique, OH is chemically converted to H_2SO_4 and detected using mass spectrometry. The differences between the techniques are an advantage as they might not be affected by the same interferences.

2.1.1. DOAS

As for the FAGE, the DOAS technique is a spectroscopic method. It is based on the extinction of a UV-light beam travelling in the atmosphere by absorption of OH over a long absorption path according to the Beer Lambert law

$$\ln\left(\frac{I_0}{I}\right) = \sigma_{OH} \times [OH] \times l \qquad \text{Eq. 5}$$

where I and I_0 are the light intensities after and before travelling through the air sampled, σ_{OH} is the absorption cross section in cm², [OH] is the OH concentration in molecule cm^{-3}, l is the absorption path length in cm.

DOAS was one of the first methods that was able to detect OH radicals in the troposphere with a first measurement reported in 1975 (Perner et al., 1976). As it is an absorption method, the measurement is absolute and the accuracy relies only on l and on σ_{OH} (accuracy of 7%). In consequence, the DOAS technique is often considered as a reference measurement. OH is detected using the strong well-resolved absorption rotational lines around 308 nm ($\sigma_{OH} \approx 10^{-16}$ cm²). DOAS instruments have a minimum detectable optical density of $\ln(I_0/I) \approx 10^{-5}$ - 10^{-6} so

in order to detect $[OH]_{min}=2.5 \times 10^5$ cm^{-3} the absorption path length needs to be in the range of 0.4 to 4 km.

Usually, DOAS instruments are composed of 4 different elements:

- a broadband light source that encompass more than one OH absorption line (often 6 absorption lines). It eases the spectral analysis especially in the subtraction of other molecules (e.g. HCHO, SO_2, and Naphthalene) fine structure absorptions in the same spectral range. The light intensity needs also to have a high luminance due to the long path length and a homogeneous spectral profile for each laser pulse is necessary.
- an open multiple reflexion cell that improves the spatial resolution. At first, single path set-ups were used over a long absorption length (up to 10.6 km at Fritz Peak (Mount and Eisele, 1992)) which resulted in the averaging of the measured OH concentration over a large spatial range. The long absorption length needed in order to achieve a good limit of detection is nowadays reached using a multi pass system where an entrance mirror and two rear mirrors are separated by 10 to 40 m (Heard and Pilling, 2003). The light beam travels approximately hundred times which gives an effective path length up to 4 km. DOAS instruments are nowadays using multi path system (Hausmann et al., 1997; Brauers et al., 2001) that improves the spatial resolution.
- a high resolution spectrograph (~500 000) to obtain a differential optical absorption of the narrow OH line transitions (2.5 pm due to Doppler and pressure broadening)
- a cooled (-45°C) photo diode array detector.

The limit of detection is ~1×10^6 cm^{-3} for 5 min average and a path length of 3 km (Dorn et al., 1995; Brauers et al., 2001).

One of the disadvantages of the DOAS technique is the difficulty to extract the OH absorption lines from the absorption spectrum which is the convolution of all the different ambient species that absorb in the same range. Moreover, since DOAS instruments do not measure at one “point” contrary to ancillary measurements, additional errors can be introduced in the measured to modelled comparison. Complex and time consuming numerical analysis are needed to retrieve the OH concentrations. The advantages are the calibration free and in-situ measurement without possible losses on walls or sampling nozzles. The DOAS installed in the SAPHIR chamber in Juelich is the only in service (Stone et al., 2012).

2.1.2. CIMS

The CIMS technique is a mass spectrometry technique where OH is chemically converted in a reactor at atmospheric pressure into a molecule that can be ionized and then detected using a mass spectrometer (Eisele and Tanner, 1991; Eisele, 1995; Berresheim et al., 2000; Kukui et al., 2008).

Air is sampled into a reactor where OH rapidly reacts (10-20 ms or 1-2 ms) with isotopically labelled $^{34}SO_2$ to produce $H_2{}^{34}SO_4$ via the following mechanism

$$^{34}SO_2 + OH + M \rightarrow H^{34}SO_3 + M \quad \text{(R 22)}$$
$$H^{34}SO_3 + O_2 \rightarrow {}^{34}SO_3 + HO_2 \quad \text{(R 23)}$$
$$^{34}SO_3 + H_2O + M \rightarrow H_2{}^{34}SO_4 + M \quad \text{(R 24)}$$

$H_2{}^{34}SO_4$ is detected as $H^{34}SO_4^-$ after its chemical ionization using NO_3^- ion. NO_3^- ions are generated separately in a sheath from HNO_3 by either a radioactive source or a corona discharge.

$$H_2{}^{34}SO_4 + NO_3^- \rightarrow H^{34}SO_4^- + HNO_3 \quad \text{(R 25)}$$

$H^{34}SO_4^-$ is then measured using a quadrupole mass spectrometer. Background signal is low due to the low abundance of ^{34}S isotope compare to ^{32}S (4.3% compare with 94.9%). The OH concentration measured is determined from the $H^{34}SO_4^-/NO_3^-$ ratio, the reaction time and the rate coefficient of the ionization reaction (R 25). However, the rate coefficient of the ionization reaction is not well known and the CIMS technique is calibrated using a H_2O photolysis calibration procedure (see 3.4). The limit of detection of the CIMS is below 10^5 cm^{-3} for 5 min average (Eisele et al., 1996) and so it is the most sensitive of all techniques measuring OH.

The main disadvantage of the technique is the sensitivity to high NO concentration where the HO_2 formed in (R 23) can generate OH and cause an artificial signal. Care was taken in order to reduce this effect by lowering the reaction time (Kukui et al., 2008; Tanner and Eisele, 1995) nevertheless corrections are needed when measuring in highly polluted environments. High concentrations of propane are added downstream to the reaction zone between ambient OH and SO_2 to remove additional OH formed from HO_2 recycling with NO. Finally, reactions that would oxidize $^{34}SO_2$ into $^{34}SO_3$ would cause an artificial $H_2{}^{34}SO_4$ signal. Mauldin et al. (Mauldin et al., 2012) recently found out that stabilized Criegee intermediates were oxidizing SO_2 into H_2SO_4 in their CIMS instrument.

2.2. Measurement techniques for HO_2

Three methods are used to detect HO_2 radicals, the MIESR (Matrix Isolation Electron Spin-Resonance) technique, the FAGE technique and improved methods of the PERCA (peroxy radical chemical amplifier) technique. Even if the time resolution of the MIESR (Matrix Isolation Electron Spin-Resonance) technique is far less than the other techniques described here, it should be mentioned as it is the only available direct and absolute method for the measurement of ambient HO_2. HO_2 radicals are trapped onto a D_2O matrix held at 77 K before being detected off line using electron spin resonance spectroscopy. The FAGE technique measured HO_2 after its conversion to OH by addition of NO. OH is then measured by LIF. It is the most sensitive technique for HO_2 with LOD better than 0.1 ppt. More recently, new techniques (3 CIMS and 1 LIF) based on PERCA were developed to measure selectively HO_2. PERCA measures the sum of peroxy radicals ($[HO_2] + [RO_2]$) and is not selective to HO_2. HO_2 and RO_2 are simultaneously converted into OH and NO_2 by addition of NO and CO via the reaction mechanism (R 26) to (R 33).

$RO_2 + NO \rightarrow RO + NO_2$	(R 26)
$\mathbf{RO + O_2 \rightarrow R'CHO + HO_2}$	(R 27)
$RO_2 + NO + M \rightarrow RO_2NO + M$	(R 28)
$\mathbf{RO + NO + M \rightarrow RONO + M}$	(R 29)
$HO_2 + NO \rightarrow OH + NO_2$	(R 30)
$HO_2 + NO \rightarrow HONO_2$	(R 31)
$OH + NO + M \rightarrow HONO + M$	(R 32)
$OH + CO + O_2 + M \rightarrow HO_2 + CO_2 + M$	(R 33)

A chain reaction is triggered which leads to the formation of several hundreds of NO_2 molecules for one initial HO_2. NO_2 can be detected by chemiluminescence after its reaction with an aqueous luminol solution (Cantrell and Stedman, 1982; Cantrell et al., 1984). For the three CIMS methods, the competition between the reactions (R 27) and (R 29) is use to enhance or reduce the conversion of RO_2 to HO_2. One method varies the O_2 concentration (Hanke et al., 2002), a second one varies the NO concentration (Edwards et al., 2003) and the most recent one varies both $[O_2]$ and [NO] (Hornbrook et al., 2011). OH radicals produced from (R 30) are converted to H_2SO_4 [(R 22)-(R 25)] which is then detected by mass spectrometry. For the LIF method (Miyazaki et al., 2010), HO_2 and RO_2 are separated in a pre-reactor using their different loss rate on surfaces. RO_2 or HO_2+RO_2 are converted to NO_2 using the PERCA method before being detected by LIF.

Table 1 summarizes the different technique that measure HO_2 with the exception of the MIESR. These methods are able to measure the sum of all the peroxy radicals and with some speciation to HO_2 given as α.

The lack of direct measurement techniques is due to the physico-chemical properties of HO_2. For spectroscopic methods, it has a broad absorption in the UV (σ_{HO2}(200 nm)= 4.35×10^{-18} cm^2 $molecule^{-1}$ (Crowley et al., 1991) along with many other peroxy radicals and it does not fluoresce. It has been detected in the near IR region but the best limit of detection that can be obtained is 10^{10} molecule cm^{-3} in a low pressure (50 Torr) cell using the CRDS (Cavity Ring Down Spectroscopy) method (Thiébaud and Fittschen, 2006). A new cavity method called NICE-OHMS (Noise-Immune Cavity-Enhanced Optical Heterodyne Molecular Spectroscopy) was used for the detection of HO_2 radicals and showed promising sensitivities (4×10^{10} molecule cm^{-3}) but still not sufficient for atmospheric measurement (Bell et al., 2012). For mass spectrometry methods, its ionization potential energy is relatively high (IP=11.5 eV (Foner and Hudson, 1955)) and at this energy other molecules present in the atmosphere would fragment and so the mass spectrum would be difficult to interpret.

2.2.1. MIESR

The MIESR is a technique that is capable of measuring simultaneously and selectively different radical species HO_2, RO_2, $CH_3C(O)O_2$, NO_2, and NO_3 using electron spin-resonance spectroscopy (ESR) after collecting radicals on a cold matrix. At first HO_2, RO_2 and $CH_3C(O)O_2$ could not be properly distinguished in the spin resonance spectrum but after the replacement of the initially used H_2O matrix with D_2O and the improvement of the numerical analysis the ability to measure selectively HO_2 compared to other peroxy radicals was achieved (Mihelcic et al., 1978, 1985, 1990).

Air is sampled (20 L/h) after gas expansion through a nozzle into a vacuum chamber (0.1 mbar). The radicals are trapped onto a polycrystalline ice (D_2O) matrix placed on a coldfinger held at 77 K using liquid nitrogen. To collect enough radicals on a coldfinger the sampling time is usually about 30 min. Samples are stored at 77 K (up to 2 weeks without radical losses) and analysed afterwards in the laboratory using electron spin resonance. The scan of one sample takes 1 hour however 5 h are needed in order to thermally stabilize the ESR cavity and to do the intrinsic spectrum of the coldfinger (after warming up the chamber).

The method is in principle absolute because all the radicals collected on the matrix are detected using ESR. However losses of radicals through collision with surfaces of the orifice

Table 1. Techniques for selective measurement of HO_2 using chemical method.

Instruments	Speciation			Detection		Time response	Calibration			Reference
	Method	α_{RO2}		Chemical specie	Method		Method	LOD (ppt) (S/N=2)	Acc. (2σ)	
		$[HO_2]$; $[RO_2]$*	$\sum([HO_2]+RO_2)$							
ROx-MAS	sample dilution in O_2 or N_2	0.25-0.30	0.90	HSO_4^-	MS	1 min	H_2O photolysis/ calibrated lamp flux	0.5 ppt for 1 min	30 %	(Hanke et al., 2002)
PerCIMS 1	variation of NO	0.10-0.15	0.80-0.90	HSO_4^-	MS	30 min	H_2O photolysis/N_2O actinometry	0.41 ppt for 15 s	41 % (HO_2 mode) 35% (RO_2 mode)	(Edwards et al., 2003)
PerCIMS 2	variation of NO and O_2	0.15	~ 1.0	HSO_4^-	MS	1 min	H_2O photolysis/ calibrated lamp flux	2 ppt for 1 min	35 %	(Hornbrook et al., 2011)
Selective PERCA-LIF	denuder	α_{CH3O2}=0.85* α_{HO2}=0.10*	~ 1.0	NO_2	LIF	1 min	H_2O photolysis/O_3 actinometry	0.41 ppt for 1 min	-	(Miyazaki et al., 2010)

MS: Mass Spectrometry, LIF: Laser Induced Fluorescence, α_{RO2} is the conversion efficiency of RO_2 to HO_2.
* For the selective PERCA-LIF, the two modes are $[RO_2]$ and $\sum([HO_2]+[RO_2])$. For the RO_2 mode, the sampled air passed through the denuder and the 90% of HO_2 is removed whereas 15% RO_2 is removed. For more details see text. ** Interference with certain RO_2 within the FAGE cell was discovered later (Fuchs et al., 2011), α_{RO2} (isoprene)=1.21 probably due to the RO_2 interference.

and signal losses in the ESR measurement are difficult to quantify and so generally the method is calibrated (Schultz et al., 1995). For the calibration, HO_2 radicals are produced by breaking H_2 molecules using a corona discharge to form H atoms. Then, H reacts with O_2 to generate HO_2. HO_2 are then titrated using NO to form NO_2 and OH. A previously calibrated NO_2 signal is used to calibrate the HO_2 signal. A high NO concentration is needed to ensure that all the OH produced from the reaction of HO_2 with NO are lost to form HONO (via OH + NO + M → HONO + M) and not HO_2 via the reaction of OH with H_2 (H_2 + OH + O_2 → HO_2 + H_2O) that recycles back HO_2. The total error of the calibration for HO_2 is estimated to be ±15% (Mihelcic et al., 1985). The limit of detection is 2.5×10^7 cm^{-3} (1 ppt).

The main disadvantage of the technique is the time resolution with a sampling rate of one coldfinger in 30 min (also limited by the number of available coldfinger) and the time consuming analysis.

The MIESR method was deployed on field and aircraft measurements (Mihelcic et al., 1985) but only one recent measurement was reported for the intercomparison with the FZJ-ROx-LIF in the SAPHIR chamber (Fuchs et al., 2009).

2.2.2. Selective PERCA/LIF

Recently, Miyazaki et al. (Miyazaki et al., 2010) proposed a new method to measure selectively HO_2 and RO_2. In order to effectively separate HO_2 from other peroxy radicals, they took advantage of the fact that the HO_2 loss rate on surfaces is more important than the loss rate for other peroxy radicals (e.g CH_3O_2).

They added to a previously built PERCA-LIF (Sadanaga et al., 2004a) a pre-inlet where sampled air is passed through a glass tube filled with spherical glass beads (1 mm diameter) called a denuder. As air passed through the denuder, due to the different heterogeneous loss rate of HO_2 compared to RO_2, 90% of HO_2 can be removed when only 15% of CH_3O_2 are lost. By either passing through the denuder or not, they can either only measure RO_2 or the sum of HO_2 and RO_2. Then sampled air is brought to a PERCA reaction chamber where CO and NO are added in order to produce high NO_2 concentration (100 times the initial concentration of peroxy radicals) via a chain reaction. NO_2 is finally detected in a low pressure cell using LIF.

They have tested different types of material for the denuder (two types of Teflon: PFA, PTFE and glass) and observed that HO_2 and RO_2 losses were less sensitive to relative humidity using the glass denuder.

The limit of detection for HO_2 is 1×10^7 cm^{-3} (< 1 ppt) for 1 min of measurement. The new method has been tested for ambient measurements and shown encouraging results. However, CH_3O_2 is the only peroxy radical which has been tested and no measurements from field campaign were reported.

2.2.3. CIMS methods for HO_2 measurements

Up to date, 3 instruments were developed (Edwards et al., 2003; Hanke et al., 2002; Hornbrook et al., 2011) for the selective measurement of HO_2 and $\sum([HO_2]+RO_2)$ which are all based on the CIMS technique (Eisele and Tanner, 1991). HO_2 and RO_2 radicals are detected after NO is first added into a reaction chamber to convert OH via (R 30). OH is then converted to H_2SO_4 after its reaction with SO_2 in the presence of H_2O and O_2 (see 2.1.2). Finally, $H^{34}SO_3^-$ is detected using mass spectrometry [(R 22) to (R 25)]. For the measurement of OH, isotopically labelled $^{34}SO_2$ is needed to differentiate $H_2{}^{34}SO_4$ produced in the reaction chamber with ambient $H_2{}^{32}SO_4$ which have concentration in the same order of magnitude than OH. However, HO_2 concentrations are 100 times higher than H_2SO_4(g) therefore isotopically labelled $^{34}SO_2$ is not needed.

The 3 instruments are based on the PERCA technique that is using chemical amplification to convert HO_2 and RO_2 to NO_2 by adding NO and CO. However, PERCA is not selective and so recent methods adjusted conversion time, [NO] and [O_2] to select HO_2 from $\Sigma(RO_2)$. Therefore, measurements are made in two different modes, "HO_2-mode" and "HO_2+RO_2-mode". After adding NO to the sampled air, the chemical mechanism is the following [(R 26) to (R 32)]. (R 26), (R 27) and (R 30) are radical propagation reactions whereas (R 28) and (R 29) are termination reactions. By adjusting the ratio [NO]/[O_2], the authors are able to chose one mode to another using the competition between (R 27) and (R 29). For the "HO_2-mode", high NO concentrations are used to favour (R 29) compared to (R 27). When the NO concentration is low, the HO_2 and RO_2 are both measured; it is the "HO_2+RO_2-mode". Comparison between the different instruments can be done by looking at the conversion efficiencies for each mode. In the "HO_2-mode", α_{RO2} (i.e. conversion efficiency for RO_2 species) needs to be as low as possible whereas in the "HO_2+RO_2-mode", $\alpha_{RO2+HO2}$ is aimed to be close to unity. For CIMS technique, calibration is needed and known amount of HO_2 radicals are produced by H_2O photolysis using a Hg lamp at 185 nm. The lamp flux needed for knowing the HO_2 concentration is obtained either by actinometric methods (O_3 or N_2O) or by calibrating the Hg lamp flux using a calibrated UV phototube.

All three instruments follow a similar measurement procedure. Air is sampled via a nozzle into a low pressure chamber (0.2-0.3 mbar) where RO_2 and HO_2 are selectively converted to OH by addition of NO. SO_2 is simultaneously added so that the OH generated is converted to H_2SO_4 in the presence of H_2O. H_2SO_4 is then reacted with NO_3^- in a ion-molecule reactor before being detecting as HSO_4^- using a quadrupole mass spectrometer. The yield of H_2SO_4 molecules per initial HO_2 molecule (also called chain length) is controlled by the reaction time and the ratio between the $[SO_2]/[NO]$ ratio (i.e competition between (R 22) and (R 32)). Usual reaction time is of 0.1 s and depending on instruments chain length varied from 5 to 15.

Hanke et al. (Hanke et al., 2002) developed an instrument named ROxMAS where sampled air is diluted by a factor of 9 either in N_2 for the "HO_2-mode" or in O_2 for the "HO_2+RO_2-mode". For the "HO_2-mode", O_2 concentration is reduced down to approximately 2% to decrease the rate of the reaction (R 27) and so most of the H_2SO_4 measured comes from the ambient HO_2 converted to OH via (R 30). For the "HO_2+RO_2-mode", the sampled air is diluted in O_2 ($[O_2]$ > 70 %), in this case, removal of peroxy radicals and alkoxy radicals via reactions (R 26), (R 28) and (R 29) is reduced and the total peroxy is measured. The conversion efficiency for the "HO_2-mode" is between 0.25 and 0.30 and 0.90 for the "HO_2+RO_2 mode".

On the other hand, Edwards et al. (Edwards et al., 2003) varied the NO concentration to measure selectively HO_2 and RO_2. Under high NO concentration (NO ~ 2300 ppm), the reaction (R 29) is favoured compared to the reaction (R 27), it corresponds to the "HO_2-mode". Under low NO concentrations (NO~5 ppm), the opposite happens and this is the "HO_2 + RO_2 mode". The conversion efficiencies reached are 0.10 to 0.15 and 0.80 to 0.90 for the "HO_2-mode" and the "HO_2+RO_2 mode" respectively. By varying the NO concentration, the SO_2 concentration must be varied simultaneously to keep the same chain length. The drawback of this method is the long time (30 min) needed to purge the NO-line between the two modes (Hornbrook et al., 2011).

The most recent development for HO_2 measurements using CIMS technique were made by Hornbrook et al. (Hornbrook et al., 2011). They combined the methods of Hanke et al. (Hanke et al., 2002) (dilution in O_2 or N_2) and Edwards et al. (Edwards et al., 2003) (variation of NO concentration) to obtain a more selective technique for HO_2 and RO_2. They did an extensive analysis of the conversion efficiency over a wide range of $[NO]/[O_2]$ ratio (10^{-6} to 10^{-2}). In measurement conditions, under low $[NO]/[O_2]$ (i.e. equal to 2.53×10^{-5}) they measured a

conversion efficiency of 100 % for RO_2 and HO_2. For the "HO_2-mode", at high [NO]/[O_2] (i.e. equal to 6.80×10^{-4}), they obtained a conversion efficiency of approximately 15 %. Under their optimal conditions, they studied the conversion efficiencies for a variety of hydrocarbons (alkanes, alkenes and aromatics) in the two different measurement modes as can be seen in Table 2. The large range of conversion efficiencies in both measurement modes reflects the complexity of chemical mechanism involved in the conversion of RO_2 to HO_2 by addition of NO.

Table 2. Conversion efficiencies measured by Hornbrook et al. (Hornbrook et al., 2011) for different RO_2 precursors.
Comparison between CH_4 and the alkanes (without CH_4), the alkenes and the aromatics tested.

RO_2 precursor	α_{RO2}	
	"HO_2+RO_2-mode"	"HO_2-mode"
CH_4	1.22	0.17
alkanes*	0.94 – 1.41	0.28 – 1.03
alkenes	1.18 – 1.52	1.11 – 1.37
aromatics	0.89 – 0.94	0.75 – 0.89

*methylpropane was not taken into account. Measurements showed very low conversion efficiency in both modes due to the absence of α-hydrogen in the RO_2 structure.

At very low [NO]/[O_2] ratio (below 10^{-5}) they observed conversion efficiencies greater than 1 (up to 1.5) that could not be explained by the standard chemical mechanism (R 22) to (R 32). More than one HO_2 is produced from the conversion of RO_2 to HO_2 or SO_2 is oxidized to SO_3 via an additional mechanism. Including decomposition or isomerisation processes of RO that could lead to the formation of additional HO_2 into the model did not fully explain these observations. However, the oxidation of SO_2 to SO_3 via a combination of 3 complex mechanisms summarized in reaction (R 34) involving RO_2 (or RO), NO and O_2 gave a good agreement between the measurement and the model.

$$RO_2\,(\text{or RO}) + SO_2 + NO + O_2 \rightarrow\rightarrow RO_2\,(\text{or RO}) + NO_2 + SO_3 \qquad \text{(R 34)}$$

However, many kinetic parameters were not known and a study of the oxidation of SO_2 under low NO condition is needed.

3. Review of the FAGE instruments

Prior to the first attempt to measure OH radical concentration in the troposphere, OH concentration measurements in the stratosphere using LIF were made (Anderson, 1976). OH is one of the natural chemical species (along with H, NO, Cl, Br) that catalytically destroy O_3 in the stratosphere (Wayne, 2000) and its measurement is of great importance in order to model the O_3 concentration in the stratosphere. The technical advances made by the Harvard group (Wennberg et al., 1994) for their aircraft LIF helped grandly in the development of other techniques that measured troposheric OH. The characteristics of the set up were a high repetition rate CVL (copper vapour laser) laser at 282 nm (O_3 interference reduced in the stratosphere due to lower amount of H_2O), White-cell, measurement cycle for signal and background (on- and off-resonance), C_3F_6 as chemical modulator, reference cell and a gated PMT.

The first measurements of OH and HO_2 from the early 1970s up to the 1990s using LIF at atmospheric pressure were subject to controversy due to the high level of the O_3 interference. In the 1980s, at the same time as the LIF measurement at atmospheric pressure, a new technique called FAGE (Fluorescence Assay by Gas Expansion) was developed in which air is sampled in a low pressure cell and OH is detected by LIF. The FAGE technique improved the quality of the measurements as the level of the O_3 interference was reduced. The FAGE technique has been nowadays developed by many groups and is recognized as reliable and sensitive.

3.1. First attempts to measure OH and HO_2 using LIF

Early measurements of ambient OH concentrations using LIF were made by exciting the OH at 282 nm $A^2\Sigma^+$ (v'=1) ← $X^2\Pi_i$ (v''= 0) and collecting the fluorescence at 308 nm at atmospheric pressure as it is used commonly for other applications (kinetic, combustion, plasma,…). The excitation/detection scheme is convenient as the fluorescence emission can be separated from the laser emission using an interference filter. The excitation laser was fired using a low repetition rate laser (e.g. 0.1 Hz and 6 mJ) in ambient air at atmospheric pressure. In consequence, the excited OH radical were mainly relaxing to the ground state via non radiative collisional quenching and only few excited OH fluoresced. The fluorescence lifetime was shorter (τ_{fluo}~ 1 ns, at 1 atm) than the laser pulse (τ_{laser}~20 ns). In addition, at atmospheric pressure, Rayleigh scattering as well as Raman scattering by O_2, N_2 and H_2O were degrading

the sensitivity with high non resonant fluorescence background. Wang and Davis (Wang and Davis, 1974) measured OH concentration up to 1.5×10^8 cm^{-3} in the early afternoon and below 5×10^6 cm^{-3} at night. However, they later (Wang et al., 1976) found out that they were producing a high amount of OH (ca. 200 to 1000 times higher than in clean atmosphere) in the photolysis pulse via the photolysis of O_3. One characteristic was that the 2-photon production and excitation of OH occurred within the same laser pulse due to the high laser energy density. Davis et al. characterized this interference experimentally (Davis et al., 1981a) and theoretically (Davis et al., 1981b) and shown that the artefact OH was much higher than the ambient OH. Improvements were made by shortening the laser pulse or expanding the laser beam (Wang et al., 1981). However detection of OH by LIF at atmospheric pressure was abandoned after the controversial OH measurements during the NASA GTE/CITE campaign where the OH concentration measured were biased with artefact OH generated from the O_3 photolysis (Crosley, 1995; Heard and Pilling, 2003).

A laboratory method using a 2-photon excitation was developed to overcome the difficulties encountered with the first LIF instruments (Bradshaw et al., 1984). For this method, the OH radical was first excited using an IR laser (e.g. $\lambda = 1.43$ µm) to the second vibrational ($v''=2$) level of the electronic ground state ($X^2\Pi$) before being excited to the first electronic state ($A^2\Sigma^+$ ($v'=1$) or $A^2\Sigma^+$ ($v'=0$)) using a UV laser (345-351 nm). The OH fluorescence was then collected at 309 nm using pass band filter and a photomultiplicator. The advantages of this technique are multiple, at 343 nm, the O_3 absorption cross section was too low and the $O(^1D)$ quantum yield close to zero and so OH generated by O_3 became negligible. In addition, the different light interferences (Rayleigh and Mie scattering) were also reduced because the detected OH fluorescence was blue-shifted. One drawback was the difficulty at that time to generate laser pulse in the near IR, they injected a 650 nm dye laser beam into a H_2 Raman cell and after using a Pellin-Broca prism they separated the 1.43 µm second Raman lines from the other Raman lines. However, this method was never applied to field measurement.

Figure 3 summarizes the 3 different schemes that were used for the measurement of the OH fluorescence at 308 nm, (a) 1-photon excitation at 282 nm and fluorescence collection at 308 nm, (b) 2-photon excitation at 1.43 µm and 351 nm followed by fluorescence collection at 308 nm and (c) 1-photon excitation at 308 nm and collection at 308 nm.

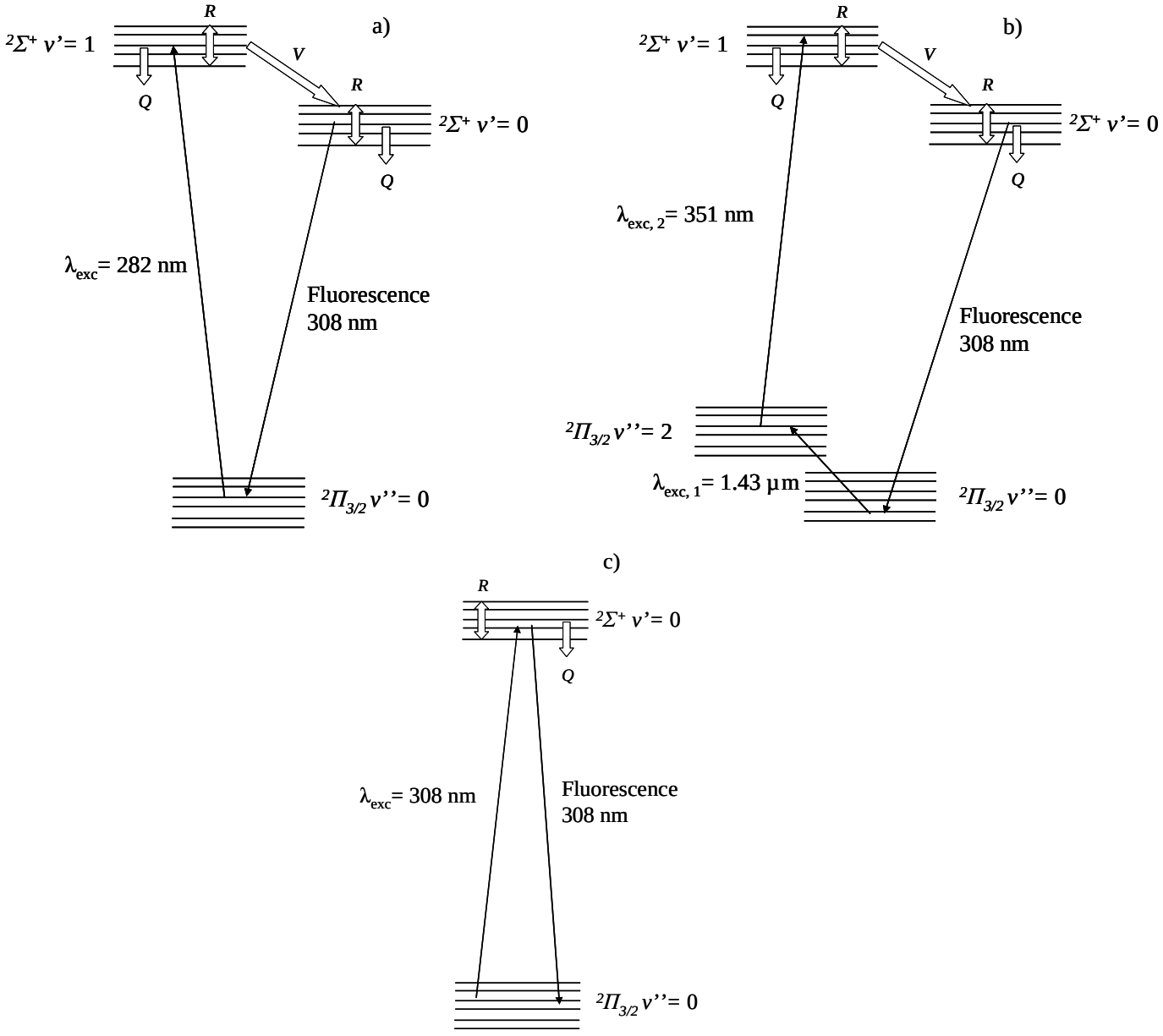

Figure 3. Schematic representation of the energy levels and transition used for the measurement of the OH fluorescence at 308 nm.
a) 1-photon excitation at λ_{exc}=282 nm, b) 2-photons excitation at $\lambda_{exc,\,1}$=1.43 µm and $\lambda_{exc,\,2}$=351 nm and c) 1-photon excitation at 308 nm. (*V*), collisional vibrational transfer. Collisional processes: rotational transfer (*R*), and quenching (*Q*). Figure adapted from Smith and Crosley (Smith and Crosley, 1990) and Bradshaw et al. (Bradshaw et al., 1984).

3.2. Developments of the FAGE technique

The FAGE technique was pioneered by Hard and O'Brien (Hard et al., 1979). Taking into account the difficulties encountered by the previous group that detected OH using LIF at atmospheric pressure they developed an instrumental set up where ambient air was sampled though an orifice into a low pressure cell. At low pressure, OH fluorescence radiative decay was then increased due to lower quenching and the non resonant fluorescence background decreased because Rayleigh and Raman scattering decreased linearly with pressure. In the first version of the FAGE (Hard et al., 1984), OH was detected at 282 nm using a low repetition rate (30 Hz) and a relatively high energy per pulse (0.6 mJ) and in consequence was subject to the O_3 interference. In order to determine the portion of the fluorescence signal coming from the O_3 photolysis, two cells were run in parallel and in one of them ambient OH was removed by reaction with a chemical modulator (i.e. isobutane) that was injected few millimetres below the nozzle. The OH fluorescence signal was then the signal in the first cell minus the signal in the second cell with the chemical modulator. However, during a field campaign at a coastal site in Oregon (Hard et al., 1986), at night they measured negative net signal that was later attributed to the reaction of isobutane with electronically excited oxygen atom, $O(^1D)$, produced in the laser pulse that generated OH radicals in the second cell while no OH fluorescence signal was measured in the first cell. These measurements were contested by different studies. Smith and Crosley (Smith and Crosley, 1990) used a photochemical model to simulate the interference of O_3 and isobutane on the measurement of OH with the FAGE technique using the conditions given by Hard et al. (Hard et al., 1986). From the simulation results, Smith and Crosley gave some requirements in order to reduce these interferences. For the O_3 interference, they advised use of a lower energy pulse as well as exciting the OH radical at a 308 nm $A^2\Sigma^+$ (v'=0) ← $X^2\Pi_i$ (v''= 0). They proposed that instead of using a low repetition rate YAG laser and a dye at 282 nm the authors should installed a high repetition rate copper vapour laser with a dye emitting at 308 nm. Indeed, the O_3 absorption cross section is 25 times lower at 308 than at 282 nm. The fact that the fluorescence is at the same wavelength as the excitation did not bring any difficulties since the OH fluorescence was already detected after the laser pulse to reduce the background signal. They also pointed out that by using high repetition rate lasers care needed to be taken that the sample flow was renewed between each laser pulse and so OH produce from the O_3 interference could not be detected in the following pulses. To reduce the interference coming

from the reaction of $O(^1D)$ with isobutane, they advised to use a hydrogen free olefin such as chlorotrifluoroethene (C_2ClF_3) for the background measurement using chemical modulation. Hard et al. (Hard et al., 1992) took into account the requirements of Crosley and Smith and the last version of the PSU FAGE owned the main characteristics of the FAGE techniques which are nowadays utilized by the different groups around the world. The characteristics were:

- Air sampled through a nozzle (~ 1 mm) into a low pressure chamber (few Torr)
- High-repetition rate laser with low energy per pulse (~1 µJ)
- Excitation of OH at 308 nm followed by fluorescence collection at 308 nm
- Gated detectors in order to limit laser scattering
- On and off resonance measurements cycle
- Calibration of the OH fluorescence signal using an external source of HOx radicals
- Measurement of HO_2 after addition of NO

Following the work made by Hard and O'Brien, 4 groups (PennState University; FZ Juelich; University of Leeds, University of Tokyo) developed instruments to measure tropospheric OH and HO_2 based on the FAGE technique. More recently, 3 groups (Indiana University, MPI Mainz, and University of Lille) built a FAGE instrument based on the instrument developed by the PennState group. Table 3 summarizes the different FAGE instruments that are currently running.

Table 3. Configurations and performances of the FAGE instruments during recent field measurements.
All these instruments have been involved in numerous field measurements in very different environments that affected their performances so the performances are given for one specific campaign.

Groups	Instruments characteristics								Reference
	Type of cell	Rep. rate / Pwr mW	Nozzle size	Detector	P_{cell} (hPa)	LOD (S/N=2) in cm^{-3}		Accuracy (2σ)	
						OH	HO_2		
University of Leeds (UK)	Single-pass ground	5 kHz / 9 to 20	0.8 mm	CPM	1.33	2.2×10^6 for 150 s	5.6×10^6 for 150 s	40 %	(Whalley et al., 2010)
FZJ (Germany)	Single-pass	8.5 kHz 10-60	0.4 mm	CPM	3.5	(0.5-1) × 10^6 for 5 min	(1-3) × 10^6 for 5 min	40 %	(Lou et al., 2010)
Pennsylvania State University (USA)	GTHOS (ATHOS) Multi-pass cell	3 kHz 1-15	1.0 mm (1.5 mm)	MCP	4-5 (3-12)	(2.5×10^5 for 1 min)	(2.5×10^6 for 1 min)	32 %	(Faloona et al., 2004; Ren et al., 2012)
Indiana University (USA)	Multi-pass cell	6 kHz 1–15	1.0 mm	MCP	5.3	7.8×10^5 for 5 min	4.4×10^6 for 8 min	40 %	(Dusanter et al., 2009)
MPI, Mainz (Germany)	HORUS Multi-pass cell	3 kHz 3-6	1.25 mm	MCP	2 5	5-10 × 10^5 for 1 min	2.0×10^6 for 1 min	20-50 %	(Martinez et al., 2010)
FRCGC, Yokohama (Japan)	Single-pass	10 kHz 5-9	1.0 mm	PMT	2.9	5.3×10^5 for 73 s	5.5×10^6 for 51 s	40%	(Fuchs et al., 2010; Kanaya et al., 2001; Schlosser et al., 2009)
University of Lille (France)	Multi-pass cell	5 kHz 1-3	1.0 mm	CPM	2.0	3.5×10^5 for 1 min	1.1×10^6 for 1 min	40%	This work

HORUS: HydrOxyl Radical measurement Unit based on fluorescence Spectroscopy, FRCGC: Frontier Research System for Global Change, GTHOS: Ground-based Tropospheric Hydrogen Oxides Sensor, ATHOS: Airborne Tropospheric Hydrogen Oxides Sensor, FZJ: Forschungszentrum Jülich, MPI: Max-Planck Institute, CPM: Channel Photomultiplier, MCP: Multi-Channel Pate, PMT: Photomultiplier

3.3. Description of the different aspect of FAGE instruments

In the following sections, we will describe in some details the different aspects of the FAGE instruments which are the gas expansion, the cell design, the type of laser, the type of detectors, the reference cells and the calibration technique.

3.3.1. Air sampling

After air is sampled through a small orifice it forms a molecular beam in a supersonic free jet expansion. In the expansion, the temperature and the pressure quickly decrease, leading to less collisions and a slower chemical reactivity. Under pressure conditions used in the FAGE, shockwave structures (i.e. large fluctuations in the temperature and the gas density) are observed that correspond to the transition from the supersonic to the subsonic gas velocity regimes. The position of the Mach disc that marks the boundary between the supersonic and the subsonic expansion, x_m can be calculated knowing the orifice diameter, d, the background pressure p_b and the external pressure p_0 by the equation given as (Miller, 1988)

$$\frac{x_m}{d} = 0.67 \times \sqrt{\frac{p_0}{p_b}} \qquad \text{Eq. 6}$$

After the Mach disc, the gas velocity enters in a subsonic regime and the temperature recovers back to ambient temperature as can be seen on Figure 4

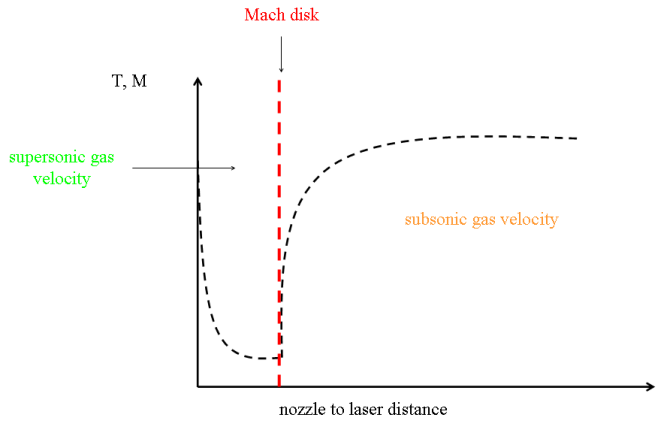

Figure 4. Schematic representation of the temperature profile in the gas expansion. Adapted from (Creasey et al., 1997b).

Creasey et al. (Creasey et al., 1997b) performed a series of experiment where they varied the distance between the nozzle and the laser by mounting the nozzle on bellows. They measured the rotational temperature by scanning the laser to excite several rotational lines looking at the distribution of the ground state rotational populations of the OH excitation spectrum. They tested different nozzle sizes (0.2 to 1.0 mm) and shapes (conical or flat). They saw that the temperature recovery after the Mach disc proceeded with different pattern in agreement with observations made by Stevens et al. (Stevens et al., 1994), Holland et al. (Holland et al., 1995) and Kanaya et al. (Kanaya et al., 2001). The distance at which the rotational temperature is recovering back to ambient was shown to be dependent on the size of the orifice, the shape of the nozzle (e.g. flat, conical) and the background pressure. Measurements showed that for a nozzle of 1 mm, ambient temperature was measured a couple of tens of centimetre (10 to 30 cm) below the nozzle. Along with the temperature and the density, the fluorescence lifetime is also varying with the distance between the nozzle and the laser probing zone. Creasey et al. (Creasey et al., 1997b) observed that the fluorescence lifetime reached a maximum in the supersonic region before the Mach disc. After the Mach disc the fluorescence lifetime was shown to follow the same profile as the temperature and decreased with the distance from the nozzle (Creasey et al., 1997b; Kanaya et al., 2001). Fluorescence lifetime dependens on the collisional quenching rate.

3.3.2. Type of cells

The first groups that developed FAGE instruments designed measurement cells that minimize stray light from the laser scattering. All cells are usually anodized black and baffles are installed along the laser path. Two type of cells have been developed, single pass type (Heal et al., 1995; Holland et al., 1995; Kanaya et al., 2001) and multi-pass type (Brune et al., 1995). The differences between single pass and multi pass cell lie in the volume sampled by the laser. For single pass, the repetition rate and the beam diameter are higher than for multi pass cells. The advantage of single pass cells is that the interference due to photolysis is reduced compared to multipass cells, whereas with the multipass cells the LIF signal is increased. Also, the background signal is expected to be higher in a multipass cells.

3.3.3. High repetition rate lasers

One of the major advances of the FAGE technique was through the use of high repetition rate lasers. At first, all groups were using Copper Vapour Laser (CVL) to pump tunable dye laser

systems (Brune et al., 1995; Heal et al., 1995; Holland et al., 1995). Nowadays, CVL are replaced by frequency doubled YAG lasers from Spectra Physics or Photonics Industries. The 532-nm wavelength is then used to pump either a Ti:Sapp solid crystal (Photonics Industries) or a dye system (e.g. Lambda Physic Scanmate, "Tintura, New Laser Generation", Harvard design, SIRAH). Usually, dyes are a mix of Rhodamine diluted in a solvent (e.g. methanol, ethanol, isopropanol) that fluoresce at 616 nm. The dye fluorescence is doubled using doubling crystal (e. g. BBO: Beta Barium Borate) to give a wavelength of 308 nm with a maximum power varying from 15 to 100 mW, linewidth from 4.5 to 7 GHz and pulsewidth from 20 to 40 ns (Dusanter et al., 2009; Kanaya et al., 2007; Lu et al., 2012). For the MPI-FAGE and the PennState FAGE, the dye cavity system is based on the Harvard design (Wennberg et al., 1994).

For the solid laser, two CLBO (Cerium Lithium Borate) non linear optical crystals are used to generate the required 308 nm wavelength. The Ti-Sapp wavelength output (924 nm) is frequency tripled to generate the required 308 nm wavelength in two stages. First, the fundamental output wavelength is doubled using a CLBO (Cerium Lithium Borate) crystal to obtain a 462 nm wavelength. In a second stage, a sum frequency generation is performed with a second CLBO crystal by mixing the 924 nm and the 462 nm wavelength (Bloss et al., 2003) to generate the 308 nm wavelength. The output power can be up to 150 mW, the pulse linewidth and the pulse length are of 0.065 cm^{-1} and 35 ns, respectively.

3.3.4. Fluorescence detection

The collection of the OH fluorescence is done at the same wavelength as the excitation (308 nm) for reasons given elsewhere (see section 3.1). At the working pressures of FAGE instruments (few hPa), the OH fluorescence lifetime (τ_{OH} ~ 300 ns) is much larger than the laser pulse (τ_{laser} ~ 20 ns). In this case, the detection of the much weaker OH fluorescence is temporally shifted from the laser pulse as can be seen on Figure 5. To do so, the detectors are gated meaning that they are switched off during the laser pulse (so they do not saturate) and rapidly switch on to collect the OH fluorescence after the laser pulse.

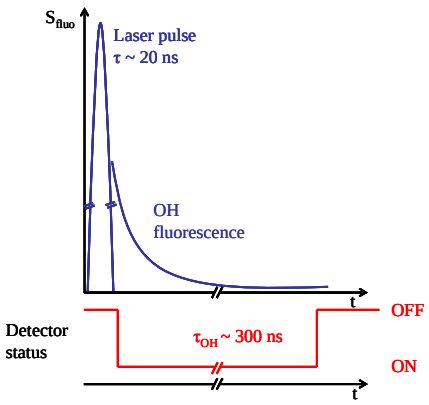

Figure 5. OH fluorescence detection using gated detector

In addition, optical systems were optimized in order to collect the maximum of the OH fluorescence emitted after the laser pulse and minimize light scattering. The set of lenses used for collecting the OH fluorescence depends on each set up but the Figure 6 shows a simplified arrangement. The OH fluorescence is collected perpendicular to the laser beam and collimated using converging lenses. Then, it passed through a narrow band filter having its maximum transmission centred on the OH fluorescence wavelengths (λ ~ 310 nm, bandwidth ~ 5 to 15 nm) to reduce solar light, red-shifted fluorescence of the walls, and potential fluorescence of other chemical species (Dusanter et al., 2009). Finally, the optical train is ended with a converging lens that focused the OH fluorescence on the detector. On the opposite side of the fluorescence detection, a concave mirror can be added to double the solid angle seen by the detector.

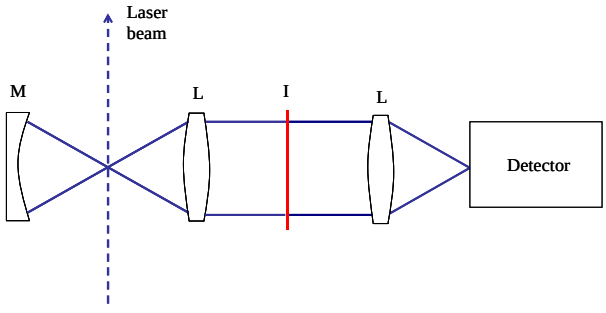

Figure 6. Simplified OH fluorescence collection
M: Concave mirror, L: Lens, I: bandpass interferometer

Three different types of detector have been used to count photons emitted from the OH fluorescence: MCP (Micro Channel Plate), CPM (Channel PhotoMultiplier) and PMT (Photomultiplier). Along with detectors, home-built switches were developed by each group

in order to turn on the detector as fast as possible after the laser pulse in order to measure as much of the OH fluorescence as possible. As the fluorescence decays exponentially, the delay between the laser pulse and the start of the fluorescence collection strongly affect the sensitivity. Detectors are usually composed of 3 elements: a photocathode, an electron multiplier and an anode. The photocathode converts the photon into electrons. Electrons are then accelerated using high-voltage potential between the photocathode and the electronmultiplier. Electronmultipliers are made of discrete dynodes for PMT, a channeltron for CPM, multiple electron multipliers for MCP. The electrons from the photocathode are amplified and detected on the anode. Important parameters to choose the type of detector are: the current gain, the quantum efficiency in the UV, its ability to be gated and the recovery time (time after the detector is "ON" after being switched "OFF"). Current gain and quantum efficiency are lower for MCP than for PMT and CPM. However, MCP detectors are internally gated using an ICCD (Intensified Charged Couple Device) so do not suffer from after pulse signal feedback and have a very short recovery time but are more expensive than the others. Among PMT and CPM, CPM exhibits a shorter recovery time and a lower after-pulsing feedback.

3.3.5. Reference cells

The OH excitation peak has a very narrow linewidth and since the laser wavelength can drift with time and ambient conditions (e.g. temperature), reference cells are used to select and stabilize the OH excitation laser wavelength. Usually, Q branch lines of the first electronic excited state are used for the excitation of OH. The modulation from on to off resonance is achieved with the reference cell by moving the laser wavelength to the side of the excitation line. Three types of reference cell are used: H_2O vapour thermolysis using a hot filament, H_2O vapour photolysis via a mercury lamp, and microwave discharge of H_2O vapour in air. The design of the different reference cells used by the different groups is similar. Air is pulled in a low pressure cell after bubbling through a water reservoir, the excitation laser passed through one axis of the cell and the OH fluorescence is collected at right angle using a detector (e.g. PMT, CPM). The On-Off resonance modulation can also be achieved using a Fabry-Perot etalon.

3.3.6. Measurement sequence

Usually, FAGE measurements follow a common pattern. First, the laser wavelength is scanned in order to find the OH excitation peak ($Q_1(1)$, $Q_1(2)$ or $Q_1(3)$) using the reference cell (the peak is chosen to be intense and easily identified in the spectrum structure). The laser wavelength is then automatically fixed on the OH excitation peak and the on-line measurement starts for several tens of seconds (5 to 90 s). Then, the laser wavelength is moved to a wavelength where OH is not absorbing and kept for several tens of second, this is the off-line measurement. The off-line measurement signal is the combination of the laser scattering, and also of possible chemical species having a broad UV absorption in the 308 nm range where OH is measured. It is subtracted from the on-line signal and after calibration the resulting signal is converted to OH concentration. Finally, the laser wavelength is moved back on-line and so on.

3.3.7. Deployment on field campaigns

The FAGE technique was developed both for ground and aircraft measurements. For ground based measurements, the laser, the electronics and the pump are set inside a container or in a building while the cells are placed on top of the container or on a tower several meters above the ground depending on the aim of the measurement (e.g. ground, above forest canopy, in a cloud). The laser beam is brought to the cell using optical fibres.

3.3.8. HO_2 measurement with FAGE

FAGE instruments are able to measure both OH and HO_2 radicals. HO_2 are detected after being converted to OH with NO. In general, FAGE experimentalist set the NO concentration to have a conversion efficiency close to 100% however at high NO concentration the reaction (R 36) becomes significant and therefore an efficiency of 100% cannot be achieved. The maximum conversion efficiency is around 90 to 95%.

$$HO_2 + NO \rightarrow NO_2 + OH \quad \text{(R 35)}$$
$$OH + NO \rightarrow HONO \quad \text{(R 36)}$$

Pure NO gas is mixed to the sample gas via a loop (e.g. Teflon) with many small holes perforated. Ascarite can be used to trap HONO that can be found in pure NO cylinder. NO is flowed through a Teflon pipe and care must be taken of leakage. In effect, if water vapour is

mixed with pure NO, nitric acid is formed and can damage the mass flow controller used to regulate the NO flow. The NO concentration added to the sample air and the conversion time vary depending on each set up from 0.04 to 0.6% for the NO concentration and 0.5 to 3 ms for the conversion time.

The possibility that RO_2 could be recycled to HO_2 was always questioned and tests were made with C1 to C4 alkanes (Creasey et al., 2002; Fuchs et al., 2010; Kanaya et al., 2001; Mather et al., 1997; Ren et al., 2004a; Stevens et al., 1994). Results showed an insignificant conversion usually inferior to 5%. This is explained by the slow reaction rate (R 38) of the alkoxy radicals (RO) with O_2 at the low pressures and thus low O_2 concentration of FAGE instruments.

$$RO_2 + NO \rightarrow RO + NO_2 \quad \text{(R 37)}$$
$$RO + O_2 \rightarrow R'CHO + HO_2 \quad \text{(R 38)}$$
$$RO + NO \rightarrow RONO \quad \text{(R 39)}$$

However, a recent work from Fuchs et al. (Fuchs et al., 2011) showed that certain alkoxy radicals (with alkenes and aromatics as parent species) could undergo fast decomposition or isomerisation that lead to high recycling of RO_2 to HO_2 within the conversion time and with NO concentrations commonly used. These findings will be discussed in section 3.6 (Interference for HO2 measurements).

3.4. Type of calibrations

Laser induced fluorescence is a direct but relative method. The fluorescence signal (in $cts.s^{-1}$) is proportional to the OH concentration, [OH] (in $molecule.cm^{-3}$), and the laser power P (in mW). The relationship that links the signal to the OH concentration is given as

$$[OH] = \frac{S}{C \times P} \qquad \text{Eq. 7}$$

where C is the sensitivity in $cts/s/molecule.cm^{-3}/mW$.

3.4.1. Theoretical sensitivity

In principle, the sensitivity can be calculated theoretically (Holland et al., 1995; Stevens et al., 1994) using the following equation

$$C = \left[\frac{B12}{c^2} \times \left(\frac{4\ln 2}{\pi} \right)^{1/2} \times (\Delta\nu_D^2 + \Delta\nu_l^2)^{-1/2} \times \frac{\Delta N}{N} \times l \right] \times \left[\varepsilon \eta T f_{gate} \right] Q \frac{\rho_{in}}{\rho_{amb}} \gamma_{sampling} \qquad \text{Eq. 8}$$

where

$$f_{gate} = \exp\left(-\frac{\Delta T_c}{\tau} \right) - \exp\left(-\frac{\Delta T_c + T_c}{\tau} \right) \qquad \text{Eq. 9}$$

$$Q = \frac{\tau}{\tau_{rad}} \qquad \text{Eq. 10}$$

and $\tau = \left(\tau_{rad}^{-1} + k_q [M] \right)^{-1}$ Eq. 11

B_{12} ($cm^3\ J^{-1}\ s^{-2}$)	Einstein B-coefficient for absorption	(Dimpfl and Kinsey, 1979) $Q_1(3)=1.01 \times 10^{24}$
$\Delta\nu_D$ (cm^{-1})	OH Doppler broadening	calculated
$\Delta\nu_l$ (cm^{-1})	laser linewidths	measured
ΔN/N	fraction of OH molecules in the rotational level being excited	calculated
l (cm)	length of the laser beam overlapping the ambient airstream	measured
ε	collection efficiency of the optics	calculated
η	detector quantum yield	from manufacturer
T	transmission of the optics	from manufacturer
f_{gate}	fraction of the OH fluorescence detected	calculated
ΔT_c	time delay of the counter gate with respect to the laser pulse	measured
T_c	length of the counter gate	measured
τ	fluorescence lifetime OH	measured
Q	quantum yield of OH fluorescence	calculated
τ_{rad}	natural radiative lifetime	(German, 1975) τ_{rad} = 688 ns
k_q	rate quenching constant of OH	(Bailey et al., 1997, 1999; Copeland and Crosley, 1986)
[M]	number density of air molecules in the gas beam	measured
ρ_{in}/ρ_{amb}	ratio of densities inside and outside the sampling chamber	calculated
$\gamma_{sampling}$	sampling efficiency for OH radicals	

The sensitivity obtained from the theoretical equation is only an approximation due to the estimations that need to be made for the excitation length, the collection efficiency of the

optics and the sampling efficiency of the OH radicals. This is the reason why calibration methods were developed to generate known amount of OH and HO_2.

3.4.2. Experimental calibrations

Several methods were developed to generate known concentrations of OH and HO_2 and they were reviewed by Dusanter et al. (Dusanter et al., 2008). The most common one is the photolysis of water vapour by a mercury lamp at λ=184.9 nm to produce an equal concentration of OH and HO_2 via the following mechanism.

$$H_2O + h\nu\ (\lambda = 184.9\ nm) \rightarrow OH + H \quad \text{(R 40)}$$
$$H + O_2 + M \rightarrow HO_2 + M \quad \text{(R 41)}$$

The quantum yield for OH and H is equal to 1 (Atkinson et al., 2004).
Hg lamps have two strong emissions in the UV at 184.9 and 253.7 nm. The photon flux is approximately 8 times higher at 253.7 nm than at 184.9 nm (Schultz et al., 1995) in consequence an interference filter is placed in front of the Hg-lamp to only select the radiation at 184.9 nm ($\sigma_{184.9}=6.9\times10^{-19}$ cm² molecule^{-1}, (Atkinson et al., 2004)) and avoid O_3 photolysis at 253.7 nm ($\sigma = 1.1 \times 10^{-17}$ cm^2 molecule^{-1}, (Atkinson et al., 2004)) that could produce extra OH via the following mechanism

$$O_3 + h\nu\ (\lambda = 253.7\ nm) \rightarrow O(^1D) + O_2 \quad \text{(R 42)}$$
$$O(^1D) + H_2O \rightarrow 2\ OH \quad \text{(R 43)}$$

However, it should be mentioned that even if residual light at 253.7 nm is irradiating the air, this process is minor because of the low concentration of O_3 (maximum 10 ppb) generated during calibration.
The OH and HO_2 concentrations are given as

$$[OH] = [HO_2] = [H_2O] \times \sigma_{H2O} \times F_{184.9} \times t \quad \text{Eq. 12}$$

where $[H_2O]$ is the concentration of H_2O in molecule cm^{-3}, σ_{H2O} is the absorption cross section in cm^2.moelcule^{-1}, $F_{184.9}$ is the lamp flux in photons cm^{-2} s^{-1} and t is the exposure time in s. The H_2O concentration is measured with an hygrometer, σ_{H2O} was measured several times and found to be 7.14×10^{-20} cm^2 molecule^{-1} (Cantrell et al., 1997; Creasey et al., 2000;

Hofzumahaus et al., 1996). Two parameters need to be measured: the lamp flux ($F_{184.9}$) and the exposure time (t) of the gas flow in front of the lamp.

A direct method is to use a detector to measure the lamp flux at 184.9 nm e.g. NIST calibrated Cs-I phototubes (Faloona et al., 2004). For this method, care must be taken to precisely characterize the photon flux distribution of the lamp as it is within the calibration tube. A precise mapping of the actinic flux is done by varying the distance of the lamp compared to the photodiode, the lamp current and the aperture size. In addition, to reduce reflexions on the wall of the calibration source, the lamp flux is collimated and the inner tube is coated with black paint so that the 185 nm photons are effectively absorbed on the wall.

Others methods are indirect, the lamp flux is obtained by actinometry either with O_2 or N_2O. When using the N_2O actinometer (see details in (Edwards et al., 2003)), the experiments need to be done separately from the calibration whereas for O_2 the method can be applied simultaneously with the H_2O photolysis, O_2 is photolyzed producing $O(^3P)$ that reacts with O_2 to from O_3 via

$$O_2 + h\nu\ (\lambda = 184.9\ nm) \rightarrow O(^3P) + O(^3P) \qquad \text{(R 44)}$$
$$O(^3P) + O_2 + M \rightarrow O_3 + M \qquad \text{(R 45)}$$

The generated O_3 concentration measured with a commercial analyzer is used to determine the lamp flux times the exposure time (F×t) via

$$(F \times t) = \frac{[O_3]}{2 \times [O_2] \times \sigma_{O2}} \qquad \text{Eq. 13}$$

At 184.9 nm, O_2 absorbs in the highly structured Schumann-Runge bands where the O_2 absorption cross sections varied within several orders of magnitude as can be seen on Figure 7. An extensive discussion was made by Dusanter et al. (Dusanter et al., 2008) concerning the previous studies that observed variations of the O_2 absorption cross sections depending on the lamp used. The conclusion was that it is highly recommended to measure regularly the absorption cross section of O_2 in the conditions used during the calibration.

Calibration procedures differ depending on the flow regime (laminar or turbulent) used in the calibration source. For laminar flows (Reynolds number < 2000), the flow is characterized by a higher flow in the centre of the tube (where the air is sampled into the FAGE) than on the walls (where the air is sampled to the O_3 analyzer). In consequence, the flow in the centre of

the tube has a shorter exposure time and the O_3 concentration (as well as the [OH] and [HO_2]) is smaller.

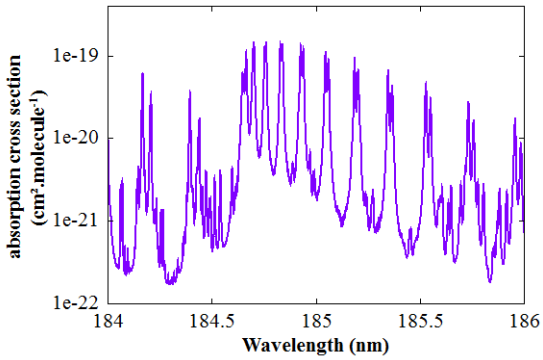

Figure 7. O_2 spectrum in the Schumann-Runge bands (Yoshino et al., 1992).

A correction factor (called P) is applied to take into account the radial velocity of the flow. The advantage of this method is the low radical losses and the relatively low gas flow but the correction factor has to be determined. Another drawback is the difficulty to place the calibration source on another FAGE setup in an intercomparison framework. For calibration using a turbulent flow, the radial velocity of the flow is flat therefore there is no need to correct the measured O_3 concentration. One drawback is the need to characterize the higher heterogeneous loss rate of radicals by moving the Hg lamp along the calibration source.

3.4.3. H_2O dependence of the sensitivity

The fluorescence lifetime of OH is function of the natural radiative lifetime and the quenching of excited OH with collision partners namely N_2, O_2 and H_2O. Knowing the quenching rate coefficients for N_2, O_2 and H_2O, the dependence of the H_2O concentration on the fluorescence lifetime can be determined. For H_2O mixing ratio of 3% and P=1.5 Torr, the fluorescence lifetime is decreasing theoretically by 20% (for more details see Chapter 2) compared to dry air.

The relative instrument sensitivity as function of H_2O was tested in the first versions of the University of Leeds (Creasey et al., 1997a) and FZJ FAGE (Hofzumahaus et al., 1996). Creasey et al. (Creasey et al., 1997a) observed a sharp decrease of the relative sensitivity with a factor of 1.74 between the calibration at [H_2O]=265 ppm and the ambient H_2O mixing ratio ([H_2O]=1%) similarly to Hofzumahaus et al. (Hofzumahaus et al., 1996) whom measured a

decrease of 2.2 of the sensitivity between the calibration H_2O concentration and the ambient H_2O concentration (see Figure 8) where the theoretical calculation predicts a decrease of 20%. The reason postulated was the formation of H_2O cluster in the supersonic expansion that would scavenge OH and HO_2 radicals. Holland et al. (Holland et al., 2003) observed that by reducing the size of the orifice from 0.75 to 0.4 mm, the H_2O effect on the sensitivity was reduced. Dusanter et al. (Dusanter et al., 2008) using an orifice nozzle of 1 mm and P_{cell}=5.3 hPa observed a dependence of the sensitivity as a function of water in agreement with the theoretical quenching of the OH fluorescence. This was also observed for the GTHOS with an orifice equal to 1 mm and a cell pressure of 5 hPa (see Figure 9).

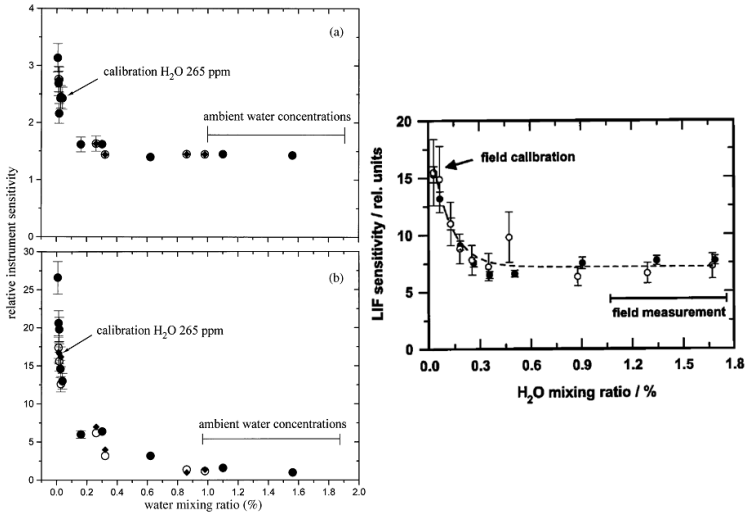

Figure 8. Relative instrument sensitivity as function of H_2O
Left: a) OH cell, b) HO_2 cell. Orifice size= 1.0 mm P_{cell}=0.59 Torr (Creasey et al., 1997a)
Right: OH cell. Orifice size= 0.75 mm P_{cell}=1.3 mbar (Hofzumahaus et al., 1996)

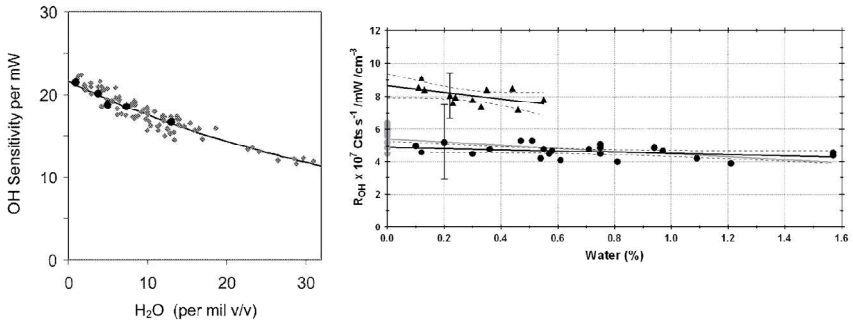

Figure 9. Instrument sensitivity as function of H_2O for the IU-FAGE (right) (Dusanter et al., 2008) and the GTHOS (left) (Faloona et al., 2004)

The behaviour of the instruments regarding the effect of the humidity on the sensitivity is strongly dependent on each apparatus (nozzle size and shape, background pressure) and needs to be tested. Ambient measurements are corrected for the quenching of the OH fluorescence with H_2O in order to get the real concentration. The FAGE instruments and the calibration process were described in this section. The next section will be dedicated to the reliability of the measurements through the presentation of the potential known interferences for the measurement of OH and HO_2.

3.5. Interference for OH measurements

Two different types of potential interferences are already well identified for OH measurements using the FAGE technique: spectral and chemical interference. Spectral interference occurs when a chemical species is fluorescing in the same wavelength range as OH. Its contribution can be subtracted from the OH fluorescence signal by the on-line and off-line wavelengths (Ren et al., 2004b). Chemical interferences are associated with the photolysis of chemical species that produce OH. They are particularly important when two laser pulses are exciting the same sampled air volume. When using high repetition rate lasers (few kHz), care should be taken to have a flow high enough to renew the sampled volume between each laser pulse in order to limit this type of interference. Additional chemical interference can be via the generation of OH radicals within the low pressure FAGE cell from "dark" reaction i.e. non-photolytic.

Extensive interference tests were made by Ren et al. (Ren et al., 2004b). In their study, spectral interferences were tested for naphthalene, sulphur dioxide and formaldehyde and chemical interferences were tested for ozone (up to 4 ppmv), hydrogen peroxide (up to 120 ppbv), nitrous acid (up to 5 ppbv), formaldehyde (up to 250 ppbv), nitric acid (up to 50 ppbv) and acetone (up to 200 ppmv). Interferences from naphthalene, ozone and acetone were identified. Except for O_3, none of the chemical species tested were affecting the OH measurement under ambient conditions. The naphthalene interference can be avoided by changing from the $Q_1(2)$ to the $Q_1(3)$ excitation line or using an offline λ lower than the $Q_1(2)$ line. In this section, more attention will be given to the ozone interference and the production of OH inside the cell by other species.

3.5.1. Ozone interference

The O_3 photolysis produces an interference signal of OH. It was observed in the first attempts to measure OH using LIF at 282 nm (for more details about the observed interference see sections 3.1 and 3.2) and even though FAGE instruments are now working at 308 nm (where the O_3 absorption is lower), O_3 is still the main chemical species affecting OH measurement which should be tested for each instrument. Ren et al. (Ren et al., 2004b) observed a quadratic dependence with the laser power of the OH interference signal meaning that a two photon process is involved (one to photolyse ozone producing $O(^1D)$ that reacts with water to form OH that is then excited by the second photon). The O_3 interference was measured to be in the range 10^2 to 10^3 cm^{-3} [OH] per ppb [O_3] which would add a slight offset in highly polluted environments. Holland et al. (Holland et al., 1995) observed that the O_3 interference signal was linear with respect to the laser power and concluded that the OH would be produced from a dark reaction on the detection cell's walls. Lu et al. (Lu et al., 2012) have reported an O_3 interference only dependent on the O_3 concentration of $(6 \pm 2) \times 10^3$ cm^{-3} [OH] per ppb [O_3] during the PRIDE campaign.

3.5.2. Internal OH production

The decomposition of chemical species in the low pressure cell that could produce OH was mentioned by Dusanter et al. (Dusanter et al., 2009). One example given was the unimolecular decomposition of Criegee intermediates that generate OH with high yields at low pressure (Kroll et al., 2001). This artificial source of OH would be linear with respect to the laser power and so the only possible way to detect it would be to use a chemical modulator.

Periodic addition of an OH scavenger (e.g. perfluoropropylene, C_3F_6) in or above the FAGE cells permits to measure which fraction of the OH LIF signal is coming from spurious OH compared to ambient OH. Indeed, ambient OH will react with C_3F_6 and if any OH signal is still detected it would correspond to artificial OH. The use of chemical modulator was often made at the beginning of the FAGE development in order to validate the technique by regularly injecting C_3F_6 into the detection cell to measure the "real" OH background (Stevens et al., 1994) however its utilization became less systematic in the following years because the measurements with C_3F_6 were close to zero.

Recently, large discrepancies between the model and the measurement of OH (up to a factor 10) were observed for several field campaigns in forestry areas (Hofzumahaus et al., 2009; Lelieveld et al., 2008; Ren et al., 2008; Whalley et al., 2011). The apparent lack of understanding of the BVOC oxidation with OH triggered the development of new oxidation mechanism of BVOC (e.g. isoprene) that could explain the higher OH concentration measured compared to the model (Butler et al., 2008; Hofzumahaus et al., 2009; Paulot et al., 2009a, 2009b; Peeters et al., 2009; Taraborrelli et al., 2009, 2012). However, Mao et al. (Mao et al., 2012b) admitted the possibility that OH measurements using FAGE were maybe affected by interferences in this kind of environment. To test this hypothesis, they carried out series of experiments during a field measurement in a forestry environment (BEARPEX09) and in the laboratory to verify if their FAGE apparatus was subject to the measurement of spurious OH. Two measurement approaches were used called "OHwave" (wavelength modulation) and "OHchem" (chemical modulation). "OHwave" is the common approach to measure OH. First, the laser wavelength is tuned on an OH excitation line for 10 s (in the case of Mao et al., variable depending on the different groups) and then the wavelength is shifted where OH is not absorbing for another 10 s to measure the background. The difference between the on-line and the off-line signals is the so-called "OHwave". For the second approach: "OHchem", a Teflon tube (dia. 1.2 cm) was placed into a small cylinder on top of the FAGE nozzle and an excess of C_3F_6 (5 sccm in ~10 L/min, approx. 500 ppm) was mixed periodically to the air sampled through 4 needles. When the C_3F_6 flow was added the measured signal corresponded to the background signal. The difference between the signal with and without C_3F_6 addition is called "OH chem.". Because no OH losses were observed by adding the cylinder on the nozzle "OHchem" can be directly compared to "OHwave". Results showed that the "OHchem" was on average twice lower than the "OHwave" indicating that artificial OH was produced inside the FAGE cell. The power dependence of the spurious OH was shown to be linear and so the possibility that a chemical species was photolyzed to produce OH in one laser shot and detected in a second laser shot was discarded. Therefore, the decomposition of chemical species (hypothetically BVOCs intermediate oxidation products) in the low pressure cell is most probable nevertheless the mechanism is not clear.

As C_3F_6 is sampled inside the FAGE cell, the OH produced inside the detection cell can also be partly removed by C_3F_6. In order to determine how much of the internal OH was removed inside the FAGE cell by C_3F_6 and obtain the "real" ambient OH concentration, laboratory experiments were conducted in which a Hg lamp was placed at three different positions

(above the inlet, below the inlet and above the detection axis) to generate OH (~100 ppt) from the H_2O photolysis via (R 40) and measure the fraction that was removed by C_3F_6

$$H_2O + h\nu\ (\lambda = 184.9\ nm) \rightarrow OH + H \qquad (R\ 40)$$

The addition of C_3F_6 showed that 95 % of the produced OH was removed when the lamp was placed above the inlet, 25 to 60% when the lamp was below the inlet and 3 to 10 % when the lamp was placed above the detection axis.

Mao et al. (Mao et al., 2012b) observed that the difference between the "OHwave" and the "OHchem" varied and was correlated with the temperature. As it is not known when FAGE instruments are subject to an interference signal via internal production of OH, both measurement approach need to be used in the field. If no differences are observed between "OHwave" and "OHchem" therefore the OH signal measured is the real concentration. However, as can be seen on Figure 10, if a difference is observed between "OHchem" and "OHwave" the real OH ($[OH]_{amb}$) concentration will be "OHchem" minus the fraction of internal OH that is not removed by C_3F_6.

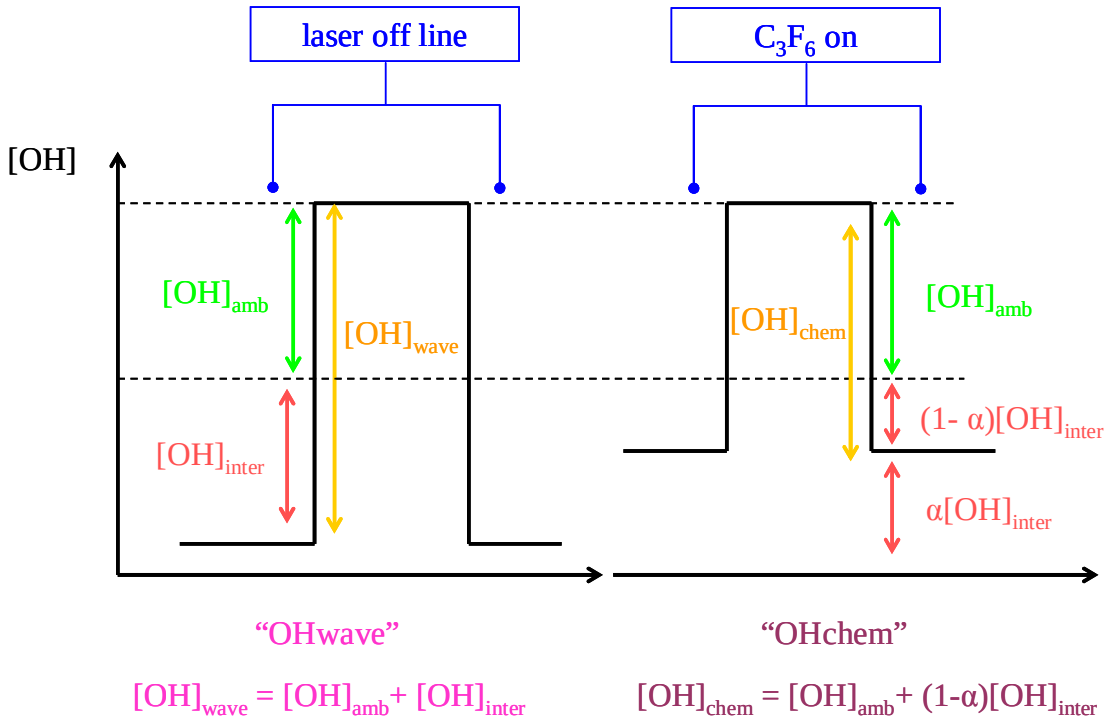

Figure 10. Schematic representation of the "OHwave" and "OHchem" measurement approaches.

The relation between $[OH]_{amb}$, $[OH]_{chem}$ and $[OH]_{wave}$ is given as (Mao et al., 2012b)

$$\frac{[OH]_{amb}}{[OH]_{chem}} = \frac{\frac{[OH]_{chem}}{[OH]_{wave}} - 1 + \alpha}{\alpha \times \frac{[OH]_{chem}}{[OH]_{wave}}} \qquad \text{Eq. 14}$$

where α is the fraction of internal OH ($[OH]_{inter}$) that is remaining with addition of C_3F_6. Mao et al. (Mao et al., 2012b) measured a value of α=0.83. During BEARPEX09, the ratio between "OHwave" and "OHchem" was 0.5 so the $[OH]_{amb}$=0.8 × $[OH]_{chem}$. Finally, the agreement between the model and the measurement was better using the OH concentration measured in the "OHchem" mode ($[OH]_{chem}/[OH]_{model}$=1.4) than for the "OHwave" mode ($[OH]_{chem}/[OH]_{model}$=3.1). From the results obtained by Mao et al. (Mao et al., 2012b), it is now essential that OH measurements using FAGE instruments, especially in forestry areas, must characterized the generation of OH inside the cells.

3.6. Interference for HO_2 measurements

For long, it was thought that the FAGE instruments were only selective to HO_2 radicals and the reactions that convert peroxy radicals to HO_2 with NO addition were too slow (see paragraph 3.3.8). RO_2 radicals from C1 to C4 alkanes have been found to have a low conversion to HO_2 within the conversion time and it was assumed that other peroxy radicals would follow the same scheme.

Intercomparative measurement for HO_2 showed in general good agreement (see more details in Chapter 3) however during the HOxComp intercomparative measurement (Fuchs et al., 2010), differences beyond their respective uncertainties were observed in ambient air as well as in the chamber between the 3 LIF instruments that participated in the intercomparative measurement. It gave some hints that either the calibration or the measurement technique was suffering from potential unknown interferences.

To understand the observed differences, Fuchs et al. (Fuchs et al., 2011) extended the interference analysis to other peroxy radical species such as alkenes and aromatics. The methodology was the following: VOC species were injected into the calibration source placed above the FAGE nozzle and VOC concentrations were in excess compare to the OH radical concentrations (~10^9 cm^{-3}) so that all OH radicals were consumed. After reaction with OH

produced from the photolysis of water, they formed peroxy radicals. The possibility that the hydrocarbons would produce radicals from the photolysis by the mercury lamp at 185 nm was tested by injecting dry air into the calibration source. No LIF signal was observed and so the hydrocarbon photolysis was assumed to be negligible (except for propane). Since the origin of the interference is generation of HO_2 by the reaction of RO_2 with NO in the FAGE, three parameters are essential: the NO concentration, the conversion time and how well NO mixes into the jet. The NO concentration was varied over almost 4 orders of magnitude (~10^{12} to 10^{16} cm^{-3}) and the conversion time was changed by modifying the orifice size (0.2 and 0.4 mm). The conversion time was measured experimentally by fitting with the MCMv3.1 mechanism the conversion of HO_2 to OH with different NO concentrations. For the 0.4 mm orifice the measured conversion time was 2.7 ms while for the 0.2 mm orifice it was reduced to 0.18 ms. The relative detection sensitivity of each RO_2 was obtained from the ratio of the detection sensitivity of the RO_2 specie against the sensitivity toward HO_2. The hydrocarbons chosen were methane, ethane, cyclohexane, ethene, propene, isoprene, MVK, MACR and benzene. In their usual measurement conditions (orifice size=0.4 mm, [NO]~10^{14} cm^{-3}) they observed as expected that the relative sensitivity of alkanes was low (<0.05) whereas for the other species the relative sensitivity was up to 80%. By changing the conversion time (using the 0.2 mm orifice), the relative sensitivity for all the tested RO_2 was much lower for the same NO concentration.

The general oxidation mechanism of any hydrocarbons is shown in Figure 11. From the reaction of hydrocarbon with OH, a peroxy radicals RO_2 is formed. RO_2 is then reacting with NO to produce an alkoxy radicals. Then two different channels are proposed for the alkoxy radical either an abstraction reaction with O_2 to form a carbonyl species and HO_2 or the unimolecular decomposition (or isomerisation) of the alkoxy radical to form a carbonyl species. The abstraction reaction is slow for any alkoxy radical while the unimolecular reaction is dependent on the hydrocarbon parent. An example is given for ethane and ethene in Figure 12. For ethane, the fate of the alkoxy radical goes only via the slow abstraction reaction to form HO_2. On the other hand, for ethene, there is a competition for the β-hydroxylalkyl alkoxy radical between the decomposition and the reaction with O_2. For most alkenes, the rate of decomposition is dominant and in the case of ethene at P=1.5 Torr, the decomposition channel is three orders of magnitudes faster than the O_2-abstraction reaction.

Similar isomerisation or decomposition mechanism exists for dialkenes (e.g isoprene) and aromatics (e.g. benzene).

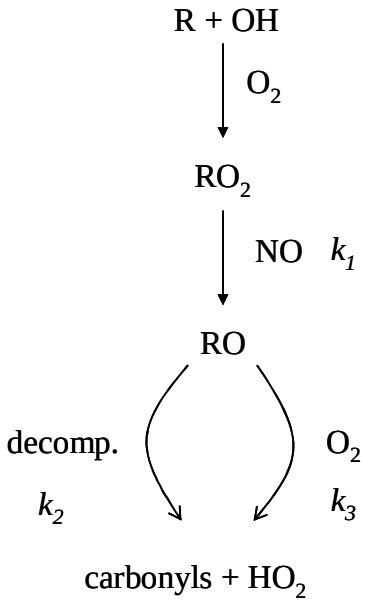

Figure 11. Oxidation mechanism of hydrocarbon

Since all the FAGE groups used NO concentration leading to conversion efficiencies for HO_2 greater than 0.9, it is not surprising that all FAGE instruments suffered from this interference. Similar RO_2 detection sensitivity were measured for the MPI FAGE (Fuchs et al., 2011) and the ATHOS (Ren et al., 2012). The University of Leeds FAGE determined an RO2 detection sensitivity of 12% for the OP3 set up (Whalley et al., 2011).

The impact of the RO_2 detection on the previous HO_2 measurement by the different LIF will vary depending where the field measurement took place as the interference is only significant for unsaturated hydrocarbons and aromatics which are mainly emitted in polluted environments and in areas where the atmosphere is loaded with BVOC (e.g forest).

Reducing the NO concentration and/or the conversion time will reduce the sensitivity of the FAGE instruments to RO_2 but also reduce their sensitivity to HO_2. Fuchs et al. (Fuchs et al., 2011) reduced the conversion time by changing the orifice size which reduces by a factor 4 their sensitivity to HO_2 and the sensitivity the different RO_2 was below 0.2. Most of the FAGE instruments were having LOD for HO_2 below 1 ppt and as the concentration of ambient levels of HO_2 is above this limit, therefore the reduced condition for the conversion of HO_2 to OH will not affect the ability to measure HO_2 in many different environments. However, even by reducing the NO concentration and the conversion time, a fraction of RO_2 is detected and the HO_2 detection using FAGE instrument is never fully selective.

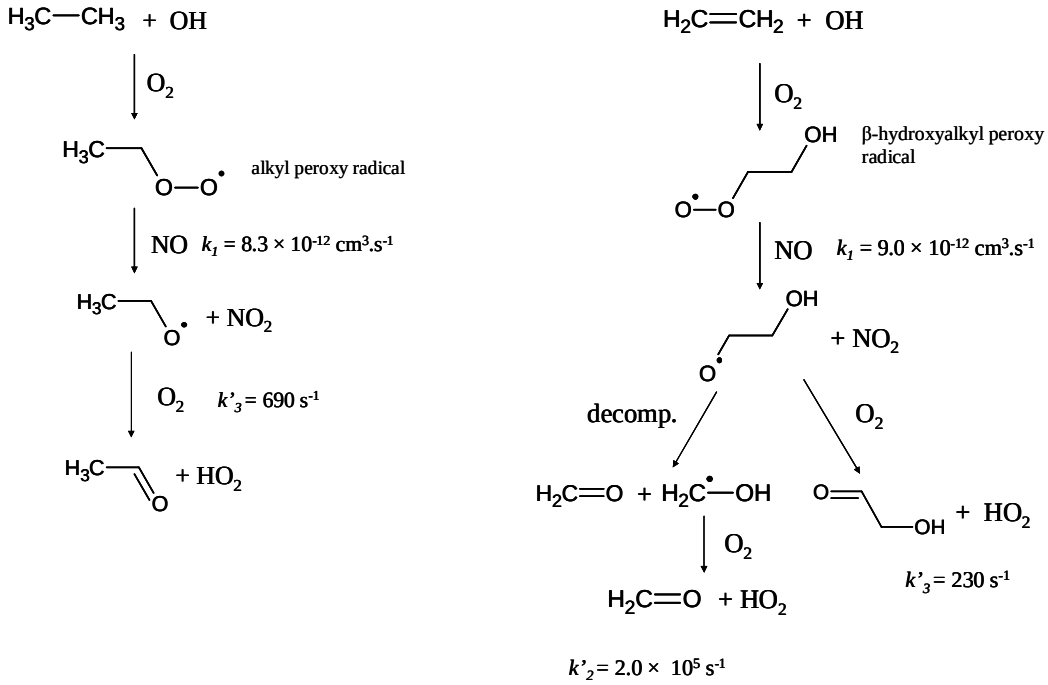

Figure 12. Oxidation mechanism (MCMv3.1) with OH for ethane (left) and ethene (right) The rate coefficients are given at T=300 K, and P=1.5 Torr ($[O_2] = 9.7 \times 10^{15}$ cm^{-3}). To ease the comparison, the rate of the $RO+O_2$ reactions are given in the 1st order.

This paragraph was dedicated to the description of the FAGE instruments in the quantification mode. As mentioned in the introduction, the OH reactivity measurement (OH lifetime) is an important parameter to measure in field campaigns in order to get the most complete estimation of the HOx budget. For that, as the FAGE instruments can detect OH in the atmosphere, with some modifications, it can also be used in a reactivity mode. This configuration as well as other techniques measuring OH reactivity is presented in the following part.

4. Review of the OH reactivity techniques

Three methods were developed to measure routinely the loss rate of OH. For two of them, the OH decay rate is directly measured with time by following OH decay by LIF using a FAGE instrument. For the third one, the OH reactivity is obtained relatively meaning that instead of measuring the OH decay directly, they measure the concentration variations of a known reactant ([X]) in the presence of artificially generated OH in zero air and ambient air due to the competition of the reactions of OH with [X] and the trace gases present in ambient air. Table 4 summarizes the performance of the different apparatus that are currently being used to measure total OH reactivity. It can be mentioned that Jeanneret et al. (Jeanneret et al., 2001) built a set-up for OH reactivity measurement using a pump and probe LIDAR technique but since this technique is not deployed in the field, the description is not given here.

4.1. Flow tube OH reactivity method

The OH reactivity flow tube method, based on the discharge-flow technique, was first developed by Kovacs and Brune (Kovacs and Brune, 2001) for ground base measurements. The technique was then adapted for airborne measurement (Mao et al., 2009). Also, a very similar flow tube reactivity system was built at the University of Leeds (Ingham et al., 2009) and deployed on several ground base field campaigns.

In this method, the OH radicals (several hundred of ppt) are produced continuously by photolysis of H_2O using a Hg lamp - (R 40) - placed inside a movable injector. Ambient air is pulled inside a turbulent flow tube where it is mixed with the OH radicals. In presence of ambient air, OH is reacting with the trace gases and detected using the FAGE technique by sampling one portion of the flow into a low pressure cell and detecting OH using LIF (more details in section 3). By varying the distance (d) between the OH source and the OH detection, at a constant flow (v), the reaction time (t) is changed and so the OH signal measured by LIF (S). The logarithm of the OH fluorescence signal is plotted against the reaction time (see Figure 13) and using a non-linear regression analysis the OH loss rate k' is derived (Eq. 10). The loss rate k' is the sum of the reactivity of each individual species present in the mixture and of the loss rate of OH due to physical processes (i.e. heterogeneous loss, diffusion loss)

$$\ln\left(\frac{S}{S_0}\right) = k' \times t \qquad \text{Eq. 15}$$

where $k' = k'_{wall} + \sum k_{X+OH}[OH]$

The different reaction times are obtained by moving the injector from the OH detection using a stepping motor. Usually 8 to 15 points are measured in order to retrieve the loss rate. As the absolute OH signal is measured, the background signal (S_0) due to laser scattering needs to be measured by moving the excitation wavelength off the OH resonance using a reference cell.

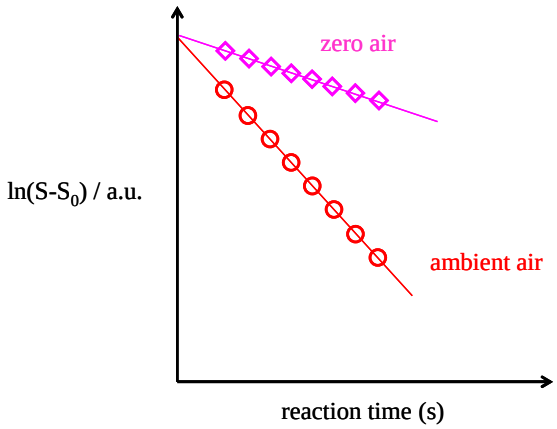

Figure 13. OH decay measured with the flow tube OH reactivity method

The critical parameter to be determined in this method is the reaction time *t* which is the distance *d* divided by the flow velocity *v*. The flow velocity is constantly measured with a hot wire anemometer placed downstream of the sampling cell. The anemometer is then calibrated by injecting a known concentration of a trace gas X that reacts with OH. By varying the concentration of the trace gas, the bimolecular rate coefficient is obtained from the pseudo-first order plot and compared with literature values. The good agreement indicates the accurate determination of the flow rate.

From the H_2O photolysis, simultaneous to the OH production, HO_2 radicals are formed via (R 40). In the presence of high concentration of NO (> 1 ppb), HO_2 is recycled back to OH via the reaction $HO_2 + NO \rightarrow OH + NO_2$ and the measured OH decays are curved. The result will be an underestimation of the total OH reactivity. A correction method was described by Shirley et al. (Shirley et al., 2006) in which the ratio of the absolute concentration of [OH]

and [HO_2] is calculated in order to determine the portion of the measured OH signal that is coming from the OH-recycling reaction.

4.2. Flash photolysis OH reactivity method

The flash photolysis method was developed at the Tokyo Metropolitan University (Sadanaga et al., 2004b). It was deployed in numerous field campaigns and was applied to the study of car exhaust in laboratory experiments (Nakashima et al., 2010).

In this method, ambient air is pulled into a photolysis cell and the OH radical are produced from the photolysis of O_3 at 266 nm in the presence of water vapour and detected by LIF at 308 nm in a low pressure cell placed perpendicular the reactor

$$O_3 + h\nu\ (\lambda = 266\ nm) \rightarrow O(^1D) + O_2 \qquad \text{(R 46)}$$
$$O(^1D) + H_2O \rightarrow 2\ OH \qquad \text{(R 47)}$$

After the photolysis laser pulse, OH decays through the reaction with the trace gases present in the photolysis cell or via other losses (e.g. heterogeneous). The OH decay is measured by time resolved LIF using high repetition rate lasers (10 kHz i.e. 100 µs time resolution). The OH concentration produced by flash photolysis is much lower than the concentrations of the reactants present in ambient air so the pseudo first order approximation is applied and the OH concentration decay is defined as a single exponential with

$$[OH] = [OH]_0 \exp(-k' \times t) \qquad \text{Eq. 16}$$

where *k'* is the pseudo first order decay rate of OH in s^{-1}.

Sadanaga et al. (Sadanaga et al., 2004b) observed that the OH decays were displaying a strong double exponential decay where the first rapid component was hypothesised to be due to perturbations by the laser shot. In consequence, only the second component of the OH decay was taken for the total OH reactivity measurement which was the combination of the true OH reactivity and physical diffusion within the photolysis cell. By changing the laser beam profile from a Gaussian (Quanta-Ray INDI-40, Spectra Physics) to a top hat (Tempest 300, NewWave Research), they observed a change in the OH decay profile from a double exponential to a single exponential decay (Y. Nakashima; personal communication). Lou et al. (Lou et al., 2010) using the same method do not observed the same OH decay profiles as Sadanaga et al. (Sadanaga et al., 2004b). A possible explanation would be that in their set up

the laser photolysis beam is expanded to increase the ratio of the photolyzed volume versus cell volume and so reduce the first rapid loss of OH.

As for the flow tube method, the OH decays can be affected by the OH recycling reaction of HO_2 in the presence of high NO concentration. However, in contrast with the flow tube method, HO_2 is not produced simultaneously with OH and the interference is much less important. Nevertheless, HO_2 is produced from the reaction of CO+OH and from the oxidation of VOC with OH and recycling under polluted environments need to be taken into account in the data analysis. The reaction of OH with O_3 that leads to the formation of HO_2 needs also to be taken into account.

4.3. Comparative Reactivity Method (CRM)

The total OH reactivity measurement by CRM is a relative method where the OH reactivity is determined by following the decrease of the concentration of a reactant in the presence of OH in zero air and in ambient air using an appropriate detector (e.g. PTR-MS, GC-FID) (Nölscher et al., 2012a; Sinha et al., 2008). Figure 14 represents the CRM measurement pattern. First, a reactant [X], usually absent in ambient air (e.g. pyrrole), is diluted in zero air after flowing through a glass reactor and its concentration is recorded (C1). Afterwards, a steady concentration of OH, produced by photolysis of H_2O, is added to the reactor. The reactant concentration is decreasing because of the reaction of X with OH (C2). By replacing the zero air with ambient air, the reactant concentration is increasing due to the competition between the reactions of OH with X and OH with the chemical species present in ambient air C3).

The OH reactivity is then given as

$$R_{air} = \frac{C3 - C2}{C1 - C3} \times k_{pyrole+OH} \times C1 \qquad \text{Eq. 17}$$

The CRM reactor is a small glass tube which was designed specifically in order to reduce the photolysis of VOC present in sampled air by the UV radiation emitted from the Hg. It has three inlets for the injection of the reagent, (pyrrole, C_4H_5N), the ambient or the zero air and the OH radicals. The sampled air is diluted in zero air and introduced inside the reactor in the presence of OH and pyrrole. The pyrrole concentration is monitored either with a PTR-MS (m/z=68) or a GC-FID. First versions were improved by placing the sampling pump downstream of the reactor (reduce loss of VOC inside the pump) and a catalytic converter is now used for air zero measurement to keep the humidity constant between zero air and

ambient air measurements as humidity is affecting PTR-MS measurement (Nölscher et al., 2012a).

As for the flow tube method, HO_2 is produced simultaneously to OH and in the presence of high NO concentration OH-recycling is observed and corrected when needed.

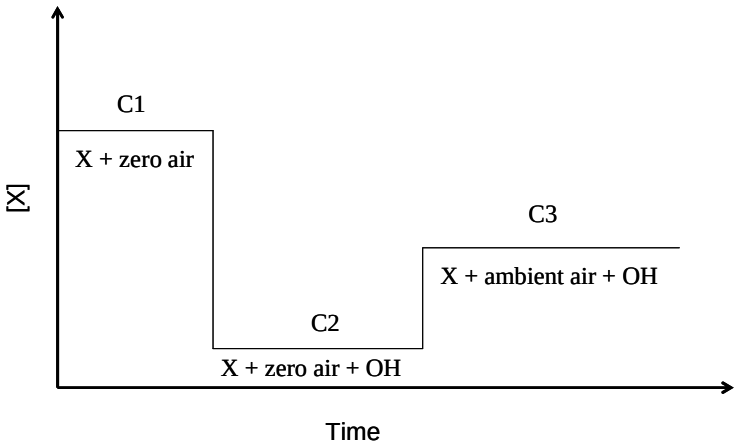

Figure 14. Schematic representation of the CRM measurement pattern (Sinha et al., 2008)

Table 4. Performances of the different OH reactivity measurement techniques
[OH] is the artificial OH concentration generated; t is the time resolution

Groups	Technique	Typical sampling flow rate / slpm	[OH] / ppt	k'_{wall} / s^{-1} (zero air)	NO correction factor for specific [NO]**	LOD / s^{-1} (2σ)	t / s	Uncertainty (1σ)	Reference
University of Leeds (UK)	Flow tube / LIF	300-900	~ 4	1.6	1.39 at 3.74 ppb	0.8	300	10-13 %	(Ingham et al., 2009)
Penn State University (USA)	Flow tube / LIF (ground base)	140	10-100	5.2	< 1.05 at < 0.05 ppb 1.08 at 1 ppb 1.4 at 5 ppb 2 at 10 ppb	1.6	240	15 %	(Kovacs and Brune, 2001; Kovacs et al., 2003)
	Flow tube / LIF (aircraft)	~130	100	2.9	1.1 at 1 ppb	0.3	210	8 – 18 %	(Mao et al., 2009)
TMU (Japan)	Flash photolysis / LIF	20	~ 40	4.0	<1.05 at 20 ppb	0.4	120	15 %	(Sadanaga et al., 2004b)
FZJ (Germany)	Flash photolysis / LIF	20	<200	1.4	1.05 at < 5 ppb 1.1 at > 5 ppb	0.6	60-180	4 – 10 %	(Lou et al., 2010)
MPI, Mainz (Germany)	CRM / PTR-MS	0.03-0.3	~10^4	-	<1.05 at <3.5 ppb ~1.5 at 10 ppb	3-4	10-60	16-20 %	(Sinha et al., 2008)
	CRM / GC-FID	0.05-0.25	~10^4	-		3-6	60-70	25-46 %	(Nölscher et al., 2012a)
LSCE (France)	CRM / PTR-MS	0.245	-*	-	1.13 at 5 ppb 1.29 at 10 ppb 1.82 at 20 ppb	3	120	20 %	(Dolgorouky et al., 2012)
University of Lille (France)	Flash-photolysis / LIF	10-15	40	4.5	-	0.6	30-120	15 %	This work

MPI: Max Planck Institute, TMU: Tokyo Metropolitan University, LSCE : Laboratoire des Sciences du Climat et de l'Environnement, FZJ : Forschungszentrum Jülich
* OH concentrations not given however from MPI-CRM, [OH] should be in the range of 10 ppb.
**factor by which the measured reactivity need to be multiplied to correct for OH-recycling

Conclusion

Among other methods described in this chapter, the FAGE technique was shown to be a technique that can be adapted to the measurement of tropospheric OH and HO_2 as it owns the necessary sensitivity and the time resolution. Recently, discrepancies for OH and HO_2 between the model and the measurement with FAGE were observed and attributed to interferences. The new interferences were observed since FAGE instruments were deployed in an increasing variety of environments especially the ones rich in BVOC species. For the detection of a fraction of RO_2 in the measurement of HO_2, the reduction of the NO and/or the reaction time was found to be an appropriate solution for future measurements. However, for previous measurements, the measured concentration of HO_2 was in fact [HO_2*] which is the sum of [HO_2] plus a fraction of [RO_2]. No attempt is made to obtain the true [HO_2]. Instead, the sum of HO_2 and RO_2 is modelled and the sensitivities of each RO_2 for specific NO concentration obtained from laboratory experiments are used to compare the $[HO_2^*]_{measured}$ with the $[HO_2^*]_{modelled}$. The newly discovered unknown OH generation inside the FAGE cells is a new challenge for the groups that runs FAGE instruments. The systematic application of a chemical modulator to measure the OH interference signal is now needed. In addition, each FAGE instruments owns its specific characteristics (i.e. geometry, flow profile) and the amplitude of the interferences will vary from one instrument to another and laboratory experiments to characterize those interferences are in progress.

The OH reactivity methods are relatively new compared to the FAGE instruments. They are a powerful tool to improve atmospheric chemistry models and their importance in field campaigns is indisputable.

At the University of Lille a FAGE instrument for the measurement of OH, HO_2 and OH reactivity was developed over the last 6 years. The detailed description of each component is given in the next chapter.

5. References

Anderson, J. G.: The absolute concentration of OH($X^2\pi$) in the Earth's stratosphere, Geophys. Res. Lett., 3(3), 165–168, doi:10.1029/GL003i003p00165, 1976.

Apel, E. C., Brauers, T., Koppmann, R., Bandowe, B., Boßmeyer, J., Holzke, C., Tillmann, R., Wahner, A., Wegener, R., Brunner, A., Jocher, M., et al.: Intercomparison of oxygenated volatile organic compound measurements at the SAPHIR atmosphere simulation chamber, J. Geophys. Res., 113(D20), D20307, doi:10.1029/2008JD009865, 2008.

Atkinson, R., Baulch, D. L., Cox, R. A., Crowley, J. N., Hampson, R. F., Hynes, R. G., Jenkin, M. E., Rossi, M. J. and Troe, J.: Evaluated kinetic and photochemical data for atmospheric chemistry: Volume I - gas phase reactions of Ox, HOx, NOx and SOx species, Atmos. Chem. Phys., 4(6), 1461–1738, doi:10.5194/acp-4-1461-2004, 2004.

Bailey, A. E., Heard, D. E., Henderson, D. A. and Paul, P. H.: Collisional quenching of OH(A 2Σ+, v′=0) by H2O between 211 and 294 K and the development of a unified model for quenching, Chemical Physics Letters, 302(1–2), 132–138, doi:10.1016/S0009-2614(99)00076-7, 1999.

Bailey, A. E., Heard, D. E., Paul, P. H. and Pilling, M. J.: Collisional quenching of OH (A 2Σ+, v′ = 0) by N2, O2 and CO2 between 204 and 294 K. Implications for atmospheric measurements of OH by laser-induced fluorescence, J. Chem. Soc., Faraday Trans., 93(16), 2915–2920, doi:10.1039/A701582H, 1997.

Bell, C. L., Van Helden, J.-P. H., Blaikie, T. P. J., Hancock, G., Van Leeuwen, N. J., Peverall, R. and Ritchie, G. A. D.: Noise-Immune Cavity-Enhanced Optical Heterodyne Detection of HO2 in the Near-Infrared Range, J. Phys. Chem. A, 116(21), 5090–5099, doi:10.1021/jp301038r, 2012.

Bloss, W. J., Gravestock, T. J., Heard, D. E., Ingham, T., Johnson, G. P. and Lee, J. D.: Application of a compact all solid-state laser system to the in situ detection of atmospheric OH, HO2, NO and IO by laser-induced fluorescence, J. Environ. Monit., 5(1), 21–28, doi:10.1039/B208714F, 2003.

Bradshaw, J. D., Rodgers, M. O. and Davis, D. D.: Sequential two-photon laser-induced fluorescence: a new technique for detecting hydroxyl radicals, Appl. Opt., 23(13), 2134–2145, doi:10.1364/AO.23.002134, 1984.

Brauers, T., Hausmann, M., Bister, A., Kraus, A. and Dorn, H.-P.: OH radicals in the boundary layer of the Atlantic Ocean 1. Measurements by long-path laser absorption spectroscopy, J. Geophys. Res., 106(D7), 7399–7414, doi:10.1029/2000JD900679, 2001.

Brune, W. H., Stevens, P. S. and Mather, J. H.: Measuring OH and HO 2 in the Troposphere by Laser-Induced Fluorescence at Low Pressure, Journal of the Atmospheric Sciences, 52(19), 3328–3336, doi:10.1175/1520-0469(1995)052<3328:MOAHIT>2.0.CO;2, 1995.

Butler, T. M., Taraborrelli, D., Brühl, C., Fischer, H., Harder, H., Martinez, M., Williams, J., Lawrence, M. G. and Lelieveld, J.: Improved simulation of isoprene oxidation chemistry with

the ECHAM5/MESSy chemistry-climate model: lessons from the GABRIEL airborne field campaign, Atmos. Chem. Phys., 8(16), 4529–4546, doi:10.5194/acp-8-4529-2008, 2008.

Campbell, M. J., Farmer, J. C., Fitzner, C. A., Henry, M. N., Sheppard, J. C., Hardy, R. J., Hopper, J. F. and Muralidhar, V.: Radiocarbon tracer measurements of atmospheric hydroxyl radical concentrations, Journal of Atmospheric Chemistry, 4(4), 413–427, doi:10.1007/BF00053843, 1986.

Cantrell, C. A. and Stedman, D. H.: A possible technique for the measurement of atmospheric peroxy radicals, Geophys. Res. Lett., 9(8), 846–849, doi:10.1029/GL009i008p00846, 1982.

Cantrell, C. A., Stedman, D. H. and Wendel, G. J.: Measurement of atmospheric peroxy radicals by chemical amplification, Anal. Chem., 56(8), 1496–1502, doi:10.1021/ac00272a065, 1984.

Cantrell, C. A., Zimmer, A. and Tyndall, G. S.: Absorption cross sections for water vapor from 183 to 193 nm, Geophys. Res. Lett., 24(17), 2195–2198, doi:10.1029/97GL02100, 1997.

Carlo, P. D., Brune, W. H., Martinez, M., Harder, H., Lesher, R., Ren, X., Thornberry, T., Carroll, M. A., Young, V., Shepson, P. B., Riemer, D., et al.: Missing OH Reactivity in a Forest: Evidence for Unknown Reactive Biogenic VOCs, Science, 304(5671), 722–725, doi:10.1126/science.1094392, 2004.

Copeland, R. A. and Crosley, D. R.: Temperature dependent electronic quenching of OH(A 2Σ+, v′=0) between 230 and 310 K, The Journal of Chemical Physics, 84(6), 3099–3105, doi:doi:10.1063/1.450291, 1986.

Creasey, D. J., Halford-Maw, P. A., Heard, D. E., Pilling, M. J. and Whitaker, B. J.: Implementation and initial deployment of a fieldinstrument for measurement of OH and HO2 in thetroposphere by laser-induced fluorescence, J. Chem. Soc., Faraday Trans., 93(16), 2907–2913, doi:10.1039/A701469D, 1997a.

Creasey, D. J., Heard, D. E. and Lee, J. D.: Absorption cross‐section measurements of water vapour and oxygen at 185 nm. Implications for the calibration of field instruments to measure OH, HO2 and RO2 radicals, Geophys. Res. Lett., 27(11), 1651–1654, doi:10.1029/1999GL011014, 2000.

Creasey, D. J., Heard, D. E. and Lee, J. D.: Eastern Atlantic Spring Experiment 1997 (EASE97) 1. Measurements of OH and HO2 concentrations at Mace Head, Ireland, J. Geophys. Res., 107(D10), 4091, doi:10.1029/2001JD000892, 2002.

Creasey, D. J., Heard, D. E., Pilling, M. J., Whitaker, B. J., Berzins, M. and Fairlie, R.: Visualisation of a supersonic free-jet expansion using laser-induced fluorescence spectroscopy: Application to the measurement of rate constants at ultralow temperatures, Applied Physics B: Lasers and Optics, 65(3), 375–391, doi:10.1007/s003400050285, 1997b.

Crosley, D. R.: The Measurement of OH and HO 2 in the Atmosphere, Journal of the Atmospheric Sciences, 52(19), 3299–3314, doi:10.1175/1520-0469(1995)052<3299:TMOOAH>2.0.CO;2, 1995.

Crowley, J. N., Simon, F. G., Burrows, J. ., Moortgat, G. K., Jenkin, M. E. and Cox, R. A.: The HO2 radical UV absorption spectrum measured by molecular modulation, UV/diode-

array spectroscopy, Journal of Photochemistry and Photobiology A: Chemistry, 60(1), 1–10, doi:10.1016/1010-6030(91)90001-A, 1991.

Crutzen, P.: A discussion of the chemistry of some minor constituents in the stratosphere and troposphere, Pure and Applied Geophysics, 106(1), 1385–1399, doi:10.1007/BF00881092, 1973.

Crutzen, P. J.: Photochemical reactions initiated by and influencing ozone in unpolluted tropospheric air, Tellus, 26(1-2), 47–57, doi:10.1111/j.2153-3490.1974.tb01951.x, 1974.

Davis, D. D., Rodgers, M. O., Fischer, S. D. and Asai, K.: An experimental assessment of the O3/H2O interference problem in the detection of natural levels of OH via laser induced fluorescence, Geophys. Res. Lett., 8(1), 69–72, doi:10.1029/GL008i001p00069, 1981a.

Davis, D. D., Rodgers, M. O., Fischer, S. D. and Heaps, W. S.: A theoretical assessment of the O3/H2O interference problem in the detection of natural levels of OH via laser induced fluorescence, Geophys. Res. Lett., 8(1), 73–76, doi:10.1029/GL008i001p00073, 1981b.

Dimpfl, W. L. and Kinsey, J. L.: Radiative lifetimes of OH(A2Σ) and Einstein coefficients for the A-X system of OH and OD, Journal of Quantitative Spectroscopy and Radiative Transfer, 21(3), 233–241, doi:10.1016/0022-4073(79)90014-1, 1979.

Dolgorouky, C., Gros, V., Sarda-Esteve, R., Sinha, V., Williams, J., Marchand, N., Sauvage, S., Poulain, L., Sciare, J. and Bonsang, B.: Total OH reactivity measurements in Paris during the 2010 MEGAPOLI winter campaign, Atmospheric Chemistry and Physics Discussions, 12(4), 10937–10994, doi:10.5194/acpd-12-10937-2012, 2012.

Dorn, H.-P., Neuroth, R. and Hofzumahaus, A.: Investigation of OH absorption cross sections of rotational transitions in the A2∑+, (υ′=0)←X2Π, (υ″=0) band under atmospheric conditions: Implications for tropospheric long-path absorption measurements, J. Geophys. Res., 100(D4), 7397–7409, doi:10.1029/94JD03323, 1995.

Dusanter, S., Vimal, D. and Stevens, P. S.: Technical note: Measuring tropospheric OH and HO2 by laser-induced fluorescence at low pressure. A comparison of calibration techniques, Atmos. Chem. Phys., 8(2), 321–340, doi:10.5194/acp-8-321-2008, 2008.

Dusanter, S., Vimal, D., Stevens, P. S., Volkamer, R. and Molina, L. T.: Measurements of OH and HO2 concentrations during the MCMA-2006 field campaign – Part 1: Deployment of the Indiana University laser-induced fluorescence instrument, Atmos. Chem. Phys., 9(5), 1665–1685, doi:10.5194/acp-9-1665-2009, 2009.

Edwards, G. D., Cantrell, C. A., Stephens, S., Hill, B., Goyea, O., Shetter, R. E., Mauldin, R. L., Kosciuch, E., Tanner, D. J. and Eisele, F. L.: Chemical Ionization Mass Spectrometer Instrument for the Measurement of Tropospheric HO2 and RO2, Anal. Chem., 75(20), 5317–5327, doi:10.1021/ac034402b, 2003.

Eisele, F. L. and Tanner, D. J.: Ion-Assisted Tropospheric Oh Measurements, J. Geophys. Res., 96(D5), 9295–9308, doi:10.1029/91JD00198, 1991.

Eisele, F. L., Tanner, D. J., Cantrell, C. A. and Calvert, J. G.: Measurements and steady state calculations of OH concentrations at Mauna Loa Observatory, J. Geophys. Res., 101(D9), 14665–14,679, doi:10.1029/95JD03654, 1996.

Faloona, I. C., Tan, D., Lesher, R. L., Hazen, N. L., Frame, C. L., Simpas, J. B., Harder, H., Martinez, M., Di Carlo, P., Ren, X. and Brune, W. H.: A Laser-induced Fluorescence Instrument for Detecting Tropospheric OH and HO₂: Characteristics and Calibration, Journal of Atmospheric Chemistry, 47(2), 139–167, doi:10.1023/B:JOCH.0000021036.53185.0e, 2004.

Foner, S. N. and Hudson, R. L.: Ionization Potential of the Free HO2 Radical and the H ☒ O2 Bond Dissociation Energy, The Journal of Chemical Physics, 23(7), 1364–1365, doi:doi:10.1063/1.1742299, 1955.

Fuchs, H., Bohn, B., Hofzumahaus, A., Holland, F., Lu, K. D., Nehr, S., Rohrer, F. and Wahner, A.: Detection of HO2 by laser-induced fluorescence: calibration and interferences from RO2 radicals, Atmospheric Measurement Techniques, 4(6), 1209–1225, doi:10.5194/amt-4-1209-2011, 2011.

Fuchs, H., Brauers, T., Dorn, H.-P., Harder, H., Häseler, R., Hofzumahaus, A., Holland, F., Kanaya, Y., Kajii, Y., Kubistin, D., Lou, S., et al.: Technical Note: Formal blind intercomparison of HO2 measurements in the atmosphere simulation chamber SAPHIR during the HOxComp campaign, Atmos. Chem. Phys., 10(24), 12233–12250, doi:10.5194/acp-10-12233-2010, 2010.

Fuchs, H., Brauers, T., Häseler, R., Holland, F., Mihelcic, D., Müsgen, P., Rohrer, F., Wegener, R. and Hofzumahaus, A.: Intercomparison of peroxy radical measurements obtained at atmospheric conditions by laser-induced fluorescence and electron spin resonance spectroscopy, Atmospheric Measurement Techniques, 2(1), 55–64, doi:10.5194/amt-2-55-2009, 2009.

German, K. R.: Direct measurement of the radiative lifetimes of the A 2Σ+ (V′ = 0) states of OH and OD, The Journal of Chemical Physics, 62(7), 2584–2587, doi:doi:10.1063/1.430840, 1975.

Haagen-Smit, A. J.: Chemistry and Physiology of Los Angeles Smog, Ind. Eng. Chem., 44(6), 1342–1346, doi:10.1021/ie50510a045, 1952.

Hanke, M., Uecker, J., Reiner, T. and Arnold, F.: Atmospheric peroxy radicals: ROXMAS, a new mass-spectrometric methodology for speciated measurements of HO2 and ∑RO2 and first results, International Journal of Mass Spectrometry, 213(2–3), 91–99, doi:10.1016/S1387-3806(01)00548-6, 2002.

Hard, T. M., Chan, C. Y., Mehrabzadeh, A. A., Pan, W. H. and O'Brien, R. J.: Diurnal cycle of topospheric OH, Nature, 322, 617–620, doi:doi:10.1038/322617a0, 1986.

Hard, T. M., Mehrabzadeh, A. A., Chan, C. Y. and O'Brien, R. J.: FAGE Measurements of Tropospheric HO With Measurements and Model of Interferences, J. Geophys. Res., 97(D9), 9795–9817, doi:10.1029/91JD01664, 1992.

Hard, T. M., O?Brien, R. J., Cook, T. B. and Tsongas, G. A.: Interference suppression in HO fluorescence detection, Appl. Opt., 18(19), 3216–3217, doi:10.1364/AO.18.003216, 1979.

Hard, T. M., O'Brien, R. J., Chan, C. Y. and Mehrabzadeh, A. A.: Tropospheric free radical determination by fluorescence assay with gas expansion, Environ. Sci. Technol., 18(10), 768–777, doi:10.1021/es00128a009, 1984.

Hausmann, M., Brandenburger, U., Brauers, T. and Dorn, H.-P.: Detection of tropospheric OH radicals by long-path differential-optical-absorption spectroscopy: Experimental setup, accuracy, and precision, J. Geophys. Res., 102(D13), 16011–16,022, doi:10.1029/97JD00931, 1997.

Heal, M. R., Heard, D. E., Pilling, M. J. and Whitaker, B. J.: On the Development and Validation of FAGE for Local Measurement of Tropospheric OH and H0 2, Journal of the Atmospheric Sciences, 52(19), 3428–3441, doi:10.1175/1520-0469(1995)052<3428:OTDAVO>2.0.CO;2, 1995.

Heard, D. E. and Pilling, M. J.: Measurement of OH and HO2 in the Troposphere, Chem. Rev., 103(12), 5163–5198, doi:10.1021/cr020522s, 2003.

Hofzumahaus, A., Aschmutat, U., Heßling, M., Holland, F. and Ehhalt, D. H.: The measurement of tropospheric OH radicals by laser‐induced fluorescence spectroscopy during the POPCORN Field Campaign, Geophys. Res. Lett., 23(18), 2541–2544, doi:10.1029/96GL02205, 1996.

Hofzumahaus, A., Rohrer, F., Lu, K., Bohn, B., Brauers, T., Chang, C.-C., Fuchs, H., Holland, F., Kita, K., Kondo, Y., Li, X., et al.: Amplified Trace Gas Removal in the Troposphere, Science, 324(5935), 1702–1704, doi:10.1126/science.1164566, 2009.

Holland, F., Hessling, M. and Hofzumahaus, A.: In Situ Measurement of Tropospheric OH Radicals by Laser-Induced Fluorescence—A Description of the KFA Instrument, Journal of the Atmospheric Sciences, 52(19), 3393–3401, doi:10.1175/1520-0469(1995)052<3393:ISMOTO>2.0.CO;2, 1995.

Holland, F., Hofzumahaus, A., Schäfer, J., Kraus, A. and Pätz, H.-W.: Measurements of OH and HO2 radical concentrations and photolysis frequencies during BERLIOZ, J. Geophys. Res., 108(D4), 8246, doi:10.1029/2001JD001393, 2003.

Hornbrook, R. S., Crawford, J. H., Edwards, G. D., Goyea, O., Mauldin III, R. L., Olson, J. S. and Cantrell, C. A.: Measurements of tropospheric HO2 and RO2 by oxygen dilution modulation and chemical ionization mass spectrometry, Atmospheric Measurement Techniques, 4(4), 735–756, doi:10.5194/amt-4-735-2011, 2011.

Ingham, T., Goddard, A., Whalley, L. K., Furneaux, K. L., Edwards, P. M., Seal, C. P., Self, D. E., Johnson, G. P., Read, K. A., Lee, J. D. and Heard, D. E.: A flow-tube based laser-induced fluorescence instrument to measure OH reactivity in the troposphere, Atmospheric Measurement Techniques, 2(2), 465–477, doi:10.5194/amt-2-465-2009, 2009.

Jeanneret, F., Kirchner, F., Clappier, A., Bergh, H. van den and Calpini, B.: Total VOC reactivity in the planetary boundary layer 1. Estimation by a pump and probe OH experiment, J. Geophys. Res., 106(D3), 3083–3093, doi:10.1029/2000JD900602, 2001.

Jenkin, M. E., Saunders, S. M., Wagner, V. and Pilling, M. J.: Protocol for the development of the Master Chemical Mechanism, MCM v3 (Part B): tropospheric degradation of aromatic volatile organic compounds, Atmos. Chem. Phys., 3(1), 181–193, doi:10.5194/acp-3-181-2003, 2003.

Kanaya, Y., Cao, R., Kato, S., Miyakawa, Y., Kajii, Y., Tanimoto, H., Yokouchi, Y., Mochida, M., Kawamura, K. and Akimoto, H.: Chemistry of OH and HO2 radicals observed at Rishiri

Island, Japan, in September 2003: Missing daytime sink of HO2 and positive nighttime correlations with monoterpenes, J. Geophys. Res., 112(D11), D11308, doi:10.1029/2006JD007987, 2007.

Kanaya, Y., Sadanaga, Y., Hirokawa, J., Kajii, Y. and Akimoto, H.: Development of a Ground-Based LIF Instrument for Measuring HOx Radicals: Instrumentation and Calibrations, Journal of Atmospheric Chemistry, 38(1), 73–110, doi:10.1023/A:1026559321911, 2001.

Kovacs, T. A. and Brune, W. H.: Total OH Loss Rate Measurement, Journal of Atmospheric Chemistry, 39(2), 105–122, doi:10.1023/A:1010614113786, 2001.

Kovacs, T. A., Brune, W. H., Harder, H., Martinez, M., Simpas, J. B., Frost, G. J., Williams, E., Jobson, T., Stroud, C., Young, V., Fried, A., et al.: Direct measurements of urban OH reactivity during Nashville SOS in summer 1999, J. Environ. Monit., 5(1), 68–74, doi:10.1039/B204339D, 2003.

Kroll, J. H., Clarke, J. S., Donahue, N. M. and Anderson, J. G.: Mechanism of HOx Formation in the Gas-Phase Ozone−Alkene Reaction. 1. Direct, Pressure-Dependent Measurements of Prompt OH Yields†, J. Phys. Chem. A, 105(9), 1554–1560, doi:10.1021/jp002121r, 2001.

Kubistin, D., Harder, H., Martinez, M., Rudolf, M., Sander, R., Bozem, H., Eerdekens, G., Fischer, H., Gurk, C., Klüpfel, T., Königstedt, R., et al.: Hydroxyl radicals in the tropical troposphere over the Suriname rainforest: comparison of measurements with the box model MECCA, Atmos. Chem. Phys., 10(19), 9705–9728, doi:10.5194/acp-10-9705-2010, 2010.

Kukui, A., Ancellet, G. and Le Bras, G.: Chemical ionisation mass spectrometer for measurements of OH and Peroxy radical concentrations in moderately polluted atmospheres, Journal of Atmospheric Chemistry, 61(2), 133–154, doi:10.1007/s10874-009-9130-9, 2008.

Lee, J., Young, J., Read, K., Hamilton, J., Hopkins, J., Lewis, A., Bandy, B., Davey, J., Edwards, P., Ingham, T., Self, D., et al.: Measurement and calculation of OH reactivity at a United Kingdom coastal site, Journal of Atmospheric Chemistry, 64(1), 53–76, doi:10.1007/s10874-010-9171-0, 2009.

Lelieveld, J., Butler, T. M., Crowley, J. N., Dillon, T. J., Fischer, H., Ganzeveld, L., Harder, H., Lawrence, M. G., Martinez, M., Taraborrelli, D. and Williams, J.: Atmospheric oxidation capacity sustained by a tropical forest, Nature, 452(7188), 737–740, doi:10.1038/nature06870, 2008.

Levy, H.: Normal Atmosphere: Large Radical and Formaldehyde Concentrations Predicted, Science, 173(3992), 141–143, doi:10.1126/science.173.3992.141, 1971.

Lewis, A. C., Carslaw, N., Marriott, P. J., Kinghorn, R. M., Morrison, P., Lee, A. L., Bartle, K. D. and Pilling, M. J.: A larger pool of ozone-forming carbon compounds in urban atmospheres, Nature, 405(6788), 778–781, doi:10.1038/35015540, 2000.

Lou, S., Holland, F., Rohrer, F., Lu, K., Bohn, B., Brauers, T., Chang, C. C., Fuchs, H., Häseler, R., Kita, K., Kondo, Y., et al.: Atmospheric OH reactivities in the Pearl River Delta – China in summer 2006: measurement and model results, Atmos. Chem. Phys., 10(22), 11243–11260, doi:10.5194/acp-10-11243-2010, 2010.

Lu, K. D., Rohrer, F., Holland, F., Fuchs, H., Bohn, B., Brauers, T., Chang, C. C., Häseler, R., Hu, M., Kita, K., Kondo, Y., et al.: Observation and modelling of OH and HO2 concentrations in the Pearl River Delta 2006: a missing OH source in a VOC rich atmosphere, Atmos. Chem. Phys., 12(3), 1541–1569, doi:10.5194/acp-12-1541-2012, 2012.

Mao, J., Ren, X., Brune, W. H., Olson, J. R., Crawford, J. H., Fried, A., Huey, L. G., Cohen, R. C., Heikes, B., Singh, H. B., Blake, D. R., et al.: Airborne measurement of OH reactivity during INTEX-B, Atmos. Chem. Phys., 9(1), 163–173, doi:10.5194/acp-9-163-2009, 2009.

Mao, J., Ren, X., Zhang, L., Van Duin, D. M., Cohen, R. C., Park, J.-H., Goldstein, A. H., Paulot, F., Beaver, M. R., Crounse, J. D., Wennberg, P. O., et al.: Insights into hydroxyl measurements and atmospheric oxidation in a California forest, Atmos. Chem. Phys., 12(17), 8009–8020, doi:10.5194/acp-12-8009-2012, 2012a.

Mao, J., Ren, X., Zhang, L., Van Duin, D. M., Cohen, R. C., Park, J.-H., Goldstein, A. H., Paulot, F., Beaver, M. R., Crounse, J. D., Wennberg, P. O., et al.: Insights into hydroxyl measurements and atmospheric oxidation in a California forest, Atmos. Chem. Phys., 12(17), 8009–8020, doi:10.5194/acp-12-8009-2012, 2012b.

Martinez, M., Harder, H., Kubistin, D., Rudolf, M., Bozem, H., Eerdekens, G., Fischer, H., Klüpfel, T., Gurk, C., Königstedt, R., Parchatka, U., et al.: Hydroxyl radicals in the tropical troposphere over the Suriname rainforest: airborne measurements, Atmos. Chem. Phys., 10(8), 3759–3773, doi:10.5194/acp-10-3759-2010, 2010.

Mather, J. H., Stevens, P. S. and Brune, W. H.: OH and HO2 measurements using laser-induced fluorescence, J. Geophys. Res., 102(D5), 6427–6436, doi:10.1029/96JD01702, 1997.

Mihelcic, D., Ehhalt, D. H., Klomfass, J., Schmitz, J., Trainer, M. and Helten, M.: Nachweis von RO2- und NO2-Radikalen in der Troposphäre mit Hilfe von Matrixisolationstechnik und EPR-Spektroskopie, Berichte der Bunsengesellschaft für physikalische Chemie, 82(11), 1146–1146, doi:10.1002/bbpc.19780821111, 1978.

Mihelcic, D., Müsgen, P. and Ehhalt, D. H.: An improved method of measuring tropospheric NO2 and RO2 by matrix isolation and electron spin resonance, Journal of Atmospheric Chemistry, 3(3), 341–361, doi:10.1007/BF00122523, 1985.

Mihelcic, D., Volz-Thomas, A., Pätz, H. W., Kley, D. and Mihelcic, M.: Numerical analysis of ESR spectra from atmospheric samples, Journal of Atmospheric Chemistry, 11(3), 271–297, doi:10.1007/BF00118353, 1990.

Miller, D. R.: In Atomic and Molecular Beam methods, by G. Scoles., Oxford University Press, New York., 1988.

Miyazaki, K., Parker, A. E., Fittschen, C., Monks, P. S. and Kajii, Y.: A new technique for the selective measurement of atmospheric peroxy radical concentrations of HO_2 and RO_2 using a denuding method, Atmospheric Measurement Techniques, 3(6), 1547–1554, doi:10.5194/amt-3-1547-2010, 2010.

Monks, P. S.: Gas-phase radical chemistry in the troposphere, Chem. Soc. Rev., 34(5), 376–395, doi:10.1039/B307982C, 2005.

Mount, G. H. and Eisele, F. L.: An Intercomparison of Tropospheric OH Measurements at Fritz Peak Observatory, Colorado, Science, 256(5060), 1187–1190, doi:10.1126/science.256.5060.1187, 1992.

Nakashima, Y., Kamei, N., Kobayashi, S. and Kajii, Y.: Total OH reactivity and VOC analyses for gasoline vehicular exhaust with a chassis dynamometer, Atmospheric Environment, 44(4), 468–475, doi:10.1016/j.atmosenv.2009.11.006, 2010.

Nič, M., Jirát, J., Košata, B., Jenkins, A. and McNaught, A., Eds.: quenching, in IUPAC Compendium of Chemical Terminology, IUPAC, Research Triagle Park, NC. [online] Available from: http://goldbook.iupac.org/Q05007.html (Accessed 3 October 2012), 2006.

Nölscher, A. C., Sinha, V., Bockisch, S., Klüpfel, T. and Williams, J.: A new method for total OH reactivity measurements using a fast Gas Chromatographic Photo-Ionization Detector (GC-PID), Atmospheric Measurement Techniques Discussions, 5(3), 3575–3609, doi:10.5194/amtd-5-3575-2012, 2012a.

Nölscher, A. C., Williams, J., Sinha, V., Custer, T., Song, W., Johnson, A. M., Axinte, R., Bozem, H., Fischer, H., Pouvesle, N., Phillips, G., et al.: Summertime total OH reactivity measurements from boreal forest during HUMPPA-COPEC 2010, Atmos. Chem. Phys., 12(17), 8257–8270, doi:10.5194/acp-12-8257-2012, 2012b.

Paulot, F., Crounse, J. D., Kjaergaard, H. G., Kroll, J. H., Seinfeld, J. H. and Wennberg, P. O.: Isoprene photooxidation: new insights into the production of acids and organic nitrates, Atmos. Chem. Phys., 9(4), 1479–1501, doi:10.5194/acp-9-1479-2009, 2009a.

Paulot, F., Crounse, J. D., Kjaergaard, H. G., Kürten, A., Clair, J. M. S., Seinfeld, J. H. and Wennberg, P. O.: Unexpected Epoxide Formation in the Gas-Phase Photooxidation of Isoprene, Science, 325(5941), 730–733, doi:10.1126/science.1172910, 2009b.

Peeters, J., Nguyen, T. L. and Vereecken, L.: HOx radical regeneration in the oxidation of isoprene, Phys. Chem. Chem. Phys., 11(28), 5935–5939, doi:10.1039/B908511D, 2009.

Perner, D., Ehhalt, D. H., Pätz, H. W., Platt, U., Röth, E. P. and Volz, A.: OH ‐ Radicals in the lower troposphere, Geophys. Res. Lett., 3(8), 466–468, doi:10.1029/GL003i008p00466, 1976.

Ren, X., Harder, H., Martinez, M., Faloona, I. C., Tan, D., Lesher, R. L., Di Carlo, P., Simpas, J. B. and Brune, W. H.: Interference Testing for Atmospheric HO_x Measurements by Laser-induced Fluorescence, Journal of Atmospheric Chemistry, 47(2), 169–190, doi:10.1023/B:JOCH.0000021037.46866.81, 2004a.

Ren, X., Harder, H., Martinez, M., Faloona, I. C., Tan, D., Lesher, R. L., Di Carlo, P., Simpas, J. B. and Brune, W. H.: Interference Testing for Atmospheric HOx Measurements by Laser-induced Fluorescence, Journal of Atmospheric Chemistry, 47(2), 169–190, doi:10.1023/B:JOCH.0000021037.46866.81, 2004b.

Ren, X., Mao, J., Brune, W. H., Cantrell, C. A., Mauldin III, R. L., Hornbrook, R. S., Kosciuch, E., Olson, J. R., Crawford, J. H., Chen, G. and Singh, H. B.: Airborne intercomparison of HOx measurements using laser-induced fluorescence and chemical ionization mass spectrometry during ARCTAS, Atmospheric Measurement Techniques, 5(8), 2025–2037, doi:10.5194/amt-5-2025-2012, 2012.

Ren, X., Olson, J. R., Crawford, J. H., Brune, W. H., Mao, J., Long, R. B., Chen, Z., Chen, G., Avery, M. A., Sachse, G. W., Barrick, J. D., et al.: HOx chemistry during INTEX-A 2004: Observation, model calculation, and comparison with previous studies, J. Geophys. Res., 113(D5), D05310, doi:10.1029/2007JD009166, 2008.

Sadanaga, Y., Matsumoto, J., Sakurai, K., Isozaki, R., Kato, S., Nomaguchi, T., Bandow, H. and Kajii, Y.: Development of a measurement system of peroxy radicals using a chemical amplification/laser-induced fluorescence technique, Review of Scientific Instruments, 75(4), 864–872, doi:doi:10.1063/1.1666985, 2004a.

Sadanaga, Y., Yoshino, A., Watanabe, K., Yoshioka, A., Wakazono, Y., Kanaya, Y. and Kajii, Y.: Development of a measurement system of OH reactivity in the atmosphere by using a laser-induced pump and probe technique, Review of Scientific Instruments, 75(8), 2648–2655, doi:doi:10.1063/1.1775311, 2004b.

Saunders, S. M., Jenkin, M. E., Derwent, R. G. and Pilling, M. J.: Protocol for the development of the Master Chemical Mechanism, MCM v3 (Part A): tropospheric degradation of non-aromatic volatile organic compounds, Atmos. Chem. Phys., 3(1), 161–180, doi:10.5194/acp-3-161-2003, 2003.

Schlosser, E., Brauers, T., Dorn, H.-P., Fuchs, H., Häseler, R., Hofzumahaus, A., Holland, F., Wahner, A., Kanaya, Y., Kajii, Y., Miyamoto, K., et al.: Technical Note: Formal blind intercomparison of OH measurements: results from the international campaign HOxComp, Atmos. Chem. Phys., 9(20), 7923–7948, doi:10.5194/acp-9-7923-2009, 2009.

Schultz, M., Heitlinger, M., Mihelcic, D. and Volz-Thomas, A.: Calibration source for peroxy radicals with built-in actinometry using H2O and O2 photolysis at 185 nm, J. Geophys. Res., 100(D9), 18811–18,816, doi:10.1029/95JD01642, 1995.

Seinfeld, J. H. and Pandis, S. N.: Atmospheric Chemistry and Physics., 1998.

Shirley, T. R., Brune, W. H., Ren, X., Mao, J., Lesher, R., Cardenas, B., Volkamer, R., Molina, L. T., Molina, M. J., Lamb, B., Velasco, E., et al.: Atmospheric oxidation in the Mexico City Metropolitan Area (MCMA) during April 2003, Atmos. Chem. Phys., 6(9), 2753–2765, doi:10.5194/acp-6-2753-2006, 2006.

Sinha, V., Williams, J., Crowley, J. N. and Lelieveld, J.: The Comparative Reactivity Method – a new tool to measure total OH Reactivity in ambient air, Atmos. Chem. Phys., 8(8), 2213–2227, doi:10.5194/acp-8-2213-2008, 2008.

Smith, G. P. and Crosley, D. R.: A Photochemical Model of Ozone Interference Effects in Laser Detection of Tropospheric OH, J. Geophys. Res., 95(D10), 16427–16,442, doi:10.1029/JD095iD10p16427, 1990.

Stevens, P. S., Mather, J. H. and Brune, W. H.: Measurement of tropospheric OH and HO2 by laser-induced fluorescence at low pressure, J. Geophys. Res., 99(D2), 3543–3557, doi:10.1029/93JD03342, 1994.

Stone, D., Whalley, L. K. and Heard, D. E.: Tropospheric OH and HO2 radicals: field measurements and model comparisons, Chem. Soc. Rev., doi:10.1039/C2CS35140D [online] Available from: http://pubs.rsc.org.docproxy.univ-lille1.fr/en/content/articlelanding/2012/cs/c2cs35140d (Accessed 1 September 2012), 2012.

Tanner, D. J. and Eisele, F. L.: Present OH measurement limits and associated uncertainties, J. Geophys. Res., 100(D2), 2883–2892, doi:10.1029/94JD02609, 1995.

Taraborrelli, D., Lawrence, M. G., Butler, T. M., Sander, R. and Lelieveld, J.: Mainz Isoprene Mechanism 2 (MIM2): an isoprene oxidation mechanism for regional and global atmospheric modelling, Atmos. Chem. Phys., 9(8), 2751–2777, doi:10.5194/acp-9-2751-2009, 2009.

Taraborrelli, D., Lawrence, M. G., Crowley, J. N., Dillon, T. J., Gromov, S., Groß, C. B. M., Vereecken, L. and Lelieveld, J.: Hydroxyl radical buffered by isoprene oxidation over tropical forests, Nature Geoscience, 5(4), 300–300, doi:10.1038/ngeo1433, 2012.

Thiébaud, J. and Fittschen, C.: Near infrared cw-CRDS coupled to laser photolysis: Spectroscopy and kinetics of the HO2 radical, Applied Physics B: Lasers and Optics, 85(2), 383–389, doi:10.1007/s00340-006-2304-0, 2006.

Wang, C. C. and Davis, L. I.: Measurement of Hydroxyl Concentrations in Air Using a Tunable uv Laser Beam, Phys. Rev. Lett., 32(7), 349–352, doi:10.1103/PhysRevLett.32.349, 1974.

Wang, C. C., Davis, L. I., Wu, C. H. and Japar, S.: Laser‐induced dissociation of ozone and resonance fluorescence of OH in ambient air, Applied Physics Letters, 28(1), 14–16, doi:doi:10.1063/1.88561, 1976.

Wang, C. C., Jr, L. I. D., Selzer, P. M. and Munoz, R.: Improved Airborne Measurements of OH in the Atmosphere Using the Technique of Laser-Induced Fluorescence, J. Geophys. Res., 86(C2), 1181–1186, doi:10.1029/JC086iC02p01181, 1981.

Wayne, R. P.: Chemistry of Atmospheres, Third Edition., Oxford University Press., 2000.

Wennberg, P. O., Cohen, R. C., Hazen, N. L., Lapson, L. B., Allen, N. T., Hanisco, T. F., Oliver, J. F., Lanham, N. W., Demusz, J. N. and Anderson, J. G.: Aircraft‐borne, laser‐induced fluorescence instrument for the in situ detection of hydroxyl and hydroperoxyl radicals, Review of Scientific Instruments, 65(6), 1858–1876, doi:doi:10.1063/1.1144835, 1994.

Whalley, L. K., Edwards, P. M., Furneaux, K. L., Goddard, A., Ingham, T., Evans, M. J., Stone, D., Hopkins, J. R., Jones, C. E., Karunaharan, A., Lee, J. D., et al.: Quantifying the magnitude of a missing hydroxyl radical source in a tropical rainforest, Atmos. Chem. Phys., 11(14), 7223–7233, doi:10.5194/acp-11-7223-2011, 2011.

Yoshino, K., Esmond, J. R., Cheung, A. S.-C., Freeman, D. E. and Parkinson, W. H.: High resolution absorption cross sections in the transmission window region of the Schumann-Runge bands and Herzberg continuum of O2, Planetary and Space Science, 40(2–3), 185–192, doi:10.1016/0032-0633(92)90056-T, 1992.

Development of a FAGE instrument for the quantification of HOx radicals

Introduction

The hydroxyl (OH) and the hydroperoxy (HO_2) radicals can be detected using the FAGE technique pioneered by Hard et al. (Hard et al., 1979) described in the Chapter 1. At the PC2A laboratory, the development of the UL-FAGE started in 2005 and was deployed on the field for the first time in April 2010. This chapter is a description of the actual UL-FAGE set up: the instrument, the calibration and the specifications of the instrument through interference tests.

During the course of this thesis, some technical changes and major numerical advances were made from the original setup to control, record and analyze automatically the parameters needed for retrieving the HOx concentrations. Also, from each field campaign we improved our knowledge and we nowadays better anticipate the numerous problematic situations that arise on the field.

The calibration is a crucial but delicate step to get the absolute HOx concentration. The calibration source as well as the procedure will be presented. A strong dependence of the sensitivity on water vapour has been observed and is still not understood. The instrument is now running automatically with limit of detections of approximately 4×10^5 cm^{-3} and 5×10^6 cm^{-3} for 1 minute of integration time for OH and HO_2, respectively.

Possible interferences were tested both inside the SAPHIR chamber and during laboratory experiments with ozone and acetone and will be discusses in this chapter.

1. Description of the UL-FAGE

The UL-FAGE instrument shown on Figure 1 is based on the PennState design (Faloona et al., 2004). It is composed of a sampling nozzle, two fluorescence cells, a pumping system, a laser, a wavelength reference cell and an acquisition system.

Ambient air is pumped at 9.2 L/min (BOC Edwards GX6/100L) through a 1 mm orifice after gas expansion into a low pressure cell (P~1.5 Torr, Datametrics Barocell 600A pressure transducer). The first cell is for the measurement of OH. The second cell placed downstream of the first cell is for the measurement of HO_2 after the injection of NO to convert HO_2 into OH. The distance between the nozzle and the middle of the OH cell is of 144 mm and of 346 mm to the middle of the HO_2 cell. OH is excited via a well selected line in the A-X(0, 0) band around 308 nm and its fluorescence is collected perpendicularly to the laser beam and detected after the laser pulse by gated CPM. The cell pressure is decreased from atmospheric pressure to few Torr in order to increase the OH fluorescence lifetime beyond Rayleigh and Mie scattering time region making possible its selective detection.

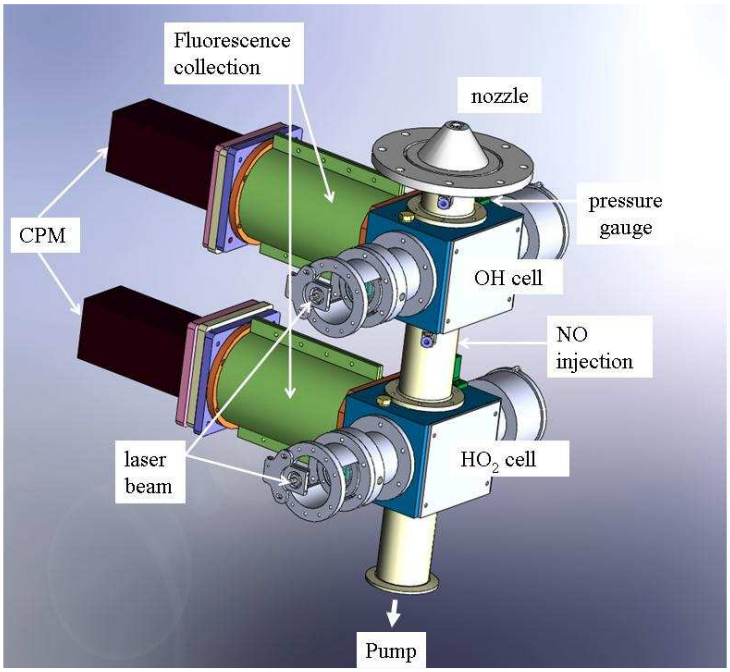

Figure 1. Drawing of the UL-FAGE.

The different parts and aspects of the UL-FAGE are described in details in the following paragraphs.

1.1. OH excitation

OH radicals are excited from the first vibrational state of the ground electronic state ($X^2\Pi$, v''=0) to the first vibrational state of the first electronic state ($A^2\Pi$, v'=0). For the UL-FAGE, the $Q_1(3)$ transition at λ = 308.1541 nm is generally used to excite OH radicals. It has a strong absorption (σ_{OH} ($Q_1(3)$) ~ 10^{-16} cm^2 $molecule^{-1}$ (Dorn et al., 1995)) and has the advantage of being part of a clearly identifiable triplet composed with the $Q_1(3)$-$Q_{21}(3)$-$P_1(1)$ as can be seen on Figure 4.

1.1.1. Laser system

The UV laser beam to excite the OH A-X (0, 0) band at 308 nm is obtained using a frequency doubled dye laser (Sirah Laser PrecisionScan PRSC-24- HPR) pumped by the frequency doubled output of a Nd:YVO_4 laser (Spectra Physics Navigator II YHP40- 532QW). The schematic of the laser is shown on Figure 2. The YAG output power is of 4.9 W with a repetition rate of 5 kHz and a pulse width of 20 ns. The dye used is a mix of 0.17 g/L of Rhodamine 610 (also called Rhodamine B) and of 0.04 g/L of Rhodamine 640 diluted in ethanol (4 Litre). The output laser power obtained is of 50 mW with a fresh dye mixture. The laser wavelength is tuned with a mirror grating with a line width of 0.15 cm^{-1}. The renewing of the dye is dependent on the measurement frequency. On the field (e.g. during HCCT), the laser dye was changed every 3 weeks for approximately 12 hours per day of measurement.

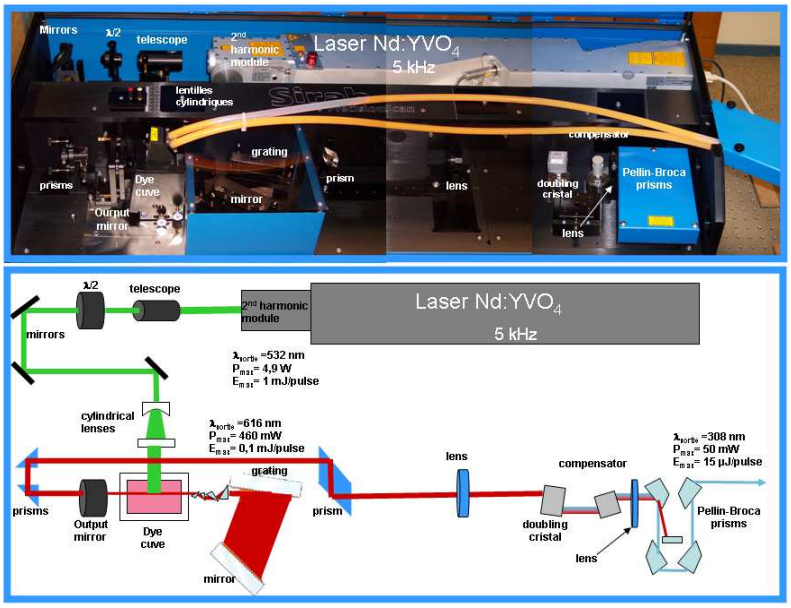

Figure 2. Schematic of the laser system used for the UL-FAGE

1.1.2. Optical train

The laser beam is delivered to the OH, the HO_2 and the reference cells by a set of optics. At the output of the laser, a telescope is used to lower the beam. The output laser beam is an "almond" shape and two cylindrical lenses (Melles-Griot LQC, f=75mm and 50 mm) are set through the beam path in order to round the laser beam reducing the losses through the fibers coupling. A first 80/20 beam splitter (Melles Griot, 16BSQ035/R80/T20) divides the laser beam to the OH fibre holder with a collimator (Melles Griot, 13 FOA 101) used to focus the beam into the fiber. A second 50/50 beam splitter (Melles Griot, 16BSQ035) divides a second time the laser beam to the HO_2 fibre mount (same as OH) and to the reference cell via a prism. After the prism (Melles Griot, AR308, 01PQB001/072), the beam is reflected on a window and the reflexion is aligned onto a photodiode (Hamamatsu, S1722). A second photodiode (Hamamatsu, S1722) is placed behind the reference cell. Photodiodes are regularly calibrated and used to record the laser power.

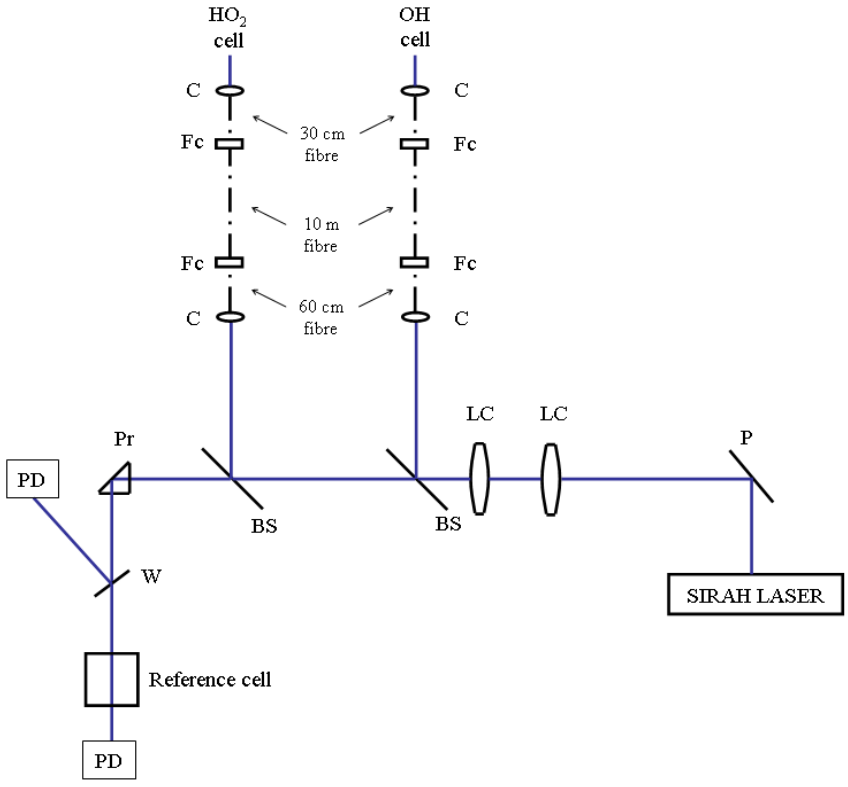

Figure 3. Schematic of the optical train

P: Periscope, LC: Cylindrical lenses, BS: Beam Splitter, W: window, C: Collimators, Fc: Fiber Connectors, PD: Photodiode, Pr: Prism

For the two OH and HO_2 cells, optical fibres (200 µm diameters) assembled with fibre connectors (sma 905) are used to bring the excitation laser beam to the FAGE cells: (i) a 60 cm fibre from the fibre holder to a vertical board on the edge of the laser table with the purpose to check regularly the aligning and the output power, (ii) a 10 m fibre (OZ optics, BFI Optilas, QMMJ-55-UVVIS-200/240-3A-3) from the vertical board to the FAGE box and (iii) a 30 cm fibre from the FAGE box to both OH and HO_2 cells. The first fibre is used to check the alignment of the optical train by measuring the laser power at the exit of the fibre and also the intensity and shape of the laser spot. The two other fibres bring the laser from the container to the FAGE cells. After exiting the last fibre, the laser beam is collimated (collimators: Melles Griot, 13 FOA 101). The optimal overall transmission is of 16% for the OH cell and of 8% for the HO_2 cell. The laser power is approximately twice higher in the OH cell compared to the second cell. The laser power at the entrance of the OH cell is in the range of 1.6 to 3 mW while it is of 0.8 to 1.5 mW at the entrance of the HO_2 cell. A detail schematic of the optical train is shown on Figure 3.

1.1.3. Gas expansion

Within the gas expansion, the temperature decreases to few Kelvin up to the Mach disc before rising up. The relative intensity of the different excitation peak can be used to determine the rotational temperature of the gas flow within the FAGE cells through the Boltzmann population distribution analysis (Creasey et al., 1997b; Kanaya et al., 2001; Stevens et al., 1994). The attempt to measure the temperature within the UL-FAGE was made by fitting the measured spectrum with the theoretical spectrum obtained with the LIFBASE software (Luque and Crosley, 2009) represented by solid lines on Figure 4. From the rotational distribution, we obtained a rotational temperature of approximately 345 K (above ambient temperature) for both OH and HO_2 cells which are distant from the nozzle from 144 mm and 346 mm respectively. The reasons of these observations are not understood. Previously, several authors observed a recovery of the temperature inside the FAGE cells up to ambient temperature when the distance between the nozzle and the laser was increased. This is in contradiction with what we observed since the exact same excitation spectrum is measured between the two cells which are separated of 200 mm. The rotational temperature was also estimated inside the reference cell where H_2O is thermalized at high temperature to form OH radicals. A rotational temperature of 855 K was estimated consistent with the water thermolysis temperature range.

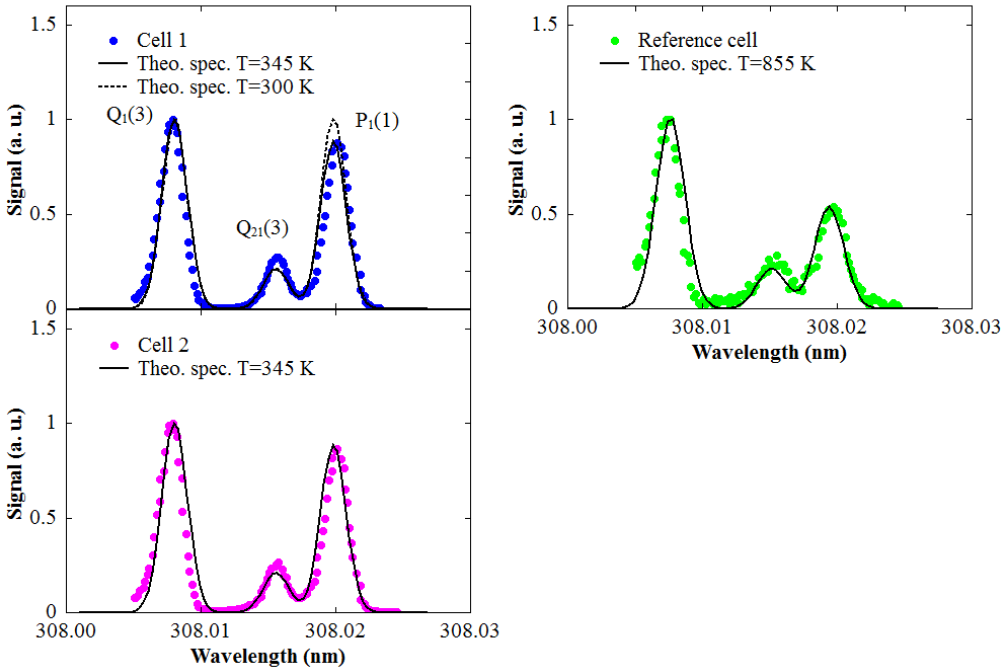

Figure 4. Normalized OH excitation spectrum measured simultaneously in the 1st cell (left - top), the 2nd cell (left - bottom) and the reference cell (left - top). The solid lines represent the theoretical spectrum obtained using the LIFBASE software (Luque and Crosley, 2009) by adjusting the temperature T (P=1.5 Torr, resolution of 0.2 nm). On the top left figure is also represented the theoretical spectrum at T=300 K (dashed line).

1.2. Multi-pass cells

As discussed in the Chapter 1, cells to detect OH fluorescence can be single or multi-pass. For the UL-FAGE, two identical multi-pass cells (10×10×10 cm) with the PennState design are used to detect OH and HO_2. Basically, a multi-pass cell is a set of 3 mirrors with one in the front and two at the back of the cuci cell. The 2 mm diameter laser beam enters the White-cell via the cut-edge of the front concave mirror (Melles Griot) and reflects on one of the two rear concave mirrors (Melles Griot). Usually, the cell is aligned so that the number of passes through the cell is of 38 to 40. Two baffles anodized with black aluminium are located after the first mirrors and before the two rear mirrors and the cells are anodized with black aluminium to reduce scattered light. Between the fibre exit and the cell entrance, a prism is placed to reflect the output beam onto a photodiode (in addition to the 2 photodiodes placed at on the optical train).

The aligning of the White cell can only be done at atmospheric pressure as the adjusting screws for the rear mirrors are placed inside the vacuum-sealed part of the cells. The stability

of the White cell aligning was proven as the FAGE cells were transported over long distances and no changing was observed.

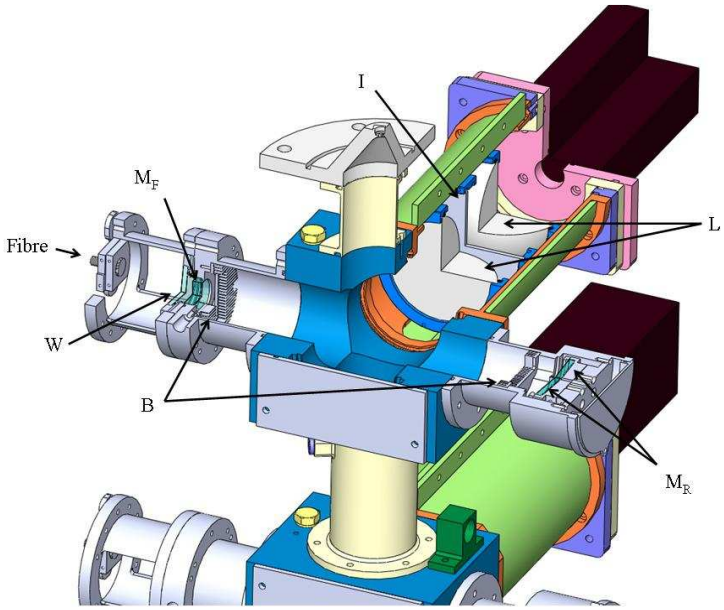

Figure 5. Sectional drawing of the FAGE cell
M_F: Front Mirror, W: Window, B: Baffles, I: Interferometer, M_R: Rear Mirrors, L: Lenses, I: Pass band interferometer.

1.3. OH fluorescence detection

The OH fluorescence is collected at right angle with respect to the laser beam. A system of two plano-convex lenses is used to collimate the fluorescence and then focus it on the detector. An interference band pass filter (Barr Associates) is placed in between the two lenses with a bandwidth of 4.7 nm centred on 308 nm and a peak transmission of 61 %.

The fluorescence is detected by CPM modules (Perkin Elmer, MP-1982) in a counting mode including a CPM tube, a power supply and electronics for discrimination, amplification and pulse shaping. This mode permits to collect each photon as an individual pulse of a few volts and a width of 25 ns. This is particularly useful in our case since the signal level is weak. CPM tubes are composed of a photocathode, a channel tube and an anode (see Figure 6). The photons from the OH fluorescence hit the photocathode (Bialkali material) and are converted into electrons via the photoelectric effect. The electrons are then accelerated from the photocathode to the channel entrance and as they hit the wall of the channel tube secondary electrons are produced which lead to an amplification f the signal (gain ~ 3×10^8).

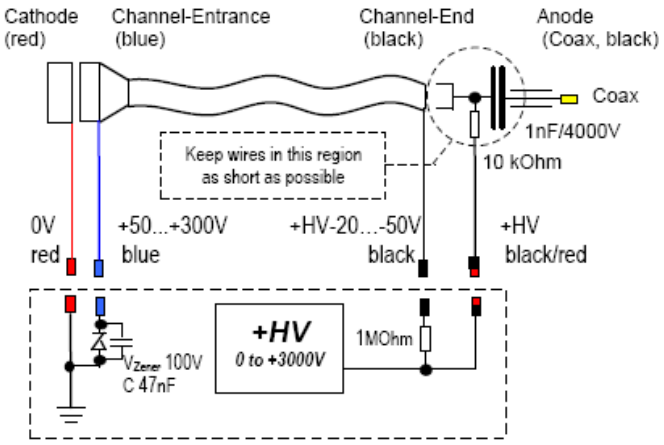

Figure 6. Schematic representation a CPM (Perkin Elmer)

To reduce the background signal and avoid the laser "blinding" the detector, the CPM is switched off during the intense laser pulse. This means that the voltage applied on the photocathode is set to be higher than the voltage applied on the channel entrance so that the electrons are not directed toward the channel entrance. Rapidly after the laser pulse, the CPM is switched on by decreasing the voltage applied to the photocathode below the channel entrance voltage. Two home made switches are used to turn the CPM on. For the OH cell, the switch is in negative mode (HV1= -1.98 kV; HV2= -2.16 kV, channel entrance=-2.09 kV), it is based after the design in Kanaya and Akimoto (Kanaya and Akimoto, 2006). The rise time for the CPM in negative mode is of 41 ns and the fall time (not displayed on the Figure 7) of 2.7 µs. These performances are not as good as the one presented by Kanaya and Akimoto where for a similar system they measured a rise time of 17 ns and a fall time of 2.08 µs, mismatches between the CPM and switch impedance could explain these discrepancies. On the Figure 7 is represented a time chart for the detection of OH in the first cell having a switch in negative mode to open the CPM 300 ns after the laser pulse. The total delay between the start of the measurement and the laser pulse is of 500 ns and the fluorescence is collected for 800 ns. The main drawback of the gated CPM is the detection of a parasitic pulse after the switched is turned on. In consequence the data acquisition is delayed to start after the CPM parasitic pulse. The CPM is gated a second time 12 µs after the laser pulse for 800 ns for the measurement of the background signal. In absence of laser, we observed that the background counts were on average 5% lower than the signal counts.

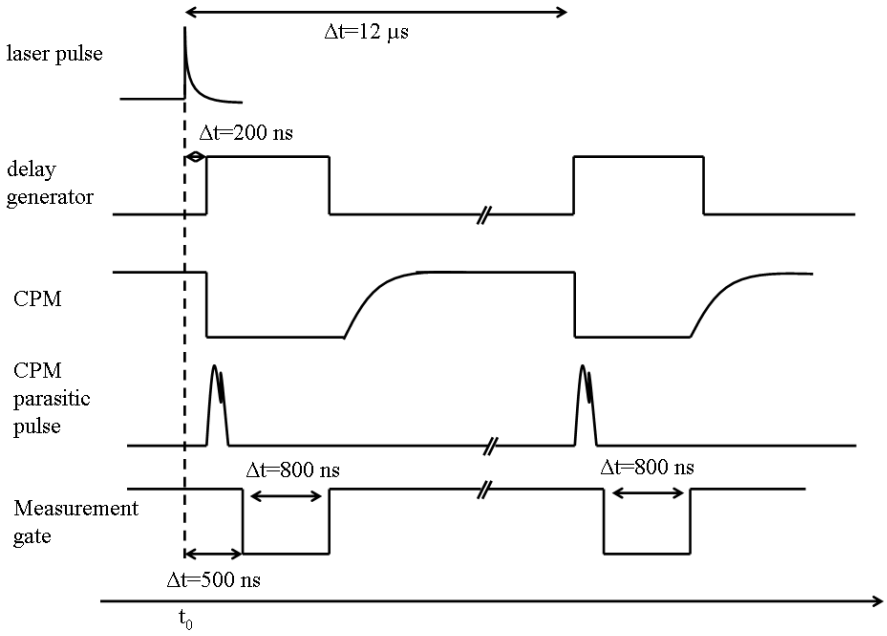

Figure 7. Time chart for the detection of the OH fluorescence with the switch in negative mode.

For the HO_2 cell, the CPM is turned on using a switch in positive mode. The CPM is switched on when the voltage applied on the photocathode decrease from 130 V to 0 V (channel entrance voltage = 50 V).

The measured fluorescence decay is shown on Figure 8. The OH fluorescence signal is the integral of the exponential decay during the measurement gate after the laser pulse. The fluorescence signal is counted from 500 ns after the laser pulse up to 1.3 µs after the laser pulse.

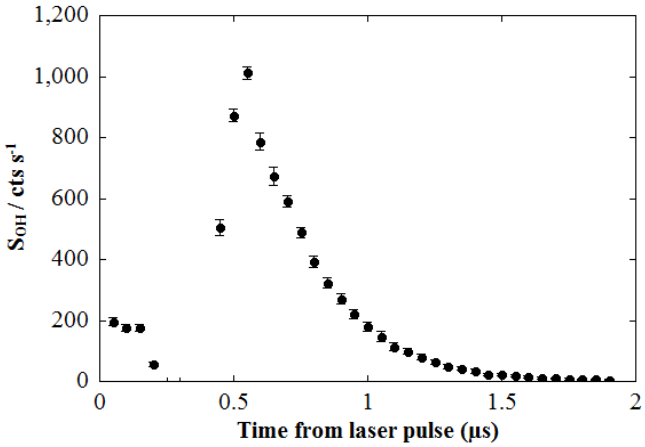

Figure 8. OH fluorescence decay after opening the detector.

1.4. Data acquisition

The pulses from the fluorescence photons collected by the CPM of the OH and the HO_2 cells are counted with National Instruments counting card (National Instruments PCI-6602). The data acquisition time is controlled by a delay generator. The delay generator (DG535, Stanford Research Systems) is triggered internally at 5 kHz and starts: the YAG, the two detector switches (for OH and HO_2 cells) and the acquisition. The photodiode signals are measured on an oscilloscope (LeCroy, WJ334-A) which is connected to a PC via a LAN connection. The data is displayed and recorded using the Labview program (v.11).

1.5. Reference cell

In order to measure the fluorescence signal for quantitative atmospheric measurements, it is necessary to set the laser wavelength on resonance with the OH excitation line. For that a reference cell where OH is produced with a high and stable concentration is used. The reference cell is a stainless steel cube (10×10×10 cm). Ambient air is drawn through a needle valve into the cell kept at approximately 2 Torr using a diaphragm pump (Pfeiffer vacuum, MVP055-3). H_2O is dissociated using a 30W-hot filament (Thermocoax, SEI 10/25) to generate OH radicals by thermolysis. A fraction of the laser beam passes through the cell via windows placed at Brewster's angle and excites the OH radicals. The fluorescence signal is collected with a non-gated CPM (Perkin Elmer MP-1982 P) and acquired on a National Instruments counting card (National Instruments PCI-6221). The reference cell is used to tune the laser dye wavelength on resonance with the OH transition and control the measurement cycles using the Labview program. The Figure 9 shows the FAGE measurement routine. First the laser wavelength is scanned over the OH transition (here $Q_1(3)$) which is the SCAN mode. The wavelength, λ, at which the signal is maximum (S_{max}) is recorded and then the laser wavelength is set on the maximum of the OH transition, this is the GO ONLINE mode. If the averaged signal over 2 points is lower than a threshold value (usually 95% of the S_{max}), the laser wavelength is incremented by 0.01 nm (RELOCK mode). The laser wavelength can be incremented up to 4 times and if the signal is still lower than the threshold value the laser wavelength is automatically scanning. On the other hand, if the signal value is over the threshold, the measurement is turned to the ONLINE mode. After 20 s, the laser wavelength is set at λ+0.05 nm for 20 s where the laser wavelength is no longer on resonance with OH transition (OFFLINE mode). Finally, the laser wavelength is set back to ONLINE and the measurement routine repeats itself. When the laser wavelength is set on resonance, the

average over 5 consecutive points needs to be over a threshold value otherwise the laser would automatically scan.

The stability of the reference cell signal is determinant for the quality of the measurement. The signal is affected by the laser wavelength, the laser power and what we call the "filament stability". Before installing the Thermocoax filament, simple "chromel alumel" filament (R=5Ω/m) were used. Under the heat (T~600°C) the filament was getting distorted and the laser beam was then hitting it causing high and variable background signal. In most cases, the measurement had to be stopped (up to 15 min every 2 hours) in order to adjust the filament and realign the laser beam inside the cell.

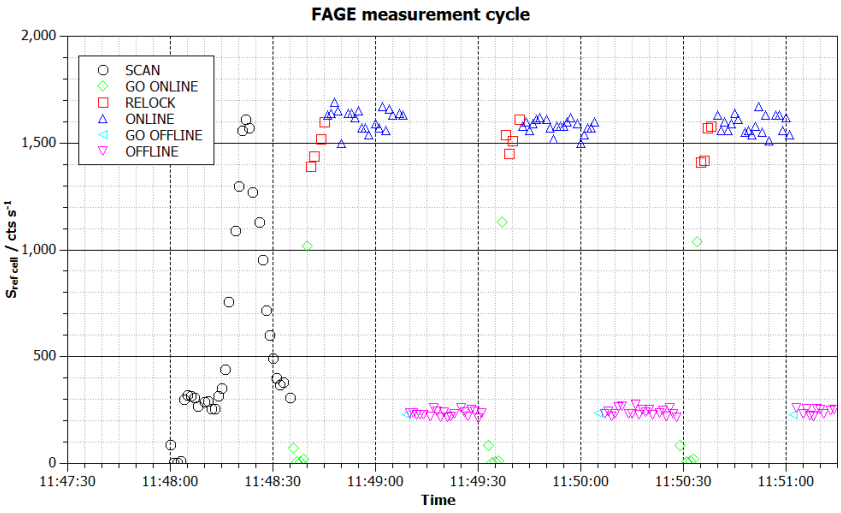

Figure 9. Reference cell signal with the different mode used for the measurement cycle.

1.6. Ambient measurements

In 2011, the University of Lille 1 invested in a measurement container to deploy the FAGE instrument during field campaigns as can be seen on Figure 10. The laser system and part of the electronics are placed inside the container whereas a platform on top of the container is set to install the FAGE box (nozzle at around 3.5 m above the ground). The FAGE box contains: the FAGE cells, the CPM switches, gas lines (for NO and N_2), and air conditioning system in order to keep the temperature constant inside the box. Only the nozzle is exiting the box. All the signal electronic cables to trigger the acquisition and collect the signal are brought from the container to the FAGE box. The 10 m and 30 cm optic fibres are used to bring the laser light to the cells.

Figure 11 is an example of an ambient measurement with the raw signals of the OH cell, the HO_2 cell and the reference cell. As can be seen, the signal of OH is only slightly coming out

of the noise whereas for the HO_2 cell the on resonance signal can clearly be observed. The measurement shown was taken around noon when the sun and we can see a strong background signal measured with the second gate on the 1st cell.

Figure 10. UL-FAGE container during CompOH.
The FAGE box is placed on top of the container.

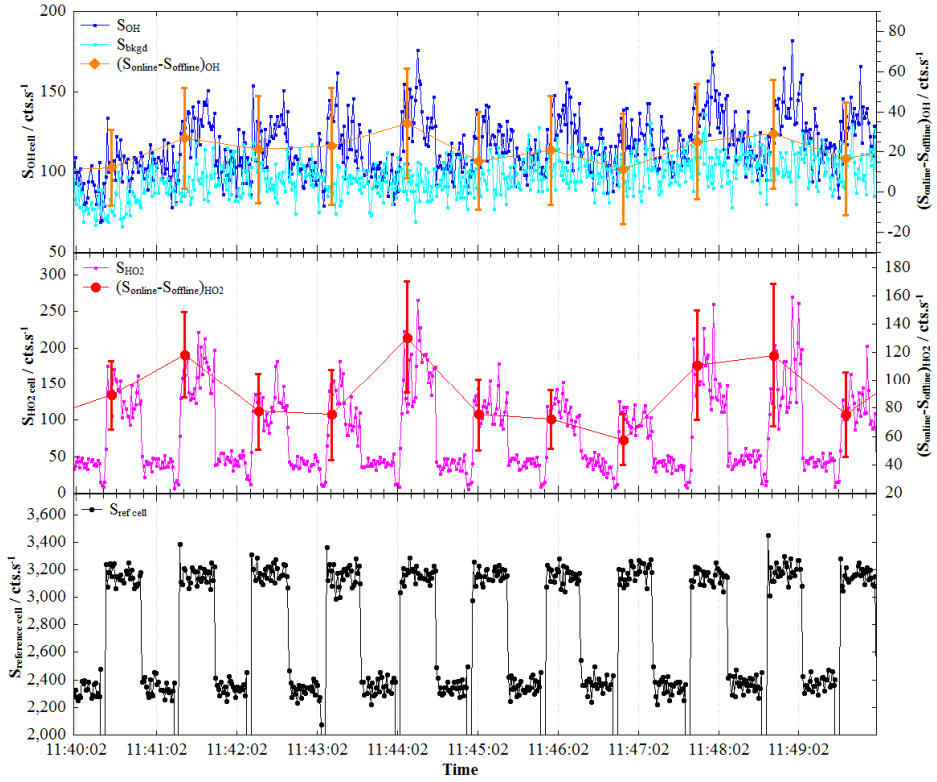

Figure 11. Raw data measured on the 01/07/2011 during CompOH campaign.
Bottom – Signal reference cell, Middle – Raw HO_2 signal and averaged data, Top – Row OH signal and averaged data. The error bars are given at 1σ.

2. Calibration

The LIF detection is a very sensitive technique but it is not absolute. The fluorescence signal needs to be calibrated to a standard. As discussed in the Chapter 1, the sensitivity of the FAGE technique can be obtained theoretically but some of the parameters are not accurately known and the calibration using an external source of HOx radicals is preferred.
The sensitivity is defined as

$$C = \frac{S_{HOx}}{[\mathrm{HOx}] \times P} \text{ in cts s}^{-1}\text{/molecule cm}^{-3}\text{/mW} \qquad \text{Eq. 1}$$

where S_{HOx} is the fluorescence signal in cts s^{-1}, [HOx] is the concentration in molecule cm^{-3} and P is the power in mW.
Several types of calibration methods are used to generate known concentrations of OH and HO_2 and calibrate the OH fluorescence signal for FAGE instruments (Dusanter et al., 2008). The one chosen for the calibration of the UL-FAGE is the UV water photolysis. H_2O photolysis at λ=184.9 nm produced an equal amount of OH radicals and H-atoms [(R 1)]. In air, H atoms are rapidly reacting with O_2 to form HO_2 via [(R 2)]

$$H_2O + h\nu\ (\lambda = 184.9\ \text{nm}) \rightarrow OH + H \qquad \text{(R 1)}$$
$$H + O_2 + M \rightarrow HO_2 + M \qquad \text{(R 2)}$$

It is usually assumed that the yield of OH and HO_2 radicals from the photolysis of water at λ=184.9 nm is equal to 1. However, the H-atoms are produced with high kinetic energy (~1.58 eV), called H*. Reactions of H* with O_2 [(R 3)] or H_2O [(R 4)] to form OH is energetically possible and are in competition with the reaction [(R 5)] that removes the excess of energy.

$$H^* + O_2 \rightarrow OH + O \qquad \text{(R 3)}$$
$$H^* + H_2O \rightarrow H_2 + OH \qquad \text{(R 4)}$$
$$H^* + M \rightarrow H + M \qquad \text{(R 5)}$$

Fuchs et al. (Fuchs et al., 2011) checked this possibility in two steps by measuring the HO_2 concentration. First, they added an excess of CO [(R 6)] to the flow so that all the OH produced from reactions (R 1), (R 3) and (R 4) are converted to HO_2. In a second step, they injected deuterated methane CD_4 to the air flow to scavenge the OH radicals produced and only measuring the HO_2 concentration from the reaction [(R 2)].

$CO + OH + O_2 \rightarrow HO_2 + CO$ (R 6)
$CD_4 + OH + O_2 \rightarrow CD_3O_2 + HDO$ (R 7)

They found that the ratio between the HO_2 concentration measured with the addition of CD_4 and with the addition of CO was equal to 0.50 and concluded that the yields of OH and HO_2 from the H_2O photolysis were indeed equal to 1.

The OH and HO_2 concentrations are proportional to the water vapour concentration $[H_2O]$ in molecules cm^{-3}, the H_2O absorption cross section σ_{H2O} at 184.9 nm in cm^2 $molecule^{-1}$, the lamp flux F in photons cm^{-2} s^{-1}, the quantum yield ϕ equal to 1, and the exposure time t in s.

$$[OH] = [HO_2] = [H_2O] \times \sigma_{H2O} \times F \times \phi \times t \quad \text{Eq. 2}$$

The flux of the lamp can be determined using the O_3 actinometry method. O_2 is photolyzed at 184.9 nm to produce two oxygen atom in their electronic ground state (Okabe, 1978) [(R 8)]. $O(^3P)$ reacts with O_2 to form O_3 [(R 9)].

$O_2 + h\nu\ (\lambda=184.9\ nm) \rightarrow O(^3P) + O(^3P)$ (R 8)
$2(O(^3P) + O_2 + M \rightarrow O_3 + M)$ (R 9)

The O_3 concentration generated is used to calculate the lamp flux knowing the O_2 absorption cross section and having a quantum yield ϕ' equal to 2.

$$[O_3] = [O_2] \times \sigma_{O2} \times F \times \phi' \times t \quad \text{Eq. 3}$$

Thus, combining Eq. 2 and Eq. 3, the OH and HO_2 concentrations are then defined as

$$[OH] = [HO_2] = \frac{1}{2} \times \frac{[O_3] \times [H_2O] \times \sigma_{H2O}}{[O_2] \times \sigma_{O2}} \quad \text{Eq. 4}$$

The water concentration is measured using a dew point hygrometer (Michell Instruments S8000) and the $[O_3]$ concentration using a commercial analyzer (Thermo 49i). The absorption cross section of H_2O is equal to $\sigma_{H2O} = 7.14 \times 10^{-20}$ cm^2 (Cantrell et al., 1997). For O_2, the absorption cross section measured by Dusanter et al. (Dusanter et al., 2009) was chosen ($\sigma_{O2} = 1.20 \times 10^{-20}$ cm^2 $molecule^{-1}$). Ideally, the O_2 absorption cross section should have been measured for each Hg lamps that were used for the calibration of the UL-FAGE since a

significant variations were measured in the lamp emission wavelength for different lamps (Hofzumahaus et al., 1997) however the experiment was not yet performed as the calibration cell need to be redesigned.

In our conditions, the O_3 concentration ranges from 2 to 8 ppb. On field campaigns, the H_2O concentrations varied from few ppm to 3000 ppm by mixing to the main flow with air that passes via a bubbler. The O_3 concentration can be decreased by lowering the Hg lamp flux by reducing the voltage of the lamp power supply.

Using the O_3 actinometry method, the concentration range is limited by the respective limits of detection of the O_3 analyser (LOD = 1 ppb) and the H_2O hygrometer (LOD=-40 °C dew point). The minimum concentrations that can be reached for OH and HO_2 are approximately 5×10^7 cm^{-3}.

2.1. Calibration source

The calibration source is shown on Figure 12. It is a rectangular tube made of aluminium (1.2 × 1.2 × 50 cm) with 5 rectangular holes in which 6-cm height Suprasil (6.0 × 1.5 × 0.2 cm) windows are placed in between rubber seals. Two blocks of aluminium are placed on each side of the tube to maintain the windows.

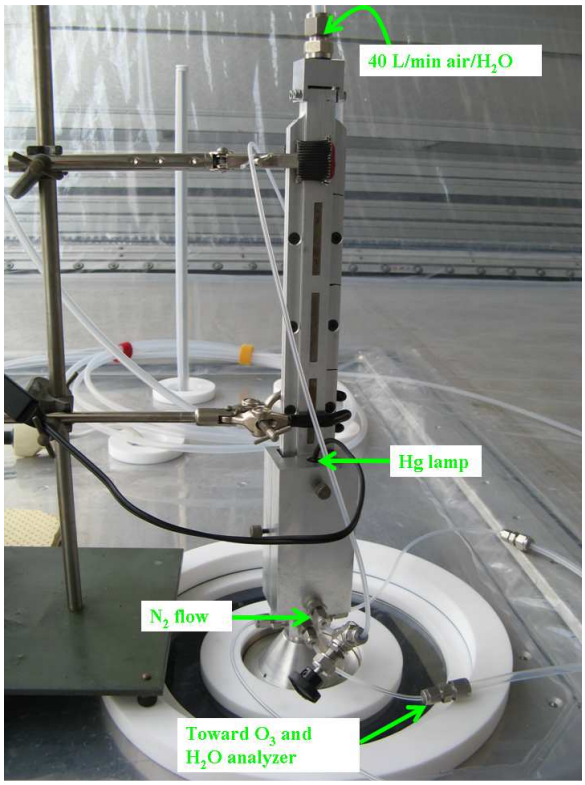

Figure 12. Photo of the calibration cell

The air flow is controlled by two mass flow controllers (30 SLPM air, 10 SLPM air, Bronkhorst) and injected in the calibration cell via 3/8'' Swagelok fitting at a flow of 40 SLPM. At this rate, the air is flowing in turbulent regime with a Reynolds number of 3700. Dusanter et al. (Dusanter et al., 2008) measured the radial air velocity profile using a pitot tube with a calibration cell (1.27 × 1.27 × 30 cm) and flow rate (50 SLPM) similar to the UL-FAGE calibration source. They measured a flow velocity 8% higher in the centre of the tube however since the flow regime is turbulent the OH and HO_2 concentrations generated inside the tube are homogeneous. The same assumption is made in our conditions.

The zero air was generated by a zero air generator (Breitfuss) where ambient air is dried, purified by two Pt catalysts (T°C= 400 °C), and filters filled with purafil and charcoal. Filters filled with Drierite are sometimes used in order to dry the air ([H_2O]<100 ppm) since the H_2O concentration coming out of the air zero generator is not constant and linked to the ambient humidity. The air purity coming out of the zero air generator was not checked and there is a possibility that this would vary depending on the purity of the air in. However, we observed that the NO_2 concentration tends to increase (up to few ppb) after a long period of use (e.g. 2 hours). During the CompOH field campaign, the air zero generator was placed in one corner of the measurement container and hypothetically due to the relatively high temperature the generator supplied air with a highly variable H_2O concentration which render the calibration impossible. Instead, air zero for the calibration was supplied from cylinder (AirLiquid, alpha 1, 5.0).

The Hg lamp is placed in an aluminium block and fixed to the calibration source using 3 screws. Nitrogen is flowed (~50 ccm) through the lamp housing mainly to cool the lamp and also to avoid absorption by O_2 that could reduce the lamp flux. The Hg lamp emits UV radiation at two intense wavelengths λ=254 nm and λ=184.9 nm. An interferometer filter (Melles Griot 185NB20) is placed inside the lamp housing to reduce the strong light emission at λ=254 nm that could photolyze O_3 (σ_{O3} (λ=254 nm) = 1.13×10^{-17} cm² molecule^{-1} (Atkinson et al., 2004)) and generate an additional OH radical concentrations via

$$O_3 + h\nu\ (\lambda=254\ nm) \rightarrow O(^1D) + O_2 \qquad (R\ 10)$$
$$O(^1D) + H_2O \rightarrow 2\ OH \qquad (R\ 11)$$

At the bottom of the calibration cell, four 1/8 Swagelok fittings are used to sample part of the excess flow towards the O_3 and the H_2O analyzers. A type K thermocouple is located at the exit of the calibration source to measure the temperature.

2.2. Calibration procedure

Figure 13 presents an example of a calibration of the OH fluorescence signal in the OH and in the HO_2 cell at a constant H_2O concentration equal to 150 ppm and a power of 2.0 mW for OH and 0.9 mW for HO_2. After the Hg lamp is switched on, the O_3 concentration along with the OH signal in the first and in the second cell is increasing. When the signal is stable, 10 sccm of NO are added downstream of the first cell to convert the HO_2 into OH. The signal is increasing in the second cell as it is the sum of the OH and HO_2 signals. Afterwards, the Hg lamp is turned off in order to measure the O_3 background signal. In order to modulate the OH and HO_2 concentration, the O_3 concentration is varied several times by adjusting the power voltage supply using a Variac.

The signal on resonance minus the signal off resonance is divided by the laser power and plotted as function of the OH concentration calculated from the O_3 and the H_2O concentrations and corrected from the losses inside the calibration source (see 2.4). A linear regression is applied to the calibration data points and the slope obtained is the sensitivity (see Figure 14).

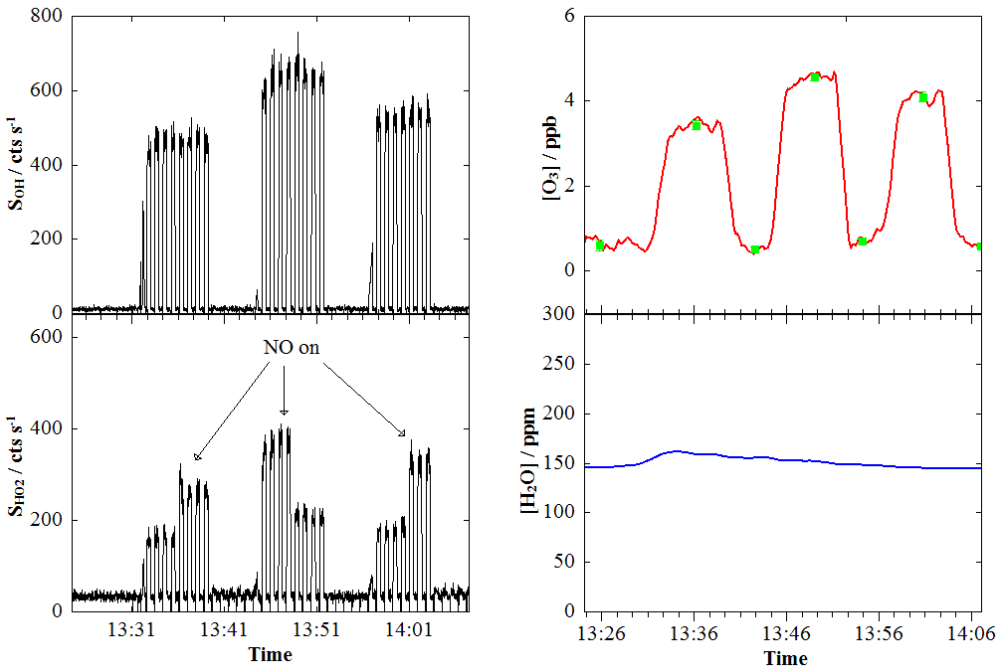

Figure 13. Example of a calibration measurement.
Top – Right: Signal in 1st cell, Bottom – Right: Signal in the 2nd cell; Top – Left: O_3 concentration, Bottom – Left: H_2O concentration

For HO_2, the sensitivity is obtained for a specific NO concentration. The signal with NO minus the signal without NO is plotted against the HO_2 concentration (same calculation than for OH but we assume that there is no HO_2 losses between the generation and the measurement, details in paragraph 2.4) and the slope obtained from the linear regression is the HO_2 sensitivity of the UL-FAGE.

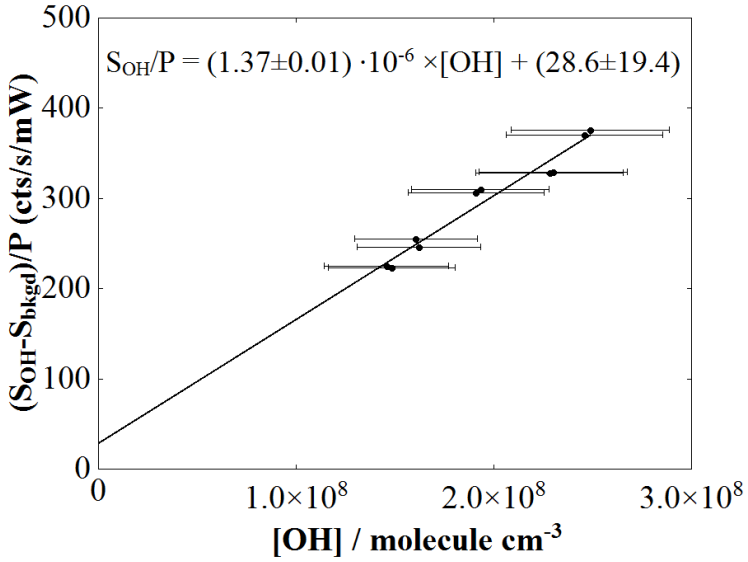

Figure 14. Calibration curve for the OH cell at $[H_2O]$=150 ppm
Signal divided by the laser power as function of the OH concentration.

2.3. Calibration uncertainty

The calibration uncertainty is mainly arising from the uncertainty on the OH and the HO_2 concentrations. While calibrating, the concentrations of OH and HO_2 are high enough that the noise is negligible compared with the OH LIF signal. The uncertainty of the parameters used for the calculation of the OH and HO_2 concentrations is given in Table 1. Using the propagation of errors method, the uncertainty on the sensitivity for the UL-FAGE was estimated to be of 23 % to 41 %. The large uncertainty range is due to the uncertainty on the O_3 measurement. By measuring the absorption cross section of O_2 with our Hg lamp, we could improve our calibration uncertainty.

Table 1. Uncertainty on the parameters used to determine the sensitivity of the UL-FAGE

Parameters	Range	Percentage
$[O_3]$	3 – 10 ppb	10 – 33 %
$[H_2O]$	150 – 3000 ppm	5 %
σ_{H2O} (Cantrell et al., 1997)	7.14×10^{-20} cm^2	3 %
σ_{O2}	1.20×10^{-20} cm^2	20 %*
Total		23 - 41 %

*Hofzumahaus et al. (Hofzumahaus et al., 1997) measured in their calibration conditions a variation of the O_2 absorption cross section depending on different Hg lamps. The O_2 absorption cross section varied from 1.1 to 1.4×10^{-20} cm^2. We did not measure the absorption cross section of O_2 in our conditions and assume it to be of 1.20×10^{-20} cm^2.

2.4. Radical losses

The advantage of using a turbulent flow within the calibration source is the homogeneity of the OH and HO_2 concentrations across the cell however the heterogeneous losses on the wall of the source are important and need to be known so the OH concentration can be corrected. To do so, the OH losses were measured by varying the distance between the exit of the calibration source and the nozzle using the different windows along the tube. The OH concentration was varied over one order of magnitude ([OH] = 10^8-10^9 cm^{-3}) in the typical calibration concentration range. OH and HO_2 radicals can be lost either via self- or cross-reactions or on the wall of the cell. Within our typical radical concentrations and reaction time between 10 (lower window) and 60 ms (higher window), radical-radical reactions are minor (less than 1 % with $[OH]=[HO_2]=1\times10^9$ cm^{-3} and t=10 ms) and the OH losses within the calibration source are mainly on the wall of the cell.

$OH + OH \rightarrow H_2O + O(^3P)$ (R 12)
$OH + HO_2 \rightarrow H_2O + O_2$ (R 13)
$HO_2 + HO_2 \rightarrow H_2O_2 + O_2$ (R 14)
$OH + wall \rightarrow losses$ (R 15)
$HO_2 + wall \rightarrow losses$ (R 16)

The Figure 15 shows the evolution of the signal as function of the distance from the exit of the calibration source. The measurement points were fitted with a linear regression. By extrapolating the signal to the origin, we measured losses for OH radicals independent of the OH concentration within our range and equal to 9.8±3.9 %. The losses for HO_2 radicals were not measured because of the experimental constraints. In order to determine the HO_2 losses, high concentration of CO (~1 %) is added to the air flow to convert all the OH radicals into HO_2 within one millisecond so that only HO_2 radicals are present in the calibration source.

However, since the air is flowing in excess above the nozzle in the room, it is not conceivable to perform this experiment.

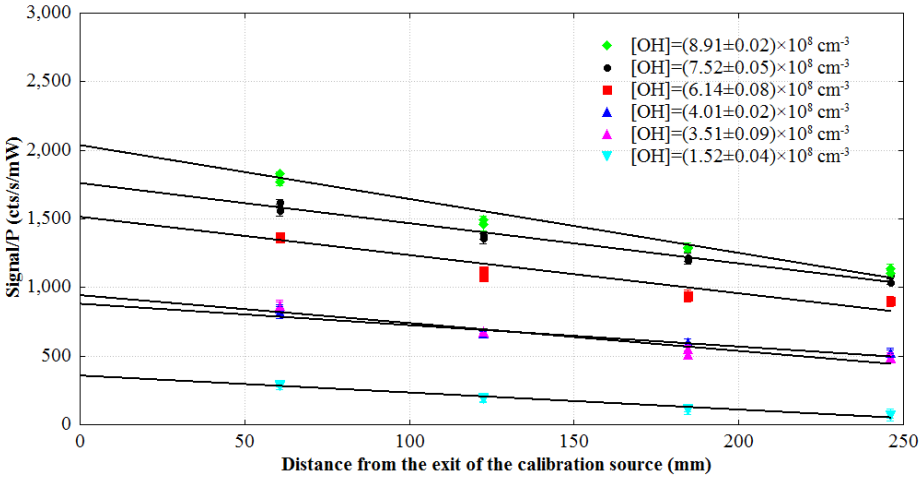

Figure 15. Evolution of the signal as function of the distance from the exit of the calibration source.
Calibrations performed at 40 SLPM for 6 OH concentrations. Errors are given at 1σ.

2.5. H_2O quenching

As already discussed in the Chapter 1, the OH fluorescence lifetime, τ, is reduced due to the quenching of the OH electronic excited ($A^2\Sigma^+$, $v'=0$) state with N_2, O_2 and H_2O via [(R 17)] affecting the sensitivity of FAGE instruments.

$$OH\ (A^2\Sigma^+, v'=0) + M \rightarrow OH\ (X^2\Pi^+, v''=0) + M \qquad \text{(R 17)}$$

The fluorescence lifetime is given by Eq. 5

$$\tau = \left(\tau_{rad}^{-1} + k_q[M]\right)^{-1} \qquad \text{Eq. 5}$$

where τ_{rad} is the natural radiative lifetime in s^{-1}, k_q is the quenching rate coefficient in $cm^3\ s^{-1}$ and [M] is the quencher concentration in molecule cm^{-3}.
A natural radiative lifetime of $\tau_{rad} = 1.45 \times 10^{-6}\ s^{-1}$ ($1/\tau_{rad} = 688$ ns) was measured by German et al. (German, 1975). The temperature dependence of the quenching rate constants for O_2, N_2 and H_2O are given in Table 2.

Table 2. Quenching rate constants of the OH ($A^2\Sigma^+$, v'=0) electronic state by N_2, O_2 and H_2O. The rate constant k_Q are given as $k_Q = A \times T^{1/2} - B \times T^{3/2} + C$ where T is the temperature in K.

Quencher	A ($cm^3.s^{-1}.K^{-1/2}$)	B ($cm^3.s^{-1}.K^{-3/2}$)	C ($cm^3.s^{-1}$)	Reference
N_2	-1.67×10^{-11}	-1.73×10^{-14}	2.31×10^{-10}	(Copeland and Crosley, 1986)
O_2	1.01×10^{-11}	1.66×10^{-14}	5.13×10^{-11}	(Copeland and Crosley, 1986)
H_2O	-4.02×10^{-10}	-4.47×10^{-13}	5.31×10^{-9}	(Bailey et al., 1999)

In the troposphere, the concentrations of N_2 and O_2 remain constant whereas the H_2O concentration is varying up to 3%. The fluorescence quantum yield Γ_{fluo} can be calculated as function of the H_2O concentration (Eq. 5) and compared with the experimental measurements. The theoretical quenching of the OH ($A^2\Sigma^+$, v'=0) electronic state as function of H_2O is shown in Figure 17 as a dashed line.

$$\Gamma_{fluo} = \frac{\tau_{nat}}{\tau_{nat} + \sum k_Q \times [M]} \qquad \text{Eq. 6}$$

The influence of the H_2O concentration on the OH fluorescence lifetime was obtained by varying the H_2O concentration from 100 to 23000 ppm within the calibration source. As H_2O is the source of OH and HO_2, when the water is increased to high level it produces high concentration of OH up to 6×10^{10} molecule cm^{-3}. At these concentrations we measured very high fluorescence signal (up to 30000 cts s^{-1}) and observed that the detector was saturating as the fluorescence signal was no longer exponential as can be seen on Figure 16. To avoid the CPM saturation the CPM gate was moved by 200 ns. All the experiments in dry and wet conditions were conducted with the CPM gate set 200 ns out. In addition, care was taken with the O_3 measurement at high humidity where differences were observed previously (Williams et al., 2006). Before and after each H_2O variation points, the zero (i.e. Hg lamp off) on the O_3 analyzer was taken. We did observed an offset that depends on the relative humidity however this offset did not vary significantly before and after each measurement. The O_3 concentration was taken as the difference between the lamp on minus the average before and after when the lamp was off (see paragraph 2.8).

On Figure 17 is shown the evolution of the sensitivity in the two cells as function of water. The comparison with the theoretical quenching (top figure - dash line) is in strong disagreement with the data points measured. Strong dependency of the sensitivity as function of water was already observed by Hofzumahaus et al. (Hofzumahaus et al., 1996) and Creasey et al. (Creasey et al., 1997a) (see Chapter 1). The explanation given was that H_2O clusters were formed in the cold gas expansion and were scavenging OH and HO_2 radicals.

Afterwards, Holland et al. (Holland et al., 2003) mentioned that by reducing the nozzle size from 0.75 to 0.4 mm and so the gas expansion temperature they could eliminate the additional losses of OH and HO_2 in the gas expansion.

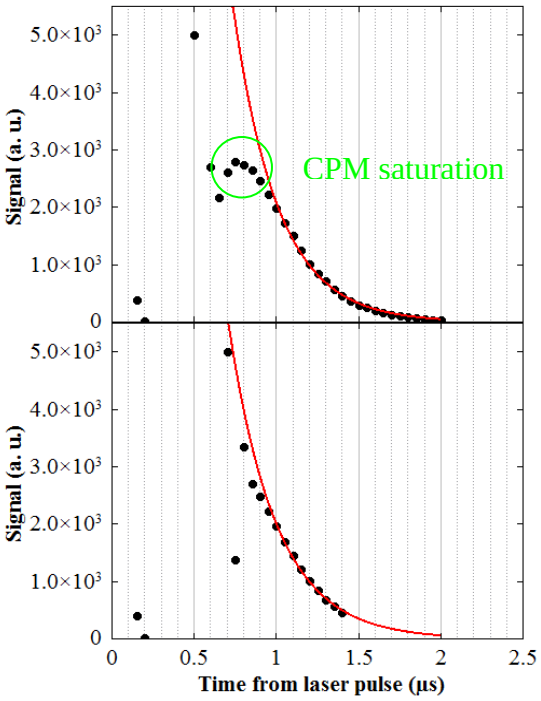

Figure 16. OH fluorescence decay during the H_2O dependence on the sensitivity experiment
Top – Before moving the CPM gate, Bottom – After moving the CPM gate
Solid lines represent a single exponential decay

At first sight, the measurements made with the UL-FAGE are similar to the observations of the two previous studies and a significant correction need to be applied to the OH and HO_2 measurement due to possible condensation of water in the gas expansion. However, the laboratory results regarding the H_2O dependence of the sensitivity are in contradiction with the observations made at the SAPHIR chamber in April 2010 where the UL-FAGE was compared with the FZJ-LIF (see Figure 18). More details about the results of the intercomparative measurement in Juelich are given in Chapter 3. Here, we only focus on the first day of the experiments and on the OH measurement when the water in the chamber was varied stepwise from 0 to 1.8 %. The HO_2 measurements can not be compared because of the RO_2 interference on both FAGE instruments that corrupted the results.

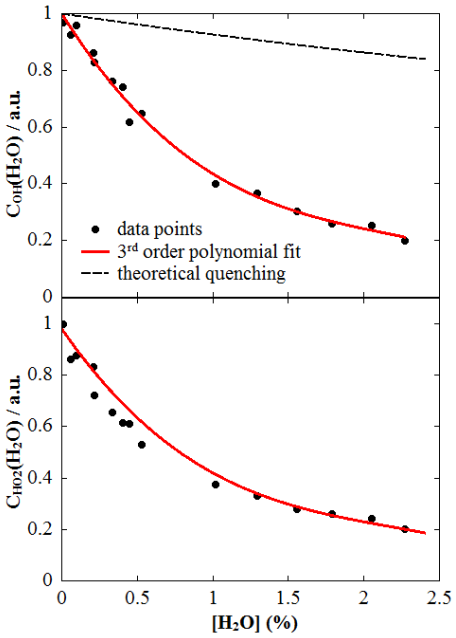

Figure 17. Evolution of the sensitivity of the UL-FAGE as function of water
Bottom - HO_2 cell, Top - OH cell
Solid lines represents a 3rd degree polynomial fit, the dashed line represents the normalized theoretical quenching $C(H_2O) = -0.05\times[H_2O]^3 + 0.34\times[H_2O]^2 - 0.86\times[H_2O] + 1$

Figure 18 displays the OH measurements by the UL-FAGE and the FZJ-LIF. The Lille OH measurements were either corrected using the theoretical quenching (top left plot) or using the H_2O dependence sensitivity obtained from laboratory experiments (bottom left plot).

The correlation plots clearly show that using the correction obtained from laboratory experiments, the two instruments are in disagreement especially when the water vapour concentration in the chamber is high. During the experiments at SAPHIR, the calibrations were performed with very low water concentration ([H_2O] < 1000 ppm) and so the sensitivity was only slightly affected by the unexplained extra loss (loss < 8%). The conclusion that can be drawn from the SAPHIR measurements is that the losses observed during a calibration are not reproduced during ambient measurements. The reasons of the losses of OH and HO_2 radicals during a calibration are not clear but seem to be linked to high concentration levels. The experiment was repeated several times and the same observations were made. Even though the concentration of OH and HO_2 produced within the calibration were high (~10^{10} cm^{-3}) at elevated H_2O concentrations, gas phase losses are unlikely due to the very short reaction time (10 ms) between the generation of the radicals and their sampling through the orifice.

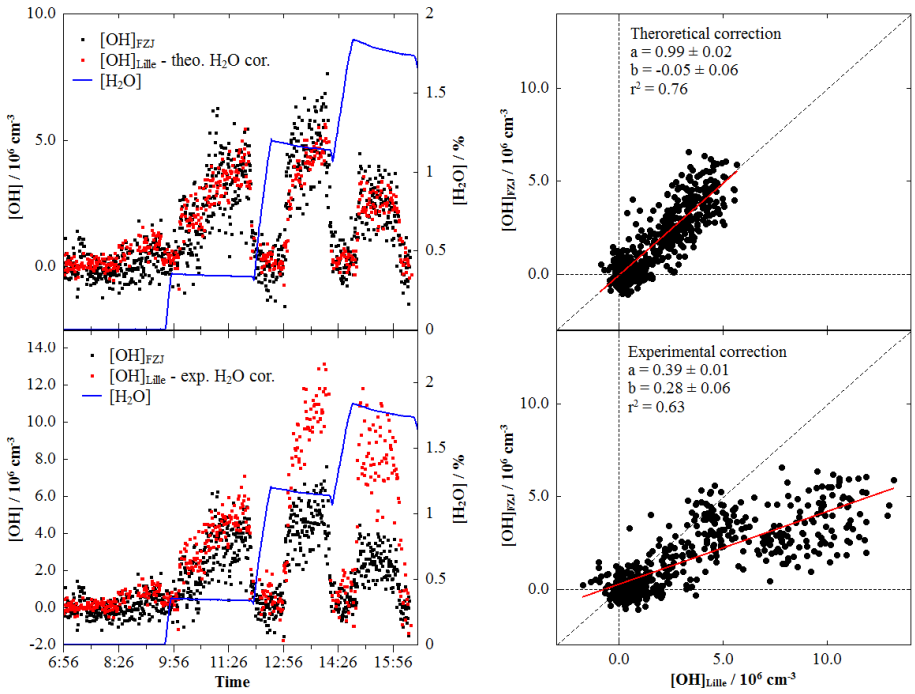

Figure 18. Comparison of the experimental and theoretical H_2O correction on the UL-FAGE measurements.
Experiments performed at the SAPHIR chamber on April 13th 2010. Left – OH measurements by the UL-FA GE (red dots) and the FZJ-LIF (black dots) with the theoretical correction (top) and the experimental correction (bottom). Right – Correlation plots between the UL-FAGE and the FZJ-LIF with the theoretical correction (top) and the experimental correction (bottom)

The nozzle geometry was raised as a possibility for the extra losses. The nozzle has a specific shape (see Figure 19) and when the high flow rate blows over the nozzle eddies can be formed between the lips and the inlet that could cause extra losses of OH and HO_2. The calibration source was placed over the FZJ-LIF nozzle and a very good agreement within their respective errors was observed when a known OH concentration (calculated using the Lille procedure) was compared with a calibrated signal from the FZJ-LIF indicating that our calibration procedure works.

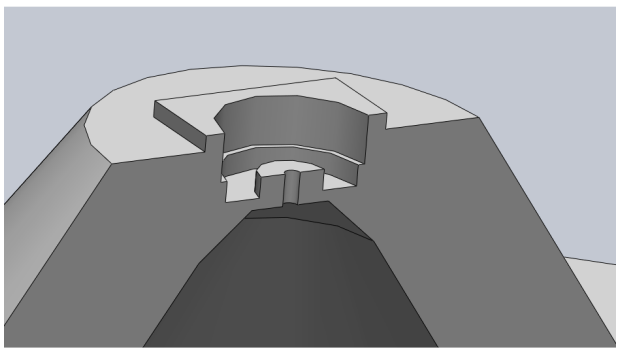

Figure 19. Representation of the UL-FAGE nozzle

Tests were made by changing the nozzle shape of the UL-FAGE (flat 1 mm, conical 400 µm) but over a too small H_2O concentration range and so conclusions can not be made if the nozzle shape has an influence on the extra loss of HOx radicals at high water concentration.
The policy that was adopted is the systematic correction of the sensitivity factor to zero air using the experimental H_2O dependence on the sensitivity. Calibrations at very low water are preferred as sensitivity dependence on water is less strong. Then, the measurement data are corrected using the theoretical fluorescence quenching. This solution is not fully satisfactory however the intercomparative measurement in Juelich and in Paris displayed good agreement using this procedure.

2.6. NO conversion

HO_2 is detected in a second cell downstream from the first cell after addition of a flow of NO to convert it to OH. In order to know the conversion efficiency, ε_{HO2}, (i.e. ratio between the converted HO_2 concentration versus the initial HO_2 concentration) and the conversion reaction time (t) one can adjust the NO concentration and plot the conversion efficiency as function of the NO concentration, $\varepsilon_{HO2} = f([NO])$. When added to the gas stream, NO can either react with HO_2 to produce OH or react with OH to form HONO.

$$HO_2 + NO \rightarrow OH + NO_2 \qquad \text{(R 18)}$$

$k_1 = 8.28 \times 10^{-12}$ cm^3 s^{-1} (Atkinson et al., 2004)

$$OH + NO + M \rightarrow HONO + M \qquad \text{(R 19)}$$

$k_2 = 7.39 \times 10^{-31}$ cm^3 s^{-1} (Atkinson et al., 2004)

The differential equation system is given as

$$\frac{d[HO_2]}{dt} = -k_1 \times [HO_2] \times [NO] \qquad \text{Eq. 7}$$

$$\frac{d[OH]}{dt} = k_1 \times [HO_2] \times [NO] - k_2 \times [OH] \times [NO] \times [M] \qquad \text{Eq. 8}$$

Hard et al. (Hard et al., 1992) solved the system of differential equations in order to obtain the conversion efficiency as function of NO. The equation solution is

$$\varepsilon_{HO2}(t) = \frac{[OH]}{[HO_2]} = \frac{k_1}{(k_2 \times [M] - k_1)} \times (\exp(-k_1 \times [NO] \times t) - \exp(-k_2 \times [NO] \times [M] \times t) \qquad \text{Eq. 9}$$

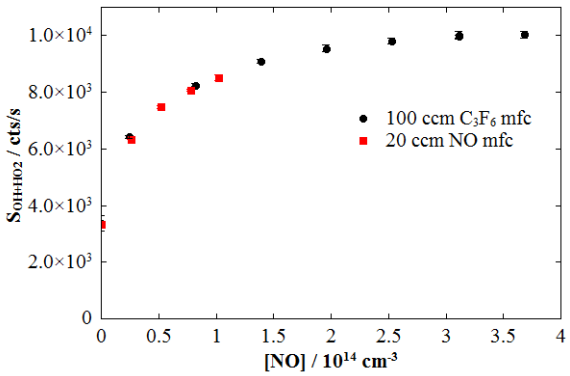

Figure 20. Evolution of the signal as function of the NO concentration.
P=1.5 Torr and $[HO_2] = 6.1 \times 10^9$ cm^{-3} during CompOH.

The experiment was made by varying the NO concentration from 4×10^{13} up to 3.5×10^{14} cm^{-3} with a constant HO_2 concentration. As the NO concentration is increased the signal measured in the second cell reached a plateau corresponding to a conversion efficiency close to 1. As can be seen on Figure 20, the signal measured in the second cell close to the full conversion is 3 times larger than without NO. In an ideal case, meaning that all the HO_2 were converted to OH, the ratio S_{HO2+OH}/S_{OH} could not exceed 2. This difference is explained by the larger lost of OH (mainly heterogeneous loss) compare to HO_2 from the calibration source to the detection zone. From the calibration of the two cells for OH radical, we know that the sensitivity for OH between the cell 1 and the cell 2 (downstream of cell 1) is twice as big.

For calculating the conversion efficiency, we made the assumption based on the calibration of the two cells for OH that 50% of OH radicals are lost between the two cells and that no losses occurred from the generation in the calibration to the detection zone in the second cell for HO_2. By multiplying the S_{OH} ([NO]=0) by 1.5 and subtracting the signal from the total signal measured in the second cell, we are able to plot the conversion efficiency as function of the NO concentration and derive the conversion time which is in these conditions t=(1.40±0.02) ms. Assuming that the losses between the two cells would be underestimated by 2% (i.e. multiply by 1.53), the conversion time would be of 1.3 ms.

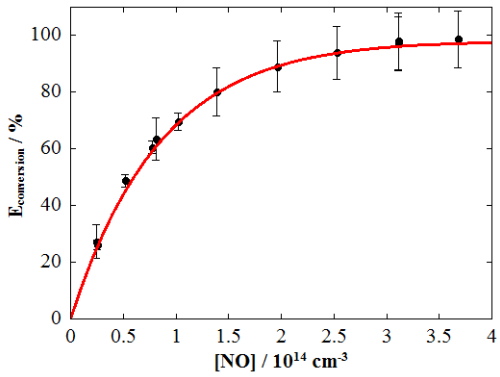

Figure 21. Conversion efficiency of HO_2 to OH as function of the NO concentration
At P=1.5 Torr and $[HO_2]= 6.1 \times 10^9$ cm^{-3}. The solid line represents the fit obtained using the equation derived by Hard et al. (Hard et al., 1992). The conversion time derived was t=1.4 ms.

Pure NO cylinders (AirLiquide) are used to convert HO_2 to OH. An interference signal is observed when NO is injected into the FAGE cells coming from the photolysis of impurities (e.g HONO) coming from the cylinder. In order to trap these impurities, Ascarite (sodium hydroxide coated silica) can be used, however, we observed that the trapping efficiency was evolving with time and so we decided to not use any trapping system. In consequence, we characterize the NO interference as function of the NO flow and the laser power (see Figure 22) and subtract it from the HO_2 signal. The artefact signal is measured regularly for each calibration. Zero air is introduced through the calibration source and the laser power is varied at the NO flow use during the measurement.

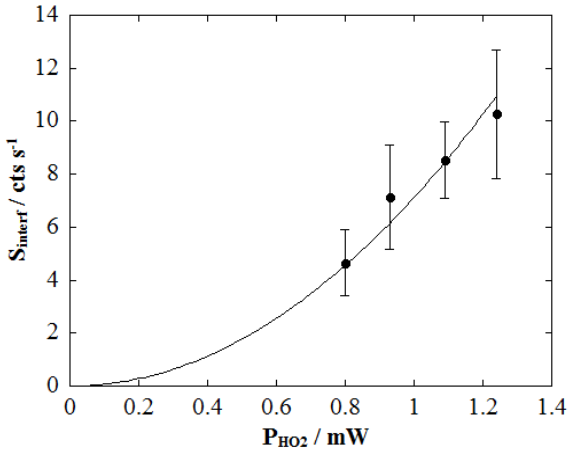

Figure 22. Power dependence of the NO impurities interference for $[NO] = 1.4 \times 10^{13}$ cm^{-3}
The solid line is a least squares power fitting with an order of 2.
Error bars are 1σ.

2.7. Limits of detection

The limit of detection is defined as

$$[OH]_{min} = \frac{S/N}{C \times P} \times \sqrt{\frac{1}{m} + \frac{1}{n}} \times \sqrt{\frac{S_{bkgd}}{t}} \qquad \text{Eq. 10}$$

where S/N is the signal to noise ratio, C the sensitivity in cts/s/molecule.cm^{-3}/mW, P the power in mW, m and n the number of measurement on and off resonance and S_{bkgd} is the background signal in cts/s, t is the measurement time in s.

The limit of detection was calculated for the different field campaigns in which the FAGE instruments was deployed and grouped in
Table 3 and in Table 4 for OH and for HO_2 respectively. As can be seen, the LOD for OH was relatively steady over the last two years as no major changes were made on the detection system. For HO_2, the limit of detection is depending on the conversion efficiency. The NO concentration was reduced in order to limit the detection of RO_2 with the UL-FAGE as explained in the next section 0.

Table 3. Evolution of the OH sensitivities and LOD for the different field campaigns
S/N=2, m=n=1, t = 40 s

	C (cts/s/molecule cm^{-3}/mW)	P (mW)	S_{bkgd} (cts/s)	[OH]min (molecule cm^{-3})
SAPHIR 2010	1.94×10^{-6}	2.04	14	4.2×10^{5}
HCCT 2010	1.13×10^{-6}	2.12	9	5.6×10^{5}
CompOH 2011	1.82×10^{-6}	1.70	9	4.3×10^{5}
Surfin 2011	1.58×10^{-6}	1.90	9	4.5×10^{5}

Table 4. Evolution of the HO_2 sensitivities and LOD for the different field campaigns
S/N=2, m=n=1, t = 40 s

	C (cts/s/molecule cm^{-3}/mW)	P (mW)	S_{bkgd} (cts/s)	ε_{HO2}	[HO_2]min (molecule cm^{-3})
SAPHIR 2010	1.64×10^{-6}	0.77	10	45 %	1.1×10^{6}
HCCT 2010	2.04×10^{-6}	0.75	37	96 %	1.8×10^{6}
CompOH 2011	4.56×10^{-7}	0.90	21	15 %	5.0×10^{6}
Surfin 2011	6.11×10^{-7}	0.92	22	15 %	3.7×10^{6}

2.8. Future improvements for the calibration

One of the drawbacks of the calibration procedure is the long response of the O_3 analyzer. For the O_3 analyzer, we observed that a rapid change in the H_2O concentration was causing a brutal decrease of the O_3 concentration read by the apparatus which lead to slow recovery to the zero (often a negative offset)

One way to reduce the calibration time would be to measure the lamp flux with a phototube placed opposite to the lamp. The phototube would need to be calibrated prior to the calibration with an O_3 analyzer or a calibrated photomultiplier. Also, the lamp flux could be reduced (nowadays limited by O_3 analyzer LOD) and so the concentration used for the calibration would be closer to the ambient concentration range for OH and HO_2.

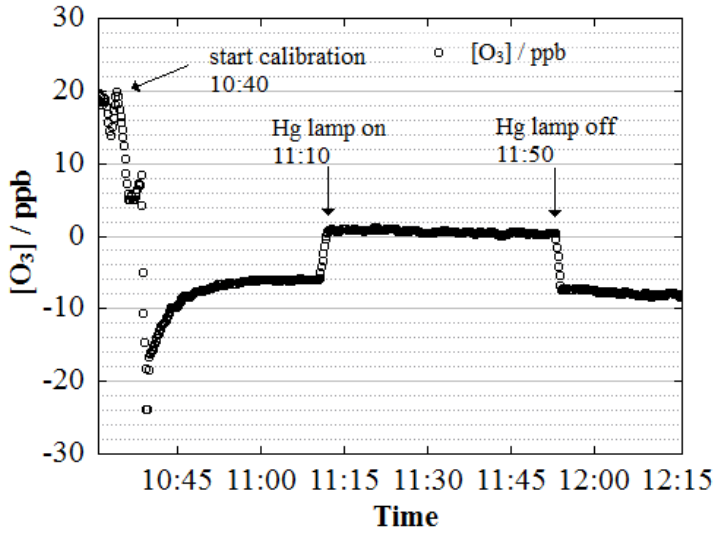

Figure 23. O_3 analyzer response to sudden change in relative humidity

3. Possible interferences

Ren et al (Ren et al., 2004) tested a large number of atmospherically relevant chemical species as potential interference source for OH measurement using the FAGE technique. The conclusion we as none of the chemical species tested would affect the OH measurement. The recent work from Mao et al. (Mao et al., 2012) which highlighted the presence of an unknown interference source of OH inside the FAGE cells in a forestry environment. Fuchs et al. (Fuchs et al., 2011) showed without any doubt that significant amount of RO_2 radical species were detected when using high NO concentration used to convert HO_2 to OH. Solutions were

proposed to reduce and characterize each FAGE instruments toward these interferences however it changed the perception on the selectivity of the FAGE technique. The magnitude of these interferences is dependent upon each setup. Parameters such as cell material, sample flow, pressure, gas expansion profile differ and could impact the interference of instrument.
The main contributor to OH interference signal is via the O_3 photolysis inside the FAGE cells that lead to the formation of OH and a lot of effort was made through the years to reduce it. For the UL-FAGE, the formation of an artificial OH signal was tested for O_3 and acetone. Tests on the RO_2 interference have not been done yet and only an impact on the field measurement is presented.

3.1. O_3 interference

The formation of OH via the photolysis is generally understood as a 2-photon process in which 1-photon photolyzes O_3 to produce an excited oxygen atom that reacts with water vapour to form OH. A second photon is then needed to detect the artificial OH formed. In consequence, the OH interference signal has a quadratic dependence with the laser power. This interference is reduced if the volume sampled by the excitation laser is renewed between each pulse. Ren et al. (Ren et al., 2004) observed a quadratic dependence of the interference signal with the laser power confirming the 2-photon process. However, Holland et al. (Holland et al., 1995) observed a strong O_3 interference which had surprisingly a linear dependence of the artificial OH signal as function of the laser power for a given concentration of O_3. It was attributed to an unknown dark reaction inside the FAGE cells in the gas phase or on the wall. They tested different sort of material (black paint, Teflon, black anodized aluminium) and observed that the interference was minimal using black anodized aluminium and by increasing the nozzle diameter. Lu et al. (Lu et al., 2012) recently reported an O_3 interference for the OH measurements of $(6\pm2) \times 10^3$ cm^{-3} only dependent on the O_3 concentration.
We have tested the O_3 interference by varying the O_3 concentration up to 1 ppm and the laser power from 0.6 to 3 mW. The experiment was done by diluting a small flow of O_3 produced from the photolysis of O_2 with a Hg lamp with zero air in the photolysis cell used for kinetic measurements. H_2O was injected ($[H_2O]$=0.3 %) by flowing an air zero flow through a water bubbler. The O_3 and H_2O concentrations were measured downstream of the flow tube using standard analyzers. First, the O_3 concentration was varied at constant laser power and repetition rate. The results are shown on Figure 24. We observed a linear increase with a slope

equal to (1.7±0.3) × 10^3 cm^{-3} [OH] per ppb of O_3. This interference would be insignificant for most of ambient measurements however OH concentration can be corrected in highly polluted environments such as cities where O_3 concentration can be as high as 200 ppb (Lei et al., 2007).

To understand through which process the OH is produced inside the FAGE cells, the 308 nm laser power was varied in the range used for ambient measurement from 0.6 to 3 mW for O_3 concentrations of 340 and 1160 ppb. The results are shown on Figure 25 and surprisingly, we observed a linear dependence of the interference signal as function of the laser power which indicates that the OH produced from O_3 is not via a 2 photon photolytic process.

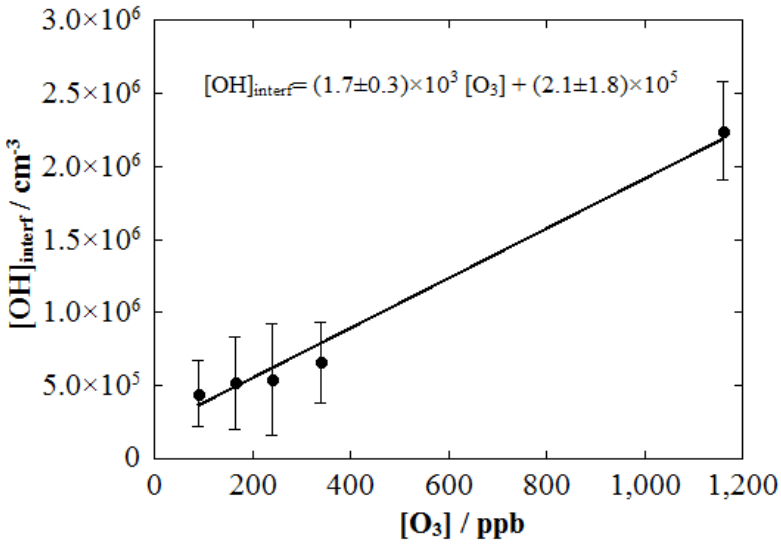

Figure 24. OH interference concentration as function of the O_3 concentration
P_{OH} = 2 mW, rep. rate = 5 kHz, [H_2O]=0.3%

This result is in disagreement with the work of Ren et al. (Ren et al., 2004) but in agreement with the study of Holland et al. (Holland et al., 1995). The reasons to explain this linear dependence of the OH formation as function of the concentration of O_3 are not clear. The possibility that OH is produced via an unknown dark reaction (i.e. non-photolytic) on the wall of the cell or in the gas phase was proposed by Holland et al. (Holland et al., 1995) can not be drawn and future test would be needed. However, as shown on Figure 24, the OH production from O_3 is insignificant under ambient conditions.

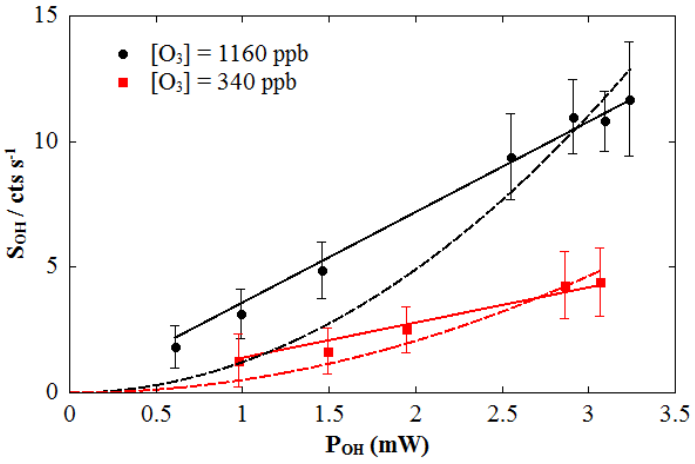

Figure 25. Power dependence of the O_3 interference. The solid lines represent a linear regression. The dashed lines represent a squared dependence of the signal as function of the laser power. rep. rate = 5 kHz, $[H_2O]$=0.3 %

One additional test was made in which the repetition rate of the laser was varied. We observed that the OH interference signal was independent on the repetition rate confirming the hypothesis that OH is produced from a dark reaction and not from a photolytic process. For this test, care was taken to keep the same energy per pulse when the repetition rate was varied.

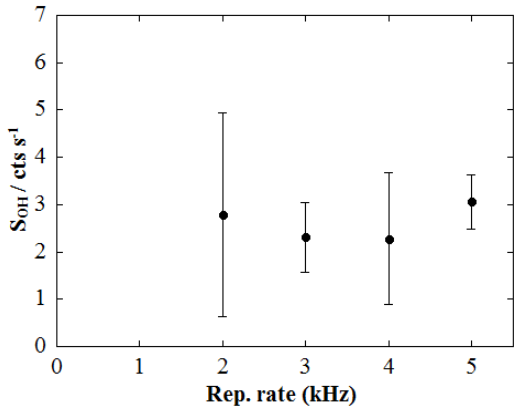

Figure 26. OH signal as function of the repetition rate.
$[O_3]$=340 ppb

3.2. Acetone interference

The photolysis of carbonyl species within the FAGE cells at 308 nm was tested with acetone. A known mixture of acetone (Sigma Aldrich) in N_2 was diluted in zero air and introduced into the photolysis cell and the OH fluorescence signal was observed. As for the test with O_3, the test was made with different concentrations of acetone and laser powers. At 308 nm

($\sigma_{acetone}(\lambda=308\ nm) = 1.61 \times 10^{-20}$ cm², (Gierczak et al., 1998)) the photolysis of acetone leads to the formation an acetyl radical (CH_3CO) and at low pressure and in the presence of O_2, high yield of OH were measured from the reaction of CH_3CO with O_2 (Blitz et al., 2002; Tyndall et al., 1997).

$$CH_3C(O)CH_3 + h\nu\ (\lambda = 308\ nm) \rightarrow CH_3CO + CH_3 \quad \text{(R 20)}$$
$$\rightarrow 2CH_3 + CO \quad \text{(R 21)}$$
$$CH_3CO + O_2 \rightarrow OH + products \quad \text{(R 22)}$$

First, the acetone concentration was varied from 1.5 to 13 ppm. The OH concentration measured as function of the acetone concentration is shown to be linear (see Figure 27). From the linear regression, we obtained that the interference signal is of 9.81×10^6 cm^{-3} per ppmv of acetone. For 10 ppbv of acetone, the OH interference would be of $\sim 1 \times 10^5$ cm^{-3}. It is slightly higher than the interference signal reported by Ren et al.(Ren et al., 2004) where an OH interference concentration of $\sim 7.5 \times 10^4$ cm^{-3} was reported for 10 ppbv of acetone. The impact of this interference is small as the ambient acetone concentration is generally lower than 10 ppbv (Finalyson-Pitts and Pitts, 2000).

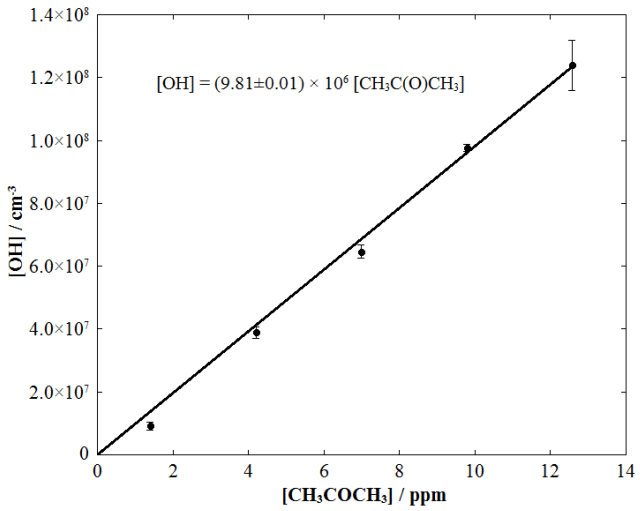

Figure 27. OH interference concentration as function of the acetone concentration
Power=2 mW, P=1.5 Torr

Contrary to O_3, the OH signal was observed to show a quadratic dependence with the laser power indicating that the OH was produced from a 2-photon process in agreement with the expectation.

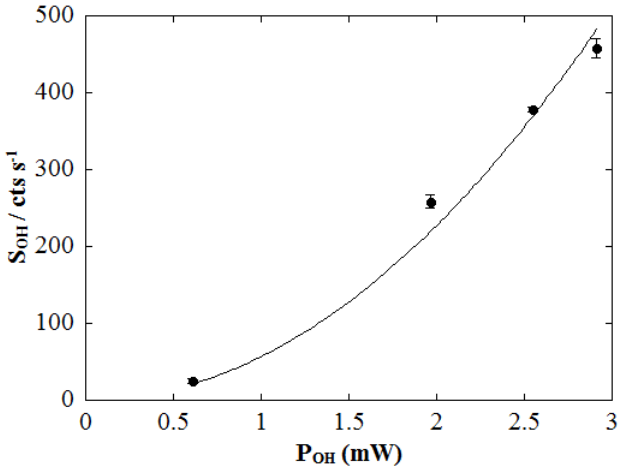

Figure 28. OH interference signal from acetone as function of the laser power
Solid line represents a least square fit with a power of 2.
[CH_3COCH_3] = 13 ppm, P=2 mW, rep. rate=5 kHz

3.3. RO_2 interference

The sensitivity of the UL-FAGE instruments toward certain RO_2 species as described by Fuchs et al. (Fuchs et al., 2011) that could affect the measurement of HO_2 with FAGE has not been tested yet. As explained by Fuchs et al. (Fuchs et al., 2011), this interference will depend on the NO concentration as well as the reaction time. The NO concentration used by the UL-FAGE was different for every field campaigns. The relative sensitivity for several RO_2 was calculated using the MCM v3.2 mechanism in our measurement conditions. As can be seen in Table 5, the HO_2 measurements were strongly affected by the RO_2 interference during the HCCT 2010 campaign while during the CompOH and the SURFIN campaigns the NO concentration was reduced limiting the sensitivity to RO_2 species. During the intercomparison in Juelich, the calculated RO_2 sensitivities were significant for 3 of the species that were injected inside the chamber i.e. isoprene, toluene and p-xylene. However, the calculated sensitivity to phenol is within our measurement uncertainty.

Table 5. Calculation of the relative sensitivity of different RO_2 species with different NO concentrations using the MCM v3.2 mechanism
The conditions were P=1.5 Torr, T=295 K and t= 1.4 ms.

	$\alpha'_{RO2} = \frac{\varepsilon_{RO2}}{\varepsilon_{HO2}}$		
Species	SAPHIR 2010 [NO] = 4.9×10^{13} cm^{-3} ε_{HO2} = 0.45	HCCT 2010 [NO] = 3.0×10^{14} cm^{-3} ε_{HO2} = 0.96	CompOH / Surfin 2011 [NO] = 1.4×10^{13} cm^{-3} ε_{HO2} = 0.15
methane	0.00	0.01	0.00
ethane	0.00	0.06	0.00
ethene	0.27	0.91	0.08
propene	0.27	0.89	0.08
isoprene	0.24	0.82	0.07
benzene	0.09	0.30	0.03
toluene	0.16	0.53	0.05
p-xylene	0.15	0.50	0.04
phenol	0.04	0.13	0.01

The chemical mechanistic information was taken from the Master Chemical Mechanism, MCM v3.2 (Bloss et al., 2005; Jenkin et al., 2003; Saunders et al., 2003), via website: http://mcm.leeds.ac.uk/MCM.
When HO_2 measurement were affected by the detection of RO_2 species, the measured HO_2 is called [HO_2*], it corresponds to the sum of the HO_2 concentration plus the sum of the RO_2 concentration of each species times the relative sensitivity (α_{RO2}) within the measurement conditions.

$$[HO_2^*] = [HO_2] + \sum \left(\alpha^i_{RO2} \times [RO_2] \right) \qquad \text{Eq. 11}$$

No measurement techniques are available for the speciation of each RO_2. These techniques CIMS or PERCA measure the sum of all the RO_2 species. In general, rather than correcting the [HO_2*] data, a model calculation is run to match the [HO_2*] by calculating the concentration of each peroxy radicals. The calculated concentration for each peroxy radicals is multiplied to the relative sensitivity of each individual RO_2 obtained from laboratory measurements or using the MCM mechanism to calculate them. The [HO_2*] measurement is then compared to the calculated [HO_2*] via Eq. 11.

Conclusion

We have presented the UL-FAGE for the quantification of OH and HO_2 radicals with the different parts described in details. With limit of detection of 4×10^5 cm^{-3} and 5×10^6 cm^{-3} for integration time of 1 minute for OH and HO_2, the UL-FAGE has a sufficient sensitivity to measure on the field HOx radicals.

The UL-FAGE was for the first time deployed in the field during the course of this thesis. The optimization of the apparatus toward a complete automation was done and we have been able to successfully measure OH and HO_2 radicals. The validation of the UL-FAGE was made by a series of two intercomparative measurements in the SAPHIR chamber in Juelich (Chapter 3) and in ambient air near Paris (Chapter 4).

Future improvements on the calibration source are planned. The installation of a photodiode to record the lamp flux will allow lower OH and HO_2 concentrations to be reached in their atmospheric concentration range. In addition, the faster response of the photodiode compare with the O_3 analyzer will make the calibration quicker. The H_2O dependence on the sensitivity using the calibration source still need to be understood and tests will be made with different nozzles size and shape.

Interferences on the FAGE system need to be characterized following the work of Mao et al (Mao et al., 2012) for OH and Fuchs et al. (Fuchs et al., 2011) for HO_2. The conclusion from these two works will be used to better prepare the UL-FAGE instruments for the next measurement campaigns. For HO_2, the NO concentration was reduced for the last field campaigns where the UL-FAGE was deployed however interference tests are needed to be made in order to obtain the relative sensitivities for the different RO_2 species for the campaigns at the SAPHIR chamber and during HCCT.

In the next chapter, we present the results of the intercomparative measurement with the FZJ-LIF at the SAPHIR chamber in Juelich in April 2010.

4. References

Atkinson, R., Baulch, D. L., Cox, R. A., Crowley, J. N., Hampson, R. F., Hynes, R. G., Jenkin, M. E., Rossi, M. J. and Troe, J.: Evaluated kinetic and photochemical data for atmospheric chemistry: Volume I - gas phase reactions of Ox, HOx, NOx and SOx species, Atmos. Chem. Phys., 4(6), 1461–1738, doi:10.5194/acp-4-1461-2004, 2004.

Bailey, A. E., Heard, D. E., Henderson, D. A. and Paul, P. H.: Collisional quenching of OH(A 2Σ+, v′=0) by H2O between 211 and 294 K and the development of a unified model for quenching, Chemical Physics Letters, 302(1–2), 132–138, doi:10.1016/S0009-2614(99)00076-7, 1999.

Blitz, M. A., Heard, D. E. and Pilling, M. J.: OH formation from CH3CO+O2: a convenient experimental marker for the acetyl radical, Chemical Physics Letters, 365(5–6), 374–379, doi:10.1016/S0009-2614(02)01484-7, 2002.

Bloss, C., Wagner, V., Bonzanini, A., Jenkin, M. E., Wirtz, K., Martin-Reviejo, M. and Pilling, M. J.: Evaluation of detailed aromatic mechanisms (MCMv3 and MCMv3.1) against environmental chamber data, Atmos. Chem. Phys., 5(3), 623–639, doi:10.5194/acp-5-623-2005, 2005.

Cantrell, C. A., Zimmer, A. and Tyndall, G. S.: Absorption cross sections for water vapor from 183 to 193 nm, Geophys. Res. Lett., 24(17), 2195–2198, doi:10.1029/97GL02100, 1997.

Copeland, R. A. and Crosley, D. R.: Temperature dependent electronic quenching of OH(A 2Σ+, v′=0) between 230 and 310 K, The Journal of Chemical Physics, 84(6), 3099–3105, doi:doi:10.1063/1.450291, 1986.

Creasey, D. J., Halford-Maw, P. A., Heard, D. E., Pilling, M. J. and Whitaker, B. J.: Implementation and initial deployment of a fieldinstrument for measurement of OH and HO2 in thetroposphere by laser-induced fluorescence, J. Chem. Soc., Faraday Trans., 93(16), 2907–2913, doi:10.1039/A701469D, 1997a.

Creasey, D. J., Heard, D. E., Pilling, M. J., Whitaker, B. J., Berzins, M. and Fairlie, R.: Visualisation of a supersonic free-jet expansion using laser-induced fluorescence spectroscopy: Application to the measurement of rate constants at ultralow temperatures, Applied Physics B: Lasers and Optics, 65(3), 375–391, doi:10.1007/s003400050285, 1997b.

Dorn, H.-P., Neuroth, R. and Hofzumahaus, A.: Investigation of OH absorption cross sections of rotational transitions in the A2∑+, (υ′=0)←X2Π, (υ″=0) band under atmospheric conditions: Implications for tropospheric long-path absorption measurements, J. Geophys. Res., 100(D4), 7397–7409, doi:10.1029/94JD03323, 1995.

Dusanter, S., Vimal, D. and Stevens, P. S.: Technical note: Measuring tropospheric OH and HO2 by laser-induced fluorescence at low pressure. A comparison of calibration techniques, Atmos. Chem. Phys., 8(2), 321–340, doi:10.5194/acp-8-321-2008, 2008.

Dusanter, S., Vimal, D., Stevens, P. S., Volkamer, R. and Molina, L. T.: Measurements of OH and HO2 concentrations during the MCMA-2006 field campaign – Part 1: Deployment of the

Indiana University laser-induced fluorescence instrument, Atmos. Chem. Phys., 9(5), 1665–1685, doi:10.5194/acp-9-1665-2009, 2009.

Faloona, I. C., Tan, D., Lesher, R. L., Hazen, N. L., Frame, C. L., Simpas, J. B., Harder, H., Martinez, M., Di Carlo, P., Ren, X. and Brune, W. H.: A Laser-induced Fluorescence Instrument for Detecting Tropospheric OH and HO₂: Characteristics and Calibration, Journal of Atmospheric Chemistry, 47(2), 139–167, doi:10.1023/B:JOCH.0000021036.53185.0e, 2004.

Finalyson-Pitts, B. J. and Pitts, J. N.: Chemistry of the Upper and the Lower atmosphere, Academic Press., 2000.

Fuchs, H., Bohn, B., Hofzumahaus, A., Holland, F., Lu, K. D., Nehr, S., Rohrer, F. and Wahner, A.: Detection of HO2 by laser-induced fluorescence: calibration and interferences from RO2 radicals, Atmospheric Measurement Techniques, 4(6), 1209–1225, doi:10.5194/amt-4-1209-2011, 2011.

German, K. R.: Direct measurement of the radiative lifetimes of the A 2Σ+ (V′ = 0) states of OH and OD, The Journal of Chemical Physics, 62(7), 2584–2587, doi:doi:10.1063/1.430840, 1975.

Gierczak, T., Burkholder, J. B., Bauerle, S. and Ravishankara, A. R.: Photochemistry of acetone under tropospheric conditions, Chemical Physics, 231(2–3), 229–244, doi:10.1016/S0301-0104(98)00006-8, 1998.

Hard, T. M., Chan, C. Y., Mehrabzadeh, A. A. and O'Brien, R. J.: Diurnal HO2 Cycles at Clean Air and Urban Sites in the Troposphere, J. Geophys. Res., 97(D9), 9785–9794, doi:10.1029/92JD00232, 1992.

Hard, T. M., O?Brien, R. J., Cook, T. B. and Tsongas, G. A.: Interference suppression in HO fluorescence detection, Appl. Opt., 18(19), 3216–3217, doi:10.1364/AO.18.003216, 1979.

Hofzumahaus, A., Aschmutat, U., Heßling, M., Holland, F. and Ehhalt, D. H.: The measurement of tropospheric OH radicals by laser‐induced fluorescence spectroscopy during the POPCORN Field Campaign, Geophys. Res. Lett., 23(18), 2541–2544, doi:10.1029/96GL02205, 1996.

Hofzumahaus, A., Brauers, T., Aschmutat, U., Brandenburger, U., Dorn, H.-P., Hausmann, M., Heßling, M., Holland, F., Plass‐Dülmer, C., Sedlacek, M., Weber, M., et al.: Reply [to "Comment on 'The measurement of tropospheric OH radicals by laser‐induced fluorescence spectroscopy during the POPCORN field campaign' by Hofzumahaus et al. and 'Intercomparison of tropospheric OH radical measurements by multiple folded long‐path laser absorption and laser induced fluorescence' by Brauers et al."], Geophys. Res. Lett., 24(23), 3039–3040, doi:10.1029/97GL02947, 1997.

Holland, F., Hessling, M. and Hofzumahaus, A.: In Situ Measurement of Tropospheric OH Radicals by Laser-Induced Fluorescence—A Description of the KFA Instrument, Journal of the Atmospheric Sciences, 52(19), 3393–3401, doi:10.1175/1520-0469(1995)052<3393:ISMOTO>2.0.CO;2, 1995.

Holland, F., Hofzumahaus, A., Schäfer, J., Kraus, A. and Pätz, H.-W.: Measurements of OH and HO2 radical concentrations and photolysis frequencies during BERLIOZ, J. Geophys. Res., 108(D4), 8246, doi:10.1029/2001JD001393, 2003.

Jenkin, M. E., Saunders, S. M., Wagner, V. and Pilling, M. J.: Protocol for the development of the Master Chemical Mechanism, MCM v3 (Part B): tropospheric degradation of aromatic volatile organic compounds, Atmos. Chem. Phys., 3(1), 181–193, doi:10.5194/acp-3-181-2003, 2003.

Kanaya, Y. and Akimoto, H.: Gating a channel photomultiplier with a fast high-voltage switch: reduction of afterpulse rates in a laser-induced fluorescence instrument for measurement of atmospheric OH radical concentrations, Appl. Opt., 45(6), 1254–1259, doi:10.1364/AO.45.001254, 2006.

Kanaya, Y., Sadanaga, Y., Hirokawa, J., Kajii, Y. and Akimoto, H.: Development of a Ground-Based LIF Instrument for Measuring HOx Radicals: Instrumentation and Calibrations, Journal of Atmospheric Chemistry, 38(1), 73–110, doi:10.1023/A:1026559321911, 2001.

Lei, W., De Foy, B., Zavala, M., Volkamer, R. and Molina, L. T.: Characterizing ozone production in the Mexico City Metropolitan Area: a case study using a chemical transport model, Atmos. Chem. Phys., 7(5), 1347–1366, doi:10.5194/acp-7-1347-2007, 2007.

Lu, K. D., Rohrer, F., Holland, F., Fuchs, H., Bohn, B., Brauers, T., Chang, C. C., Häseler, R., Hu, M., Kita, K., Kondo, Y., et al.: Observation and modelling of OH and HO2 concentrations in the Pearl River Delta 2006: a missing OH source in a VOC rich atmosphere, Atmos. Chem. Phys., 12(3), 1541–1569, doi:10.5194/acp-12-1541-2012, 2012.

Luque, J. and Crosley, D. R.: LIFBASE: Database and Spectral Simulation for diatomic molecules (v 1.6), Tech. Rep. MP 99-009, SRI International (1999) (version 2.0.64, 2008), http:// www.sri.com/psd/lifbase/.,, 2009.

Mao, J., Ren, X., Zhang, L., Van Duin, D. M., Cohen, R. C., Park, J.-H., Goldstein, A. H., Paulot, F., Beaver, M. R., Crounse, J. D., Wennberg, P. O., et al.: Insights into hydroxyl measurements and atmospheric oxidation in a California forest, Atmos. Chem. Phys., 12(17), 8009–8020, doi:10.5194/acp-12-8009-2012, 2012.

Okabe, H.: Photochemistry of small molecules, JohnWiley & Sons., New York., 1978.

Ren, X., Harder, H., Martinez, M., Faloona, I. C., Tan, D., Lesher, R. L., Di Carlo, P., Simpas, J. B. and Brune, W. H.: Interference Testing for Atmospheric HOx Measurements by Laser-induced Fluorescence, Journal of Atmospheric Chemistry, 47(2), 169–190, doi:10.1023/B:JOCH.0000021037.46866.81, 2004.

Saunders, S. M., Jenkin, M. E., Derwent, R. G. and Pilling, M. J.: Protocol for the development of the Master Chemical Mechanism, MCM v3 (Part A): tropospheric degradation of non-aromatic volatile organic compounds, Atmos. Chem. Phys., 3(1), 161–180, doi:10.5194/acp-3-161-2003, 2003.

Stevens, P. S., Mather, J. H. and Brune, W. H.: Measurement of tropospheric OH and HO2 by laser-induced fluorescence at low pressure, J. Geophys. Res., 99(D2), 3543–3557, doi:10.1029/93JD03342, 1994.

Tyndall, G. S., Orlando, J. J., Wallington, T. J. and Hurley, M. D.: Pressure dependence of the rate coefficients and product yields for the reaction of CH3CO radicals with O2, International Journal of Chemical Kinetics, 29(9), 655–663, doi:10.1002/(SICI)1097-4601(1997)29:9<655::AID-KIN2>3.0.CO;2-T, 1997.

Williams, E. J., Fehsenfeld, F. C., Jobson, B. T., Kuster, W. C., Goldan, P. D., Stutz, J. and McClenny, W. A.: Comparison of Ultraviolet Absorbance, Chemiluminescence, and DOAS Instruments for Ambient Ozone Monitoring, Environ. Sci. Technol., 40(18), 5755–5762, doi:10.1021/es0523542, 2006.

Intercomparative measurement in the SAPHIR chamber

Introduction

In April 2010, we performed a 9 days intercomparative measurement at the SAPHIR chamber (Juelich, Germany) between the FZJ-LIF (Forschungszentrum Jülich – Laser Induced Fluorescence) and the newly developed UL-FAGE (University of Lille – Fluorescence Assay by Gas Expansion) in the frame of the European project Eurochamp 2 which aims at integrating European simulation chambers for investigating atmospheric processes. The two instruments both measured OH and HO_2 radicals and the intercomparative measurement took place for both radicals.

This intercomparison provides a process for testing the reliability of the different instruments detecting OH at very low concentration in the atmosphere. Indeed, as soon as the OH radical was shown to be the primary oxidant in the troposphere, techniques that allowed detecting its very low concentration were developed. In the following years, the intercomparison of the newly developed instruments with respect to one another became of interest in order to test the reliability of the different instruments. In the first part of this chapter, we have summarized the different intercomparative measurement for OH and HO_2.

In the next section, the experiments at the SAPHIR chamber were split into two parts. In the first one following the HOxComp measurement protocol, the H_2O, O_3 and NOx concentration levels were changed stepwise in order to verify the response of the two instruments towards those three species. In the initial project, the second part was dedicated to the study of the oxidation of glyoxal ($C_2H_2O_2$). However we failed to detect any glyoxal after injecting it inside the chamber. Instead, in the 5 remaining days of measurements we studied the chemistry of CO, phenol and isoprene under different conditions of O_3 and NOx. Also by shadowing the chamber, we investigated radical chemistry in the darkness. In addition, the Lille calibration source was placed above the FZJ-LIF nozzle on both OH and HO_2 cells.

The DOAS (Differential Optical Absorption Spectroscopy) as well as the MIESR (Matrix Isolation Electron Spin Resonance) were not available during the time of the measurement so no absolute measurements were carried out. However, for the quantitative aspect of the intercomparison, we relied on the facts that the FZJ-LIF was intercompared previously with the MIESR for HO_2 (Fuchs et al., 2009; Platt et al., 2002) and with the DOAS for OH (Fuchs et al., 2012; Schlosser et al., 2007, 2009) and showed good correlation in all the intercomparative measurements. Hence, the FZJ-LIF was used as the reference method for this campaign in order to validate the UL-FAGE.

1. History of intercomparative measurement for OH and HO_2

1.1. Intercomparative measurements for OH

All reported intercomparative measurements in the recent years for the OH quantification measurement are summarized in Table 1. Most of the intercomparative measurements were made in ambient conditions during field campaigns (ground and aircraft) dedicated to the study of different environments (TOHPE 1993, POPCORN 1994, TRACE-P 2001, ARCTAS 2008). In general, intercomparative measurements have shown relatively good agreement. However due to the high temporal and local variation of the OH radical, they were subject to discrepancies that could be explained by different air masses sampled by each instrument. This can be reduced by working in large atmospheric chambers where the air sampled by each instrument should be homogeneous. Three campaigns took place in the SAPHIR chamber in 2003, 2005 and 2011 and the HOxComp campaign organized in 2005 was the only campaign dedicated specifically to the intercomparison of a large set of OH instruments.

Schlosser et al. (Schlosser et al., 2007) presented the first intercomparative measurement between the FZJ-LIF and the FZJ-DOAS techniques at the SAPHIR chamber (Simulation of Atmospheric PHotochemistry In a Large Reaction Chamber). They carried out a series of experiments in standard conditions where no trace gases were added and some others where HCHO, NO, NO_2, O_3, CO and H_2O were added in different combinations. They observed a very good agreement between the two instruments (r^2=0.93, slope=0.99) over 6 valid measurement days. 3 days where discarded from the analysis because they have shown poor correlation and differences beyond the combined systematic errors of the two instruments. The possible explanations given for the disagreement were the instability of the LIF calibration, interferences with other molecules and photochemical or chemical gradients inside the chamber volume.

In 2005, the first formal blind intercomparison of OH measurement techniques took place at SAPHIR as part of the HOxComp campaign (Schlosser et al., 2009). The instruments that were compared inside the chamber were 3 LIF (FZJ-LIF, MPI-LIF, FRCGC-LIF) and 1 DOAS (FZJ-DOAS). Over the 6 days of measurements, 3 experiments were carried out where H_2O, O_3 and NOx were varied stepwise in order to check the potential interferences of these species on each instrument. The 3 other days were dedicated to the study of the

aging of the Juelich ambient air inside the chamber, the ozonolysis of alkenes in the dark chamber and the photooxidation of several hydrocarbons. The analysis showed a very good agreement between all the instruments within 12%. The correlation between each instrument pair spanned between 0.71 to 0.91 for the correlation factor (r^2) and between 0.88 and 1.10 for the slope (a). By taking the DOAS technique as the reference measurement, no significant interferences were observed with the LIF systems depending on the H_2O, NO_x and O_3 concentration.

The most recent intercomparative measurement made at SAPHIR was made between the FZJ-LIF and the FZJ-DOAS in 2011 (Fuchs et al., 2012). The goal of the experiment was to reproduce the conditions (high VOC concentrations, low NO concentrations) observed during the Pride-PRD2006 campaign in China: under these conditions the OH concentrations measured by the FZJ-LIF were higher than the model predictions by a factor of two at low NO ([NO] < 0.3 ppb) (Lu et al., 2012). Experiments were made for CO, t-butene, isoprene, MVK, MACR, benzene, mesitylene, toluene and p-xylene. The 20 days of measurement showed a very good agreement. The slope equalled 1.02 and the linear correlation coefficient was r^2=0.86. The general good agreement between the DOAS and the FZJ-LIF reduced the possibility of an artefact OH measurement during the Pride-PRD2006. However, discrepancies were observed when looking at the individual measurement days for MVK and toluene: for both species, LIF measured 30 to 40% larger OH concentration than the DOAS showing potential interferences from these species on the FAGE measurements.

1.2. Intercomparative measurements for HO_2

Contrary to OH, intercomparative measurements for HO_2 are fewer. To date, 6 were reported, they are summarized in Table 2. Four of them were made in ambient air (Fuchs et al., 2010; Platt et al., 2002; Ren et al., 2003, 2012) and 2 others at the SAPHIR chamber (Fuchs et al., 2009, 2010). The BERLIOZ campaign (Platt et al., 2002) and the intercomparison made by Fuchs et al. (Fuchs et al., 2009a) were the only ones where an absolute technique (MIESR) was used for the intercomparative measurement. For one of them the exchange of the calibration source was performed (Ren et al., 2003).

During HOxComp, 3 LIF instruments (FZJ-LIF, FRCGC-LIF, MPI-LIF) took part in the formal blind intercomparison for HO_2 measurement techniques. The absolute measurement by MIESR failed to work so no absolute reference was available. In consequence, only the

relative variation of HO_2 by the 3 LIF was looked at. They observed that the agreement (slopes and correlation coefficients) varied from day to day. The main conclusion was that the systematic observed differences could come from chemical interferences that would cause a variable artificial HO_2 signal depending on each FAGE instruments. The conclusion was drawn since the design of the measurement cells as well as calibration procedure was similar for OH and HO_2 for the 3 instruments and the simultaneous OH intercomparison showed good agreement and so ruled out any problems link to calibration or sensitivity changes. They have shown that the differences in HO_2 were correlated with H_2O and O_3 concentration levels inside the chamber. For H_2O, a disagreement at low H_2O concentration ($[H_2O] < 0.6$ %) was shown whereas at higher humidity all the instruments agreed within their respective errors. It was concluded that an unknown parameter was influencing the HO_2 detection but not the calibration at low vapour concentration. For O_3, the agreement between the three instruments in the illuminated chamber was good however an offset in the measured HO_2 concentrations was observed between the MPI-LIF and the two other LIF for elevated O_3 concentrations (130-150 ppb) in the dark chamber. In addition, systematic differences were seen during periods of darkness between the MPI-LIF and the two other LIF but the amplitude of the disagreement varied from day to day even when similar O_3 concentrations were used. This was counter balanced by the lack of offset signal with the MPI-LIF during the ozonolysis of alkenes experiments in the darkness where the O_3 concentration maximum was 100 ppb. The difference between all the experiments in the darkness and the ozonolysis experiment was the absence of photolytically produced species which may be the source of signal in the MPI-LIF.

In 2006, an intercomparison was made at SAPHIR between the FZJ-LIF and the MIESR. 2 experiments were made, the first one was the photooxiation of CH_4 and the other one was the ozonolysis of 1-butene in the dark chamber. Due to failure of the flow system of the FZJ-LIF for the ozonolysis experiment, the experiment had to be repeated but without the MIESR that was already disconnected from the chamber. The two experiments were made in very similar conditions. The overall agreement was very good with a slope of 0.98 and a linear correlation coefficient of 0.98.

Table 1. Sum up of OH intercomparative measurements
Sum up of the different intercomparative measurements for OH radicals. N is the number of paired measurements, r^2 is the coefficient of determination, a is the slope, b is the intercept in 10^6 cm^{-3}. LIF: Laser Induced Fluoresence, FAGE, RC: ^{14}CO radiocarbon instrument, DOAS: Differential Optical Absorption Spectroscopy, CIMS: Chemical Ionization Mass Spectrometry

Campaign	Instruments x	Instruments y	N	r^2	a	b	Measurement site	Comments	Reference
CITE 1 1983/84	GaT-LIF/FMC-LIF lidar/WSU-RC		-	-	-	-	aircraft, marine and continental California, USA tropical marine Hawaii, USA	- low sensitivity which made the intercomparison irrelevant - self-generation of OH by laser photolysis of O_3 at 282 nm	(Beck et al., 1987)
1992	PSU-LIF	WSU-RC	22	0.74	2.9	0.93	clean rural environment Washington state, USA	poor sensitivities data averaged over 30 to 60 min for FAGE discrepancies in time resolution (90 s for RC) and location (different air sampling)	(Campbell et al., 1995)
TOHPE 1993	NCAR-DOAS	NCAR-CIMS	140	0.62	0.82	0.06	clean and polluted environments Colorado Rocky Montains, USA	DOAS measured 20% higher concentration than CIMS Disagreement explained by different air masses sampling	(Mount et al., 1997)
POPCORN 1994	FZJ-LIF	FZJ-DOAS	137	0.80	1.01	0.28	clean rural environment corn field, Germany	exclusion of data points when wind direction perturbed DOAS measurement	(Brauers et al., 1996)

Table 1. Continued

Campaign	Instruments x	Instruments y	N	r^2	a	b	Measurement site	Comments	Reference
PEM Tropics B 1999	ATHOS-LIF	NCAR-CIMS	-	-	-	-	aircraft (up to 8 km) very clean environment Pacific Ocean	instruments in 2 different aircrafts intercomparison made when aircrafts were on a similar location (two instances) LIF/CIMS ratio increases from 0.8 near the surface to 1.6 at 8 km height. Correction needed for ATHOS-LIF (see below)	(Eisele et al., 2001)
TRACE-P 2001	ATHOS-LIF	NCAR-CIMS	-	0.88 *(0.88)*	1.58 *(0.96)*	-0.31 *(-)*	aircraft very clean environment Pacific Ocean	instruments in 2 different aircrafts altitude dependence CIMS/LIF ratio decrease when altitude increases. *A calibration error was found for the ATHOS-LIF and data were corrected by multiplying the data by a factor of 1.6* (Mao et al., 2010; Ren et al., 2008). Italic data are after correction	(Eisele et al., 2003)

Table 1. Continued

Campaign	Instruments x	Instruments y	N	r^2	a	b	Measurement site	Comments	Reference
2003	FZJ-LIF	FZJ-DOAS	400	0.93	0.99	-0.08	SAPHIR chamber, Juelich, Germany	9 valid days of measurements correlation and regression obtained from 6 measurment days 3 measurement days were discarded from the analysis explanations given are instability of LIF calibration, interferences with other molecules, photochemical or chemical gradients inside the chamber volume	(Schlosser et al., 2007)
HOxComp 2005	FZJ-DOAS	MPI-LIF	238	0.91	0.98	10.14	SAPHIR chamber Juelich, Germany	6 days of measurements (H_2O, NO_x, O_3, aging ambient air, ozonolysis of alkenes, photooxidation of hydrocarbons) 3 LIF, 1 DOAS very good agreement within 12% of the slope from unity	(Elshorbany et al., 2012; Kanaya et al., 2012; Schlosser et al., 2009)
	FZJ-DOAS	FZJ-LIF	420	0.79	0.95	-0.23			
	FZJ-DOAS	FRCGC-LIF	399	0.77	1.09	-0.09			
	FRCGC-LIF	MPI-LIF	199	0.71	1.01	-0.41			
	FRCGC-LIF	FZJ-LIF	356	0.75	0.88	-0.01			
	FZJ-LIF	MPI-LIF	264	0.84	1.10	10			

Table 1. Continued

Campaign	Instruments x	Instruments y	N	r^2	a	b	Measurement site	Comments	Reference
HOxComp 2005	FRCGC-LIF	MPI-LIF	277	0.75	1.26	-0.63	Ambient Juelich, Germany polluted maximum concentrations NO=13 ppb, O_3=65 ppb	3 days of measurements 3 LIF, 1 CIMS heterogenity in the slopes but high correlation two distincts groups of instruments DWD-CIMS/MPI-LIF and FRCGC-LIF/FZJ-LIF, different locations for both groups that can explain the discrepancies	(Elshorbany et al., 2012; Kanaya et al., 2012; Schlosser et al., 2009)
	FRCGC-LIF	DWD-CIMS	301	0.82	0.75	-0.31			
	FRCGC-LIF	FZJ-LIF	339	0.8	1.06	-0.21			
	FZJ-LIF	MPI-LIF	395	0.76	1.29	-0.29			
	FZJ-LIF	DWD-CIMS	460	0.84	0.7	-0.04			
	MPI-LIF	DWD-CIMS	328	0.96	0.59	10.08			
2011	FZJ-DOAS	FZJ-LIF	2495	0.86	1.02	0.1	SAPHIR Juelich, Germany	20 days of measurements Photochemical degradation of VOCs (benzene, t-butene, isoprene, MVK, MCAR, toluene, mesitylene, toluene, p-xylene) under low NO concentrations (0.1-0.3 ppb) LIF measured 30-40% more for MVK and toluene experiments	(Fuchs et al., 2012)

Table 1. Continued

Campaign	Instruments x	Instruments y	N	r^2	a	b	Measurement site	Comments	Reference
ARCTAS 2008	ATHOS-LIF	NCAR-CIMS	-	0.72	0.89	0.03	aircraft measurement over Alaska (all instruments in the same aircraft)	CIMS/LIF ratios - *function of altitude* ratio ~1 below 4-5 km ratio > 1 above 4-5 km not explained same observation than TRACE-P and PEM TB - *function of water* ratio < 1; H_2O < 5000 ppm ratio~1; H_2O > 6000 ppm maybe due to CIMS (H_2O dependent reaction to produce H_2SO_4) Observed to modelled ratios - *function of altitude* good agreement below 6 km for CIMS and LIF - *function of NO* ratio > 1 at NO < 10 ppt for LIF ratio < 1 at NO>1 ppb for CIMS - *function of isoprene* ratio up to 6 for LIF and CIMS for isoprene > 1 ppb LIF interference (Mao et al., 2012), no explanations for CIMS	(Ren et al., 2012)

GaT: Georgia Institue of Technology, FMC: Ford Motor Company, PSU: Portland State University, WSU: Washington State University, NCAR: National Center for Atmospheric Research FZJ: Forschungszentrum Jülich, MPI: Max Planck Institute, FRCGC: Frontier Research Center for Global Change, ATHOS: Airborne Tropospheric Hydrogen Oxides Sensor, DWD: Deutscher Wetterdeinst

Table 2. Sum up of HO_2 intercomparative measurements
Sum up of the intercomparative measurements made for HO_2. N is the number of paired measurements, r^2 is the coefficient of determination, a is the slope, b is the intercept in ppt. MIESR: Matrix-Isolation Electron Spin Resonance, LIF: Laser-Induced Fluorescence (conversion of HO_2 to OH by addition of NO), PerCIMS: PeroxyRadical Chemical Ionization Mass Spectrometry

Campaign	Instruments x	Instruments y	N	r^2	a	b	Measurement site	Comments	Reference
BERLIOZ 1998	MIESR	FZJ-LIF	14	0.88	1.03	0.15	semi-polluted site near Berlin, Germany	2 days of measurements used for the intercomparison	(Platt et al., 2002)
2003	GTHOS-LIF	PerCIMS	-	0.85	0.93	0.60	ambient and calibration source exchange Pennsylvania, USA	4 days of intercomparison Excellent agreement from cross-calibration and sources swapping within 5%.	(Ren et al., 2003)
HOxComp 2005	FRCGC-LIF	MPI-LIF	334	0.97	1.46	1.31	ambient day time	no absolute measurement due to MIESR failure.	(Fuchs et al., 2010b)
	MPI-LIF	FZJ-LIF	506	0.92	0.59	-0.39		3 measurement days in ambient, 6 measurements in SAPHIR agreement varied from day to day bad agreement at low H_2O (<0.6%) interference partly due to O_3 in dark chamber for the MPI-LIF	
	FZJ-LIF	FRCGC-LIF	81	0.98	1.19	-0.53			
HOxComp 2005	FRCGC-LIF	MPI-LIF	138	0.93	2.95	0.51	ambient night time		
	MPI-LIF	FZJ-LIF	222	0.92	0.75	-0.45			
	FZJ-LIF	FRCGC-LIF	35	0.70	0.46	0.10			

GTHOS: Ground-based Tropospheric Hydrogen Oxides Sensor

Table 2. Continued

Campaign	Instruments x	Instruments y	N	r^2	a	b	Measurement site	Comments	Reference
HOxComp 2005	FRCGC-LIF	MPI-LIF	625 (386)	0.82 (0.97)	1.26 (1.24)	0.36 (0.84)	SAPHIR	(see above for comments)	(Fuchs et al., 2010b)
	MPI-LIF	FZJ-LIF	2201 (1347)	0.92 (0.98)	1.19 (1.22)	-0.80 (-1.31)			
	FZJ-LIF	FRCGC-LIF	573 (362)	0.93 (0.98)	0.69 (0.66)	0.28 (0.20)			
2006	MIESR	FZJ-LIF	7	0.98	0.98	-1.2	SAPHIR	2 experiments : methane photooxidation, 1-butene ozonolysis in the dark chamber (problem encounter with the LIF instrument, ozonolysis experiment repeated in the same conditions without the MIESR instrument)	(Fuchs et al., 2009)

Table 2. Continued

Campaign	Instruments x	Instruments y	N	r^2	a	b	Measurement site	Comments	Reference
2008 ARCTAS	ATHOS-LIF	PerCIMS	-	0.72	0.86	3 .9	aircraft measurement over Alaska (all instruments in the same aircraft)	CIMS/LIF ratios *function of altitude* ARCTAS A ratio ~ 1.72 ARCTAS-CARB, ARCTAS B ratio ~ 1 up to 6 km ratio > 1 up to 6 km *function of water* ratio > 1; H_2O < 3000 ppm ratio ~ 1; H_2O > 3000 ppm Observed to modelled ratios *function of altitude* good below 6 km for CIMS and LIF howevern impact of HO_2 uptake on aerosols not well parameterized, possible change on the ratio *function of NO* ratio increased for both CIMS and LIF when NO increased missing HOx source in the model *function of isoprene* little dependence of ratio observed to model LIF data corrected for RO_2 interferences, sensitivity to isoprene=0.68	(Ren et al., 2012)

2. Experimental details

The intercomparative measurement was made between the UL-FAGE and the FZJ-LIF inside the SAPHIR chamber (Figure 1). Both instruments are based on the design developed by Hard at al. (Hard et al., 1984) called FAGE. Air is sampled in a low pressure cell after gas expansion where OH is detected by LIF. In Table 3 the main characteristics of the two instruments are noted. The main difference between the two is the type of fluorescence excitation cell used: in the case of the UL-FAGE, a multi-pass cell is used whereas the FZJ-LIF used a single pass cell. Single pass cells are believed to be less sensitive to interferences due to a smaller probed volume and also to have a lower background signal. Another difference is the separation of the two cells (for OH and HO_2) for FZJ-LIF whereas for the UL-FAGE the HO_2 cell is placed downstream of the OH cell.

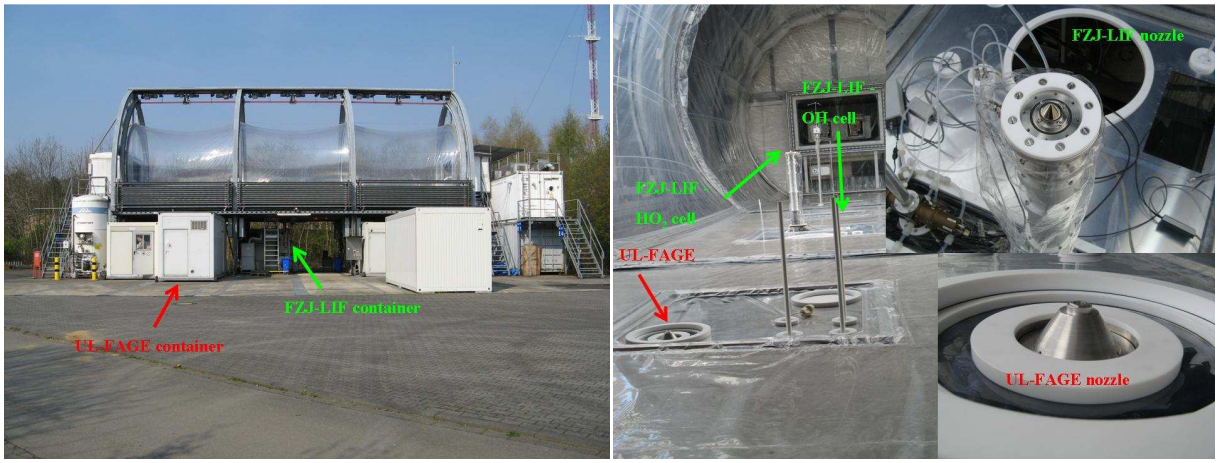

Figure 1. Photos at the SAPHIR chamber
Right – SAPHIR chamber, Left – Positions of the UL-FAGE nozzle and the FZJ-LIF nozzles inside the chamber

2.1. SAPHIR chamber

The SAPHIR chamber is in operation since 2001. It is designed to investigate tropospheric photochemistry under natural light conditions and was well characterized in different works (Bohn et al., 2005; Rohrer et al., 2005). The chamber has a volume ~ 270 m^3 (18 m long, 5 m diameter) and is constructed of a double-walled FEP (Fluorine-ethene-propene) cylinder held by a steel-frame. FEP walls have 85% transmission to UV-A and UV-B. The working pressure is held 50 Pa above ambient pressure in order to avoid ambient air contaminating the

chamber. The louvre-system allows shadowing of the chamber and changing of the photochemical conditions. Rohrer et al. (Rohrer et al., 2005) showed that HONO and HCHO are the principal sources of radicals as it is the case for most of the large atmospheric chambers.

The chamber has a large set of instruments installed permanently for the measurements of trace gases. Ancillary measurements were made for O_3 (UV absorption-spectrometry), NO (chemiluminescence), NO_2 (chemiluminescence), CO (gas chromatography), photolysis frequencies (spectroradiomater), hydrocarbons up to C_{10} (gas chromatography), H_2O (IR absorption, hygrometer) as well as temperature and pressure. Trace gases (H_2O, CO_2, O_3, NO_x, CO, toluene, p-xylene, phenol and isoprene) were added to the chamber depending on the experiments. H_2O concentration was controlled by adding to the purge flow evaporated Milli-Q water. The chamber has already been used for intercomparative measurements of different techniques that measured HCHO (Wisthaler et al., 2008), OH (Fuchs et al., 2012; Schlosser et al., 2007, 2009), HO_2 (Fuchs et al., 2009, 2010b), NO_2 (Fuchs et al., 2010a) and OVOC (Apel et al., 2008).

2.2. FZJ-LIF

The FZJ-LIF was developed in the 1990s by Hofzumahaus and Holland and a detailed descriptions can be found elsewhere (Holland et al., 1995). The instrument participated to field campaigns in different environments (POPCORN, BERLIOZ, Pride-PRD2006) and was involved in a series of intercomparative measurement for OH (POPCORN, HOxComp) and for HO_2 (BERLIOZ, HOxComp). For OH measurements, the FZJ-LIF agreed well with the DOAS at the SAPHIR chamber for 3 intercomparative measurements:

- Schlosser et al., (Schlosser et al., 2007) $r^2 = 0.93$, slope=0.99
- HOxComp (Schlosser et al., 2009) $r^2 = 0.79$, slope=0.95
- Fuchs et al., (Fuchs et al., 2012) $r^2 = 0.86$, slope=1.02

For HO_2, it is the only instrument that was compared with the only available absolute method, MIESR. During BERLIOZ (Platt et al., 2002) and an intercomparison at SAPHIR (Fuchs et al., 2009b), the agreement was very good with linear correlation equal to 0.88 and 0.98 respectively. In both cases, the slope was close to unity. However, during HOxComp, the agreement between the FZJ-LIF and 2 others LIF instruments was shown to vary from day to

day (see 1.2). Discrepancies could not be explained but the correlation between the different instruments was impacted with O_3 and H_2O. Recently, Fuchs et al. (Fuchs et al., 2011) have shown that the instrument used for the intercomparison was subject to interference due to recycling to HO_2 of certain types of RO_2 following NO addition thus generating artificial HO_2.

2.3. UL-FAGE

During the intercomparative measurement, the UL-FAGE was very similar to the set up described in Chapter 2. The main difference was the absence of a second measurement gate for the detection of the solar background on the OH cell after detecting the OH fluorescence signal (see details in Chapter 2). For the HO_2 measurements, the NO gas kit used during the campaign was borrowed from the FZJ group. NO was delivered from a 2L pure NO cylinder (99.99%) and was additionally purified with Ascarite. The flow was adjusted inside the UL-FAGE using a mass flow controller. On Figure 2 is represented the conversion efficiency as function of the NO concentration made during a calibration at SAPHIR. The solid line was obtained using the equation derived by Hard et al. (Hard et al., 1992) for a conversion time equal to 1.4 ms (details can be found in Chapter 2). During the entire campaign, the NO concentration was kept at 4.9×10^{13} cm^{-3} which corresponded to a conversion efficiency of approximately 40%.

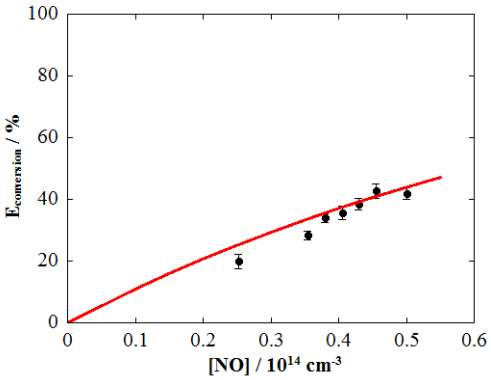

Figure 2. Representation of the conversion efficiency as function of [NO]
The solid line represents the conversion efficiency as function of the NO concentration obtained from the model given by Hard et al. (Hard et al., 1992). $[HO_2] = 4.1 \times 10^9$ cm^{-3}, P=1.5 Torr, t=1.4 ms.

The calibration factors measured for OH and HO_2 were taken from the average of 7 calibration points where the H_2O concentration was varied between 180 and 910 ppm, the O_3

concentration was on average equal to 7.7(±1.5) ppb and the laser power for OH, $Power_{OH}$= 2.04(±0.09) mW and for HO_2, $Power_{HO2}$=0.77(±0.03) mW.

Table 3. Characteristics and performances of the UL-FAGE and FZJ-LIF during the intercomparative measurement

	UL-FAGE	FZJ-LIF
cell assembly	HO_2 cell downsteram of OH cell	separate cells
inlet nozzle size (mm)	1.0	0.4
sample flow rate (litre/min)	9.5	1
distance nozzle - detection (cm)	15	10
cell pressure (hPa)	2.0	3.8
laser rep. rate (kHz)	5	8.5
laser beam shape (cell)	multi-pass (White type)	round: 8 mm diameter
time resolution (s)	55	30
dependence of sensitivity on water	fluorescence quenching	fluorescence quenching
calibration	O_2/O_3 actinometry	
type of detector	CPM[a]	MCP[a]
OH		
laser power (mW)	2-2.5	35-40
accuracy (2σ)	30 %	20 %
LOD (S/N=2) (10^5 cm^{-3})	3.8	3
HO_2		
laser power (mW)	0.8-1.2	35-40
conversion efficiency	~ 45 %	>90%
conversion time (ms)	1.4	2.7
NO concentration	0.10%	0.15%
(absolute concentration / 10^{13} cm^{-3})	(4.9)	(14)
NO purification	Ascarite (sodium hydroxide-coated silica)	
interference from NO addition	<0.3 ppt not corrected	0.2-0.3 ppt
accuracy (2σ)	30 %	20 %
LOD (S/N=2) (10^6 cm^{-3})	1.1	1

[a] CPM: Channel Photon Multiplier, MCP : MultiChannelPlate

2.4. Measurement protocol

The chamber was flushed overnight with ultra-pure synthetic air obtained by evaporation of liquid N_2 and O_2 (Linde, purity > 99.9999%). Measurements were typically done from 7:00 to 15:00 (UTC). At the beginning of each day, a concentration of approximately 100 ppm of CO_2 was added. It was used as a tracer to check the homogeneity of the air mixture inside the chamber. When the roof is open and the chamber is insolate, turbulences take place in the chamber and a complete mixing takes approximately 10 min. In the dark chamber, due to weaker convection, a fan is turned on to increase the air mixing.

For the first 4 days, toluene and p-xylene with concentration of approximately 6 ppb were injected in the dark chamber 30 to 60 min before the shutters were open. For the H_2O experiments (April 13th and 16th), a second injection of 6 ppb of toluene and p-xylene was made when the water concentration was increased for the second time. The louvre system was closed for each H_2O injection on the 13th and only for the second injection of H_2O on the 16th similarly with the experiments on the 14th and the 15th where the roof was closed only for the second injection of O_3 and NO_2 respectively.

For the other days except on the 19th, injections of the studied trace gases were made when the chamber was open and the chamber was only closed at the end of the measurement. On the 19th, the chamber stay closed for most the measurement and was open only for 90 min.

3. Results

The intercomparative measurement was carried out in the SAPHIR chamber over 9 days. The type and the measurement conditions are listed in Table 4. The first 4 days were dedicated to test the response of both instruments towards H_2O (twice), O_3 and NO_x. For the second part of the intercomparative measurement campaign, as explained in the introduction, the goal was to study the photochemistry of glyoxal. However, since glyoxal was not observed by the PTR-MS after being injected, two days were focused on CO under insolate conditions (17th) and in the dark chamber (19th). Then two experiments on phenol were made first under low ozone (April 20th) and secondly under high ozone concentration (April 21st) before studying the isoprene chemistry under high O_3 and low NOx concentration (22nd).

Table 4. List of the different experiments made during the intercomparison
The values given are the maximum for each experiment.

Date	NO ppbv	NO_2 ppbv	O_3 ppbv	H_2O %	j_{O1D} 10^{-6} s^{-1}	j_{NO2} 10^{-3} s^{-1}	j_{HONO} 10^{-4} s^{-1}	Type of experiments
13/04	0.21	0.75	4.72	1.84	7.21	5.04	8.23	H_2O
14/04	0.23	0.86	183.81	0.88	6.73	5.46	8.95	O_3
15/04 (dark)	0.03	0.17	83.71	0.87	-	-	-	O_3
15/04	0.73	6.88	83.71	0.87	9.24	5.62	9.19	NOx
16/04	0.22	0.64	1.94	1.27	6.79	4.34	7.06	H_2O
17/04	3.92	15.41	92.54	0.92	9.77	5.85	9.66	CO
19/04 (dark)	0.08	15.74	52.13	1.03	-	-	-	CO
19/04	4.49	15.74	52.13	1.03	9.50	5.35	8.82	CO
20/04	1.09	2.08	10.04	1.02	9.72	5.69	9.46	Phenol
21/04	1.39	5.40	48.11	0.79	8.89	6.41	10.76	Phenol
22/04	0.53	1.41	59.58	0.93	9.37	6.44	10.56	Isoprene

The H_2O interference experiment was repeated due to some technical problem observed with the UL-FAGE on the 13/04/2010. We found that the two photodiodes (at the exit of the OH FAGE cell and of the reference cell) that were used for the power measurements were not reliable. The photodiode signal was not responding linearly with the laser power. The photodiode signal was increasing whereas we were sure that the laser power decreased (hypothetically a temperature dependence on the photodiode signal). In order to retrieve the laser power during the 1st day of measurement, we therefore used as a power reference the off resonance signal in the first cell when the chamber was closed. The background signal is linearly dependent with respect to the laser power as it is coming from the laser scattering inside the FAGE cell. Within the chamber conditions, we assumed that through the complete day, the off-resonance signal was solely impacted by the laser power. For the rest of the intercomparative measurement, the laser power was regularly measured (ca. every 30 min) through each measurement day at the exit of the laser. From the independently measured fibre transmission we retrieved the input laser power for the OH and the HO_2 cell. In the next paragraphs (3.1-3.6), the effect of H_2O, O_3 in insolate and dark conditions, NOx, CO, phenol and isoprene on the HOx measurements is described, followed by the calibration test. In the paragraph 3.8, a statistical analysis for the overall campaign as well as a day to day analysis is presented.

3.1. H_2O interference tests

On the 13th and 16th, the water vapour was varied stepwise at four different relative humidities 0, 20, 50 and 70 %. Profiles are displayed on Figure 3. The measurements conditions were different between the two days:

- the averaged temperature was lower on the 16th (10.3 ± 2.7) °C instead of (16.2 ± 4.5) °C on the 13th) with scatter clouds whereas on the 13th the sky was clear.
- for both days, the concentration of NO was below 0.2 ppb and [NO_2] below 1 ppb.
- the O_3 concentration was higher on the 13th with a maximum equal to 5 ppb where the maximum on the 16th equalled 2 ppb
- on the 13th, the roof was closed for each H_2O injection whereas on the 16th the roof was closed only for the second H_2O injection.

On the 13th, the OH concentration profiles for both instruments were similar. The OH concentration slightly increased above the background signal for both instruments for the first insolate period and clearly above the LOD for the rest of the measurement day when the

louvre-system was open. The maximum concentration measured was approximately 6×10^6 cm^{-3}. For each dark period, the OH concentration inside the chamber was below or close to the LOD for both LIF instruments. The HO_2 measurement by the two different FAGE instruments was more contrasted. While the same concentration variations were observed by the two instruments, the ratio between the two absolute concentrations varied significantly during the course of the measurement. During the first insolate period, under dry conditions, the agreement was good. During the second insolate period (from 10:04 to 12:00), the HO_2 concentration measured by the FZJ-LIF was 40 % higher than the UL-FAGE whereas it was 80 % higher for the last two periods when the roof was open (from 12:56 to 14:10 and from 14:55 to 16:05). These differences seem to be correlated with the H_2O concentration: the HO_2 concentration ratio ($[HO_2]_{FZJ}/[HO_2]_{Lille}$) with the increase in H_2O concentration increased inside the chamber. The concentration measured by the FZJ-LIF was continuously higher by a factor of two compared to the UL-FAGE even during the third and the last dark periods (from 14:10 to 14:55, and from 16:05 to 16:30).

On the 16th, the OH concentration measured by the two instruments was three times lower than on the 13th with a maximum equal to 2×10^6 cm^{-3}. During a large part of the measurement (from 6:45 to 14:08), the OH concentration was close to the limit of detection of both instruments. As a difference from the measurement on the 13th, the HO_2 concentration was in very good agreement for both instruments in terms of variation and absolute concentration. For the first insolate period (from 8:43 to 11:00) and the first dark period (from 11:00 to 12:02), the agreement is excellent, both instruments measured the same HO_2 concentration with less than 5 % difference. For the second insolate period, the FZJ-LIF measured 20 % more than the UL-FAGE. These results are in contradiction with the ones obtained on the 13th where the agreement between the two instruments showed a dependence on the H_2O concentration inside the chamber.

From the H_2O interference test experiment, we can conclude that the OH measurements were not significantly affected by the variation of H_2O inside the chamber. However, for the HO_2 measurements we observed a strong disagreement on the 13th where the FZJ-LIF measured higher concentration than the UL-FAGE. The difference between the FZJ-LIF and the UL-FAGE increased when the H_2O concentration increased. On the 16th, the disagreement between the UL-FAGE and the FZJ-LIF was within the combined uncertainty of both instruments. We can not conclude whether the HO_2 measurement by both instrument was affected by H_2O as contrary results as observed when the H2O test experiment was repeated.

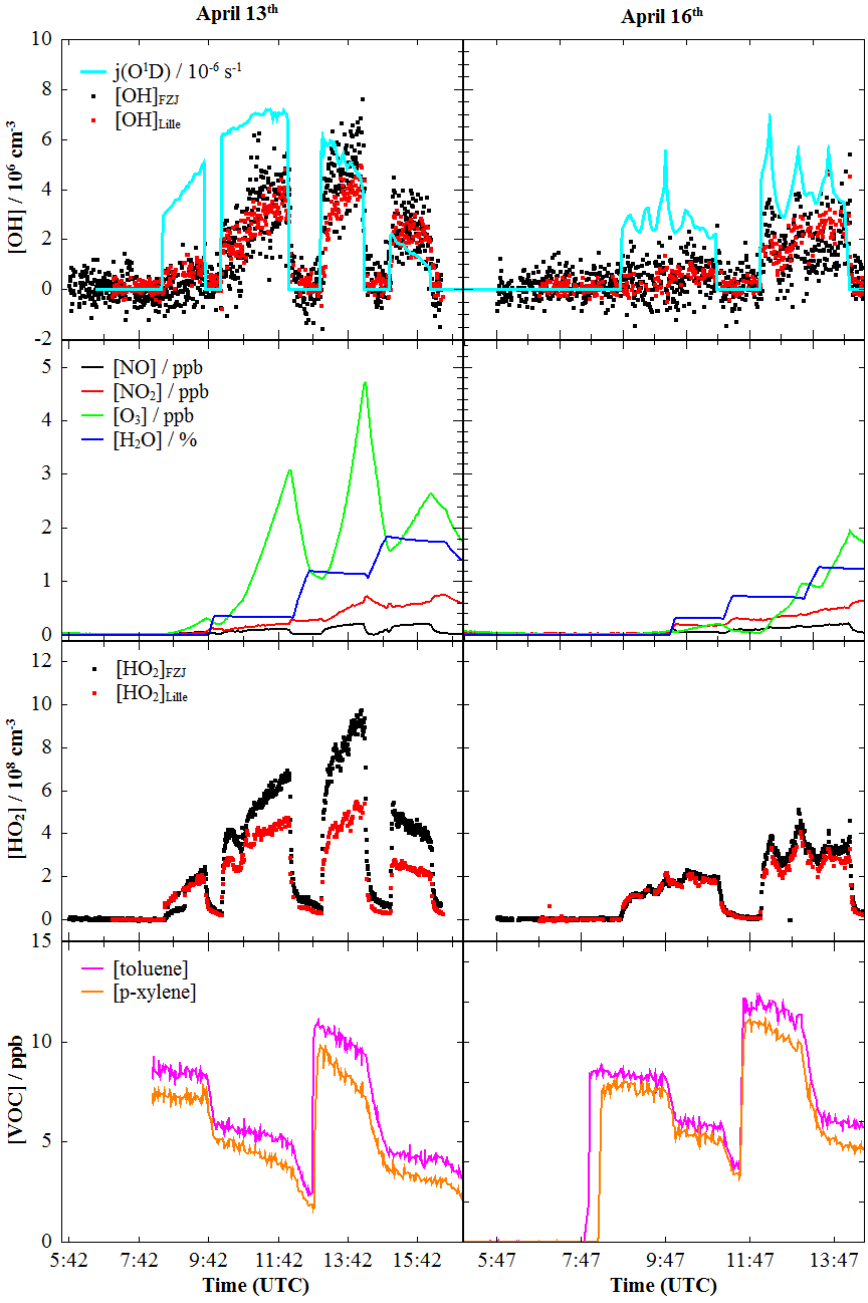

Figure 3. Measurement profiles for April 13th (Left) and April 16th (Right)
From down to up:
- VOC measurement profiles.
- HO_2 profiles for the FZJ-FAGE (black dots) and the UL-FAGE (red dots).
- Profiles of NO (solid black line), NO_2 (solid red line), O_3 (solid green line) and H_2O (solid blue line). The concentrations are given in ppb for NO, NO_2 and O_3. For H_2O, the concentration is given in %.
- OH profiles for the FZJ-FAGE (black dots), the UL-FAGE (red dots) and the $j(O^1D)$.

3.2. O_3 interference tests

The influence of O_3 on the measurement of OH and HO_2 by the two LIF was tested in two different conditions, first in the open chamber similarly to the H_2O and NO_x tests and secondly, in the dark chamber where only O_3 and H_2O were injected.

O_3 is the principal source of interference in the FAGE cell. Indeed, O_3 can be photolyzed within the FAGE cells at the OH excitation wavelength (308 nm) to form OH via the reaction between $O(^1D)$ and water vapour. The OH formed within the FAGE cell can be then probed by a second laser pulse in case the probed volume is not fully refreshed between two laser pulses. Through years, one of the reasons to change the laser excitation wavelength from 282 nm to 308 nm was to diminish the O_3 interference. Indeed, the O_3 absorption cross section is approximately 25 times lower at 308 nm than at 282 nm. On the other hand, all FAGE instruments work with high repetition rate lasers in order to increase their sensitivity. For the UL-FAGE, the repetition rate is kept at 5 kHz which means that in order to reduce any interference from the photolysis of species that forms OH the probed volume would need to be renewed every 200 µs.

The O_3 interference is relatively straightforward to characterize in laboratory by injecting a known amount of O_3 and water through the calibration source. During ambient measurements, the interference by O_3 can be corrected from it knowing the laser power, the repetition rate, the O_3 and the H_2O concentrations. However, experiments in chamber conditions can bring additional information for the O_3 interference for both instruments.

3.2.1. Open chamber

For the O_3 test measurement in the open chamber (April 14th), 4 concentrations of O_3 were reached 0, 70, 130 and 180 ppb. The water was kept constant at approximately 0.8 %, [NO] < 0.2 ppb and [NO_2] < 1 ppb. Measurement profiles are shown on Figure 5. The experiment started at 6:45 and after the gas additions (H_2O at 7:40, p-xylene and toluene at 8:48) the roof was open at 9:35. The first O_3 addition was made at 10:40 followed by a second one in the dark chamber at 12:12 and a last one at 13:21 (chamber open).

Before the roof was open, the OH and HO_2 concentrations measured by both instruments scattered around their respective limits of detection. Afterwards, the OH and HO_2 concentration increased following the O_3 photolysis frequencies $j(O^1D)$. When the second injection of O_3 (up to 130 ppb) in the dark chamber was done, the OH concentration measured by the two LIF was slightly above the detection limit of the two LIF due to the O_3 interference

that generated artificial OH inside the FAGE cells. For HO_2, the O_3 addition in the dark can be clearly seen on the none-corrected HO_2 profiles of the two instruments for the same reasons. For the last insolate period, the UL-FAGE and the FZJ-LIF measured the same OH concentration up to 4×10^6 cm^{-3}. For the two insolate periods, the HO_2 concentrations measured by the FZJ-LIF were 50 to 60 % higher than for the UL-FAGE. The maximum concentration measured by the FZJ-LIF was 10×10^8 cm^{-3} and 6×10^8 cm^{-3} for the UL-FAGE.

3.2.2. Dark chamber

On April 15th, during the first part of the experiment (from 7:20 to 10:15), the louvre system was kept close in order to check the O_3 interference for both LIF in the dark chamber. O_3 was injected stepwise 3 times to obtain concentrations of 27, 56 and 83 ppb with a constant water concentration of 0.8 %. The OH and HO_2 concentration increased slightly accordingly with the well-known ozone interference that generates artificial OH in the FAGE cells.

The concentrations of OH and HO_2 measured by the FZJ-LIF and the UL-FAGE were averaged for each stepwise addition. The results are shown on Figure 4 where the OH and HO_2 concentration for both instruments are plotted as function of the O_3 concentration inside the chamber.

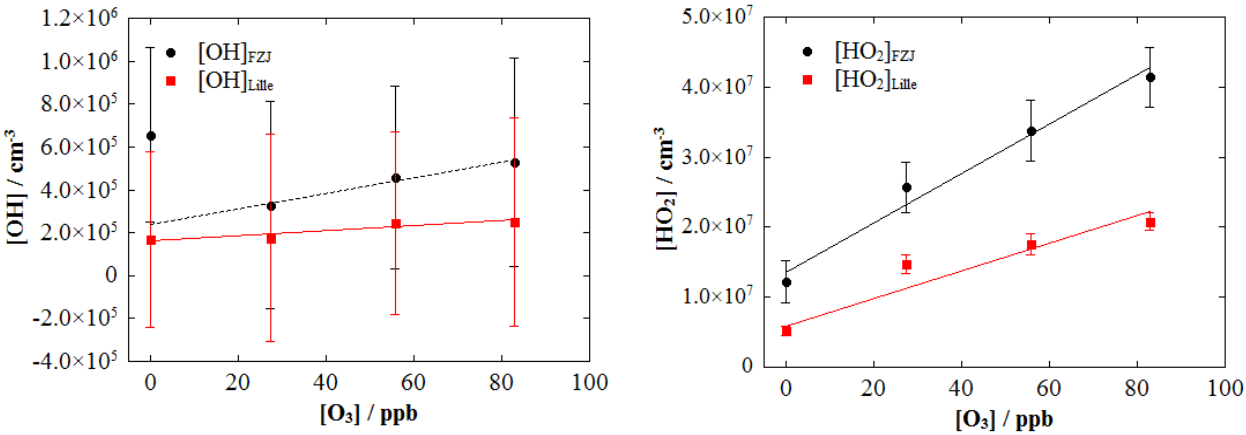

Figure 4. Representation of the [OH] (left) and [HO_2] (right) measured during the O_3 interference test in the dark chamber on April 15th. The red squares represent the OH and HO_2 concentrations measured with the UL-FAGE, the black dots the OH and HO_2 concentrations measured by the FZJ-FAGE. The solid lines represent a linear regression fit. The dashed line on the left-graph for the $[OH]_{FZJ}$ is a linear regression without taking into account the value at [O_3] = 0 ppb.

The table summarized the linear regression analysis for the O_3 interference in the dark chamber. For the UL-FAGE, we measured for OH an interference of 1.15 (± 0.72) × 10^3 cm^{-3} per ppb of O_3 and 1.99 (± 0.16) × 10^5 cm^{-3} per ppb of O_3 for HO_2. The O_3 interference for the OH cell is in agreement with the laboratory experiments (see Chapter 2 for more details, $[OH]_{interf}$ = (1.7 ± 0.72) × 10^3 cm^{-3} per ppb of O_3)

Table 5. Results of the linear regression analysis of the O_3 interference in the dark chamber.
For the UL-FAGE, rep. rate=5 kHz, P_{OH}=2.5 mW, P_{HO2}= 1.0 mW.
For the FZJ-LIF, rep. rate=8.5 kHz, P_{OH}=35 mW, P_{HO2}= 35 mW.

	a, slope in cm^{-3}[OH] / ppb[O_3]	**b, intercept in cm^{-3}**
$[OH]_{Lille}$	1.15 (± 0.72) × 10^3	1.64 (± 3.56) × 10^5
$[OH]_{FZJ}$	3.59 (± 0.58) × 10^3	2.40 (± 0.58) × 10^5
$[HO_2]_{Lille}$	1.99 (± 0.16) × 10^5	5.83 (± 0.62) × 10^6
$[HO_2]_{FZJ}$	3.55 (± 0.59) × 10^5	1.37 (± 0.27) × 10^7

For the FZJ-LIF the O_3 interference in the OH cell found was slightly lower than the one given by Lu et al. (Lu et al., 2012) where they stated an O_3 interference of 6 (± 2) × 10^3 cm^{-3} per ppb of O_3. However, for the HO_2 cell, for both instruments the interference measured was with 3.55 × 10^5 cm^{-3} much larger than previously quoted with an interference of (2 × 10^4 per ppb of O_3., (Lu et al., 2012)). This might be due to actual production of HO_2 from ozonolysis of residual hydrocarbons in the dark chamber that interfered with the O_3 test.

From the O_3 interference test in the open chamber, the OH measurements by both instruments did not seem to be affected by the increase of the O_3 concentration inside the chamber. However for HO_2, the FZJ-LIF measured higher HO_2 concentrations than the UL-FAGE throughout the measurement day. In the dark chamber, we observed a small increase of the OH and the HO_2 concentrations measured by both instruments when the O_3 concentration increased. The comparison with the laboratory experiments for OH is in agreement for both instruments. For HO_2, we concluded that an unknown dark reaction inside the chamber corrupted the interference test. For the both instruments, the OH and the HO_2 detection cells are similar and so the O_3 interference is expected to be in the same range in both cells as observed in laboratory experiments.

3.3. NOx interference test

The NOx test measurement (April 15th) was done after the O_3 test in the dark chamber. NO_2 was injected twice with concentration of 5 ppb. The first one was made at 11:22 in the open chamber leading to the increase of the NO concentration up to 0.6 ppb. The second NO_2 injection was made in the dark chamber at 13:22, the NO_2 concentration increased from 2.3 to 6.9 ppb. When the chamber was open for the second time (14:17), the NO increased up to 0.7 ppb. Because of the O_3 interference test made during the first part of the experiment, the O_3 concentration stayed at a high level ($[O_3]$ = (69 ± 5) ppb) during the NO_x interference test. After the roof was open (10:15), the OH profile observed by the two instruments were identical. The OH concentration increased up to 7×10^6 cm^{-3} during the first insolate period. During the dark period, the concentration measured was steady and close to the LOD and for the last insolate period, the maximum OH concentration was 5×10^6 cm^{-3}. As for the 13th, the HO_2 concentration ratio between the two instruments varied during the course of the measurement and for this day the agreement got improved through the course of the day. Before the first NO_2 injection, the FZJ-LIF measured 50% more HO_2 than the UL-FAGE whereas the disagreement decreased to 30% less afterwards. During the dark period, the agreement is worse and the FZJ-LIF measured 60% more than the UL-FAGE. For the last insolate period, the measured HO_2 concentration by the FZJ-LIF was only 20% higher than the concentration measured by the UL-FAGE.

The agreement between the UL-FAGE and the FZJ-LIF was better when NOx were added inside the chamber. The same observations were made during HOxComp where the MPI-LIF agreement with the two other LIF was improved for the same experiment when NOx were added. During HOxComp, the NO_x experiment was made under high CO concentration (500 - 800 ppb) and low O_3 concentration (20 ppb) while in our conditions the O_3 concentration was high (80 ppb) and no CO was added. It is interesting to notice that the NO_x concentration influences the HO_2 detection by the LIF instruments despite different conditions even though no clear explanations can be given. The NO_x concentrations are too low to have any influence on the detection inside the FAGE cells. The improvement in the agreement may result from a modification of the chemical composition inside the chamber that removes species responsible for an HO_2 interference. However, for the other measurement days when NO_x were injected inside the chamber, no clear influence of NO_x on the agreement of the two LIF can be drawn.

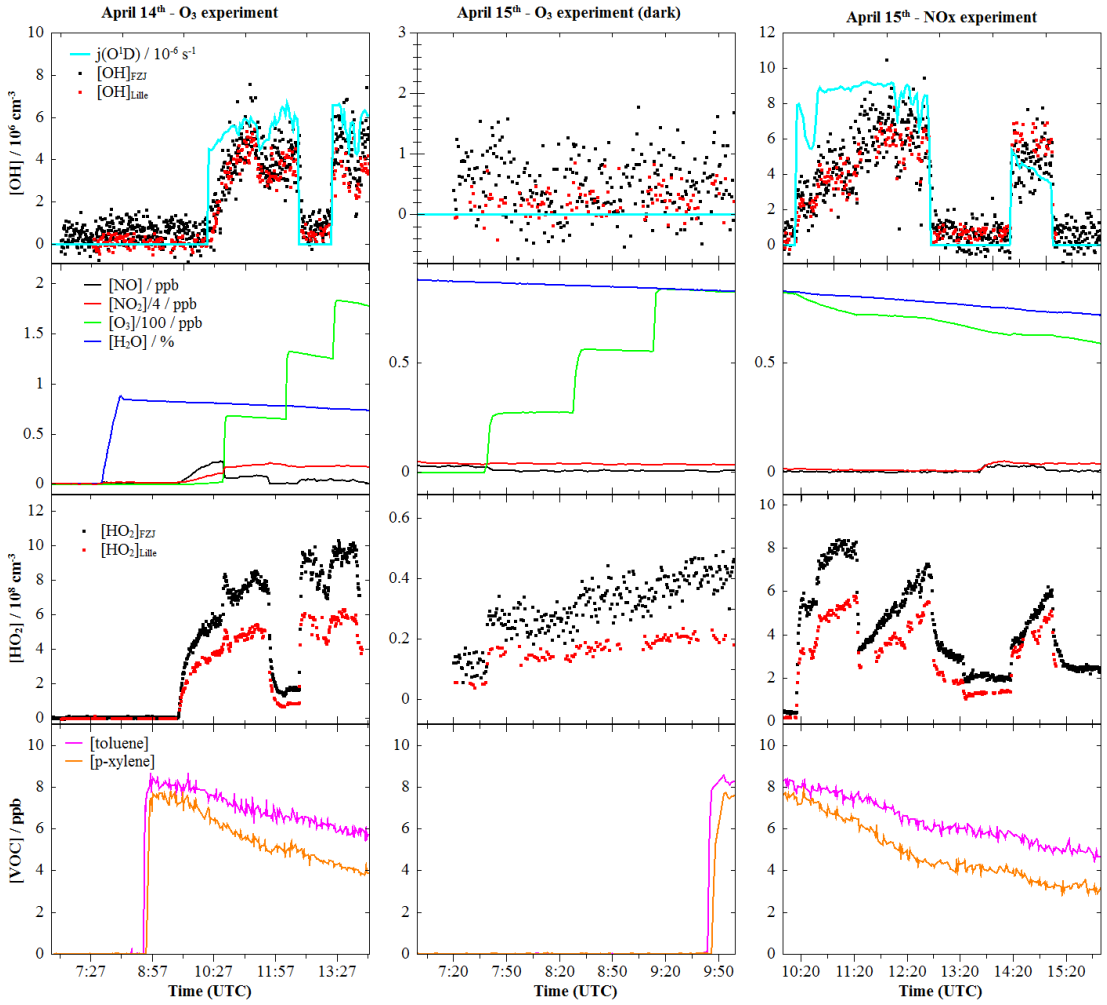

Figure 5. Measurement profiles for April 14th (Left), April 15th – dark chamber (Middle), April 15th (Right)

Caption: same as for Figure 3.

3.4. CO experiments

In order to simulate a simple chemistry but involving OH and HO_2 formation/consumption, NO and NO_2 were also injected. CO is one the main sink of OH in the troposphere. CO is emitted from combustion processes such as forest fires or car exhausts. Its concentration varies from 100 ppb in clean environments to few ppm in highly polluted areas. From its reaction with OH, it produces HO_2 which is one of the precursors of the O_3 formation in the troposphere. A simplified mechanism of the oxidation of CO with OH that leads to a net production of O_3 is given below (R 1) to (R 6)

The experiment was made on two days in different light conditions as can be seen on Figure 6.

$OH + CO \rightarrow H + CO_2$ (R 1)
$H + O_2 + M \rightarrow HO_2 + M$ (R 2)
$HO_2 + NO \rightarrow OH + NO_2$ (R 3)
$NO_2 + h\nu \rightarrow NO + O$ (R 4)
$O + O_2 + M \rightarrow O_3 + M$ (R 5)

$CO + 2O_2 + h\nu \rightarrow O_3 + CO_2$ (R 6)

On the 17th, only one injection of 1.5 ppm of CO was made (10:16). In addition, 2 injections of NO_2 (5 ppb and 10 ppb) were made which brought the NO_2 concentration up to 16 ppb. The NO concentration increased along with the NO_2 injection up to 3.9 ppb. O_3 continuously increased up to 37 ppb during the experiment and a 50 ppb addition was made at 15:45 in the dark chamber. H_2O was added to the chamber at the start of the experiment and decreased linearly from 0.90 to 0.73 % (from 8:00 to 16:45).

On the 19th, 2 injections of CO of 2 ppm each were made (at 7:48 and 9:50). A NO_2 concentration of 5 ppb was added at 8:12. From 10:06, NO was added at a constant flow rate (40 cc). At 10:22, the flow rate was first decreased by half (20 cc) and again (10 cc) from 10:55 to 11:25. During the NO addition ([NO] < 0.1 ppb), the NO_2 concentration increased up to approximately 16 ppb. A second injection of NO_2 of 10 ppb at 14:37 was made which increased the NO_2 concentration from 4.8 to 13 ppb. The NO concentration stayed below 0.1 ppb when the chamber was closed, it increased when the chamber was open to 2.5 ppb and again up to 4.5 ppb along with the second NO_2 injection. A concentration of 50 ppb of O_3 was added to the chamber at 7:23. Following the addition, the O_3 concentration decreased to 13 ppb when the chamber stayed closed before increasing again up to 32 ppb after the chamber was open (13:19). For the first part (from 6:38 to 12:18), the experiment was made in the dry chamber ([H_2O] < 0.1%), afterwards [H_2O] was constant at 1.0%.

In the beginning of the 17th, the OH profiles observed were the same for both apparatus. After the chamber was opened, the concentration increased up to 2×10^7 cm^{-3}. After the CO addition, the concentration decreased sharply down to 7×10^6 cm^{-3}. However, after the first NO_2 injection, the UL-FAGE measured systematically 20% higher OH concentrations than the FZJ-LIF. For HO_2, after the chamber was open, both instruments measured different profiles. The FZJ-LIF observed an increase up to 2.5×10^8 cm^{-3} whereas the UL-FAGE observed 1.9×10^8 cm^{-3} (25% lower). However, 1 hour after the roof was opened the

concentrations measured by both instruments were identical. After the CO addition, again, both instruments observed different profiles; the FZJ-LIF measured 30% more than the UL-FAGE, however, after 1 hour, the FZJ-LIF measured only 10% more than the UL-FAGE. When NO_2 was added (12:16), the HO_2 concentration measured by both instruments decreased sharply down to 2×10^8 cm^{-3}. After the second NO_2 injection (14:07), HO_2 decreased by a factor of two down to 1×10^8 cm^{-3}. Both instruments were in good agreement from 12:16 to 15:00. When the chamber was closed (15:00), both instruments observed an increase in the HO_2 concentration but with different magnitudes. Before the O_3 injection (15:45), the concentration measured by the FZJ-LIF was 60% higher than UL-FAGE. After the addition of 50 ppb of O_3, the FZJ-LIF measured only 30 % more HO_2 than the UL-FAGE. On the 19th, in the dark chamber, the OH concentration stayed below the LOD of both instruments and increased up to 6×10^6 cm^{-3} when the chamber was open (13:19). For HO_2, in the dark chamber, the two IF observed a slow increase of the concentration up to 3×10^7 cm^{-3} after 5 ppb of NO_2 were added (8:12) inside the chamber. After the second CO injection (9:50), the HO_2 concentration decreased below 1×10^7 cm^{-3}. The HO_2 concentration increased a second time up to 5×10^7 cm^{-3} when a small NO flow was added to the chamber (starting at 10:06). At 13:19, the chamber was opened and when the second 10 ppb NO_2 injection was made, the OH decreased down to 2×10^6 cm^{-3} before decreasing below the LOD of the two instruments after the shutter was closed at 15:52. Both instruments measured the same OH concentration within their respective uncertainty. Same observations can be made for HO_2, the concentration increased up to 2×10^8 cm^{-3} after the roof was opened and decreased down to 5×10^7 cm^{-3} when NO_2 was added. After the chamber was closed (15:52), a large discrepancy was observed in the absolute concentration measurement for HO_2: the FZJ-LIF measured on averaged 80% more HO_2 than the UL-FAGE.

For the two CO experiments, the OH concentration measured by the UL-FAGE and the FZJ-LIF were in agreement. OH was observed to increase in the dark chamber at the end of the measurement on the 17th for unknown reasons. For HO_2, the measurement was affected by unknown dark reactions that lead to the formation of HO_2 or RO_2. The agreement between the two instruments was variable depending on the conditions inside the chamber.

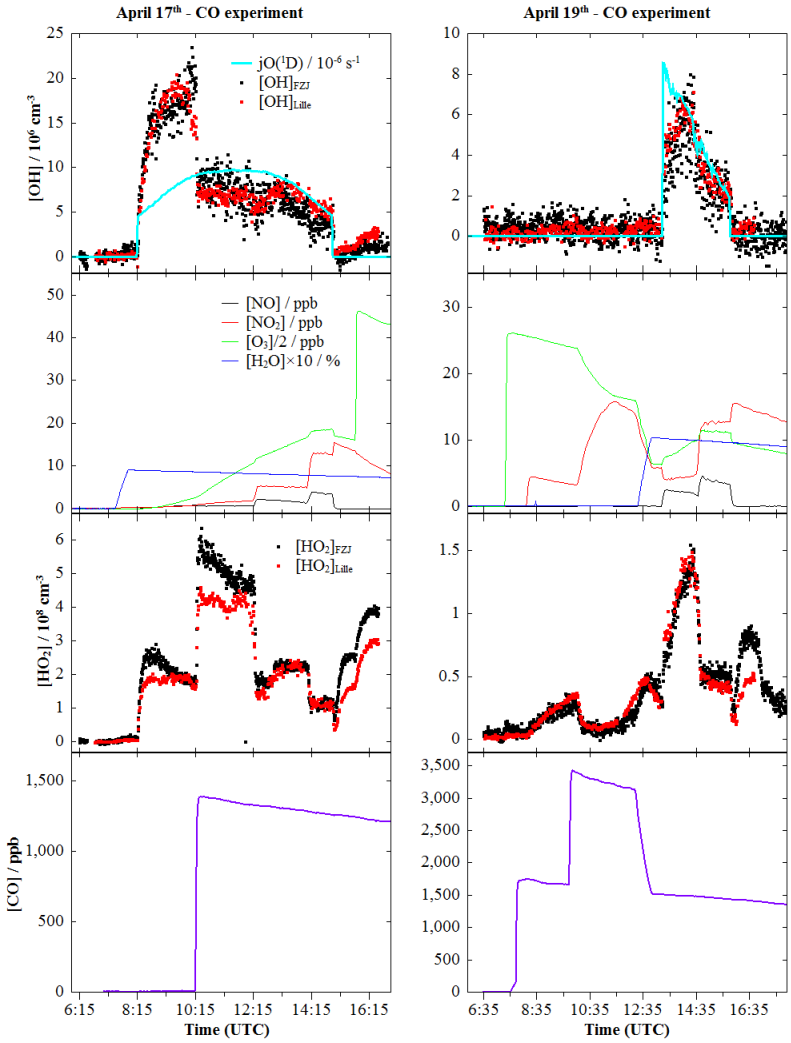

Figure 6. Measurement profiles for April 17th (Left) and April 19th (Right)
Caption: same as for Figure 3.

3.5. Phenol experiments

Phenol is one of the main products of the aromatics oxidation (e.g. benzene) with OH. Volkamer et al. (Volkamer et al., 2002) showed that under atmospheric conditions, the yield of phenol from the oxidation of benzene with OH was up to 53%. Phenol oxidation with OH was studied by Berndt and Böge (Berndt and Böge, 2003). Two different pathways are proposed for the reaction of phenol with OH. The main path (yield ~ 0.76 to 0.87) goes via the OH addition to form an OH-phenol adduct that react with O_2 to form catechol and HO_2 with a yield of 0.73 to 0.80. The minor path goes via an H-abstraction to form phenoxy radicals. Under high NOx conditions, different authors ((Berndt and Böge, 2003) and references therein) reported the formation of o-nitrophenol (yield ~ 0.036 to 0.067) and p-benzoquinone (yield ~ 0.010 to 0.037).

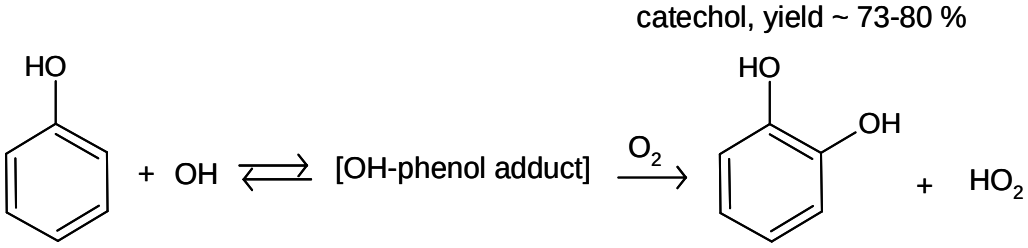

Figure 7. Simplified oxidation mechanism of phenol with OH.

The experiment on phenol was repeated twice with different O_3 concentrations. On the 20th, the ozone concentration stayed below 10 ppb while on the 21st, an O_3 injection brought the concentration up to 50 ppb (see profiles on Figure 8).

On the 20th, only phenol was injected (15 mg) when the chamber was exposed to the sunlight. The NO concentration reached a maximum of approximately 1 ppb at noon, O_3 concentration increased up to 10 ppb and NO_2 up to 2 ppb. H_2O was injected at 7:28 up to 0.95 % and decreased constantly down to 0.85 at the end of the measurement (14:10).

On the 21st, a first injection of O_3 (50 ppb) was made in the dark chamber at 8:04. The roof was then opened (8:30) and thereafter phenol (8.5 mg) was added followed by an injection of 5 ppb of NO_2. The O_3 concentration decreased from 48 to 33 ppb, the maximum concentration of NO and NO_2 was 1.5 and 5.5 ppb respectively. The 21st is marked by highly variable photolysis frequencies due to clouds.

On the 20th, the OH profiles measured by both instruments were the same. After the roof was opened (8:22), the OH concentration increased up to 2×10^7 cm^{-3}. When phenol was injected (10:40), OH decreased sharply down to 4×10^6 cm^{-3} and stayed constant up to the end of the measurement. The HO_2 profiles observed by the two instruments were slightly different. As seen already on the 17th, when the roof was first opened the HO_2 concentration measured by the FZJ-LIF was 30% higher than the UL-FAGE but after 45 min both instruments measured the same concentration for 90 min. After adding phenol, the FZJ-LIF measured continuously 30% more HO_2 than the UL-FAGE.

On the 21st, as for the 20th, the OH profiles were identical for the two instruments. The OH concentration was strongly dependent on the radiation that highly varied during that day. OH decreased from 7×10^6 cm^{-3} to 3×10^6 cm^{-3} after phenol was added (10:10) but no clear observations can be made after NO_2 was added (12:28) on the OH concentration measured by any of the two instruments. For HO_2, the FZJ-LIF measured 30 % more than the UL-FAGE during the course of the day independently of the addition of and NO_2 (12:28). After NO_2 was

added, the HO_2 concentration decreased from approximately 3×10^8 cm^{-3} down to 1×10^8 cm^{-3}.

For the two phenol experiments, the agreement between the two instruments was observed to be good for OH measurements. For HO_2, the FZJ-LIF measured higher concentration than the UL-FAGE.

3.6. Isoprene experiment

Isoprene is by far the main biogenic VOC emitted by trees in the troposphere (Guenther et al., 1995). Several recent field campaigns (Kubistin et al., 2010; Lu et al., 2012; Whalley et al., 2011) in forestry environments under high isoprene and low NOx concentrations have shown significant differences between the measured and the calculated OH concentrations indicating a missing source of OH. These disagreements have triggered many theoretical and experimental studies (Taraborrelli et al., 2012). A new chemical mechanism of the isoprene oxidation was developed (Peeters et al., 2009) in which OH is recycled from isomerisation of hydroxyperoxy radicals, from the photolysis of one of the isomerisation product, hydroxyperoxy aldehydes (HPALD) and from the reaction of HO_2 with isoprene peroxy radicals. The main oxidation products of isoprene are methylvinylketone (MVK), metacrolein (MACR) and formaldehyde.

On the last day of the campaign, we studied the isoprene oxidation under high O_3 and low NO_x concentration. O_3 was injected (12:01) up to a concentration of 50 ppb after the roof had been opened followed by a 5 ppb injection of isoprene (12:19). The water concentration varied from 0.9 to 0.8 %, the maximum NO and NO_2 concentrations were 0.5 ppb and 1.4 ppb respectively. OH profiles for both instruments were in very good agreement during the entire experiment: for the first part (from 6:58 to 10:46), the OH concentration was below the LOD of both LIF instruments. After the roof was open (10:52), the OH concentration increased up to 1.5×10^7 cm^{-3}. When isoprene was added the OH concentration decreased sharply down to 2×10^6 cm^{-3} before slowly rising to reach a concentration of approximately 5×10^6 cm^{-3} at the end of the measurement. In the case of HO_2, a large disagreement between both instruments has been observed. As for OH, before the roof was opened, the HO_2 concentration inside the chamber was below the LOD of the two instruments. After it was opened, the HO_2 concentration increased to around 2×10^8 cm^{-3} and the FZJ-LIF measured 30 % more than the UL-FAGE. When O_3 was added, the HO_2 concentration increased to 3×10^8 cm^{-3} and the FZJ-LIF measured 40 % more than the UL-FAGE. After isoprene was added, a large

disagreement was observed between the two apparatus. During the first 20 min after the injection, the FZJ-LIF measured on averaged 85% more than the UL-FAGE, this agreement decreased to around 40% more for the last 20 min before the roof was closed (15:10).

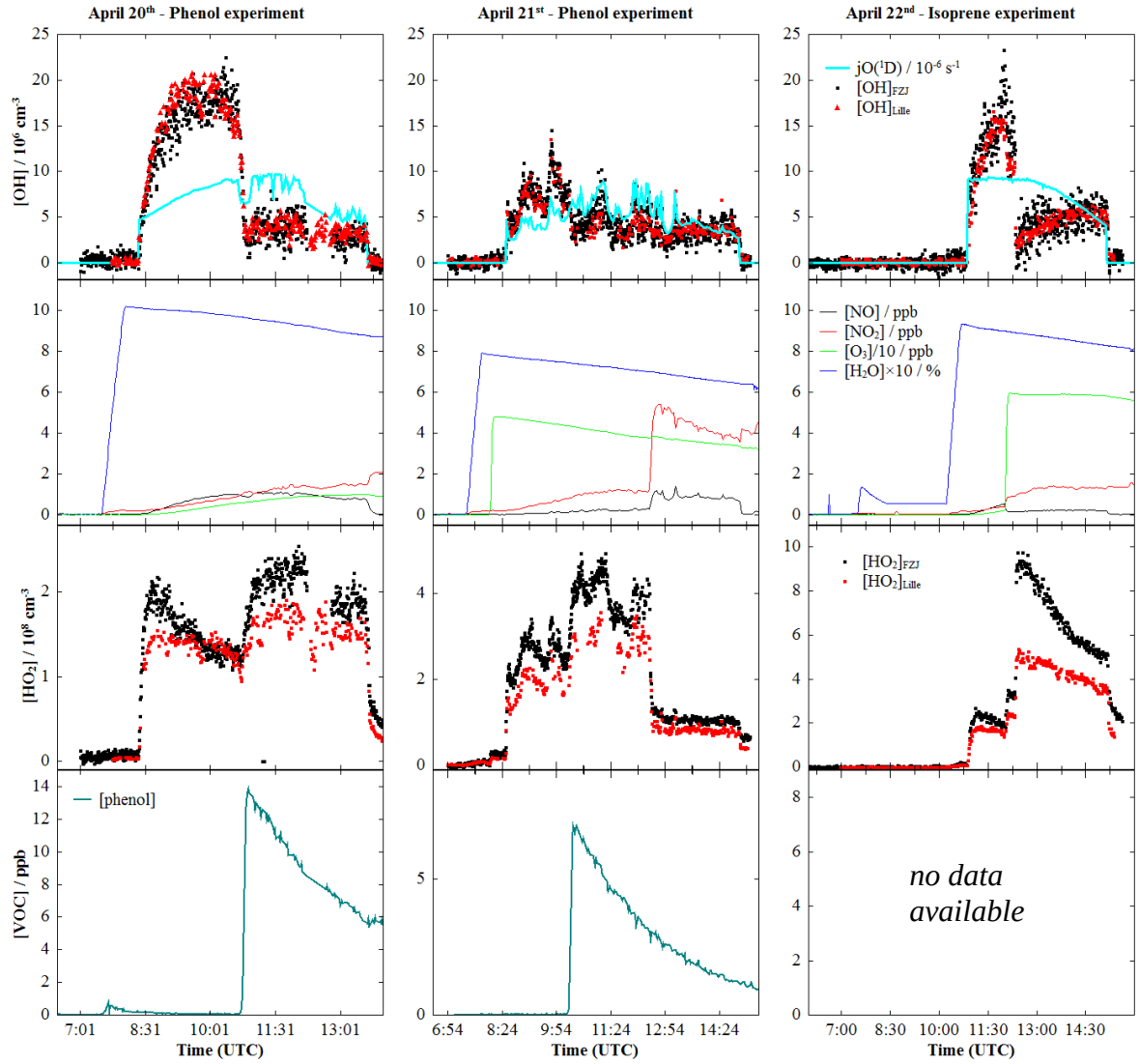

Figure 8. Measurement profiles for April 20th (Left), April 21st (Middle) and April 22nd (Right).
Caption: same as for Figure 3.

For OH, good agreement was observed between the two instruments. For HO_2, after the isoprene injection we observed a strong disagreement between the FZJ-LIF and the UL-FAGE. The difference between the HO2 measurement decreased toward the end of the measurement.

3.7. Calibration source exchange

One major possible source of discrepancy between the two similar LIF instruments comes from the calibration procedure. Even though the techniques used to generate known concentrations of OH and HO_2 are similar for both instruments, exchanging the calibration source is of great interest to check out systematic errors. Details of the UL-calibration source are given in Chapter 2 whereas a description of the FZJ calibration source is given by Aschmutat et al. (Aschmutat, U. et al., 1994). For both calibration sources, O_3 actinometry is used to determine the lamp flux. With the goal to generate lower HOx concentrations, the FZJ-LIF calibration source flushes N_2O is flushed in front of the lamp in order to reduce the lamp flux by absorption of the UV radiation by N_2O. However, the O_3 produced from the O_2 photolysis is then too low for being measured with a standard O_3 analyzer. Therefore, they use a photodiode to measure the lamp flux that was previously calibrated for higher O_3 concentration. The main difference between the two calibration sources is the use of turbulent flow for the UL-calibration source whereas the FZJ-calibration source uses a laminar flow. Therefore, the calibration source from FZJ could not be adapted to the UL-FAGE because the coupling between the UL-FAGE nozzle and the FZJ calibration source would need to be characterized precisely. Indeed, using a laminar flow the gas flow profile across the cell is not flat and the position of the cell with respect to the nozzle could impact the concentration by a factor up to 2.

We placed the UL-FAGE calibration source on the FZJ-LIF and generated known concentration of OH and HO_2. Then, the FZJ-LIF converted the signal obtained into an OH (or HO_2) concentration using their calibration factors. In Table 6 is listed the 3 calibration points made for the OH FZJ-cell at 3 different H_2O concentrations. The concentrations are given with their uncertainties which were calculated from the propagation of errors of each parameter uncertainty. The calibration source exchange measurement is represented on Figure 9.

Table 6. OH and HO_2 concentrations calculated for the calibration source exchange
The 1σ uncertainty for the FZJ-LIF is of 10% and of 15% for the UL-FAGE.

	$[O_3]$ / ppb	$[H_2O]$ / °Cdp	$[OH]_{Lille}$ / 10^9 cm^{-3}	$[OH]_{FZJ}$ / 10^9 cm^{-3}	$[OH]_{FZJ}/[OH]_{Lille}$
point 1	5.6	-20.22	1.75	1.57	0.90
point 2	5.2	-27.26	0.81	0.72	0.88
point 3	4.3	-18.77	1.57	1.42	0.91

The results show a systematic overestimation of the concentration by the UL-FAGE of approximately 10 % compared with the FZJ-LIF. This overestimation is coherent with the statistical analysis (see next paragraph 3.8) in which the data measurement points were plotted in a correlation plot $[OH]_{FZJ}=f([OH]_{Lille})$. The slope obtained from a linear regression analysis for the overall dataset was of 0.86 in agreement with the calibration source exchange.

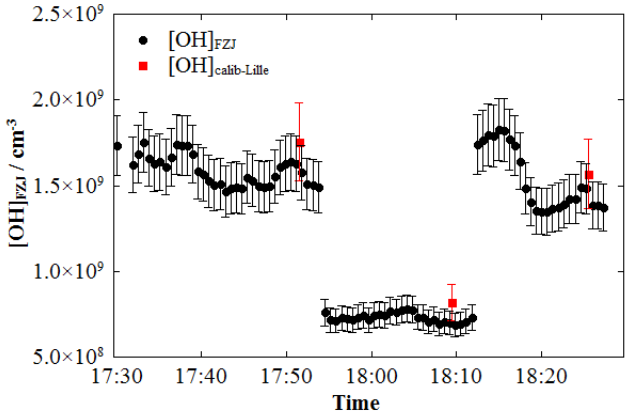

Figure 9. Calibration source exchange.
Uncertainty of 10% for the FZJ-LIF data points and of 15% for the UL-FAGE.

3.8. Statistical analysis

For the data analysis, as the measurement time resolution is different for both instrument (30 s for the FZJ-LIF and 55 s for the UL-FAGE), we used the Lille measurement time as a reference time for the whole data set and the FZJ-FAGE measurement points were linearly interpolated to each Lille measurement points when both instruments were measuring simultaneously (see Figure 10).

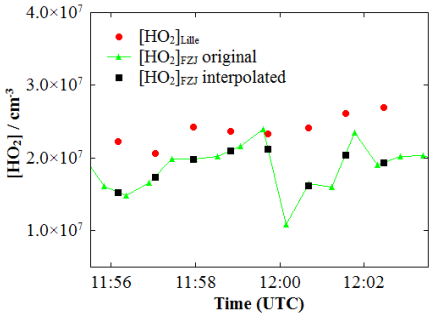

Figure 10. Data interpolation
Example of data processing made before correlating Lille and FZJ measurement data set. The original FZJ measurement points (green triangles) are linearly interpolated (black squares) with respect to the Lille measurement points (red circles).

In order to determine the correlation (i.e. linear dependence) between the concentrations measured by the two LIF instruments, the data were plotted on scatterplots where the concentration (OH or HO_2) from UL-FAGE was displayed on the x-axis and the interpolated concentration from FZJ-FAGE on the y-axis. The square of the Pearson correlation coefficient, r^2, also called coefficient of determination was used to determine the degree of association between the two data set e.g. if $r^2=1$, all variations in the OH (or HO_2) concetration observed by one instrument were also observed by the other.

A linear regression analysis was applied to the scatterplots using the linear equation y=ax+b. The slope a is used to show the quantitative relationship between the two instruments: if a = 1, both instruments measured the same concentrations within their respective errors. The intercept b allows checking if one or both instruments are having an offset.

In the first step of the data analysis we considered the all data sets independently of the conditions. In a second step, we have analyzed each day individually.

3.8.1. Analysis of the all data set

On Figure 11 are represented the scatter plots for the whole 9 days of measurements for OH (left) and HO_2 (right). With a number of 3745 measurement points, the result for OH shows a very good agreement between the FZJ-LIF and the UL-FAGE with a slope equal to 0.86 (in agreement with the exchange of the calibration source) and an insignificant intercept equal to $1.42 \pm 0.24 \times 10^5$ cm^{-3}. The correlation coefficient obtained was 0.93. For HO_2, with the same number of common measurement points, the slope obtained is 1.50 with a small positive intercept of $1.48 \pm 0.12 \times 10^7$ cm^{-3}. The correlation coefficient is very high and equal to 0.96. There is a clear discrepancy for the HO_2 measurement by both instruments beyond their additional respective errors.

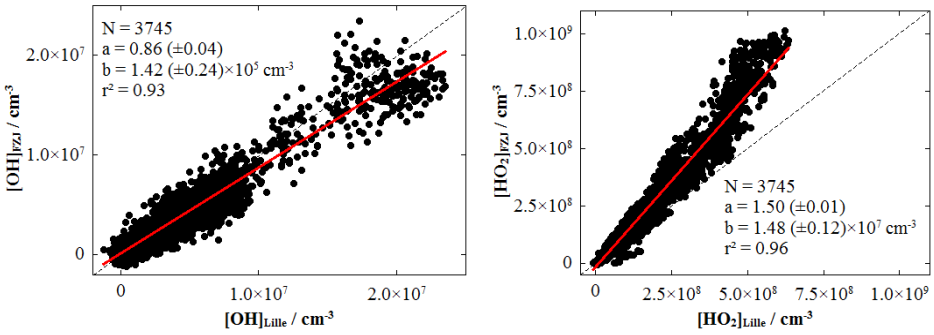

Figure 11. Scatter plots for OH and HO_2 for the 9 days of measurement.
OH (left) and HO_2 (right). The solid lines correspond to a linear regression fit using the equation y=ax+b. The dashed line represents the 1:1 line.

3.8.2. Day by day analysis

In a second analysis, each day was analyzed separately in order to give better insights for the possible differences observed between the two instruments in different conditions. The scatter plots for each OH measurements days are represented on Figure 12 with results of the statistical analysis displayed in Table 7. For HO_2, scatter plots and results of each measurement day are displayed in Figure 13 and in Table 8. The analysis for OH displayed a very good agreement from day to day ($r^2 > 0.76$) except on the 16th where the correlation was equal to 0.56. On this day, the OH concentration inside the chamber was very low during the course of the measurement reaching a maximum of 2×10^6 cm^{-3}.

For HO_2, the day by day analysis showed contrasted results as can be seen on Figure 13 and in Table 8. The correlation coefficients obtained were always greater than 0.90. However, the slopes indicating the quantitative agreement between the two apparatus vary from day to day with the FZJ-LIF measuring consistently higher concentration than the UL-FAGE except on the 19th (a=0.94) where the concentration measured in the chamber were low ($[HO_2] < 2\times 10^8$ cm^{-3}) and most of the experiment was done in the dark. On the first 3 measurement days (13-14-15), the agreement between the two LIF is the lowest with slopes greater than 1.39. On the 22nd (isoprene experiment), the correlation between the two instrument is not linear. It corresponds to days where aromatics (toluene, p-xylene) or alkenes (isoprene) species were injected inside the chamber and where the OH concentration was elevated ($[OH]_{average} > 3 \times 10^6$ cm^{-3}). This has to be compared with the measurement on the 16th where the OH concentration stayed very low during the day ($[OH]_{average} \sim 1 \times 10^6$ cm^{-3}). The agreement for HO_2 on this day was good (a=1.15) even though toluene and p-xylene were injected inside the chamber. The photolytic activity was lower due to clouds that reduced the light intensity. The experiments with addition of phenol showed a different behaviour. The analysis of the two experiments with phenol (20-21) showed a better agreement on the 20th (a=1.18) than on the 21st (a=1.32): on the 20th no O_3 was added inside the chamber but where the OH concentration was higher. For the CO experiments (17-19), a better agreement is obtained for the experiment on the 19th (a=0.94) where the chamber was dark for most of the measurement. However, for the last period of the measurement in the dark after the chamber had been opened for 90 min, a large disagreement is observed with the FZJ-LIF measuring 80% more HO_2 than the UL-FAGE. The same observations were observed on the 17th where a large disagreement is observed for the last measurement period after the chamber was closed.

Table 7. Results obtained from the day by day analysis for OH measurements.
Results obtained from the day by day analysis of the scatter plots for the OH measurements. N, is the number of points, r^2 coefficient of determination. From the linear regression fit, a is the slope, b is the intercept in 10^5 cm^{-3}, errors are 1σ.

	N	a, slope	b, intercept	r^2
13/04/2010	528	0.99 ± 0.02	-0.49 ± 0.57	0.76
14/04/2010	360	0.89 ± 0.02	0.52 ± 0.56	0.86
15/04/2010	352	0.83 ± 0.02	2.72 ± 0.69	0.86
16/04/2010	358	0.65 ± 0.03	1.85 ± 0.42	0.56
17/04/2010	513	0.90 ± 0.01	-3.20 ± 1.21	0.91
19/04/2010	524	0.73 ± 0.01	1.78 ± 0.31	0.87
20/04/2010	303	0.83 ± 0.01	0.45 ± 1.38	0.95
21/04/2010	370	0.88 ± 0.02	1.20 ± 0.91	0.86
22/04/2010	437	0.95 ± 0.01	0.68 ± 0.86	0.93

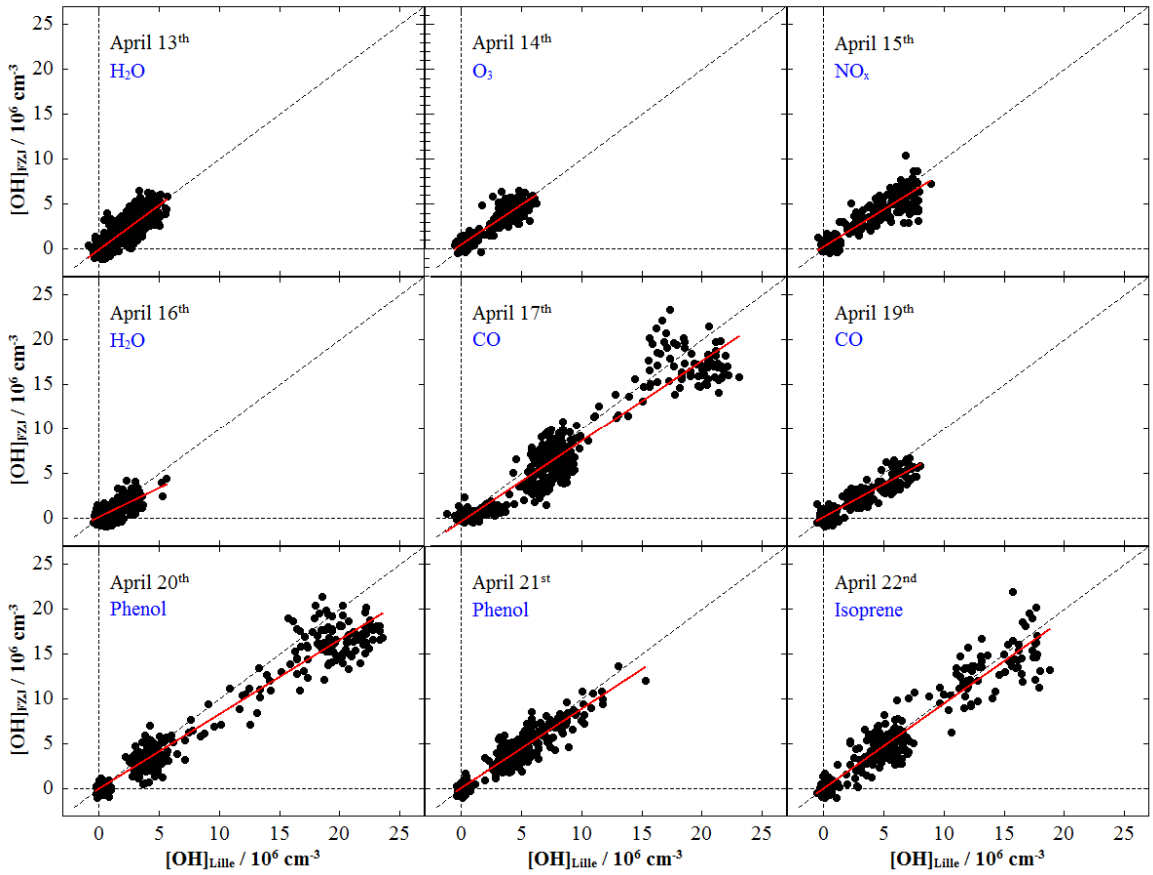

Figure 12. Day by day scatter plots for OH measurements by the UL-FAGE and the FZJ-LIF. Solid lines represent linear regression analysis.

Table 8. Results obtained from the day by day analysis for HO_2 measurements.
Results obtained from the day by day analysis of the scatter plots for the HO_2 measurements. N, is the number of points, r^2 coefficient of determination. From the linear regression fit, a is the slope, b is the intercept in 10^6 cm^{-3}, errors are 1σ.

	N	a, slope	b, intercept	r^2
13/04/2010	528	1.60 ± 0.02	-4.83 ± 4.39	0.94
14/04/2010	360	1.57 ± 0.01	6.73 ± 2.43	0.99
15/04/2010	352	1.34 ± 0.0	13.48 ± 3.84	0.97
16/04/2010	358	1.15 ± 0.01	-1.66 ± 1.51	0.98
17/04/2010	513	1.25 ± 0.01	-2.28 ± 2.98	0.95
19/04/2010	524	0.94 ± 0.01	3.62 ± 0.71	0.90
20/04/2010	303	1.18 ± 0.02	4.84 ± 2.84	0.91
21/04/2010	370	1.32 ± 0.01	2.22 ± 1.34	0.99
22/04/2010	437	1.62 ± 0.01	-13.05 ± 3.34	0.97

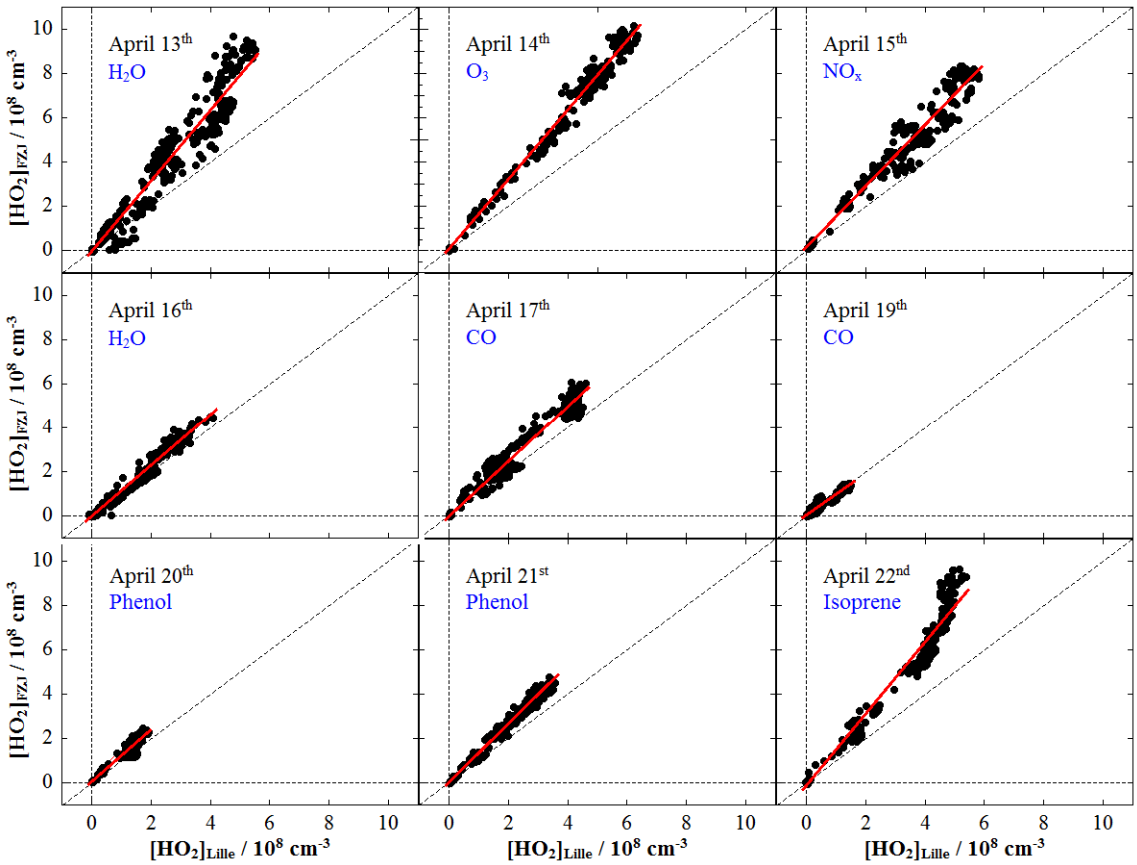

Figure 13. Day by day scatter plots for HO_2 measurements by the UL-FAGE and the FZJ-LIF. Solid lines represent linear regression analysis.

3.8.3. Precision of the two instruments

There are three parameters that define the quality of a measurement: the limit of detection, the accuracy and the precision.

The measurement in the dark chamber in the absence of OH and HO_2 were used in order to determine the precision of the two instruments. The data points were taken from each start of measurements when the chamber was close except for the 15th when the O_3 interference test was made and the 19th for the CO experiment in the dark chamber since both instruments were subject to an O_3 interference.

On Figure 14 histogram plots are used to represent the frequency distribution for OH and HO_2 for both instruments. The histogram were fitted with a normal distribution equation

$$f(x) = height \times \exp\left[-\ln(2) \times \left(\frac{x - x_0}{\sigma_{bkg}}\right)^2\right]$$

From the fit, we obtained the centre (x_0) and the HWHM (Half Width Half Maximum), σ_{bkg}.

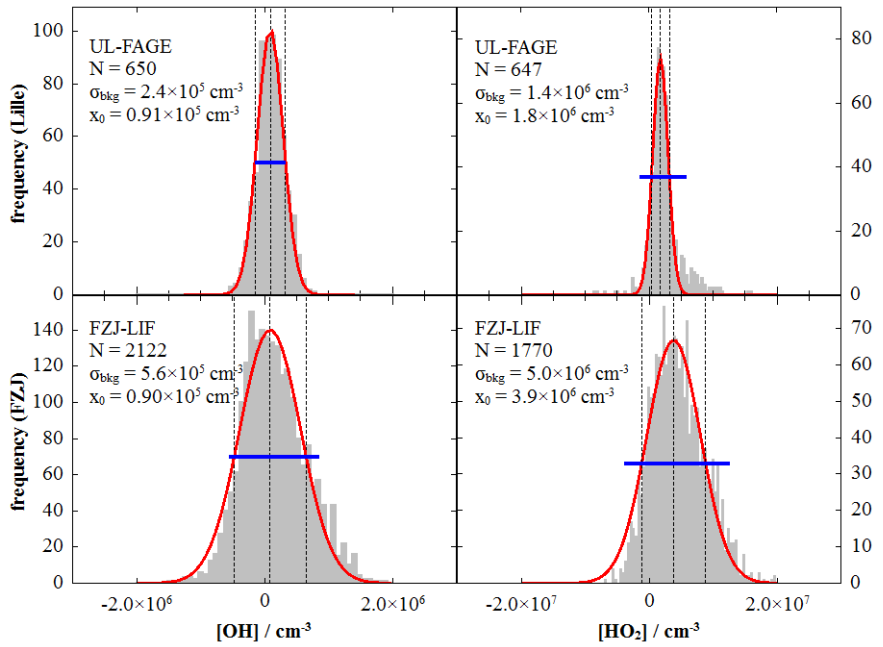

Figure 14. Frequency distribution for OH and for HO_2 for measurements in the dark chamber.

For OH and HO_2, the UL-FAGE showed a higher precision than the FZJ-LIF. For OH, the precision obtained for the UL-FAGE was 2.4 × 10^5 cm^{-3} and 5.6 × 10^5 cm^{-3} for FZJ-LIF. At least a part of this difference can be attributed to the fact that the FZJ-LIF had a better time resolution Δt=30 s instead of Δt=55 s for the UL-FAGE

4. Discussion

In this section, we shall discuss the results from the intercomparative measurement between the UL-FAGE and the FZJ-LIF by putting them in perspective with the results reported after the HOxComp campaign (Fuchs et al., 2010; Schlosser et al., 2009) and the recent work from Fuchs et al. (Fuchs et al., 2011) which described in details the newly found interference of RO_2 in the detection of HO_2 by FAGE instruments.

For OH, the agreement was very good between the two LIF instruments over the 9 days of measurements. No systematic interference was found when O_3, H_2O, NOx concentrations were varied inside the chamber. This result is coherent with what has been concluded for the OH intercomparison inside the chamber between 3 LIF (FZJ-LIF, MPI-LIF and FRCGC-LIF) and the DOAS during HOxComp (Schlosser et al., 2009).

For HO_2, the two instruments showed a very high correlation for each measurement day (r^2> 0.90). However the quantitative agreement varied from one day to another similarly to the observations made during HOxComp: here also a high correlation was observed between the measurements but the absolute concentrations could not be assessed due to unknown interferences. In addition they found that the measurement by the 3 LIF was correlated towards O_3 and H_2O. As already mentioned by Fuchs et al. (Fuchs et al., 2010), the good agreement for the OH measurements (Schlosser et al., 2009) eliminated several possible explanations for the systematic observed differences: inhomogeneous sampled air, systematic error in the calibration, lack of reproducibility of the calibration and intrinsic variable instrument sensitivities. Two possible reasons were given, unknown dependencies of the detection sensitivities on chemical compositions and chemical interferences that could cause artificial HO_2 signal. These arguments were reinforced afterwards by Fuchs et al. (Fuchs et al., 2011) whom found that RO_2 radicals formed during the oxidation of certain chemical species (e.g. alkenes, aromatics) could recycle fast enough HO_2 from their reaction with NO within the FAGE cell, thus leading to an artificial HO_2 signal. They showed that within their measurement conditions ([NO] = 1.3×10^{14} cm^{-3} and $t_{conversion}$=2.7 ms), artificial HO_2 was generated with a different number of species (cyclohexane, ethene, propene, isoprene, MVK, MACR and benzene) with for some of them relative sensitivities up to 80% i.e. each RO_2 radical generates a LIF signal corresponding to 0.8 HO_2 radicals. This new interference is dependent on the NO concentration as well as the conversion time within the FAGE and thus different from one apparatus to another. They also tested the possibility of water dependence

on the sensitivity of HO_2 such as observed during HOxComp and showed that water vapour was not influencing the conversion of HO_2 to OH within their measurement conditions.

4.1. Intercomparison for OH

The intercomparison between the two LIF instruments showed an excellent agreement over the 9 measurement days inside the SAPHIR chamber. Out of 3745 concurrent measurement points, we obtained from the linear regression analysis a slope equal to 0.86 and an intercept of $1.42 \pm 0.24 \times 10^5$, below the limit of detection of both instruments. The coefficient of determination was equal to 0.93 which indicated that a great part of the concentration variations as well as the absolute concentrations inside the chamber were observed by the two FAGE instruments. This result is interesting knowing that the conditions (chemistry, photochemistry) were very different from one day to another. The measured OH concentration range varied over two orders of magnitude approximately from 2.0×10^5 to 2.4×10^7 cm^{-3}.

From the day by day analysis, the slope varied from 0.73 to 1.12 and the intercept from -3.20×10^5 to 5.25×10^5 cm^{-3}. 8 out of the 9 days of measurements showed a high correlation between the two instruments with r^2 ranging from 0.76 to 0.95. On April 16th, the coefficient of determination r^2=0.56. The averaged concentration measured by the UL-FAGE was $[OH]_{ave} = 7.58 \pm 9.78 \times 10^5$ only two times higher than our limit of detection ($7.64 \pm 10.3 \times 10^5$ for the FZJ-FAGE). During half of the day, the OH concentration inside the chamber was below the limit of detection of both instruments. Thus, the correlation analysis may not be valid.

The calibration source exchange helped understanding the difference between the two instruments. The ratio ($[OH]_{FZJ}/[OH]_{Lille}$) obtained when UL-FAGE calibration source was placed on top of the FZJ-LIF nozzle, is in very good agreement with the ratio obtained for the all data set.

4.2. Intercomparison for HO_2

The linear regression analysis of the all data sets for the HO_2 measurements gave a slope of 1.50 and an intercept of $1.48 \pm 0.12 \times 10^7$ cm^{-3}. It showed that over the 9 measurement days the FZJ-FAGE measured 50% higher HO_2 concentration than the UL-FAGE. The overall uncertainty given by both instruments can not explain the differences observed by both

instruments. As it was observed during the HOxComp, the O_3 and H_2O dependency on the correlation were tested.

It can be concluded that the interference due to the RO_2 radicals had a significant impact on the HO_2 measurement. The two FAGE instruments were probably subject to the RO_2 interference with different magnitudes. In Table 9 is summarized the relative sensitivities of the two instruments toward the RO_2 of the hydrocarbon introduced inside the chamber during the intercomparative measurement. Lu et al (Lu et al., 2012) described a procedure that allows estimating the impact of the detection of RO_2 radicals on the measured HO_2 concentration measured. A strong effect of this interference was observed on April 22nd during the isoprene experiment. When isoprene was injected inside the chamber, the FZJ-LIF measured concentration up to 2 times higher than the UL-FAGE indicating that the peroxy radicals generated during isoprene oxidation gave rise to higher HO_2 signal in the FZJ-LIF than in the UL-FAGE. In Table 9 are summarized for both instruments the relative sensitivity of RO_2 radicals generated from the different species that were injected inside the chamber. It can be seen that the sensitivity for the isoprene-RO_2 is 3 times higher for the FZJ-LIF than for the UL-FAGE. This is in agreement with the large discrepancy observed on April 22nd.

Instead of correcting the HO_2 concentration for the interference, a model is used to compare the measured HO_2 concentration with $[HO_2^*]$ corresponding to the concentration of HO_2 plus a fraction of RO_2 detected as HO_2 ($[HO_2^*] = [HO_2] + \Sigma\alpha_{RO2}[RO_2]$). The relative sensitivity of each RO_2 obtained experimentally is used for the comparison. The modelling of HO_2 and RO_2 inside the SAPHIR chamber was not performed yet and so no conclusions will be given on the impact of RO_2 on the detection of HO_2 for both instruments. In addition, for the UL-FAGE, the relative sensitivity of the different RO_2 was not yet measured in the laboratory and only the one obtained from the MCM could be used.

During the course of the intercomparative measurement, unexplained formation of HO_2 was observed in the dark chamber especially on April 17th and on April 19th after the chamber was closed at then end of the measurement. These effects were already observed in previous measurement in the SAPHIR chamber and are due to some chamber effects which are not well characterized probably heterogeneous reactions on the wall of the chamber. It is interesting to observe that the response of both apparatus toward the unexplained HO_2 formation is contrasted. During the morning dark experiment on April 19th, both instruments agreed well within their respective errors whereas on April 17th and April 19th when the chamber was closed strong disagreement was observed between the two LIF. This

disagreement could indicate that RO_2 species are formed inside the chamber. These unknown HO_2 formation processes render the modelling even more complex.

Table 9. Comparison of the sensitivity to RO_2 species, α_{RO2}, for the UL-FAGE and the FZJ-LIF.
For the UL-FAGE, the sensitivities were obtained using the MCM v3.2. For the FZJ-LIF, the different sensitivities were obtained experimentally (Fuchs et al., 2011; Lu et al., 2012).

Species	UL-FAGE [NO] = 4.9×10^{13} cm^{-3} $\varepsilon_{HO2} = 0.45$	FZJ-LIF [NO] = 1.3×10^{14} cm^{-3} $\varepsilon_{HO2} > 0.90$
isoprene	0.24	0.79[a]
toluene	0.16	0.86[b]
p-xylene	0.15	0.86[b]
phenol	0.04	-

[a] Experimental values, [b] Estimation from benzene

4.2.1. Impact of H_2O on HO_2 measurements

During HOxComp, Fuchs et al. (Fuchs et al., 2010) reported that HO_2 measurements between the LIF instruments had larger discrepancy at low water concentration (0-0.6%) than at higher once (0.6-1.8%). For the present measurement, the water interference test was made twice: first on the 13th and repeated on the 16th. The protocol varied between these measurements and the HOxComp measurements. For the H_2O test, p-xylene and toluene were injected twice inside the chamber whereas only water was injected during HOxComp.

As already mentioned in the Results part, contradictory results were observed between the two instruments for both measurement days (see on Figure 15). To check the possibility of H_2O interference on the detection of HO_2 we binned the measurement data in 4 different ranges of H_2O concentration. On the 13th, we observed without any doubt a dependence of the HO_2 concentration measured by the two instruments on the water vapour whereas on the 16th the water dependence is less clear. In Table 10 are grouped the coefficients obtained from the regression analysis for each water concentration range. At low water ($[H_2O] < 0.1$ %), the slope is close to unity. For higher H_2O concentrations ($0.1\% < [H_2O] < 0.6\%$), the FZJ-LIF measured 38% more than the UL-FAGE. Above 0.6%, the slopes do not evolve and from the linear regression we obtained a slope of approximately 1.8. On the other hand, on the 16th, the H_2O dependence is less obvious. We did observe an increase in the slopes when the H_2O increase but only from 0.94 to 1.18.

The possible explanations for the observed differences are not clear knowing that the experiments were repeated using the same exact conditions. The observed H_2O dependency might have been actually biased by the RO_2 interference described by Fuchs et al. (Fuchs et al., 2011). In effect, p-xylene and toluene are both aromatics species and candidates to form RO_2 that can recycle OH after addition of NO inside the FAGE cells. Assuming that the main differences observed by the two LIF were due to different detection sensitivities towards these RO_2, the different results observed on the 13th and on the 16th showed the difficulty to apply any correction to the HO_2 measurements. The detection sensitivity of these RO_2 can be established in separate laboratory experiments nevertheless the RO_2 concentration inside the chamber will also depend on the oxidation conditions. On the 16th, the OH concentration measured inside the chamber was 3 times lower than on the 13th due to a lower light intensity that might have affected the RO_2 concentration and so the HO_2 measurements. From these measurements, we can not assess if the two LIF were influenced by water vapour due to this additional interference that render the analysis complex.

Table 10. Results obtained from the linear regression fit for the HO_2 data as function of [H_2O]. N is the number of points, a is the slope, b is the intercept in 10^6 cm^{-3}, r² is the coefficient of determination.

	[H_2O] = 0.00 to 0.10%		[H_2O] = 0.10 to 0.60%	
	April 13th	April 16th	April 13th	April 16th
N	149	143	145	60
a, slope	1.04 ± 0.00	0.94 ± 0.01	1.38 ± 0.08	1.04 ± 0.03
b, intercept	-0.23 ± 0.03	0.15 ± 0.05	0.46 ± 2.72	0.65 ± 0.42
r²	0.87	0.98	0.97	0.96
	[H_2O] = 0.60 to 1.20%		[H_2O] = 1.20 to 1.90%	
	April 13th	April 16th	April 13th	April 16th
N	111	97	123	58
a, slope	1.77 ± 0.13	1.18 ± 0.03	1.78 ± 0.15	1.12 ± 0.05
b, intercept	0.37 ± 4.66	0.31 ± 0.66	1.18 ± 2.68	1.65 ± 1.17
r²	0.99	0.99	0.99	0.97

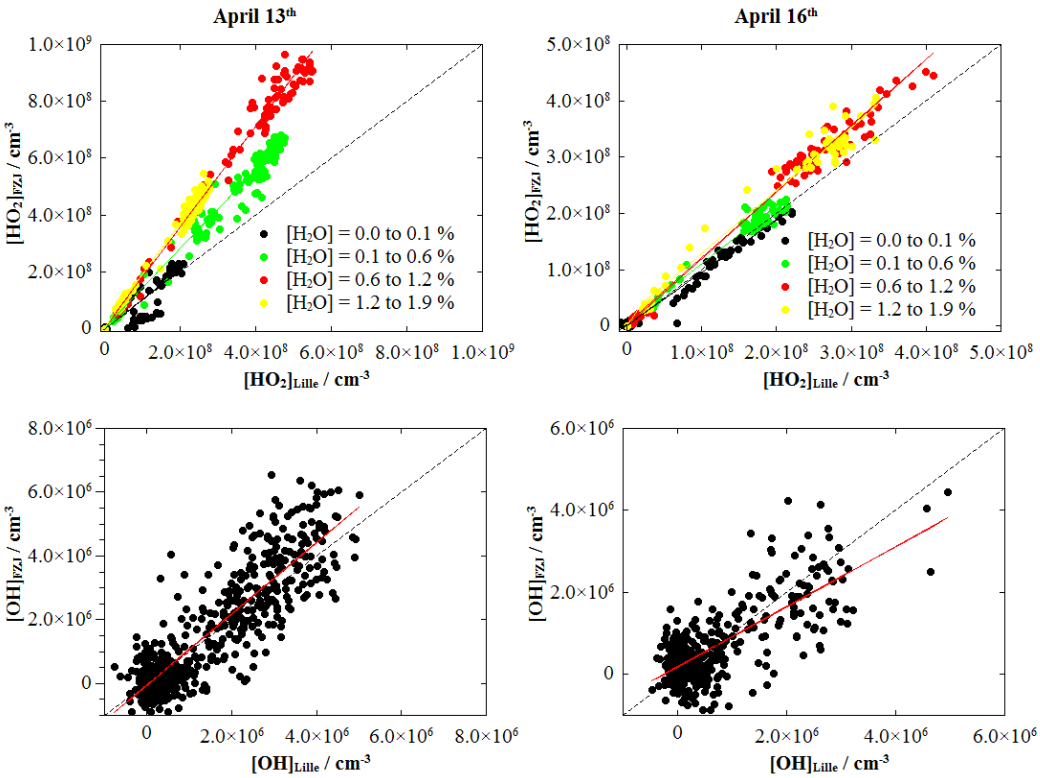

Figure 15. Scatter plots for the HO_2 and OH measurements on April 13th (left) and April 16th (right).
Top. For HO_2, the data were divided in groups of different water vapour concentration in the chamber between 0.0 to 0.1 % (black dots), 0.1 to 0.6 % (green dots), 0.6 to 1.2 % (red dots) and 1.2 to 1.9 % (yellow dots). Bottom. For OH, the correlation plots are shown for the all data set. The solid lines corresponds to a linear regression fit using the y=ax+b equation. The dashed line is the 1:1 line.

4.2.2. Impact of O_3 on HO_2 measurements

O_3 concentration inside the chamber was seen to influence the correlation between the different LIF instruments during HOxComp in dark conditions. Fuchs et al. (Fuchs et al., 2010) reported that the MPI-LIF measured higher HO_2 in the dark chamber than the two other LIF in the presence of O_3 whereas no correlation toward O_3 was observed when the chamber was illuminated. The results of the O_3 test made on the 14th were binned into different concentration range and as can be seen on Figure 16, the O_3 concentration did not influence the correlation between the two instruments when the chamber was illuminated as observed during HOxComp.

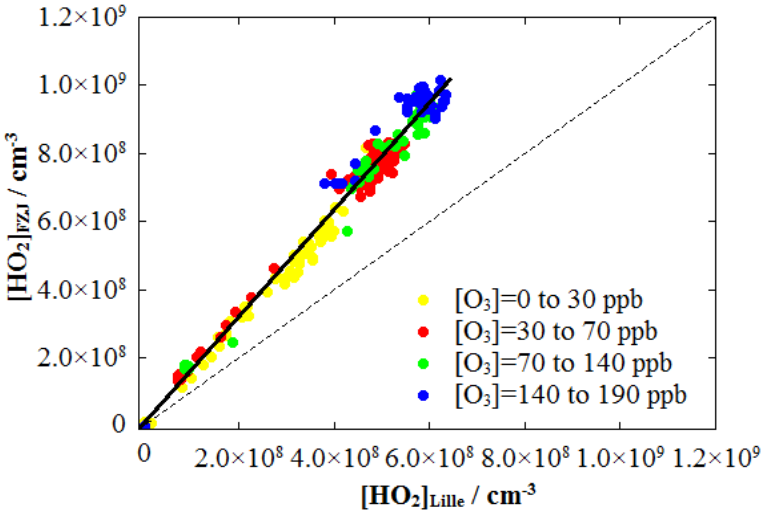

Figure 16. Scatter plots of HO_2 concentration on the 14th when the ozone concentration was varied.

Conclusion

The intercomparative measurement between the UL-FAGE and the FZJ-LIF was a success. The absence of absolute measurement techniques for OH and HO_2 made the quantitative analysis difficult however the FZJ-LIF was intercompared with the DOAS for OH (3 times) and with the MIESR for HO_2 (2 times) and has shown excellent agreement. In consequence, the FZJ-LIF can be considered as the reference instrument in this intercomparative measurement. Following the measurement protocol of the HOxComp campaign the two instruments were tested in a series of experiments where H_2O, O_3, NOx and VOC concentrations were varied in order to check their respective response.

For OH, the instruments agreed really well over the 9 days of measurements and none of them seemed to suffer from any significant interference.

For HO_2, the contrasted results showed the sensitivity of the two instruments towards the recently discovered RO_2 interference. The FZJ-LIF measured consistently higher concentration than the UL-FAGE. During the first 4 days of the intercomparative measurement. H_2O, O_3 and NOx were varied in order to determine the response of HO2 measurements to these species. However, the presence of toluene and p-xylene and their respective oxidation products in the chamber biased the results and no conclusions can be drawn on the possible interference on the detection of HO_2 towards H_2O, NOx and O_3. The isoprene experiment confirmed the high potential of this alkene to produce RO_2 radicals that can recycle OH inside the FAGE cells after the addition of NO. The strongly different results

observed on the 13th and the 16th when the H_2O interference test was repeated showed the difficult task that will arise when previous HO_2 measurements need to be corrected towards the RO_2 interference will be needed. Not only the concentration of the primary emitted VOC is needed but also a model calculation model with a detailed oxidation mechanism of each VOC species is needed to estimate the total RO_2 concentration.

From the phenol experiments, we observed that the disagreements between the two apparatus were less important than when toluene, p-xylene or isoprene were added to the chamber which could indicate that the peroxy radicals produced from the oxidation of phenol have a lower detection sensitivity in the HO_2 cell.

5. References

Apel, E. C., Brauers, T., Koppmann, R., Bandowe, B., Boßmeyer, J., Holzke, C., Tillmann, R., Wahner, A., Wegener, R., Brunner, A., Jocher, M., et al.: Intercomparison of oxygenated volatile organic compound measurements at the SAPHIR atmosphere simulation chamber, J. Geophys. Res., 113(D20), D20307, doi:10.1029/2008JD009865, 2008.

Aschmutat, U., Hessling, M., Holland, F. and Hofzumahaus, A.: A tunable source of hydroxyl (OH) and hydroperoxy (HO2) radicals: In the range between 10^6 and 10^9 cm-3., Physico-Chemical behaviour of Atmospheric Pollutants, G. Angeletti and G. Restelli, Proc. EUR 15609, 811-816., 1994.

Beck, S. M., Bendura, R. J., McDougal, D. S., Jr, J. M. H., Gregory, G. L., Jr, H. J. C., Davis, D. D., Bradshaw, J., Rodgers, M. O., Wang, C. C., Davis, L. I., et al.: Operational Overview of NASA GTE/CITE 1 Airborne Instrument Intercomparisons: Carbon Monoxide, Nitric Oxide, and Hydroxyl Instrumentation, J. Geophys. Res., 92(D2), 1977–1985, doi:10.1029/JD092iD02p01977, 1987.

Berndt, T. and Böge, O.: Gas-phase reaction of OH radicals with phenol, Phys. Chem. Chem. Phys., 5(2), 342–350, doi:10.1039/B208187C, 2003.

Bohn, B., Rohrer, F., Brauers, T. and Wahner, A.: Actinometric measurements of NO2 photolysis frequencies in the atmosphere simulation chamber SAPHIR, Atmos. Chem. Phys., 5(2), 493–503, doi:10.5194/acp-5-493-2005, 2005.

Brauers, T., Aschmutat, U., Brandenburger, U., Dorn, H.-P., Hausmann, M., Heßling, M., Hofzumahaus, A., Holland, F., Plass‐Dülmer, C. and Ehhalt, D. H.: Intercomparison of tropospheric OH radical measurements by multiple folded long‐path laser absorption and laser induced fluorescence, Geophys. Res. Lett., 23(18), 2545–2548, doi:10.1029/96GL02204, 1996.

Campbell, M. J., Hall, B. D., Sheppard, J. C., Utley, P. L., O'brien, R. J., Hard, T. M. and George, L. A.: Intercomparison of Local Hydroxyl Measurements by Radiocarbon and FAGE Techniques, Journal of the Atmospheric Sciences, 52(19), 3421–3428, doi:10.1175/1520-0469(1995)052<3421:IOLHMB>2.0.CO;2, 1995.

Eisele, F. L., Mauldin, L., Cantrell, C., Zondlo, M., Apel, E., Fried, A., Walega, J., Shetter, R., Lefer, B., Flocke, F., Weinheimer, A., et al.: Summary of measurement intercomparisons during TRACE-P, J. Geophys. Res., 108(D20), 8791, doi:10.1029/2002JD003167, 2003.

Eisele, F. L., Mauldin, R. L., Tanner, D. J., Cantrell, C., Kosciuch, E., Nowak, J. B., Brune, B., Faloona, I., Tan, D., Davis, D. D., Wang, L., et al.: Relationship between OH measurements on two different NASA aircraft during PEM Tropics B, J. Geophys. Res., 106(D23), 32683–32,689, doi:10.1029/2000JD900714, 2001.

Elshorbany, Y. F., Kleffmann, J., Hofzumahaus, A., Kurtenbach, R., Wiesen, P., Brauers, T., Bohn, B., Dorn, H.-P., Fuchs, H., Holland, F., Rohrer, F., et al.: HOx budgets during HOxComp: A case study of HOx chemistry under NOx-limited conditions, J. Geophys. Res., 117(D3), D03307, doi:10.1029/2011JD017008, 2012.

Fuchs, H., Ball, S. M., Bohn, B., Brauers, T., Cohen, R. C., Dorn, H.-P., Dubé, W. P., Fry, J. L., Häseler, R., Heitmann, U., Jones, R. L., et al.: Intercomparison of measurements of NO2 concentrations in the atmosphere simulation chamber SAPHIR during the NO3Comp campaign, Atmospheric Measurement Techniques, 3(1), 21–37, doi:10.5194/amt-3-21-2010, 2010a.

Fuchs, H., Bohn, B., Hofzumahaus, A., Holland, F., Lu, K. D., Nehr, S., Rohrer, F. and Wahner, A.: Detection of HO2 by laser-induced fluorescence: calibration and interferences from RO2 radicals, Atmospheric Measurement Techniques, 4(6), 1209–1225, doi:10.5194/amt-4-1209-2011, 2011.

Fuchs, H., Brauers, T., Dorn, H.-P., Harder, H., Häseler, R., Hofzumahaus, A., Holland, F., Kanaya, Y., Kajii, Y., Kubistin, D., Lou, S., et al.: Technical Note: Formal blind intercomparison of HO2 measurements in the atmosphere simulation chamber SAPHIR during the HOxComp campaign, Atmos. Chem. Phys., 10(24), 12233–12250, doi:10.5194/acp-10-12233-2010, 2010b.

Fuchs, H., Brauers, T., Dorn, H.-P., Harder, H., Häseler, R., Hofzumahaus, A., Holland, F., Kanaya, Y., Kajii, Y., Kubistin, D., Lou, S., et al.: Technical Note: Formal blind intercomparison of HO2 measurements in the atmosphere simulation chamber SAPHIR during the HOxComp campaign, Atmos. Chem. Phys., 10(24), 12233–12250, doi:10.5194/acp-10-12233-2010, 2010c.

Fuchs, H., Brauers, T., Dorn, H.-P., Harder, H., Häseler, R., Hofzumahaus, A., Holland, F., Kanaya, Y., Kajii, Y., Kubistin, D., Lou, S., et al.: Technical Note: Formal blind intercomparison of HO2 measurements in the atmosphere simulation chamber SAPHIR during the HOxComp campaign, Atmos. Chem. Phys., 10(24), 12233–12250, doi:10.5194/acp-10-12233-2010, 2010d.

Fuchs, H., Brauers, T., Häseler, R., Holland, F., Mihelcic, D., Müsgen, P., Rohrer, F., Wegener, R. and Hofzumahaus, A.: Intercomparison of peroxy radical measurements obtained at atmospheric conditions by laser-induced fluorescence and electron spin resonance spectroscopy, Atmospheric Measurement Techniques, 2(1), 55–64, doi:10.5194/amt-2-55-2009, 2009a.

Fuchs, H., Brauers, T., Häseler, R., Holland, F., Mihelcic, D., Müsgen, P., Rohrer, F., Wegener, R. and Hofzumahaus, A.: Intercomparison of peroxy radical measurements obtained at atmospheric conditions by laser-induced fluorescence and electron spin resonance spectroscopy, Atmospheric Measurement Techniques, 2(1), 55–64, doi:10.5194/amt-2-55-2009, 2009b.

Fuchs, H., Dorn, H.-P., Bachner, M., Bohn, B., Brauers, T., Gomm, S., Hofzumahaus, A., Holland, F., Nehr, S., Rohrer, F., Tillmann, R., et al.: Comparison of OH concentration measurements by DOAS and LIF during SAPHIR chamber experiments at high OH reactivity and low NO concentration, Atmospheric Measurement Techniques, 5(7), 1611–1626, doi:10.5194/amt-5-1611-2012, 2012.

Guenther, A., Hewitt, C. N., Erickson, D., Fall, R., Geron, C., Graedel, T., Harley, P., Klinger, L., Lerdau, M., Mckay, W. A., Pierce, T., et al.: A global model of natural volatile organic compound emissions, J. Geophys. Res., 100(D5), 8873–8892, doi:10.1029/94JD02950, 1995.

Hard, T. M., Chan, C. Y., Mehrabzadeh, A. A. and O'Brien, R. J.: Diurnal HO2 Cycles at Clean Air and Urban Sites in the Troposphere, J. Geophys. Res., 97(D9), 9785–9794, doi:10.1029/92JD00232, 1992.

Hard, T. M., O'Brien, R. J., Chan, C. Y. and Mehrabzadeh, A. A.: Tropospheric free radical determination by fluorescence assay with gas expansion, Environ. Sci. Technol., 18(10), 768–777, doi:10.1021/es00128a009, 1984.

Holland, F., Hessling, M. and Hofzumahaus, A.: In Situ Measurement of Tropospheric OH Radicals by Laser-Induced Fluorescence—A Description of the KFA Instrument, Journal of the Atmospheric Sciences, 52(19), 3393–3401, doi:10.1175/1520-0469(1995)052<3393:ISMOTO>2.0.CO;2, 1995.

Kanaya, Y., Hofzumahaus, A., Dorn, H.-P., Brauers, T., Fuchs, H., Holland, F., Rohrer, F., Bohn, B., Tillmann, R., Wegener, R., Wahner, A., et al.: Comparisons of observed and modeled OH and HO2 concentrations during the ambient measurement period of the HOxComp field campaign, Atmos. Chem. Phys., 12(5), 2567–2585, doi:10.5194/acp-12-2567-2012, 2012.

Kubistin, D., Harder, H., Martinez, M., Rudolf, M., Sander, R., Bozem, H., Eerdekens, G., Fischer, H., Gurk, C., Klüpfel, T., Königstedt, R., et al.: Hydroxyl radicals in the tropical troposphere over the Suriname rainforest: comparison of measurements with the box model MECCA, Atmos. Chem. Phys., 10(19), 9705–9728, doi:10.5194/acp-10-9705-2010, 2010.

Lu, K. D., Rohrer, F., Holland, F., Fuchs, H., Bohn, B., Brauers, T., Chang, C. C., Häseler, R., Hu, M., Kita, K., Kondo, Y., et al.: Observation and modelling of OH and HO2 concentrations in the Pearl River Delta 2006: a missing OH source in a VOC rich atmosphere, Atmos. Chem. Phys., 12(3), 1541–1569, doi:10.5194/acp-12-1541-2012, 2012.

Mao, J., Jacob, D. J., Evans, M. J., Olson, J. R., Ren, X., Brune, W. H., Clair, J. M. S., Crounse, J. D., Spencer, K. M., Beaver, M. R., Wennberg, P. O., et al.: Chemistry of hydrogen oxide radicals (HOx) in the Arctic troposphere in spring, Atmos. Chem. Phys., 10(13), 5823–5838, doi:10.5194/acp-10-5823-2010, 2010.

Mount, G. H., Eisele, F. L., Tanner, D. J., Brault, J. W., Johnston, P. V., Harder, J. W., Williams, E. J., Fried, A. and Shetter, R.: An intercomparison of spectroscopic laser long-path and ion-assisted in situ measurements of hydroxyl concentrations during the Tropospheric OH Photochemistry Experiment, fall 1993, J. Geophys. Res., 102(D5), 6437–6455, doi:10.1029/96JD02342, 1997.

Peeters, J., Nguyen, T. L. and Vereecken, L.: HOx radical regeneration in the oxidation of isoprene, Phys. Chem. Chem. Phys., 11(28), 5935–5939, doi:10.1039/B908511D, 2009.

Platt, U., Alicke, B., Dubois, R., Geyer, A., Hofzumahaus, A., Holland, F., Martinez, M., Mihelcic, D., Klüpfel, T., Lohrmann, B., Pätz, W., et al.: Free Radicals and Fast Photochemistry during BERLIOZ, Journal of Atmospheric Chemistry, 42(1), 359–394, doi:10.1023/A:1015707531660, 2002.

Ren, X., Edwards, G. D., Cantrell, C. A., Lesher, R. L., Metcalf, A. R., Shirley, T. and Brune, W. H.: Intercomparison of peroxy radical measurements at a rural site using laser-induced fluorescence and Peroxy Radical Chemical Ionization Mass Spectrometer (PerCIMS) techniques, J. Geophys. Res., 108(D19), 4605, doi:10.1029/2003JD003644, 2003.

Ren, X., Mao, J., Brune, W. H., Cantrell, C. A., Mauldin III, R. L., Hornbrook, R. S., Kosciuch, E., Olson, J. R., Crawford, J. H., Chen, G. and Singh, H. B.: Airborne intercomparison of HOx measurements using laser-induced fluorescence and chemical ionization mass spectrometry during ARCTAS, Atmospheric Measurement Techniques, 5(8), 2025–2037, doi:10.5194/amt-5-2025-2012, 2012.

Ren, X., Olson, J. R., Crawford, J. H., Brune, W. H., Mao, J., Long, R. B., Chen, Z., Chen, G., Avery, M. A., Sachse, G. W., Barrick, J. D., et al.: HOx chemistry during INTEX-A 2004: Observation, model calculation, and comparison with previous studies, J. Geophys. Res., 113(D5), D05310, doi:10.1029/2007JD009166, 2008.

Rohrer, F., Bohn, B., Brauers, T., Brüning, D., Johnen, F.-J., Wahner, A. and Kleffmann, J.: Characterisation of the photolytic HONO-source in the atmosphere simulation chamber SAPHIR, Atmos. Chem. Phys., 5(8), 2189–2201, doi:10.5194/acp-5-2189-2005, 2005.

Schlosser, E., Bohn, B., Brauers, T., Dorn, H.-P., Fuchs, H., Häseler, R., Hofzumahaus, A., Holland, F., Rohrer, F., Rupp, L., Siese, M., et al.: Intercomparison of Two Hydroxyl Radical Measurement Techniques at the Atmosphere Simulation Chamber SAPHIR, Journal of Atmospheric Chemistry, 56(2), 187–205, doi:10.1007/s10874-006-9049-3, 2007.

Schlosser, E., Brauers, T., Dorn, H.-P., Fuchs, H., Häseler, R., Hofzumahaus, A., Holland, F., Wahner, A., Kanaya, Y., Kajii, Y., Miyamoto, K., et al.: Technical Note: Formal blind intercomparison of OH measurements: results from the international campaign HOxComp, Atmos. Chem. Phys., 9(20), 7923–7948, doi:10.5194/acp-9-7923-2009, 2009a.

Schlosser, E., Brauers, T., Dorn, H.-P., Fuchs, H., Häseler, R., Hofzumahaus, A., Holland, F., Wahner, A., Kanaya, Y., Kajii, Y., Miyamoto, K., et al.: Technical Note: Formal blind intercomparison of OH measurements: results from the international campaign HOxComp, Atmos. Chem. Phys., 9(20), 7923–7948, doi:10.5194/acp-9-7923-2009, 2009b.

Taraborrelli, D., Lawrence, M. G., Crowley, J. N., Dillon, T. J., Gromov, S., Groß, C. B. M., Vereecken, L. and Lelieveld, J.: Hydroxyl radical buffered by isoprene oxidation over tropical forests, Nature Geoscience, 5(4), 300–300, doi:10.1038/ngeo1433, 2012.

Volkamer, R., Klotz, B., Barnes, I., Imamura, T., Wirtz, K., Washida, N., Becker, K. H. and Platt, U.: OH-initiated oxidation of benzene, Phys. Chem. Chem. Phys., 4(9), 1598–1610, doi:10.1039/B108747A, 2002.

Whalley, L. K., Edwards, P. M., Furneaux, K. L., Goddard, A., Ingham, T., Evans, M. J., Stone, D., Hopkins, J. R., Jones, C. E., Karunaharan, A., Lee, J. D., et al.: Quantifying the magnitude of a missing hydroxyl radical source in a tropical rainforest, Atmos. Chem. Phys., 11(14), 7223–7233, doi:10.5194/acp-11-7223-2011, 2011.

Wisthaler, A., Apel, E. C., Bossmeyer, J., Hansel, A., Junkermann, W., Koppmann, R., Meier, R., Müller, K., Solomon, S. J., Steinbrecher, R., Tillmann, R., et al.: Technical Note: Intercomparison of formaldehyde measurements at the atmosphere simulation chamber SAPHIR, Atmos. Chem. Phys., 8(8), 2189–2200, doi:10.5194/acp-8-2189-2008, 2008.

Ambient HOx measurements: CompOH, SURFIN

Introduction

In this chapter is presented the results obtained from the deployment of the UL-FAGE in two different campaigns CompOH and Surfin. The UL-FAGE was also deployed for 7 weeks September-October 2010 in Goldlauter (Germany) during the HCCT campaign. The results from this measurement will not be presented in this thesis. The aim of the CompOH campaign was to intercompare the UL-FAGE with the LATMOS-CIMS for OH measurements. This campaign is complementary to the first intercomparison between the UL-FAGE and the FZJ-LIF in the SAPHIR chamber in April 2010. Firstly, contrary to the Juelich comparison, the two instruments use OH detection systems which are fundamentally different, mass spectrometry for the CIMS and LIF for the FAGE. The interest is that they will be subject to different kinds of interferences. Secondly, the intercomparison was held in ambient air, contrary to the controlled conditions in the atmospheric simulation chamber in Juelich. One of the drawbacks to intercompare two instruments in ambient air is the possibility that they are sampling different air masses which might bias the results. In addition, the chemistry is more complex and the variety of species is greater and therefore more realistic. The campaign was held in July 2011 near Paris. The preliminary results are presented here.

In the second part, we present the results obtained during the SURFIN campaign that was held in downtown Marseille at the end of July 2011. The goal of SURFIN was to understand the chemical mechanism that lead to the formation of pollutant such as HONO indoors. HOx radicals are known to play a role in the indoor chemistry however their concentrations are expected to be very low and no direct OH and HO_2 measurements were reported. Up to now, the role of radicals in the indoor chemistry is considered as minor. During the indoor field campaign, OH and HO_2 radicals were observed above the detection limit of the UL-FAGE up to 1.5×10^6 cm^{-3} for OH and 2.0×10^7 cm^{-3} for HO_2. A correlation between the HONO concentration, the HONO photolysis rate and the measured OH concentration was established indicating the key role of HONO as a source of OH radicals. The preliminary results are presented.

1. CompOH

The CompOH field campaign took place in Palaiseau near Paris from the 1st to the 12th of July 2011. The field campaign had two main objectives. The first one was the intercomparison between the UL-FAGE and the LATMOS-CIMS (Kukui et al., 2008) in ambient conditions for 5 days. In the second part of the campaign, 3 different instruments that measure OH reactivity were compared: the LSCE-CRM, the MPI-CRM and the UL-OH reactivity system (see Chapter 5).

In this part, the interest will be focused on the intercomparison between the CIMS and the FAGE instruments for the quantification of OH radicals. The CIMS and the FAGE techniques are the main instruments available for the measurement of OH radicals. Both techniques own sufficient time resolution and detection limit for atmospheric measurement. The description of the CIMS technique was given in the Chapter 1. Basically, OH radicals are converted into H_2SO_4 after addition of SO_2 into a reactor at atmospheric pressure. H_2SO_4 is then ionized and measured as HSO_4^- using mass spectrometry. It is the most sensitive technique for the measurement of OH radicals with limit of detection close to 1×10^5 cm^{-3}. The fundamental differences between the two techniques are of interest as they will be subject to different kinds of interferences.

The CIMS and the FAGE techniques have already been compared in the past and the results can be found in Table 1 of Chapter 3. Three intercomparison were made between the ATHOS-LIF and the NCAR-CIMS during airborne measurements: PEM Tropics B (Eisele et al., 2001), TRACE-P (Eisele et al., 2003) and ARCTAS (Ren et al., 2012). For the PEM Tropics B and the TRACE-P campaigns, the two instruments were set in two different aircrafts and the intercomparison took place when they were at the same location. For TRACE-P, the two instruments showed a very good correlation with r^2=0.88 and a slope equal to a=0.96 (after correction, for more details see Chapter 3) indicating an excellent agreement between the two instruments. However, for both PEM Tropics B and TRACE-P campaigns the ratio between the CIMS and the LIF decreases for higher altitudes. During ARCTAS, a very detailed analysis was made for the results of the intercomparison between the NCAR-CIMS and the ATHOS-LIF. Contrary to the two first airborne campaigns, the two instruments were located inside the same aircraft. The agreement between the two instruments was good with a correlation r^2=0.72 and a slope a=0.89. The differences were in most cases explained by the combined measurement uncertainty of the instruments. The OH

measurement by the NCAR-CIMS and the ATHOS-LIF were compared to a box model. The observed-to-modeled OH ratio was compared as function of the NO and isoprene concentrations. For very low NO concentration, the observed-to-model OH ratio was higher for the LIF than for the CIMS whereas the opposite is seen at high NO where the observed-to-model OH ratio was higher for the CIMS than for the LIF indicating differences between the instruments. Both instruments observed an increase of the observed-to-model OH ratio when isoprene concentration increased. This indicates that either isoprene oxidation mechanisms are incomplete or both techniques suffered from the same interference in environments dominated by BVOC.

Another intercomparison between the DWD-CIMS and 3 other LIF instruments (FZJ-LIF, FRCGC-LIF, MPI-LIF) was made in 2005 during HOxComp in ambient air in Juelich, Germany (Schlosser et al., 2009). The correlation between the LIF instruments and the CIMS was good with r^2>0.82. Each instrument pair showed good correlation. On the other hand, the slopes were in a range between 0.59 and 0.75 indicating that the LIF instruments systematically measured higher concentration than the CIMS instruments. The measured differences were explained due to the instrument locations which impacted the intercomparative measurement as different air masses were sampled. The intercept was insignificant between the DWD-CIMS and two LIF instruments (FZJ-LIF and FRCGC-LIF) whereas it was important between the DWD-CIMS and the MPI-LIF but was not explained. The DWD-CIMS was not intercompared in the chamber due to some technical problems.

The instruments intercompared in this study are the UL-FAGE and the LATMOS-CIMS. The UL-FAGE was compared with the FZJ-LIF inside the SAPHIR chamber and showed a very good correlation r^2=0.93 and a slope equal to 0.86 with an insignificant intercept over a large range of conditions (see Chapter 3). The small observed difference could be explained in great part by differences in the calibration of the two instruments. The LATMOS-CIMS was intercompared with another FAGE instrument in the EUPHORE atmospheric chamber in Valencia. Differences were observed depending on the relative humidity. The agreement was very good at low humidities (RH< 10 %) whereas strong disagreement was observed at high humidities. The LATMOS-CIMS was deployed during the MEGAPOLI campaign on the same site as the present work (Michoud et al., 2012) and during OPALE (Oxidant production over Antarctica land and its export) in Antarctica (Kukui et al., 2012; Preunkert et al., 2012).

HOx measurements in urban and suburban areas were reviewed previously in different studies (Dusanter et al., 2009; Stone et al., 2012). Measurements in such areas are of importance as they help to understand and characterize the coupling between HOx and NOx in the presence

of VOCs that leads to the formation of pollutants species like O_3 and particles. The comprehension of the urban chemistry is essential to draw strategies aiming at reducing anthropogenic impact on air quality. These environments are characterized with high concentrations of O_3 and NOx up to hundreds of ppb. Measured HOx concentrations were observed to be as high as 20×10^6 cm^{-3} during the SOS campaign in Nashville (Martinez et al., 2003) and as low as 1.4×10^6 cm^{-3} during the PMTACS winter campaign in New-York (Ren et al., 2006). During day time, the HONO photolysis, the carbonyl photolysis and the reaction of O_3 with alkenes was identified as important sources of HOx radicals (Stone et al., 2012). Detection of HOx radicals during night-time measurements in urban environments is rare because their concentrations are close to the limit of detection of most instruments. At night, if the NO concenctration is low enough, the main oxidants are O_3 and NO_3 which reacts rapidly with unsaturated hydrocarbons to produce OH and HO_2 radicals. During BERLIOZ, concentrations of 1.8×10^5 cm^{-3} and 1.0×10^8 cm^{-3} were observed for OH and HO_2 respectively (Geyer et al., 2003). Similar concentrations were observed during the TORCH campaign (Lee et al., 2009). The highest OH concentration reported at night was measured during the PROPHET campaign (Sillman et al., 2002) with concentration of 0.04 ppt (~1.0×10^6 cm^{-3}). The HO_2 concentration was 5.0×10^7 cm^{-3} during the same period.

1.1. Experimental section

1.1.1. Site description

The intercomparative measurement campaign between the UL-FAGE and the LATMOS-CIMS took place between the 1st and 5th July 2012 at the SIRTA (“Site Instrumental de Recherche par Télédétection Atmosphérique”) observatory (Haeffelin et al., 2005; Pietras et al., 2007). The SIRTA is a French national atmospheric observatory dedicated to cloud and aerosol research and is located at Palaiseau in “Ecole Polytechnique” area (48.718°N, 2.207°E), 20 km south-west of Paris (France) in a semi-urban environment. The site is downwind of Paris under anticyclonic conditions and receives oceanic air masses from west from the France the rest of the time (Freutel et al., 2012).

1.1.2. Ancillary measurements

The intercomparative measurement was supported by a set of ancillary measurements. Other than OH, the UL-FAGE measured HO_2 and the LATMOS-CIMS measured the sum of peroxy

radicals $\Sigma(RO_2+HO_2)$ species. Total OH reactivity measurement were made with the MPI-CRM (Nölscher et al., 2012; Sinha et al., 2008) and the LSCE-CRM (Dolgorouky et al., 2012). Photolysis frequencies measurement (j(O1D), $j(NO_2)$, j(HONO), j(HCHO) and $j(NO_3)$) were made using a spectroradiometer (B. Bohn, "Institut für Energie und Klimaforschung", Forschungszentrum Jülich). The spectroradiometer was placed on top of the Lille container. The stable species measured were O_3 (Thermo 49 i), NOx (Thermo 42 i), CO (GC), HONO (NitroMac, (Huang et al., 2002)), HCHO (Le Calvé et al., 2009), VOC (GC, cartridge) and meteorological parameters (T, P, RH, wind direction). The VOC species were not measured during the first days (start on the 4th) of the campaign and so their measurements are not being discussed here, more attention will be given in the Chapter 5. The location of the different instruments is displayed on Figure 1.

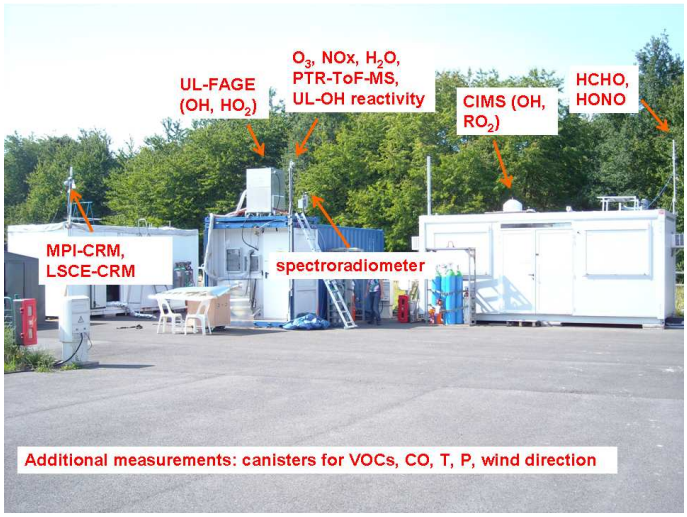

Figure 1. Photograph of the measurement site during CompOH with the location of the different instruments.

The LATMOS-CIMS measured OH and RO_2 radicals from the 2nd up to the 10th of July. The UL-FAGE measured OH and HO_2 radicals from the 1st to the 5th. On the 5th, the maxima of the two OH profiles measured by the UL-FAGE and the LATMOS-CIMS were shifted by approximately 2 hours with maximum of approximately 1.5×10^7 cm^{-3} for both instruments. This disagreement was already discussed during a data workup meeting in Ocober 2011 and no explanations have been found yet. It is worth noticing that on the 5th, the UL-FAGE suffered from some troubles with the mass flow controller that regulate the NO flow. In consequence, we intervened on top of the UL-FAGE container to replace the faulty MFC with

a spare one. During this operation, the NO line had to be open and burst of NO was released on the site. However, changing the MFC took only 15 min and it is unlikely that the NO concentration released into the atmosphere had such an impact on the local chemistry knowing that the two instruments were only separated by approximately 4 meters. In consequence, the intercomparative measurement is limited to the first 3 common measurement days (02/07, 03/07, 04/07) and the night between the 4th and the 5th.

The performances of the two instruments during CompOH are given in Table 1. The UL-FAGE was calibrated at the beginning of the campaign (30/06) and at the end of the intercomparison (05/07). The average of the two calibration points was used for obtaining the OH concentration, C_{OH}= (1.83±0.21) × 10^{-6} cts/s/cm^{-3}/mW. The UL-FAGE calibration source was placed on top of the LATMOS-CIMS inlet. The results have not been analyzed yet and so will not be shown in this work. The LATMOS-CIMS was also calibrated after the campaign with a calibration cell based also on the water photolysis.

Table 1. Performances of the UL-FAGE and the LATMOS-CIMS for OH measurement

Instruments	LOD /cm^{-3}	Time resolution / s	Uncertainty 1σ
UL-FAGE	4.5 × 10^5	60	15 %
LATMOS-CIMS	5.0 × 10^5	600	15 %

1.2. Results and discussion

The first five days of the CompOH campaign are displayed on Figure 2. The conditions were similar for the 5 measurement days. The temperature increased slowly from the 1st to the 5th. The temperature average was of 290 K with a maximum of 302 K during the day and a minimum of 281 K at night. The sky was almost cloud free for the entire measurement period. The average relative humidity was ~51 %. On the morning of the 4th, a pollution plume from the morning traffic was measured at the site with NO concentration increasing up to 15 ppb, NO_2 up to 25 ppb and CO up to 220 ppb. It corresponded to the highest reactivity measurement during this period with k'_{OH}=15 s^{-1}. Generally, the OH reactivity measured spanned between 1 and 7 s^{-1}. The O_3 concentration displayed a diurnal profile with a maximum in the afternoon and a minimum at night. From the 1st to the 3rd, the O_3 concentration observed were similar with maximum of 60 ppb during the day and a minimum of 20 ppb at night. On the 4th, the O_3 concentration increased sharply up to 80 ppb and during

the night between the 4th and the 5th the O_3 observed concentrations stayed at approximately 40 ppb. The OH concentration profiles were similar from the 1st up to the 4th with exception of the 5th where higher concentrations were measured. The HONO concentration was only partially measured since the NITROMAC instrument suffered from technical problems. The maximum concentration was observed on the morning of the 4th with a value of [HONO]~10 ppt. The formaldehyde concentration was relatively steady with an averaged concentration of 3.2 ppb. In Table 3 and Table 2 are summarized the different species measured along with their mean, maximum and minimum values.

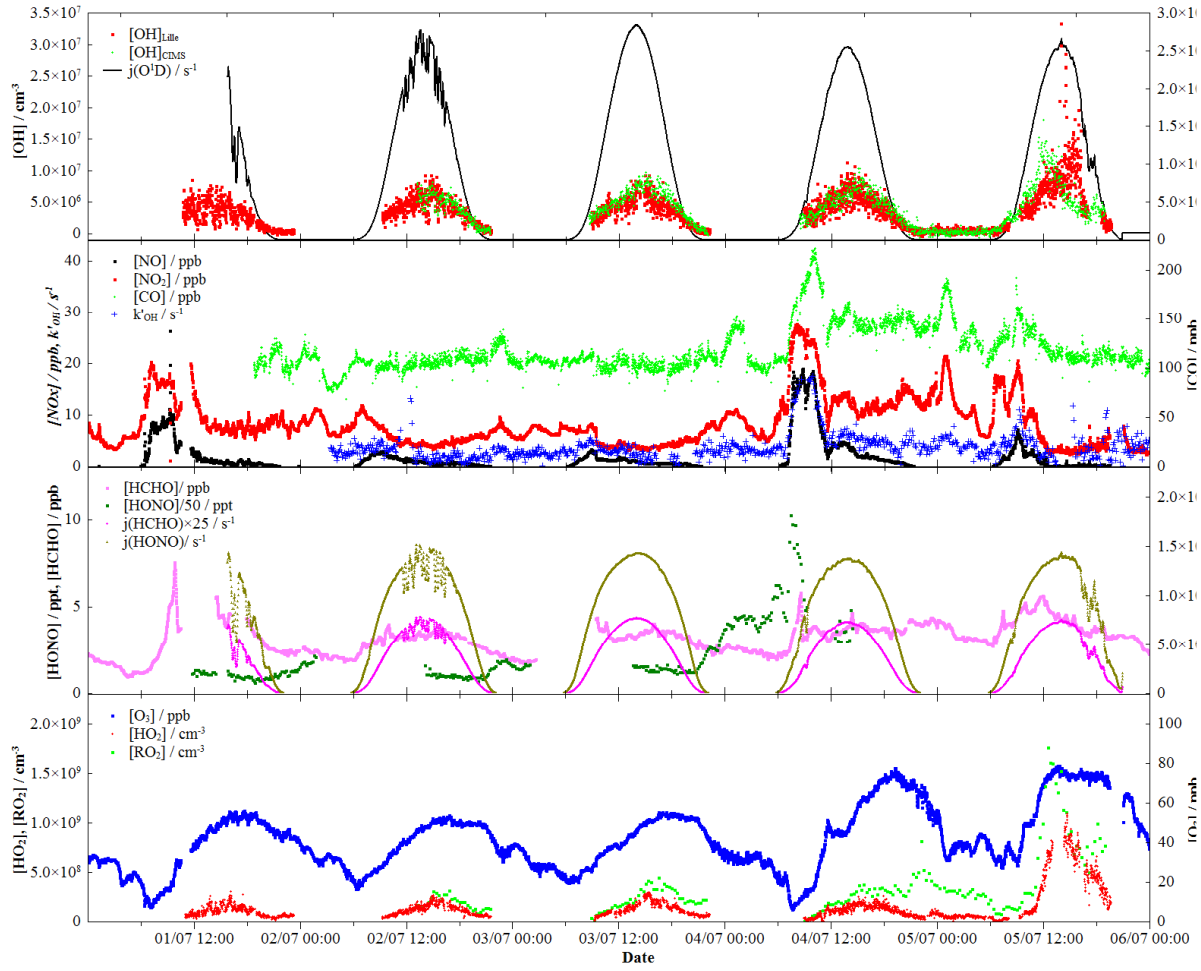

Figure 2. Measurement profiles during the OH quantification intercomparison
Top – OH measurement profiles for the UL-FAGE and the CIMS in cm^{-3}, $j(O^1D)$ in s^{-1}
2nd window – NO_x and CO measurement profile in ppb, k_{OH} (MPI-CRM) in s^{-1}
3rd window – HCHO and HONO measurement profiles in ppb and ppt respectively, j_{HCHO} and j_{HONO} in s^{-1}
Bottom – HO_2 and RO_2 measurement profiles in cm^{-3}, O_3 in ppb

Table 2. [OH], [HO_2] and [RO_2] concentrations measured during CompOH
The data measured on the 5th were not taken into account.

	[OH] / 10^6 cm^{-3}		[HO_2] / 10^8 cm^{-3}		[RO_2] / 10^8 cm^{-3}	
	mean	max	mean	max	mean	max
UL-FAGE	3.49 ± 2.62	12.49	1.04 ± 0.59	3.27	-	-
LATMOS-CIMS	3.63 ± 2.66	10.29	-	-	2.43 ± 1.18	8.17

Table 3. Summary of the mean, maximum and minimum of the ancillary measurements during CompOH from 01/07 to 04/07.

Species	mean	min	max
NO / ppb	2.4 ± 3.6	0.1	19.8
NO_2 / ppb	8.4 ± 4.7	0.9	27.7
O_3 / ppb	41.8 ± 16.4	0.5	79.0
CO / ppb	118.8 ± 22.9	75.3	222.5
HCHO / ppb	3.2 ± 0.9	0.10	7.6
HONO / ppt	111.7 ± 90.0	31.0	512.1
Photolysis rates			
$j(O^1D)$ / 10^{-6} s^{-1}	7.6 ± 9.4	0	28.4
j(HONO) / 10^{-4} s^{-1}	5.8 ± 5.5	0	15.2
j(HCHO) /10^{-5} s^{-1}	1.1 ± 1.1	0	3.2
$j(H_2O_2)$ / 10^{-6} s^{-1}	2.6 ± 2.6	0	7.3
OH reactivity			
k'_{OH} / s^{-1}	3.6 ± 2.3	*-1.5*	17.5

1.2.1. Intercomparative measurement

The data for both instruments were interpolated to 1 min. All the scatter plots are shown on Figure 3 and the results are summarized in Table 4. During the 3 measurement days 1630 data points were measured simultaneously. By taking the entire data set and plotting $[OH]_{CIMS}$ as function of the $[OH]_{FAGE}$ on a scatter plot, we obtained a slope of a=0.87 ± 0.01 and a correlation coefficient of r^2=0.75. The intercept obtained from the linear regression analysis was of b=(5.74 ± 0.54) × 10^5 cm^{-3}. The analysis was repeated for each individual measurement days as well as the night between the 4th and the 5th (from 22:00 to 6:00). Disparities are observed between the different measurement days with a slope varying from 0.69 on the 4th to 0.94 on the 3rd. We also observed significant intercepts above the detection limit of both instruments when looking at individual measurement days with a maximum intercept equal to (14.27 ± 1.21) × 10^5 cm^{-3} on the 4th. The difference between the relatively low intercept obtained from the analysis of the all data set with the large intercepts obtained on the 3rd and the 4th is due to the presence of the night data where the LATMOS-CIMS

measured on averaged 50 % less OH than the UL-FAGE. Indeed, during the night measurement a strong disagreement is observed between the two instruments. The night was characterized by a high and steady O_3 concentration. High HO_2 concentrations were also measured with the UL-FAGE. A detailed description of the night measurement is given in the paragraph 1.2.2.

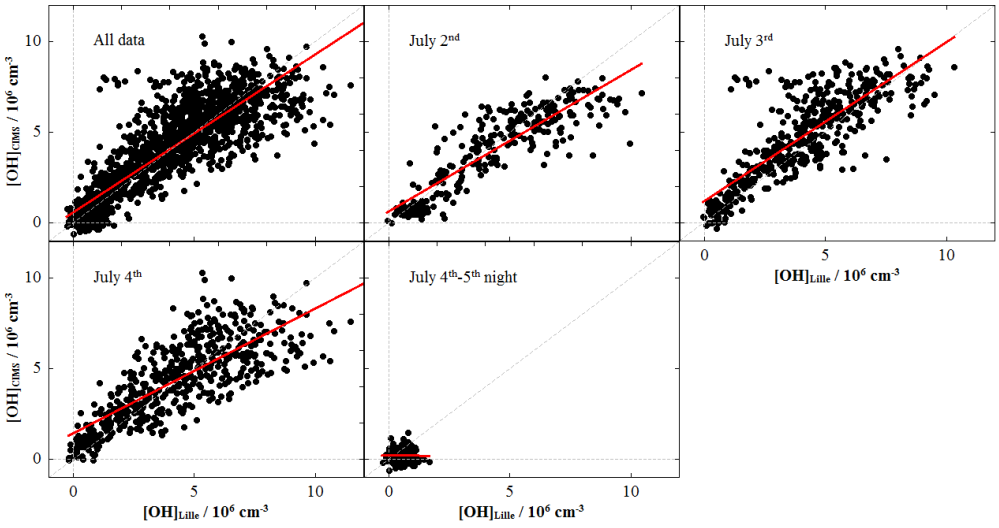

Figure 3. Scatter plots of day by day OH measurements and for all OH measurements during CompOH.
Solid lines represent linear regression analysis.

Table 4. Results obtained from the statistical analysis for OH measurements.
N is number of common points. a, is the slope, b is the intercept in 10^5 cm^{-3} obtained from the linear regression analysis using the equation $y=ax + b$. a_0 is the slope obtained from the $y=a_0x$ equation.

Date	N	a, slope	b, intercept	r^2	a_0
02/07/2011	279	0.78 ± 0.03	6.25 ± 1.24	0.77	0.89 ± 0.01
03/07/2011	463	0.94 ± 0.02	11.52 ± 0.90	0.61	1.10 ± 0.02
04/07/2011	534	0.69 ± 0.02	14.27 ± 1.21	0.61	0.94 ± 0.01
04-05/07/2011 night	269	-	-	-	-
All	1630	0.87 ± 0.01	5.74 ±0.54	0.75	0.98 ± 0.01

The results obtained from the day by day analysis indicate that at least one of the instruments suffers from an interference affecting the measurement. Nevertheless, the slopes are in the same range than for the other intercomparisons, with higher concentrations measured for the FAGE compared to the CIMS, like reported by Schlosser et al. (Schlosser et al., 2009) during HOxComp. Therefore, our results are consistent with the results obtained at HOxComp. Also,

similarly to the (DWD-CIMS – MPI LIF) instrument pair we observed a significant intercept that can not be explained. The correlation is not as good as the previous intercomparitive measurement (from 0.61 to 0.77 for this campaign compared to r^2>0.72 for previously reported studies, see Chapter 3). Taking into account the combined uncertainties of the two instruments and the fact that ambient air masses were probed, we can consider that the instruments are in a relatively good agreement.

In order to understand the differences observed between the two instruments, we plotted the $[OH]_{CIMS}/[OH]_{Lille}$ concentration ratio as function of different chemical species. The dependence of the $[OH]_{CIMS}/[OH]_{Lille}$ concentration ratio as function of NO, O_3, H_2O and $[OH]_{Lille}$ is shown on Figure 4. On the NO dependence, the agreement is observed to be better at higher NO concentrations. For O_3, the agreement is good between the two instruments except when $[O_3]$ >70 ppb with a ratio equal to 1.44. The UL-FAGE is subject to an O_3 interference which was observed to be independent of the laser power (1.7×10^3 [OH] cm^{-3} per ppb of O_3). However under the O_3 concentration range measured during CompOH the interference signal would not exceed 1×10^5 cm^{-3}. Therefore, the UL-FAGE OH measurements were not corrected for the known O_3 interference. For the dependence on H_2O, the agreement is worse for higher H_2O concentrations but the observed difference is within the combined uncertainties (±56% at 2σ). When we plot the $[OH]_{CIMS}/[OH]_{Lille}$ concentration ratio as function of the $[OH]_{Lille}$, we see that the ratio is varying from 0.7 at high OH concentration to 1.4 at low OH concentration. This confirms that the correlation between the two instruments is not linear over the measured concentration range. The UL-FAGE measured higher concentrations than the CIMS in the high OH concentration range. In the low concentration range, the UL-FAGE measured lower concentrations than the CIMS. It is interesting to notice that the opposite is observed during the night time measurement (low OH concentrations) where the UL-FAGE measured higher concentration than the LATMOS-CIMS. From these results, no clear correlation can be made between the variation of the concentration of O_3, NO and H_2O and the discrepancies between the instruments. In order to characterize the differences between the two instruments, a chemical model will be performed as it has been done by Ren et al. (Ren et al., 2012) for ARCTRAS.

Here, we have presented the preliminary results of the intercomparative measurement between the UL-FAGE and the LATMOS-CIMS. The general agreement is good however significant observed discrepancies need to be understood.

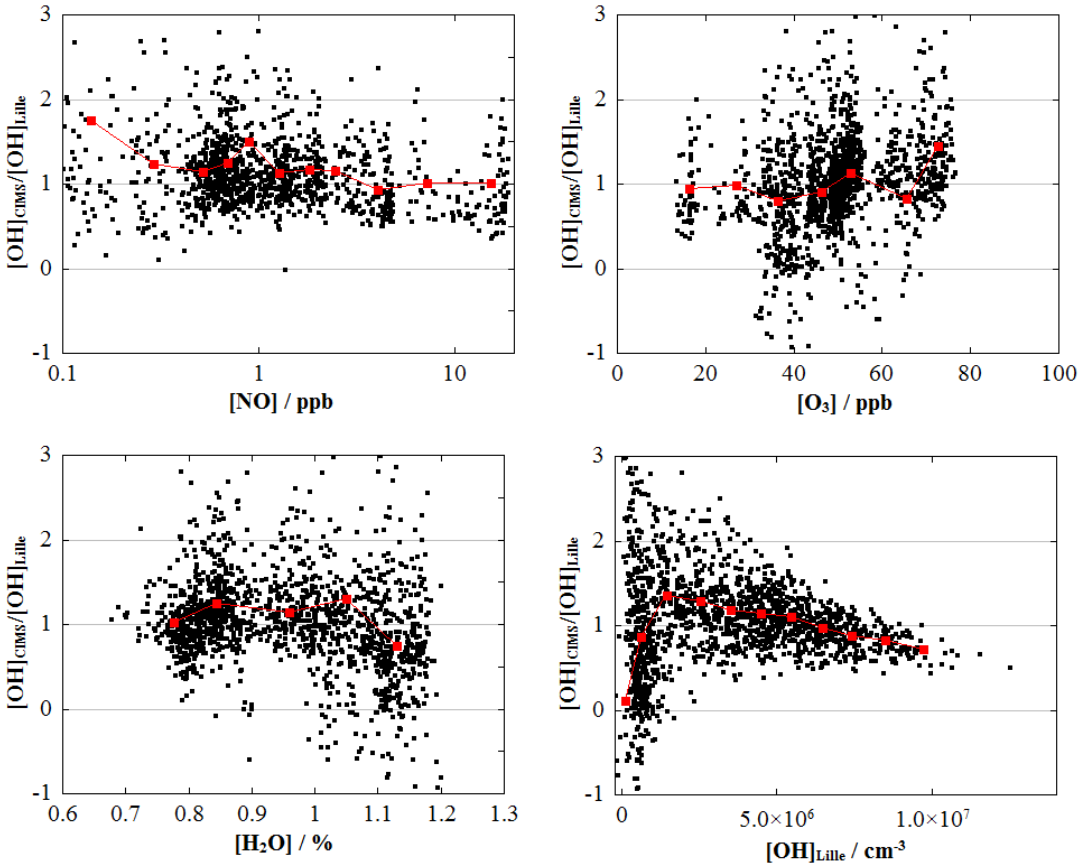

Figure 4. Dependence of the $[OH]_{CIMS}/[OH]_{Lille}$ ratio as function of NO (left), O_3 (right) and H_2O (bottom)
The data point are interpolated to 1 min.
The red square are the averaged calculated on binned NO, O_3 and H_2O data

1.2.2. Nighttime measurement

During CompOH, measurements of OH and HO_2 were made during the night between the 4th and the 5th. The mean and maximum concentrations of the different species measured are given in Table 5. As can be seen on Figure 5, the CO along with the NO_2 concentration reached a maximum at around 1 am. The ozone concentration decreased through the night from ~70 ppb to ~35 ppb and was on averaged of 44 ppb. The NO concentration decreased rapidly below the detection limit (0.1 ppb) of the analyzer after twilight. VOC measurement were made with cartridges during the night measurement and mean values are shown in Table 6. Toluene and m,p-xylene were having the highest concentration with 2.54 ppb and 1.56 ppb respectively. The VOC concentration increased along with the CO and NO_2 concentration during the night indicating that the measurement site certainly received the plume from Paris.

We observed that the OH concentration decreased for both instruments along with the ozone photolysis rate, $j(O^1D)$. The UL-FAGE measured higher OH concentration than the LATMOS-CIMS. The ratio between the $[OH]_{CIMS}/[OH]_{Lille}$ was of 0.54 and improved to 0.65 when the UL-FAGE data were corrected for the O_3 interference. The measurement of HO_2 showed a more complex profile. First the HO_2 concentration decreased from 7×10^8 cm^{-3} to 4×10^8 cm^{-3} at 22:00. Afterwards, we observed an increase of the HO_2 concentration up to 1.3×10^8 cm^{-3} around midnight before the HO_2 concentration decreases while CO and NO_2 increased up to 5×10^8 cm^{-3}. Then, the HO_2 concentration stayed constant until 6 am. A sharp decreased down to 1×10^7 cm^{-3} is then observed when the NO_2 concentration increased.

Table 5. Mean and maximum values for the different measurement between 22:00 and 6:00 on the 4th to 5th night.

Species	Mean	Max
$[OH]_{Lille}$ / cm^{-3}	$4.20 \pm 3.28 \times 10^5$	1.67×10^6
$[OH]_{Lille}$ / cm^{-3} (O_3 correction)	$3.45 \pm 3.28 \times 10^5$	-
$[OH]_{CIMS}$ / cm^{-3}	$2.25 \pm 3.49 \times 10^5$	1.54×10^6
$[HO_2]_{Lille}$ / cm^{-3}	$5.96 \pm 4.84 \times 10^7$	1.27×10^8
$[RO_2]_{CIMS}$ / cm^{-3}	$3.40 \pm 1.22 \times 10^8$	8.17×10^8
k'_{OH} / s^{-1}	2.68 ± 1.98	7.79
[NO] / ppb	<0.1	<0.1
$[NO_2]$ / ppb	11.9 ± 4.0	21.5
$[O_3]$ / ppb	44.3 ± 9.8	69.3
[HCHO] / ppb	3.6 ± 0.5	4.4
[CO] / ppb	122.7 ± 50.7	191.8
$j(O^1D)$ / s^{-1}	$<1.7 \times 10^{-8}$	-

Table 6. Mean and standard deviation of VOC measurements during the 4th to 5th night.

VOC species	Mean / ppb	SD / ppb	VOC species	Mean / ppb	SD / ppb
benzene	0.21	0.04	1,3,5 TMB	0.26	0.06
ethyl benzene	0.53	0.08	1,2,4 TMB	0.51	0.13
heptane	0.17	0.03	1,2,3 TMB	0.13	0.03
octane	0.18	0.04	m,p xylene	1.56	0.29
toluene	2.54	0.38	isoprene	3×10^{-3}	4×10^{-2}
o-xylene	0.52	0.09			

The observed variation in the HO_2 concentration during that night indicates that the HOx chemistry was rather complex. The discrepancy between the OH measurement between the UL-FAGE and the LATMOS-CIMS is not clear however the measurement was supported with extensive ancillary measurements and a future box model simulation might help to understand these differences.

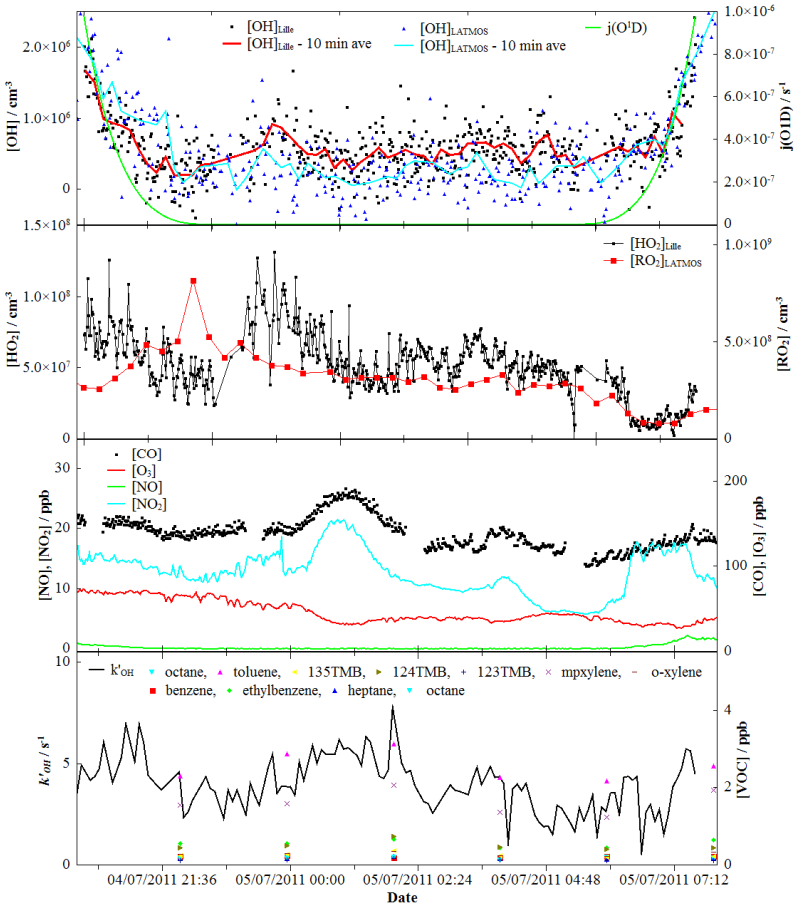

Figure 5. Nighttime measurement during CompOH between the 4th and the 5th.
1st plate (top) – OH measurements from the LIF (black dots) and the CIMS instrument (blue triangles). The red and blue solid line are the 10 min average for the $[OH]_{Lille}$ and the $[OH]_{CIMS}$ respectively. The green line is the ozone photolysis rate, $j(O^1D)$.
2nd plate – HO_2 (black squares) and RO_2 (red squares) measurements from the LIF and the CIMS instruments
3rd plate – Measurement of CO (black squares), O_3 (red line), NO (green line) and NO_2 (blue line)
4th plate – OH reactivity measurement by the MPI-CRM, VOC measurements

1.2.3. Profile interpretation

In order to interpret the profiles obtained, another type of analysis can be performed based on a simple calculation of the main production and consumption pathways. As already discussed in Chapter 1, the primary production of OH is from the photolysis of O_3 to produce an excited oxygen atom that reacts with H_2O to form OH (reactions (R 1) and (R 2)).

$O_3 + h\nu\ (\lambda<310\ nm) \rightarrow O(^1D) + O_2$ (R 1)

$O(^1D) + H_2O \rightarrow 2\ OH$ (R 2)

The primary production P(OH) is then given as

$$P(OH) = 2 \times f \times [O_3] \times j(O^1D) \quad \text{Eq. 1}$$

where $j(O^1D)$ is the photolysis rate of ozone and f is

$$f = \frac{k_{O^1D+H_2O}[H_2O]}{k_{O^1D+H_2O}[H_2O] + k_{O^1D+N_2}[N_2] + k_{O^1D+O_2}[O_2]} \quad \text{Eq. 2}$$

where the $k_{O1D+H2O}$, k_{O1D+N2} and k_{O1D+O2} are the reaction rates for the reaction with H_2O and the quenching reaction with O_2 and N_2.

The highly complex mechanism of OH consumption renders the prediction of the OH concentration difficult however it was observed that the OH concentration followed a linear relationship with respect to the $j(O^1D)$ ozone photolysis rate (Ehhalt and Rohrer, 2000). The steady state OH concentration can be assumed to the ratio between the OH production from the O3 photolysis, P(OH) divided by the OH losses, L(OH) via the reaction of OH with its different sinks (e.g. hydrocarbons, NO_2)

$$[OH] = \frac{P(OH)}{L(OH)} \quad \text{Eq. 3}$$

A similar relationship can be obtained for HO_2 and $j(O^1D)$. Under low NOx conditions, HO_2 is lost mainly via its self reaction so the HO_2 concentration will be proportional to the square root of $j(O^1D)$.

The empirical equation that described the relationship between the OH concentration and the ozone photolysis rate is given by

$$[OH \text{ or } HO_2] = a \times j(O^1D)^b + c \quad \text{Eq. 4}$$

where the coefficients *a*, *b* and *c* represent the average influence of the chemical environment at a specific location on OH (Rohrer and Berresheim, 2006). The exponent *b* reflects the combined effect of the different photolytic processes (photolysis of O_3, H_2O_2, HONO, HCHO and NO_2). The coefficient *a* represents the chemical sources and sinks of OH and the term c reflects the contribution of all the light independent processes. High linear correlation using

this equation reflects that the chemistry involved can be well represented by a simple model based on the OH steady state assumption and is mainly driven by variations of $j(O^1D)$. The coefficients a, *b* and *c* for different campaigns were summarized by Stone et al. (Stone et al., 2012).

On Figure 6 is shown the correlation plots of $j(O^1D)$ with OH and HO_2 during CompOH. For OH the correlation was observed to be independent of the NO concentration. The data were fitted using Eq. 4 by fixing the coefficient b to 1 (linear fit) and by letting the coefficient b free. The correlation obtained were similar for both fit (0.67 for b=1 and 0.69 for b free) indicating that 70 % of the OH variation can be explained by the variation of $j(O^1D)$. Dusanter et al (Dusanter et al., 2009) observed a very low linear correlation between OH and $j(O^1D)$ (r^2= 0.16) during the MCMA campaign in Mexico in a very polluted environment. The slope (a) representing the specificity of the local chemistry was of 3.33×10^{11} cm^{-3} (2.05×10^{11} cm^{-3} when b=1). This value is one of the highest reported (see Table 8) however most of the campaigns were in remote areas (e.g MBL, Antarctica). During the TORCH campaign, Emmerson et al. (Emmerson et al., 2007) observed a slope of 1.07×10^{11} cm^{-3} for a power coefficient b equal to 1.06. In our case, the coefficient b was obtained to be of 0.62. This reflects that in our condition the HOx chemistry was complex and that a steady state approach in which OH is mainly produced via the O_3 photolysis is not appropriate.

For HO_2, the linear correlation between HO_2 and $j(O^1D)$ for the all data sets was low with r^2=0.36. Nevertheless, we observed as expected that the correlation varied depending on the NO concentration In previous studies, the “low NO regime” was set to be below 130 ppt for Holland et al. (Holland et al., 2003) and below 300 ppt for Kanaya et al. (Kanaya et al., 2001). The “low NO regime” is defined when the main loss of HO_2 is through its self reaction. The correlation between $j(O^1D)$ and HO_2 was observed to be dependent to the square root of $j(O^1D)$ between 0.1 and 1.0 ppb with b=0.55. A correlation r^2=0.76 was obtained for NO concentration below 0.5 ppb lower than the correlation obtained by Vaughan et al. (Vaughan et al., 2012) during the SOS campaign in Cap Verde (see Table 9). Between 1 and 2 ppb, no correlation can be observed between $j(O^1D)$ and $[HO_2]$, this transitional regime was observed between 0.3 and 1 ppb by Kanaya et al. (Kanaya et al., 2001). Above 2 ppb, the correlation between $j(O^1D)$ and HO_2 was observed to be linear indicating that HO_2 radicals might be lost principally by reactions with molecules other than HO_2 (Kanaya et al., 2001). All the results from the data analysis for OH and HO_2 are given in Table 7.

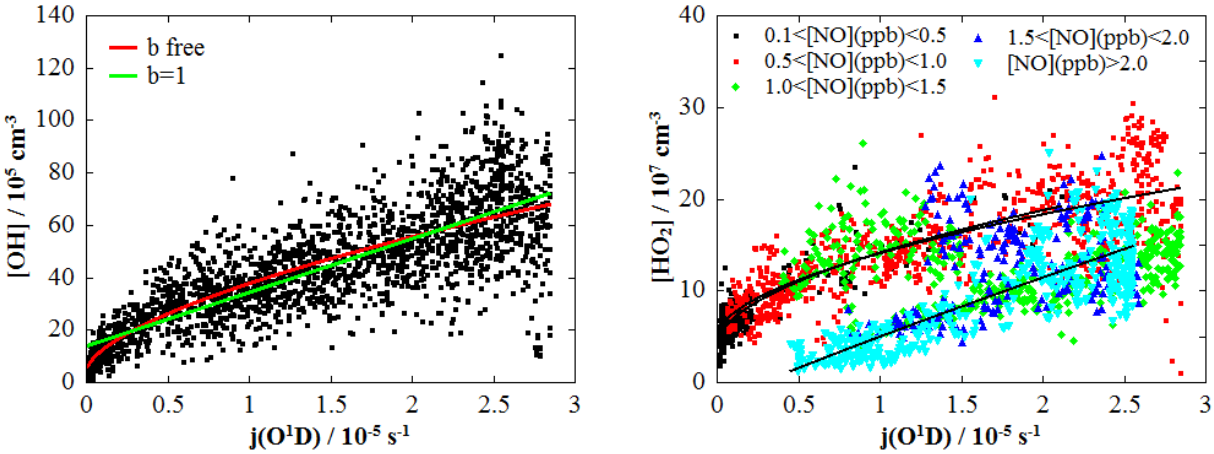

Figure 6. Correlation of $j(O^1D)$ with OH (left) and HO_2 (right).

The correlation coefficients r^2 for linear regression analysis are 0.67 for OH and 0.36 for HO_2 for the all data set.
Left panel – The solid lines correspond to the non-linear regression fit using Eq. 4 for a fixed b and for a fee b. Right panel – Correlation of $j(O^1D)$ with HO_2 with different NO concentration.
The data were binned in different categories corresponding to different NO concentration range. Black squres: 0.1<NO(ppb)<0.5; Red squares: 0.5<NO(ppb)<1.0, Green lozenges: 1.0<NO(ppb)<1.5, Dark blue triangles: 1.5<NO(ppb)<2.0, Light blue triangles NO(ppb)>2.0

Table 7. Summary of the coefficients obtained from Eq. 4 for OH and HO_2

		a / 10^{11} cm^{-3}	b	c / 10^6 cm^{-3}	r^2
[OH]		3.33 ± 0.15	0.62 ± 0.03	0.46 ± 0.12	0.69
		(2.05 ± 0.03)	(1)	(1.40 ± 0.05)	(0.67)
		a / 10^{12} cm^{-3}	b	c / 10^7 cm^{-3}	r^2
	0.1<NO(ppb)<0.5	1.00 ± 0.46	0.55 ± 0.05	4.16 ± 0.37	0.76
	0.5<NO(ppb)<1.0	9.06 ± 1.38	0.55 ± 0.08	5.04 ± 1.24	0.58
[HO_2]	1.0<NO(ppb)<1.5	-	-	-	0.08
	1.5<NO(ppb)<2.0	-	-	-	0.17
	NO(ppb)>2.0	7.32 ± 2.10	0.91 ± 0.19	-2.24 ± 2.06	0.69

The concentration of OH showed good correlation as function of $j(O^1D)$. The coefficients obtained are in the same range as previously observed. For HO_2, we observed a dependence of the correlation with $j(O^1D)$ as function of the NO concentration. Under low NO condition (NO < 1.0 ppb), the HO_2 concentration was dependent to the square of $j(O^1D)$ whereas the dependence was observed to be linear at high NO concentrations (NO > 2.0 ppb).

1.2.4. HO_2/OH concentration ratio

The HO_2/OH ratio is an interesting parameter as it depends on the processes that interconvert HOx radicals. The HO_2/OH ratio depends on the NOx and the VOC concentration. OH reacts with VOC, CO and O_3 to produce HO_2 whereas HO_2 reacts with NO and O_3 to regenerate OH thus the ratio HO_2/OH is decreasing when the concentration of NO increased. During the CompOH campaign, the NO concentration was on averaged of 2.4 ± 3.6 ppb with peaks up to ~20 ppb. On Figure 7 is represented the HO_2/OH ratio measured as function of the NO concentration. Observed ratio varied between 10 and 120 for NO concentration between 0.1 and 20 ppb.

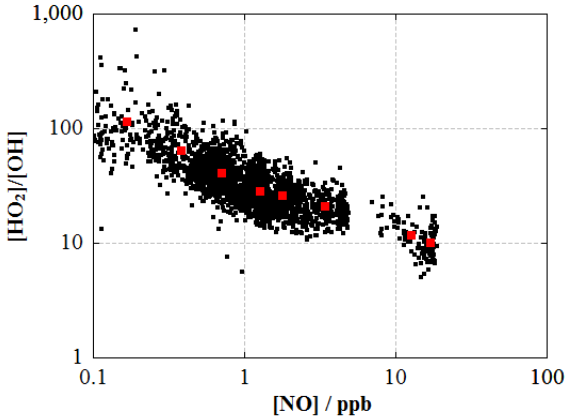

Figure 7. Correlation plot between the HO_2/OH ratio and NO
Red squares are the mean calculated on binned NO data

Dusanter et al. (Dusanter et al., 2009) summarized the campaigns in urban and in suburban areas in which the HO_2/OH ratio was measured. The results obtained during CompOH are consistent with the previous observations. During TORCH campaign, the HO_2/OH ratio varied from 10 to 70 for NO concentrations between 0.3 and 9.9 ppb similar to our conditions (Emmerson et al., 2007).

Table 8. Summary of the correlation between [OH] and $j(O^1D)$
a, b and c are in molecules cm^{-3}. Adapted from Stone et al. (Stone et al., 2012)

Campaign	Location	Year	$a/10^{11}$	b	$c/10^6$	r^2	References
POPCORN	Rural Germany	1994	3.9	0.95	0.04 ± 0.01	0.86	(Holland et al., 1998; Rohrer and Berresheim, 2006)
ALBATROSS	Remote Atlantic Ocean	1996	1.4	1.3	0.20 ± 0.21	0.72	(Brauers et al., 2001; Rohrer and Berresheim, 2006)
BERLIOZ	Rural Germany	1998	2.0	0.95	0.43 ± 0.02	0.91	(Holland et al., 2003; Rohrer and Berresheim, 2006)
MOHp	Rural Germany	1998–2003	2.4	0.93	0.13 ± 0.01	0.88	(Rohrer and Berresheim, 2006)
MINOS	Coastal Crete	2001	2.2	0.68	0.01 ± 0.05	0.90	(Berresheim et al., 2003; Rohrer and Berresheim, 2006)
NAMBLEX	Coastal Ireland	2002	1.47 ± 0.08	0.84 ± 0.05	0.44 ± 0.06	-	(Sommariva et al., 2006)
TORCH	Urban UK	2003	1.07 ± 0.04	1.16 ± 0.05	0.62 ± 0.03	-	(Emmerson et al., 2007; Stone et al., 2012)
CHABLIS	Antarctica	2005	0.25 ± 0.16	0.74 ± 0.04	0.11 ± 0.12	-	(Bloss et al., 2007; Stone et al., 2012)
RHaMBLe	Coastal Cape Verde	2007	1.73 ± 0.57	0.90 ± 0.25	0.9 ± 0.45		(Stone et al., 2012; Whalley et al., 2010)
OP3	Tropical forest Borneo	2008	0.94 ± 0.11	0.61 ± 0.09	0.20 ± 0.07	-	(Stone et al., 2012; Whalley et al., 2011)
SOS	Coastal Cape Verde	2009	1.19	0.98 ± 0.05	0.50	0.59	(Vaughan et al., 2012)
OPALE	Antarctica	2011	1.58	0.56	0.03	0.71	(Kukui et al., 2012)

Table 9. Summary of the correlation between $[HO_2]$ and $j(O^1D)$
a, b and c are in molecules cm^{-3}. [NO] is in ppb.

Campaign	Location	Year	[NO]	a	b	$c/10^6$	r^2	References
SOAPEX	Coastal Tasmania	1999	<0.002	-	0.49 ± 0.03	-	-	(Creasey et al., 2003)
ORION99	Coastal Okinawa	1999	<0.3	-	~0.5	-	-	(Kanaya et al., 2001)
			>1		~1.0			
BERLIOZ	Rural Germany	1998	all data	-	-	-	0.36	(Holland et al., 2003)
SOS	Coastal Cape Verde	2009	<0.1	4.72	0.53 ± 0.02	7.5	0.88	(Vaughan et al., 2012)

1.3. Summary of the CompOH campaign

The intercomparative measurement between the UL-FAGE and the LATMOS-CIMS was a success. The two instruments measured simultaneously during 3and a half days. The last day of the intercomparison was not taken into account as the two instruments measured very different profiles. The reasons for these observations are not clear and investigation is under way. The correlation between the two instruments was good with r^2=0.75. The slope indicating the absolute agreement between the LIF and the CIMS was of 0.87 within the uncertainty errors of the two instruments and an intercept of 5.74×10^5 cm^{-3}. However, when analyzing individual days we observed a great disparity with significant intercepts. During the nighttime measurement the UL-FAGE measured 40% more than the LATMOS-CIMS. The possibility that one or both instruments were subject to interferences is raised. For the UL-FAGE, no discrepancies were observed when it was compared with the FZJ-LIF in the SAPHIR chamber. A future model study might help to understand these disparities.

In a second part, the interpretation of the OH and HO_2 profile as function of the photolysis frequency was made. For OH, we observed that the chemistry during CompOH could not be assimilated to a simple steady state. The HO_2 concentration was observed to be dependent to the square root of $j(O^1D)$ at low NO concentration (NO< 0.5 ppb) in agreement with previous studies. For NO concentration higher than 2 ppb, the dependence between HO_2 and $j(O^1D)$ was linear. The ratio HO_2/OH was shown to vary between 10 and 120 for NO concentration varying between 0.3 and 20 ppb.

2. SURFIN

The project SURFIN was lead by the Laboratoire Chimie Provence (University of Provence) in collaboration with the PC2A (University of Lille) and the LISA (University of Paris 7 and 12). The aim of the project was to study indoor chemistry and its impact on air quality.

In recent years, more attention was given on indoor air quality as people in urban areas spend almost 90% of their time indoor (Finalyson-Pitts and Pitts, 2000). The main indoor pollutants can be emitted from indoor sources, transported from outdoor or produced indoor through chemical reactions. Sources of indoor pollutants are various from cooking to cleaning products or smoking with emissions of particles, CO, NOx and VOC.

For NOx species, observations have shown that indoor concentrations were generally higher than outdoor concentrations especially when combustion sources were present in the room. Otherwise, the indoor and outdoor concentrations were shown to have similar concentration profiles since removal of NO and NO_2 is relatively slow on surfaces (Finalyson-Pitts and Pitts, 2000). HONO is a major indoor pollutant (Finlayson-Pitts et al., 2003) and the reaction of NO_2 on surfaces in the presence of H_2O via (R 3) is known as a major source

$$2NO_2 + H_2O \xrightarrow{surface} HONO + HNO_3 \qquad \text{(R 3)}$$

HONO can also be directly emitted from gas stoves and concentrations up to several tens of ppb were measured in indoor environments (Febo and Perrino, 1991). HONO concentrations increased rapidly in an unvented room in the presence of NO_2 whereas they decrease rapidly when the room is vented (e.g. windows open). For VOC species, indoor sources are numerous (e.g. carpets, furniture polish, room freshener,…) with concentrations generally higher than outdoor. OVOCs such as aldehydes and ketones are also among the volatile species which are directly emitted indoors. In contrast with the other gas species, concentrations of ozone, a strong outdoor pollutant, are generally lower indoor compared to outdoor since it is decomposed on surfaces or titrated with NO to produce NO_2 (Finalyson-Pitts and Pitts, 2000).

Indoor gas phase reactions are mainly dominated by the ozonolysis of alkenes which initiates radical chemistry through the formation of OH. The chemistry is then similar to the outdoors chemistry where hydrocarbon species are oxidized by OH to produce peroxy radicals which generate HO_2 in the presence of NO. Finally, HO_2 is recycled to OH via the reaction with NO. Reactions of O_3 with alkenes are slow and steady state OH concentrations were estimated to be of 1.7×10^5 cm^{-3} assuming indoor O_3 concentration of 20 ppb (Weschler and Shields,

1996) and typical alkenes concentrations (up to few ppb). Weschler and Shields (Weschler and Shields, 1997) reported the first indirect indoor OH measurements. They measured the decay of 1,3,5-trimethylbenzene concentration after injecting O_3 (~100 ppb) and d-limonene (~100 ppb) inside a room. 1,3,5-trimethylbenzene has the advantage of only reacting with the OH produced from the ozonolysis of d-limonene. An average OH concentration of 7.5×10^5 cm^{-3} was found. For more information, indirect measurements and model study of the OH indoor chemistry were reviewed by White et al. (White et al., 2010).

One of the major differences between indoor and outdoor is the lower photolysis rates. Outdoor the radical chemistry is driven by photochemical reactions which are initiated by the photolysis of species such O_3 or HONO. Indoor, photolytic sources of radicals are strongly reduced as regular windows (BK7) have only a low transmission in the UV spectral range and the ratio of visible light transmitted versus UV light transmitted was estimated to be of ~3 to 5 (Carslaw, 2007). On Figure 8 is represented the HONO spectrum in the UV along with the light transmission through a BK7 glass window.

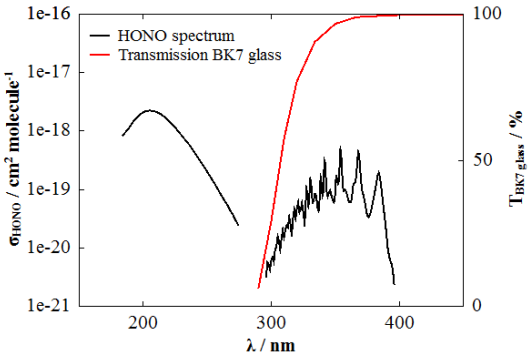

Figure 8. HONO spectrum and light transmission through a BK7 glass window

Carslaw (Carslaw, 2007) performed a model study in which a detailed chemical model (MCM) was used to investigate indoor air chemistry. The results predicted OH concentration up to 4×10^5 cm^{-3} and up to 10 ppt (~2.4×10^8 cm^{-3}) for HO_2. In the base case scenario, the outdoor photolysis rates were calculated using a 2-stream scattering model (Hough, 1988) and the transmission in the visible was assumed to be $T_{visible}$=10% and in the UV T_{UV}= 3%. Sensitivity tests were made for different photolysis rate intensities considering the only two previous studies from Nazaroff and Cass (Nazaroff and Cass, 1986) ($T_{visible}$=0.7%, T_{UV}=0.15%) and from Drakou et al. (Drakou et al., 1998) ($T_{visible}$=25-30%, T_{UV}=70-80%). Using the light conditions from Drakou et al. (Drakou et al., 1998), the OH concentration was increased by 248% and by 54% for HO_2 whereas using the light conditions from Nazaroff and

Cass, the OH concentration decreased by 41% along with the HO_2 concentration by 8%. These findings highlighted the importance of the indoor photolysis rate intensities. Especially the transmission in the UV causes uncertainties concerning the concentration of OH which can be produced indoor through photolysis phenomena. This is why as recommended by Weschler (Weschler, 2011) in a recent review on indoor air, direct indoor measurements of OH concentrations are strongly needed.

The OH radical concentration measurement indoor was attempted in a classroom in Marseille city centre in July 2011. OH and HO_2 radicals were measured using the UL-FAGE, others measured species were HONO, O_3, NOx, aldehydes, photolysis frequencies and VOC.

2.1. Instrumentation

The UL-FAGE performance during the SURFIN campaign is given Table 10. The UL-FAGE was calibrated twice at the beginning of the campaign and in the middle of the second week.

Table 10. Performance of the UL-FAGE during SURFIN
C is the sensitivity in cts/s/cm^{-3}/mW, LOD is the limit of detection in cm^{-3} for S/N=2

	C	LOD (1 min)	LOD (10 min)
OH	1.58×10^{-6}	4.5×10^{5}	1.4×10^{5}
HO_2	6.11×10^{-7}	3.7×10^{6}	1.2×10^{6}

The UL-FAGE was placed close to a window (approximately 1.5 m) on the West-East axis so that the nozzle was irradiated by direct sunlight in the late afternoon from 17:00 to 19:00. The LICOR instrument (LI-1800) that measured the photolysis rate frequencies was placed close to the FAGE nozzle. All the other measuring instruments were located in the adjacent room.

The following instruments were used in the campaign: ozone analyzer (TEI, 42i), NOx analyzer (TEI,49i TL), a specific analyzer for the measurement of HONO (NITROMAC), a Fluorescence Assay by Gas expansion instrument (FAGE), a Proton Transfer Reaction Mass Spectrometer Time of Flight (PTR-TOF-MS), a SMPS (Scan Mobility Particle Sizer) and photolysis rates were measured with a spectroradiometer (LI-1800). Four powerful fans were installed in each corner to ensure air homogeneity inside the room. A stainless steel sampling line was setup from the middle of the measurement classroom through the door to the communicating classroom where all the instruments were set up (Figure 9).

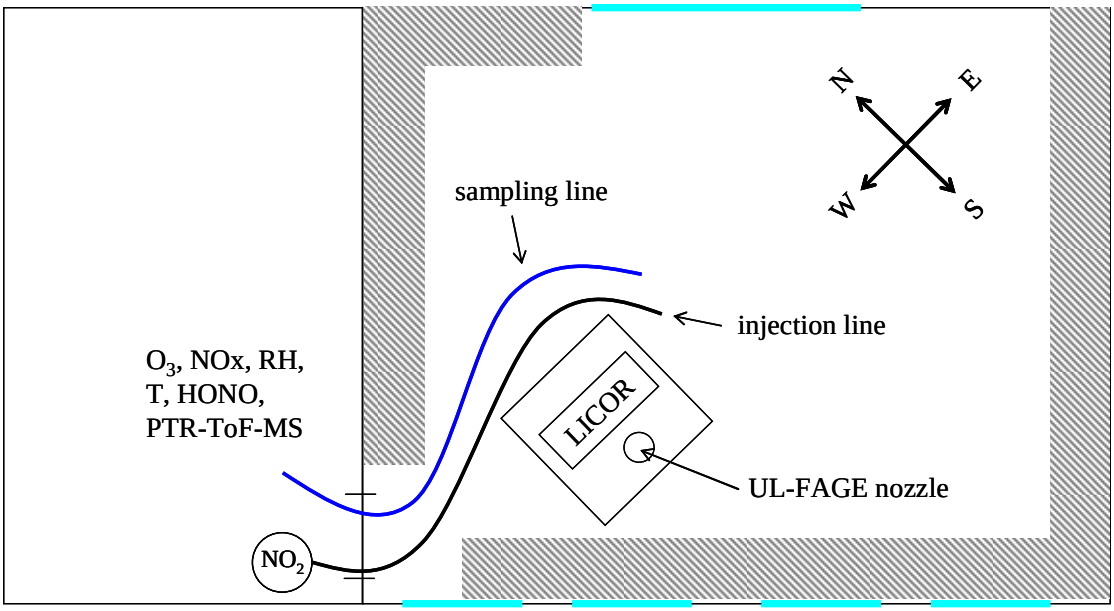

Figure 9. Schematic representation of the position of the UL-FAGE and the LICOR in the classroom.

2.2. Measurement protocol

The measurements were performed between July, 19 and July, 28 2011 in a classroom with dimensions of 7.00×6.50×3.74 m (total volume 170 m^3). The air exchange rate (ARE) was obtained by measuring the decay of acetonitrile that was injected through the main door before each experiments.

Two to three experiments of 4 hours were carried out at different times of the day, corresponding to different light intensity levels: in the morning (11 00 a.m. to 15.00 p.m.), afternoon (15.00 p.m. to 19.00 p.m.) and night (21.00 p.m. to 00:30 a.m.). The first hour of each experiment was used as a blank before different NO_2 concentration levels were injected (from 50 to 180 ppb) inside the room with different relative humidities (from 30 to 80 %) to enhance the production of HONO. Between each experiment the room was vented by opening the windows and the main door for 30 min. In two experiments, no NO_2 was injected inside the room so the measurement was made with ambient NO_2.

2.3. Results and discussion

The indoor photolysis frequencies of HONO, HCHO and O_3 indoors were measured continuously. The photolysis rate of HONO, j_{HONO}, was in the range of 4 to 8 × 10^{-5} s^{-1} for the time period in which direct sunlight shone onto the LICOR (in the evening between 17:00 and 19:00). For the rest of the day, j_{HONO} was in the range of 2 to 4 × 10^{-5} s^{-1}. The photolysis frequencies of other species (ozone and formaldehyde) which could potentially represent a source of OH and HO_2 were always below the detection limits of the spectroradiometer (10^{-7} s^{-1}). The transmission spectrum of the light through the window was not characterized. The O_3 concentration stayed always below 10 ppb during all experiments. Measured HONO concentrations varied from 5 to 15 ppb depending on the NO_2 concentration and the relative humidity.

On Figure 10 is displayed the averaged concentration profile averaged over 6 days of measurements (from the 20th up to the 25th) where the conditions were similar. On the 19th, the LICOR instrument was located further away from the FAGE nozzle. Afterwards, considering the sun trajectory, the LICOR was placed on the same axis to the FAGE nozzle. On the 3 last days, experiments introducing pesticides and burning candles within the room were conducted for other purposes (study of the impact of soot particles on indoor chemistry or degradation of pesticides indoor) and in consequence are not taken into account in the present analysis. In the morning measurement period, the OH concentration was approximately of 4 × 10^5 cm^{-3}, whereas for the night measurement period the OH concentration stayed below or close to the limit of detection of the UL-FAGE around 2 × 10^5 cm^{-3}. When the sunlight was directly striking onto the nozzle concentrations up to 1.5 × 10^6 cm^{-3} were measured. For HO_2, the concentration stayed always below 2.5 × 10^7 cm^{-3} (1 ppt). The HO_2 concentration did follow the OH profile when light was on the nozzle.

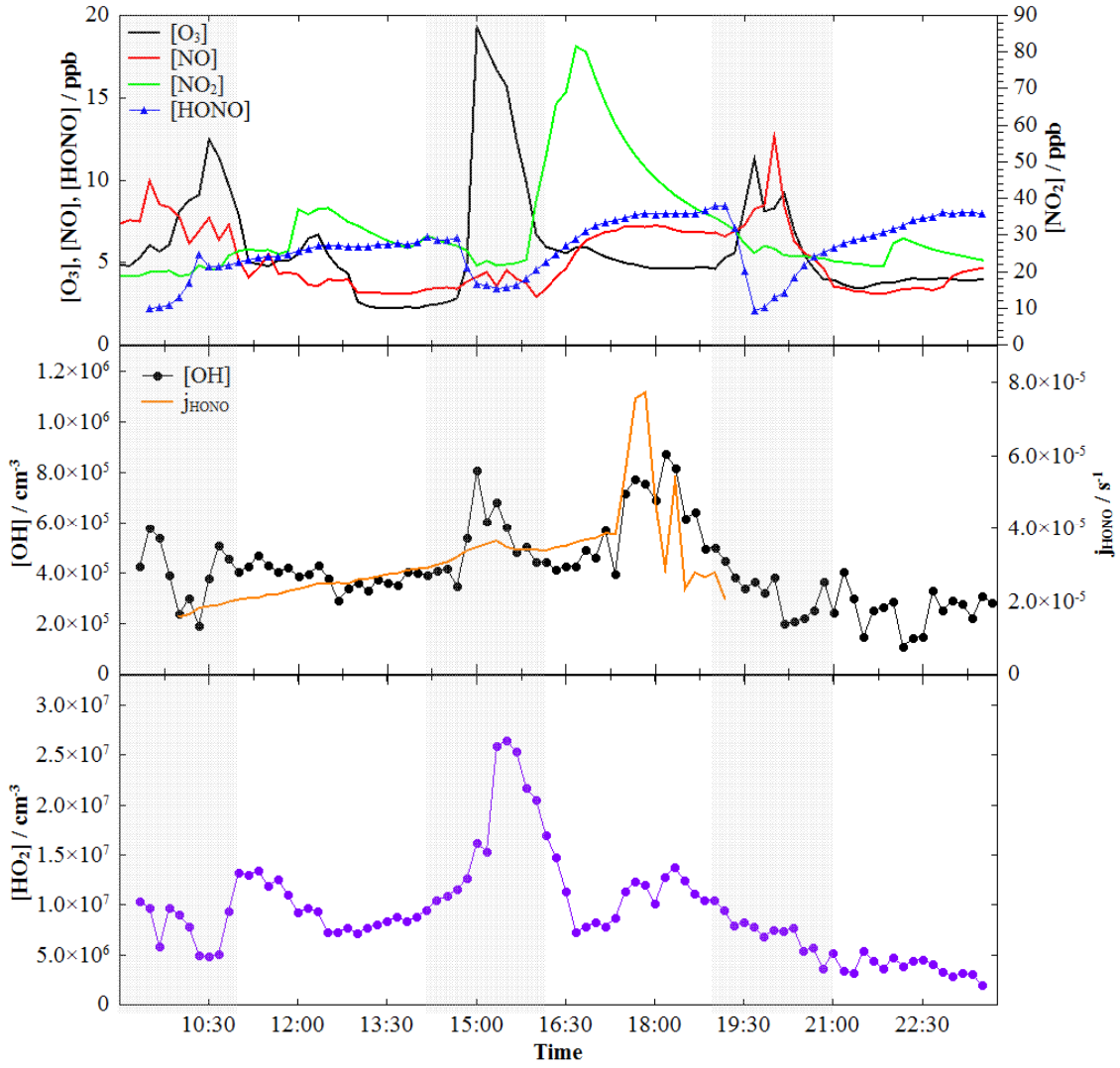

Figure 10. Averaged over 6 measurement days
The grey zone corresponds to the time period when the room was purged.

On Figure 11 is represented the measurement performed on July 21st. Two experiments were carried out from 11:00 to 15:00 in which 50 ppb of NO_2 were injected and from 15:30 to 19:30 where no NO_2 was injected. The door and windows were closed at 11:00 and the HONO concentration increased up to 5 ppb. After the first NO_2 injection, the HONO concentration continued to increase up to 7 ppb. At 15:00, the door and windows were opened. The HONO concentration decreased rapidly whereas we saw an increase in the O_3 and NO concentration due to the high exchange rate with outdoors. After closing the door and windows (15:30), the NO_2 concentration increased while the NO and O_3 concentrations decreased indicating that NO was titrated with O_3 to produce NO_2. The HONO concentration increased up to 6 ppb. The OH concentration measured during the morning experiment was

between 2 to 5 × 10^5 cm^{-3} and increased up to 1.2 × 10^6 cm^{-3} when sunlight hit the FAGE nozzle around 17:30. The OH and HO_2 concentrations followed the HONO photolysis rate.

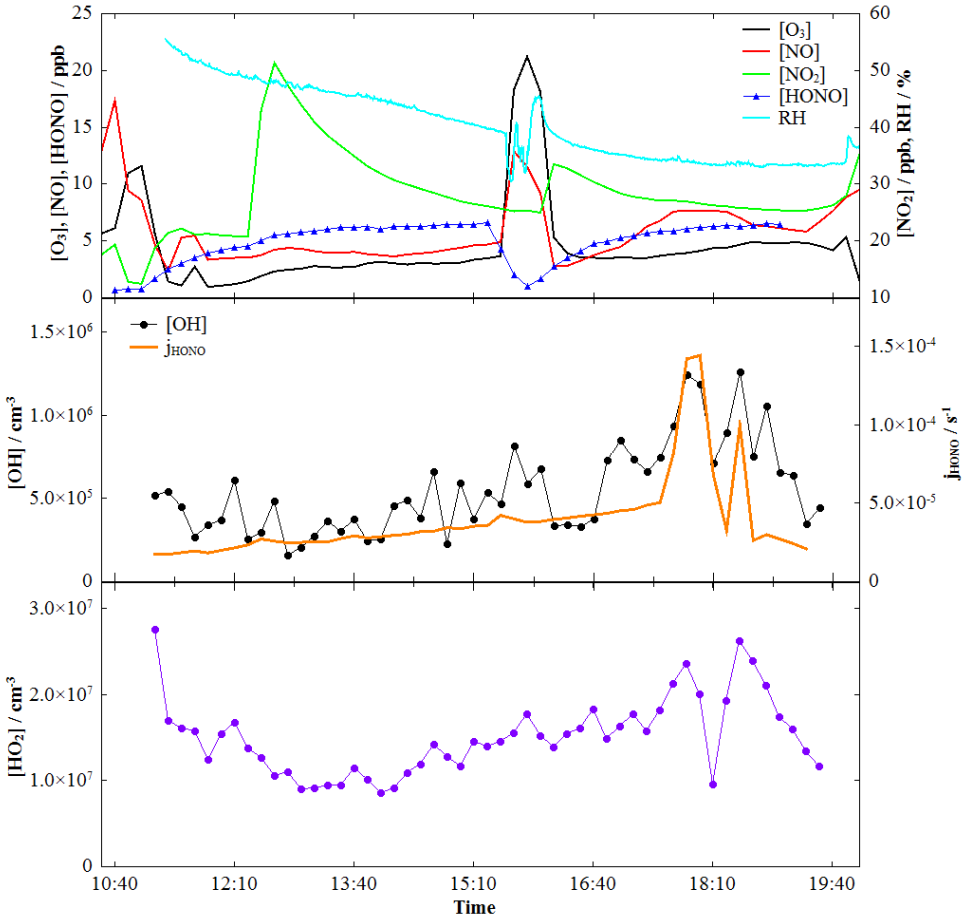

Figure 11. Measurement on the 21/07.
All data were interpolated or averaged to 10 min.

It is clear that the OH formation observed in the late afternoon is linked with the HONO photolysis rate intensity. All the measurement data were either interpolated or averaged to 10 min and scatter plots were made to parameterize the OH formation. The data analysis was limited to the afternoon period (16:00 to 19:00) when the sunlight was passing through the room as for the rest of the time periods no significant OH formation was observed. The averaged data were used to plot the OH concentration as function of the product of the HONO photolysis rate times the HONO concentration. The correlation coefficient obtained from the linear regression analysis was r^2=0.50 (see Figure 12). Another source could be the photolysis of NO_2, producing O_3, reacting with alkenes, so that the O_3 concentration stays low but the OH production increases.

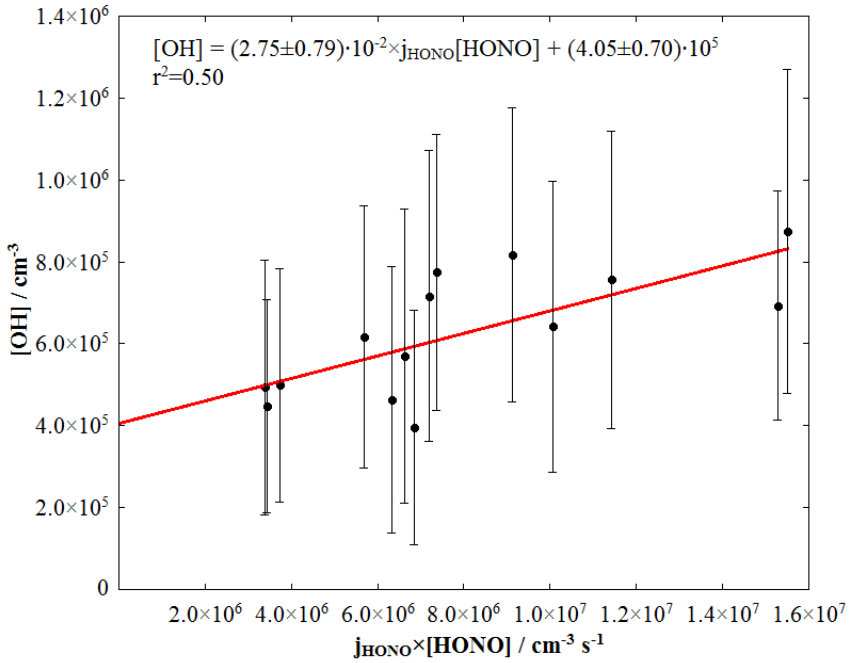

Figure 12. Scatter plot: [OH] vs j_{HONO}× [HONO]
[OH] as function of the product of the HONO photolysis rate and of the [HONO], [OH] = $(2.75 \pm 0.79) \times 10^{-2}$ (j_{HONO} × [HONO]) + $(4.05 \pm 0.70) \times 10^5$, r^2=0.50;
Errors are given at 1σ.

The concentration of 1.4×10^6 cm^{-3} (j_{HONO}=1.5×10^{-5} s^{-1}, [HONO] = 6 ppb) is to our knowledge the highest OH concentration measured indoor. It is interesting to remark that the chemical model from Carslaw (Carslaw, 2007) predicted similar OH concentrations similar to the concentrations measured by the UL-FAGE in the classroom in Marseille. Of course, the model study by Carslaw (Carslaw, 2007) was not run in our conditions and so the absolute measured data can not be compared. When the light was only scattered through the room, the averaged OH concentration was of 4×10^5 cm^{-3} whereas the averaged maximum OH was 8×10^5 cm^{-3} when the sunlight directly stoke the UL-FAGE nozzle. Carslaw (Carslaw, 2007) ran chemical models with different scenarios in which the light intensities was varied. In the base case scenario a modelled OH concentration of 4×10^5 cm^{-3} was obtained. The major OH source was the ozonolysis of aromatics ($P(OH)_{alkenes}$=53×10^5 cm^{-3} s^{-1}) whereas the photolysis of HONO ($P(OH)_{HONO}$=7×10^5 cm^{-3} s^{-1}) was a minor source. Monoterpenes measurement were made using the PTR-ToF-MS but were not available at the time of the redaction and so the estimation of the production rate can not be made. In a second scenario, the UV transmission was increased and the modelled OH concentration increased up to 1.3×10^6 cm^{-3} now with a strong contribution of the HONO photolysis as a source of OH similarly to our

measurement when the light struck onto the nozzle. This scenario is similar to our measurement when the light struck onto the nozzle. During this period, the OH production rate from the HONO photolysis peaks up to 2×10^6 cm^{-3} s^{-1}.

However, for HO_2, the predicted maximum concentration was of 8 ppt in the base case scenario and 12 ppt in the second scenario, 10 times higher than the maximum HO_2 concentration measured during the entire campaign. The ratio $([HO_2]/[OH])_{modelled}$ was of 600 whereas it was of approximately 20 during the entire measurement period. A possible explanation would be that during the same period, the NO concentration in the room spanned between 3 to 7 ppb whereas in the model study by Carslaw (Carslaw, 2007) the NO concentration indoor was for most of the day below 1 ppb which in consequence increases the lifetime of HO_2 and so its concentration. The low NO concentration in the model is explained by the reaction of NO with O_3,

$$NO + O_3 \rightarrow NO_2 + O_2 \qquad \text{(R 4)}$$

The ratio $[HO_2]/(OH)$ as function of the NO concentration is represented on Figure 13. It can be seen that for most of the measurements the [NO] concentration was higher than 1 ppb and so the $[HO_2]/[OH]$ was lower than the low NO condition as presented by Carslaw (Carslaw, 2007).

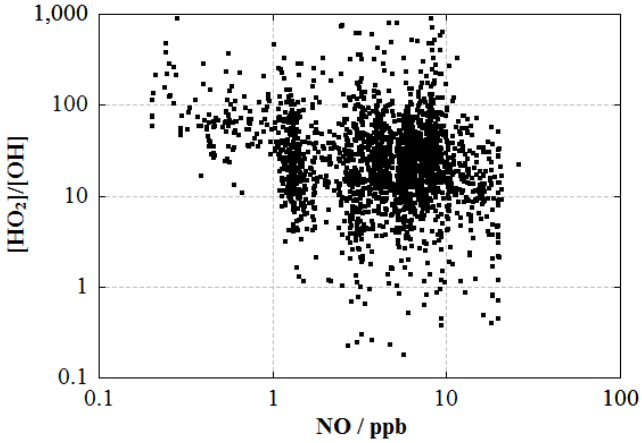

Figure 13. Correlation plot between $[HO_2]/[OH]$ ratio and NO.
All data were interpolated to 1 min for OH and HO_2 and averaged to 1 min for NO

A simulation of the chemistry occurring under our conditions will be performed and will help to understand the concentration profile of OH as well as the low HO_2 measured concentrations.

In recent studies (see Chapter 1, Interferences), it was observed that the OH and HO_2 measurements using the FAGE technique were subject to interferences. For HO_2, the NO concentration used to convert HO_2 into OH was set to a low value so that the interference due to the detection of RO_2 species was diminished. For OH, some tests using C_3F_6 were performed at the end of the field campaign in the period when the nozzle was exposed to direct sunlight. But due to the short direct sunlight period and the weak sunlight on this day, no conclusion can be drawn. However, the fact that the OH signal was very low except when the sun was striking the nozzle proves that photolysis by sunlight is the major source of OH signal, while interferences due to species like HONO, present in similar concentrations during sunlight period and in the shade do not affect the measurement. A potential interference could only be due to other short live species linked to a photolysis process.

2.4. Summary of the SURFIN campaign

The first direct measurement of OH and HO_2 indoor was a success. We observed OH concentration up to 1.4×10^6 cm^{-3} when the sunlight was striking directly onto the sampling nozzle. Concentrations of 4×10^5 cm^{-3} were observed when the room was not directly insolate. At night, the measured OH concentrations were close or below the limit of detection of the UL-FAGE (LOD = 2×10^5 cm^{-3}) indicating that even during the morning when only scattered light entered the room, non-negligible photolytic sources of OH existed. OH was observed in both forced conditions when NO_2 was injected inside the room to enhance the HONO formation as well as when no injections were made. The indoor photolysis of HONO is confirmed as a potential source of OH radicals with production rates. The HO_2 concentration was always measured below 1 ppt. The OH concentration was observed to be highly dependent on the photolysis rate intensities which vary during the course of the day. The orientation of the room as well as the size of the windows will affect the OH concentration and thus the position of the measuring instruments is determinant. The modeling of the experiment will probably help to understand the observed profiles. For future investigations of the indoor radical chemistry, the choice of the room is of high importance. It is also clear that the radical concentrations throughout the room will be variable with higher concentrations close the window and lower in the center of the room. The time of the day as well as the time of the year will be determinant.

Conclusion

In this chapter we have presented the preliminary results of the two campaigns in which the UL-FAGE was deployed in the summer 2011. The UL-FAGE was intercompared for a second time during CompOH: after the intercomparison to another FAGE within the SAPHIR chamber, a comparison was made in ambient air and this time with another technique, the LATMOS-CIMS. The results obtained show a good correlation between the two instruments however some discrepancies were observed: during the day significant intercepts were obtained from the linear regression analysis and at night the UL-FAGE measured 40% more than the LATMOS-CIMS. We hope that a box model might help to understand the discrepancies as no clear correlation of the ratio $[OH]_{CIMS}/[OH]_{Lille}$ was observed as function of NO, O_3 and H_2O.

During SURFIN, we reported the first direct measurement of OH indoor. Concentrations as high as 1.5×10^6 cm^{-3} were measured when the sunlight was shinning over the FAGE nozzle. The correlation between $j_{HONO}[HONO]$ and the OH concentration indicated that [HONO] was a major source of OH indoor. Background day OH concentrations of 4.5×10^5 cm^{-3} were measured on average. At night, the OH concentration was below or close to our limit of detection, 2.0×10^5 cm^{-3}. During the day time, the correlation between $j_{HONO}[HONO]$ and the OH concentration indicated that [HONO] was one of the major source of OH indoor.

.

3. References

Berresheim, H., Plass-Dülmer, C., Elste, T., Mihalopoulos, N. and Rohrer, F.: OH in the coastal boundary layer of Crete during MINOS: Measurements and relationship with ozone photolysis, Atmos. Chem. Phys., 3(3), 639–649, doi:10.5194/acp-3-639-2003, 2003.

Bloss, W. J., Lee, J. D., Heard, D. E., Salmon, R. A., Bauguitte, S. J.-B., Roscoe, H. K. and Jones, A. E.: Observations of OH and HO2 radicals in coastal Antarctica, Atmos. Chem. Phys., 7(16), 4171–4185, doi:10.5194/acp-7-4171-2007, 2007.

Brauers, T., Hausmann, M., Bister, A., Kraus, A. and Dorn, H.-P.: OH radicals in the boundary layer of the Atlantic Ocean 1. Measurements by long-path laser absorption spectroscopy, J. Geophys. Res., 106(D7), 7399–7414, doi:10.1029/2000JD900679, 2001.

Carslaw, N.: A new detailed chemical model for indoor air pollution, Atmospheric Environment, 41(6), 1164–1179, doi:10.1016/j.atmosenv.2006.09.038, 2007.

Creasey, D. J., Evans, G. E., Heard, D. E. and Lee, J. D.: Measurements of OH and HO2 concentrations in the Southern Ocean marine boundary layer, J. Geophys. Res., 108(D15), 4475, doi:10.1029/2002JD003206, 2003.

Dolgorouky, C., Gros, V., Sarda-Esteve, R., Sinha, V., Williams, J., Marchand, N., Sauvage, S., Poulain, L., Sciare, J. and Bonsang, B.: Total OH reactivity measurements in Paris during the 2010 MEGAPOLI winter campaign, Atmospheric Chemistry and Physics Discussions, 12(4), 10937–10994, doi:10.5194/acpd-12-10937-2012, 2012.

Drakou, G., Zerefos, C., Ziomas, I. and Voyatzaki, M.: Measurements and numerical simulations of indoor O3 and NOx in two different cases, Atmospheric Environment, 32(4), 595–610, doi:10.1016/S1352-2310(97)00335-X, 1998.

Dusanter, S., Vimal, D., Stevens, P. S., Volkamer, R. and Molina, L. T.: Measurements of OH and HO2 concentrations during the MCMA-2006 field campaign – Part 1: Deployment of the Indiana University laser-induced fluorescence instrument, Atmos. Chem. Phys., 9(5), 1665–1685, doi:10.5194/acp-9-1665-2009, 2009.

Ehhalt, D. H. and Rohrer, F.: Dependence of the OH concentration on solar UV, J. Geophys. Res., 105(D3), 3565–3571, doi:10.1029/1999JD901070, 2000.

Eisele, F. L., Mauldin, L., Cantrell, C., Zondlo, M., Apel, E., Fried, A., Walega, J., Shetter, R., Lefer, B., Flocke, F., Weinheimer, A., et al.: Summary of measurement intercomparisons during TRACE-P, J. Geophys. Res., 108(D20), 8791, doi:10.1029/2002JD003167, 2003.

Eisele, F. L., Mauldin, R. L., Tanner, D. J., Cantrell, C., Kosciuch, E., Nowak, J. B., Brune, B., Faloona, I., Tan, D., Davis, D. D., Wang, L., et al.: Relationship between OH measurements on two different NASA aircraft during PEM Tropics B, J. Geophys. Res., 106(D23), 32683–32,689, doi:10.1029/2000JD900714, 2001.

Emmerson, K. M., Carslaw, N., Carslaw, D. C., Lee, J. D., McFiggans, G., Bloss, W. J., Gravestock, T., Heard, D. E., Hopkins, J., Ingham, T., Pilling, M. J., et al.: Free radical

modelling studies during the UK TORCH Campaign in Summer 2003, Atmos. Chem. Phys., 7(1), 167–181, doi:10.5194/acp-7-167-2007, 2007.

Febo, A. and Perrino, C.: Prediction and experimental evidence for high air concentration of nitrous acid in indoor environments, Atmospheric Environment. Part A. General Topics, 25(5–6), 1055–1061, doi:10.1016/0960-1686(91)90147-Y, 1991.

Finalyson-Pitts, B. J. and Pitts, J. N.: Chemistry of the Upper and the Lower atmosphere, Academic Press., 2000.

Finlayson-Pitts, B. J., Wingen, L. M., Sumner, A. L., Syomin, D. and Ramazan, K. A.: The heterogeneous hydrolysis of NO2 in laboratory systems and in outdoor and indoor atmospheres: An integrated mechanism, Phys. Chem. Chem. Phys., 5(2), 223–242, doi:10.1039/B208564J, 2003.

Freutel, F., Schneider, J., Drewnick, F., von der Weiden-Reinmüller, S.-L., Crippa, M., Prévôt, A. S. H., Baltensperger, U., Poulain, L., Wiedensohler, A., Sciare, J., Sarda-Estève, R., et al.: Aerosol particle measurements at three stationary sites in the megacity of Paris during summer 2009: meteorology and air mass origin dominate aerosol particle composition and size distribution, Atmospheric Chemistry and Physics Discussions, 12(8), 22199–22268, doi:10.5194/acpd-12-22199-2012, 2012.

Geyer, A., Bächmann, K., Hofzumahaus, A., Holland, F., Konrad, S., Klüpfel, T., Pätz, H.-W., Perner, D., Mihelcic, D., Schäfer, H.-J., Volz-Thomas, A., et al.: Nighttime formation of peroxy and hydroxyl radicals during the BERLIOZ campaign: Observations and modeling studies, J. Geophys. Res., 108(D4), 8249, doi:10.1029/2001JD000656, 2003.

Haeffelin, M., Barthès, L., Bock, O., Boitel, C., Bony, S., Bouniol, D., Chepfer, H., Chiriaco, M., Cuesta, J., Delanoë, J., Drobinski, P., et al.: SIRTA, a ground-based atmospheric observatory for cloud and aerosol research, Ann. Geophys., 23(2), 253–275, doi:10.5194/angeo-23-253-2005, 2005.

Holland, F., Aschmutat, U., Heßling, M., Hofzumahaus, A. and Ehhalt, D. H.: Highly Time Resolved Measurements of OH during POPCORN Using Laser-Induced Fluorescence Spectroscopy, Journal of Atmospheric Chemistry, 31(1), 205–225, doi:10.1023/A:1005868520002, 1998.

Holland, F., Hofzumahaus, A., Schäfer, J., Kraus, A. and Pätz, H.-W.: Measurements of OH and HO2 radical concentrations and photolysis frequencies during BERLIOZ, J. Geophys. Res., 108(D4), 8246, doi:10.1029/2001JD001393, 2003.

Hough, A. M.: The calculation of photolysis rates for use in global tropospheric modelling studies, Her Majesty's Stn. Off., Norwich, England, AERE Report, R-13259, 1988.

Huang, G., Zhou, X., Deng, G., Qiao, H. and Civerolo, K.: Measurements of atmospheric nitrous acid and nitric acid, Atmospheric Environment, 36(13), 2225–2235, doi:10.1016/S1352-2310(02)00170-X, 2002.

Kanaya, Y., Sadanaga, Y., Nakamura, K. and Akimoto, H.: Behavior of OH and HO2 radicals during the Observations at a Remote Island of Okinawa (ORION99) field campaign. 1. Observation using a laser-induced fluorescence instrument, J. Geophys. Res., 106(D20), 24197–24,208, doi:10.1029/2000JD000178, 2001.

Kukui, A., Ancellet, G. and Le Bras, G.: Chemical ionisation mass spectrometer for measurements of OH and Peroxy radical concentrations in moderately polluted atmospheres, Journal of Atmospheric Chemistry, 61(2), 133–154, doi:10.1007/s10874-009-9130-9, 2008.

Kukui, A., Legrand, M., Ancellet, G., Gros, V., Bekki, S., Sarda-Estève, R., Loisil, R. and Preunkert, S.: Measurements of OH and RO2 radicals at the coastal Antarctic site of Dumont d'Urville (East Antarctica) in summer 2010–2011, J. Geophys. Res., 117(D12), D12310, doi:10.1029/2012JD017614, 2012.

Lee, J., Young, J., Read, K., Hamilton, J., Hopkins, J., Lewis, A., Bandy, B., Davey, J., Edwards, P., Ingham, T., Self, D., et al.: Measurement and calculation of OH reactivity at a United Kingdom coastal site, Journal of Atmospheric Chemistry, 64(1), 53–76, doi:10.1007/s10874-010-9171-0, 2009.

Martinez, M., Harder, H., Kovacs, T. A., Simpas, J. B., Bassis, J., Lesher, R., Brune, W. H., Frost, G. J., Williams, E. J., Stroud, C. A., Jobson, B. T., et al.: OH and HO2 concentrations, sources, and loss rates during the Southern Oxidants Study in Nashville, Tennessee, summer 1999, J. Geophys. Res., 108(D19), 4617, doi:10.1029/2003JD003551, 2003.

Michoud, V., Kukui, A., Camredon, M., Colomb, A., Borbon, A., Miet, K., Aumont, B., Beekmann, M., Durand-Jolibois, R., Perrier, S., Zapf, P., et al.: Radical budget analysis in a suburban European site during the MEGAPOLI summer field campaign, Atmospheric Chemistry and Physics Discussions, 12(6), 15883–15943, doi:10.5194/acpd-12-15883-2012, 2012.

Nazaroff, W. W. and Cass, G. R.: Mathematical modeling of chemically reactive pollutants in indoor air, Environ. Sci. Technol., 20(9), 924–934, doi:10.1021/es00151a012, 1986.

Nölscher, A. C., Sinha, V., Bockisch, S., Klüpfel, T. and Williams, J.: A new method for total OH reactivity measurements using a fast Gas Chromatographic Photo-Ionization Detector (GC-PID), Atmospheric Measurement Techniques Discussions, 5(3), 3575–3609, doi:10.5194/amtd-5-3575-2012, 2012.

Pietras, C., Boitel, C., Dupont, J. C., Haeffelin, M., Lapouge, F., Morille, Y., Noel, V. and Romand, B.: SIRTA, a multi-sensor platform for clouds and aerosols characterization in the atmosphere: infrastructur, objective and prospective - atr. no 67501A, Lidar Technologies, Techniques, and Measurements for Atmospheric Remote Sensing, Proceedings of the Society of Photo-Optical Instrumentation Engineers (Spie), A7501–A7501, 2007.

Preunkert, S., Ancellet, G., Legrand, M., Kukui, A., Kerbrat, M., Sarda-Estève, R., Gros, V. and Jourdain, B.: Oxidant Production over Antarctic Land and its Export (OPALE) project: An overview of the 2010–2011 summer campaign, J. Geophys. Res., 117(D15), D15307, doi:10.1029/2011JD017145, 2012.

Ren, X., Brune, W. H., Mao, J., Mitchell, M. J., Lesher, R. L., Simpas, J. B., Metcalf, A. R., Schwab, J. J., Cai, C., Li, Y., Demerjian, K. L., et al.: Behavior of OH and HO2 in the winter atmosphere in New York City, Atmospheric Environment, 40, Supplement 2(0), 252–263, doi:10.1016/j.atmosenv.2005.11.073, 2006.

Ren, X., Mao, J., Brune, W. H., Cantrell, C. A., Mauldin III, R. L., Hornbrook, R. S., Kosciuch, E., Olson, J. R., Crawford, J. H., Chen, G. and Singh, H. B.: Airborne intercomparison of HOx measurements using laser-induced fluorescence and chemical

ionization mass spectrometry during ARCTAS, Atmospheric Measurement Techniques, 5(8), 2025–2037, doi:10.5194/amt-5-2025-2012, 2012.

Rohrer, F. and Berresheim, H.: Strong correlation between levels of tropospheric hydroxyl radicals and solar ultraviolet radiation, Nature, 442(7099), 184–187, doi:10.1038/nature04924, 2006.

Schlosser, E., Brauers, T., Dorn, H.-P., Fuchs, H., Häseler, R., Hofzumahaus, A., Holland, F., Wahner, A., Kanaya, Y., Kajii, Y., Miyamoto, K., et al.: Technical Note: Formal blind intercomparison of OH measurements: results from the international campaign HOxComp, Atmos. Chem. Phys., 9(20), 7923–7948, doi:10.5194/acp-9-7923-2009, 2009.

Sillman, S., Carroll, M. A., Thornberry, T., Lamb, B. K., Westberg, H., Brune, W. H., Faloona, I., Tan, D., Shepson, P. B., Sumner, A. L., Hastie, D. R., et al.: Loss of isoprene and sources of nighttime OH radicals at a rural site in the United States: Results from photochemical models, J. Geophys. Res., 107(D5), 4043, doi:10.1029/2001JD000449, 2002.

Sinha, V., Williams, J., Crowley, J. N. and Lelieveld, J.: The Comparative Reactivity Method – a new tool to measure total OH Reactivity in ambient air, Atmos. Chem. Phys., 8(8), 2213–2227, doi:10.5194/acp-8-2213-2008, 2008.

Sommariva, R., Bloss, W. J., Brough, N., Carslaw, N., Flynn, M., Haggerstone, A.-L., Heard, D. E., Hopkins, J. R., Lee, J. D., Lewis, A. C., McFiggans, G., et al.: OH and HO2 chemistry during NAMBLEX: roles of oxygenates, halogen oxides and heterogeneous uptake, Atmos. Chem. Phys., 6(4), 1135–1153, doi:10.5194/acp-6-1135-2006, 2006.

Stone, D., Whalley, L. K. and Heard, D. E.: Tropospheric OH and HO2 radicals: field measurements and model comparisons, Chem. Soc. Rev., doi:10.1039/C2CS35140D [online] Available from: http://pubs.rsc.org.docproxy.univ-lille1.fr/en/content/articlelanding/2012/cs/c2cs35140d (Accessed 1 September 2012), 2012.

Vaughan, S., Ingham, T., Whalley, L. K., Stone, D., Evans, M. J., Read, K. A., Lee, J. D., Moller, S. J., Carpenter, L. J., Lewis, A. C., Fleming, Z. L., et al.: Seasonal observations of OH and HO2 in the remote tropical marine boundary layer, Atmos. Chem. Phys., 12(4), 2149–2172, doi:10.5194/acp-12-2149-2012, 2012.

Weschler, C. J.: Chemistry in indoor environments: 20 years of research, Indoor Air, 21(3), 205–218, doi:10.1111/j.1600-0668.2011.00713.x, 2011.

Weschler, C. J. and Shields, H. C.: Production of the Hydroxyl Radical in Indoor Air, Environ. Sci. Technol., 30(11), 3250–3258, doi:10.1021/es960032f, 1996.

Weschler, C. J. and Shields, H. C.: Measurements of the Hydroxyl Radical in a Manipulated but Realistic Indoor Environment, Environ. Sci. Technol., 31(12), 3719–3722, doi:10.1021/es970669e, 1997.

Whalley, L. K., Edwards, P. M., Furneaux, K. L., Goddard, A., Ingham, T., Evans, M. J., Stone, D., Hopkins, J. R., Jones, C. E., Karunaharan, A., Lee, J. D., et al.: Quantifying the magnitude of a missing hydroxyl radical source in a tropical rainforest, Atmos. Chem. Phys., 11(14), 7223–7233, doi:10.5194/acp-11-7223-2011, 2011.

Whalley, L. K., Furneaux, K. L., Goddard, A., Lee, J. D., Mahajan, A., Oetjen, H., Read, K. A., Kaaden, N., Carpenter, L. J., Lewis, A. C., Plane, J. M. C., et al.: The chemistry of OH and HO2 radicals in the boundary layer over the tropical Atlantic Ocean, Atmos. Chem. Phys., 10(4), 1555–1576, doi:10.5194/acp-10-1555-2010, 2010.

White, I. R., Martin, D., Muñoz, M. P., Petersson, F. K., Henshaw, S. J., Nickless, G., Lloyd-Jones, G. C., Clemitshaw, K. C. and Shallcross, D. E.: Use of Reactive Tracers To Determine Ambient OH Radical Concentrations: Application within the Indoor Environment, Environ. Sci. Technol., 44(16), 6269–6274, doi:10.1021/es901699a, 2010.

OH reactivity set-up: Application to ambient and laboratory measurements

Introduction

The OH radical due to its high reactivity governs the lifetime of most trace gases of biogenic and anthropogenic origins present in the troposphere. As mentioned in Chapter 1, the oxidation of hydrocarbons with OH radicals in the presence of NOx leads to the formation of secondary products such as O_3 and PAN. The rate at which OH radicals react with most of trace gases is called OH reactivity. Three different techniques have been developed for the measurement of the OH reactivity and were described in Chapter 1. In Lille, in parallel to the development of the FAGE instrument for the quantification of HOx radicals, we adapted the set-up for the measurement of the total OH reactivity by coupling the FAGE cells with a laser photolysis cell such as developed by Sadanaga et al. (Sadanaga et al., 2004). In the first part of this chapter, we describe the Lille instrument and the different tests that were run in order to validate the instrument. In a second part, we present the results of the intercomparative measurement between the UL-OH reactivity instruments with two other instruments based on the CRM method during the CompOH campaign in July 2011. This is the first report of an intercomparative measurement of OH reactivity techniques in ambient air. In addition to OH reactivity measurements, the OH reactivity set-up was used to perform kinetic measurements. In the last part of this chapter, we present the results of the study of the reaction between excited NO_2 with H_2O as a potential source of OH radicals in the troposphere.

1. Development of the UL-OH reactivity system

The UL-OH reactivity system was built following the work of Sadanaga et al. (Sadanaga et al., 2004). A photolysis cell was coupled to a FAGE cell to measure time resolved OH radicals by LIF at λ=308 nm. OH radicals are produced in the photolysis cell from the UV photolysis (λ=266 nm) of O_3 in the presence of water vapour.

$$O_3 + h\nu\ (\lambda=266\ nm) \rightarrow O(^1D) + O_2 \qquad (R\ 1)$$
$$O(^1D) + H_2O \rightarrow 2\ OH \qquad (R\ 2)$$

The OH decays are measured taking advantage of the high repetition rate of the fluorescence excitation laser used on FAGE instruments that provides high time resolution up to 100 µs. For the UL-FAGE, the high repetition rate laser was generally triggered at 5 kHz and so a time resolution of 200 µs was achieved.

Two different configurations were tested; either the photolysis cell was set along the FAGE cells (called "on-line configuration", OLC) or perpendicular to them (called "ninety degree configuration", NDC) as shown on Figure 1.

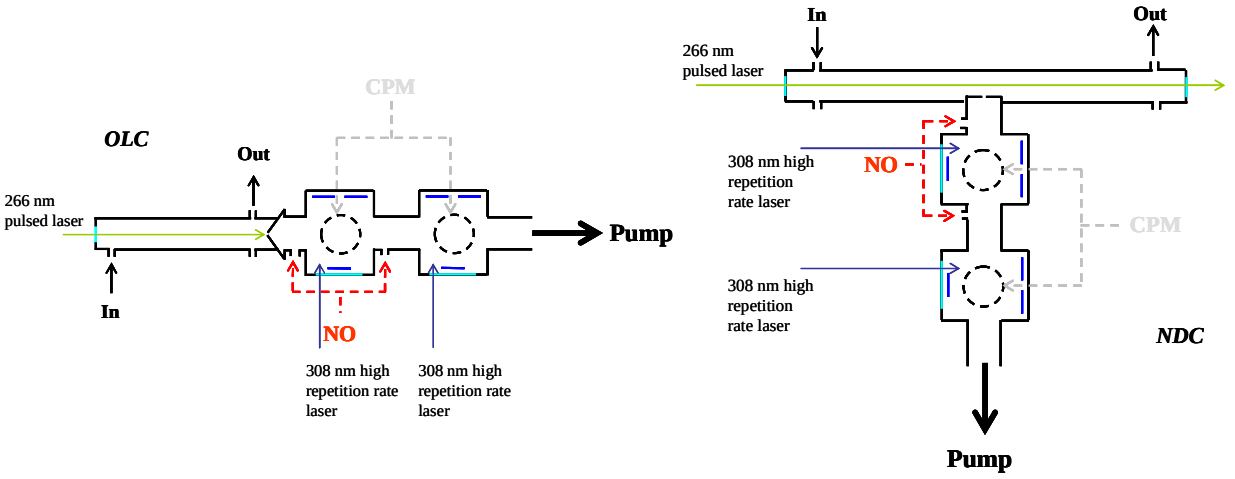

Figure 1. Configuration set up for kinetic and reactivity measurement.
Left – On line configuration, Right – Ninety Degree configuration

Generally, the photolysis laser and the excitation were running independently. The photolysis laser repetition rate can be varied from 0.1 to 10 Hz however we usually preferred a rate of 1 or 2 Hz depending on the flow conditions in order to refresh the gas mixture between each photolysis laser pulse.

One delay generator was used to trigger the detection system, i.e. the FAGE system including the LIF laser, the switches, the CPM, the reference cell signal acquisition. But contrary to the quantification mode, the start of the acquisition of OH and the HO_2 cell signals was triggered with the Q-switch of the photolysis laser. The photolysis laser is either triggered internally or using a second delay generator depending on the type of photolysis laser (different models have been used during this thesis). Since the 5 kHz excitation laser is running independently from the photolysis laser, all points recorded within a time window of 200 µs are considered equivalent, giving a resolution time of 200 µs. This method is possible, because the kinetic decay rates generally measured are on the tens of millisecond timescale, so the jitter of 100 µs resulting from the non-synchronization of the two lasers can be considered negligible.

Both photolysis cells are made of aluminium, closed on one side by a Suprasil quartz window (CVI Melles Griot) mounted on flanges which allow the photolysis laser beam to enter. In the OLC, the photolysis cell is a cylinder of 48 cm long with an internal diameter of 5 cm. The other end is connected to the sampling cone of the FAGE cell. In the NDC, the photolysis cell is a square tube of 100 cm long with an internal side of 6 cm. The distance between one end and the sampling nozzle to the FAGE is of 50 cm. For the NDC, the other end is equipped with a window similar to the first one and a beam dump is used to trap the laser beam. For both cells, gas is introduced *via* Swagelok fittings at the quartz window end, at the other end four more Swagelok fittings are mounted equally spaced around the cylinder: these fittings allow a pump to be attached along with additional sampling instruments (O_3, NOx, H_2O) as well as pressure/temperature monitoring.

The validation of the two configurations was subject of a paper by Amedro et al. (Amedro et al., 2012) and only the main results are presented here. In principle the measurement is straightforward: OH radical are generated from the photolysis of O_3 and the OH decay is recorded however the profile analysis needed to get the OH reactivity is subject to careful considerations. Sadanaga et al. (Sadanaga et al., 2004) observed that the OH decays were displaying a strong double exponential decay where the first rapid component was hypothesised to be due to perturbations by the laser shot. In consequence, only the second component of the OH decay was taken for the total OH reactivity measurement which was the combination of the true OH reactivity and OH physical diffusion in the flow tube. By changing the laser beam profile from a Gaussian (Quanta-Ray INDI-40, Spectra Physics) to a top hat (Tempest 300, NewWave Research), they observed a change in the OH decay profile from a double exponential to a single exponential decay (Y. Nakashima; personal communication). Lou et al. (Lou et al., 2010) using the same method did not observed the

same OH decay profiles as Sadanaga et al. (Sadanaga et al., 2004). A possible explanation would be that in their set up the laser photolysis beam is expanded to increase the ratio of the photolyzed volume versus cell volume and so reduce the first rapid physical loss of OH.

Using the flash photolysis method, the main uncertainty is due to the choice of the starting time of the exponential fit relative to the photolysis shot. Indeed, during the first few ms, both physical diffusion of the OH in the photolysis cell and chemical processes are affecting the OH decay. In consequence, the start of the fit needs to be determined. This can be done by measuring the bimolecular rate coefficients of a known reaction. This will also affect the range of decay rates that can be measured by the flash photolysis method because longer the physical phenomena last, the later the fitting time can start thus limiting the measurement of fast decay due to the lack of measurement points. For example, decay faster than 40 s^{-1} for the TMU instrument (Y. Nakashima, personal communication) and 60 s^{-1} for the FZJ instrument are not measured accurately. Lou et al. (Lou et al., 2010) observed a deviation from the linearity between the calculated and the measured for decays greater than 60 s^{-1} (-18% deviation for decays of 100 s^{-1}).

For the UL-FAGE, a series of tests were carried out in order to understand the physical processes occurring after the laser photolysis pulse. In both configurations, the OH decay profiles are composed of a rise followed by a decay which can either be represented as a single or double exponential. The main issue is to determine when the chemical reaction does dominate over the physical diffusion. Several fitting procedure were tested to reproduce the observed signals: single exponential decay, single exponential rise follow by a single exponential decay and single exponential rise followed by a double exponential decay. For reactivity measurement purposes, care was taken to chose a starting time for the fits where physical effects were diminished and so the use of a single exponential equation to fit the decay profile was possible.

Strong physical diffusion phenomena occur when OH radicals are produced only in a small volume compare to the cell volume. It takes longer to reach homogeneity of the OH concentration inside the photolysis cell is longer to reach and will thus affect the decay profile. By expanding the laser beam the impact of the physical effect can be reduced as shown on Figure 2. However as the laser beam is expanded the energy density is decreased along with the signal intensity. To validate the technique and the fitting procedure rate constants of well known reaction was measured for both configurations. The kinetic measurements were made under pseudo first order conditions where the concentration of the reactant, X was much

higher than the concentration of OH. The kinetic measurement was made for reactions of OH with CH_4, CO and C_3H_8 in both configurations. Results are given in Table 1.

$$CH_4 + OH \rightarrow CH_3 + H_2O \quad \text{(R 3)}$$
$$CO + OH + O_2 \rightarrow CO_2 + HO_2 \quad \text{(R 4)}$$
$$C_3H_8 + OH \rightarrow C_3H_7 + H_2O \quad \text{(R 5)}$$

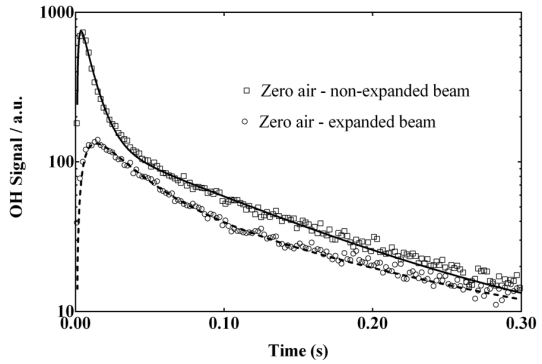

Figure 2. Comparison between two OH time decay profiles in zero air in the NDC: Non-expanded beam (dia~0.6 cm), expanded beam (dia~2.0 cm). The solid line corresponds to a fit using single exponential rise followed by a double exponential decay, k'_0=9.7 s^{-1}. The dashed line represents a fit using a single exponential decay, k'_0 = 13.9 s^{-1}.

Table 1. Summary of the rate coefficients measured in both configutations at 296 K
Reference values are given from (Atkinson et al., 2006)

	k_{CH4+OH}		k_{CO+OH}	$k_{C3H8+OH}$
	Non-Expanded	Expanded	Non-Expanded	Non-Expanded
NDC	$(7.2 \pm 0.7) \times 10^{-15}$	$(5.8 \pm 0.1) \times 10^{-15}$	$(2.7 \pm 0.2) \times 10^{-13}$	$(1.04 \pm 0.7) \times 10^{-12}$
OLC	$(6.2 \pm 0.2) \times 10^{-15}$		$(2.5 \pm 0.7) \times 10^{-13}$	-
Reference	$(6.0 \pm 0.2) \times 10^{-15}$		$(2.3 \pm 0.7) \times 10^{-13}$	$(1.05 \pm 0.7) \times 10^{-12}$

The advantages and drawbacks of the OLC can be compared to those of the NDC. In the OLC air is sampled from the centre of the photolysed volume, in line with the macroscopic gas flow direction, therefore the influence of physical effects such as diffusion are decreased. As the initial increase in signal is fast but non-exponential, the fitting of the OH decay is started after a fixed delay with respect to the photolysis laser. This delay has been deduced empirically by measuring well-known rate constants. From the measurement of well-known rate constants, we estimated that decays of up to 200 s^{-1} can be measured in this configuration. Beyond 200 s^{-1}, the linearity was not fulfilled. In the NDC air is sampled from the extremity of the photolyzed volume at 90° with respect to the macroscopic gas flow direction. Therefore,

in this configuration physical effects such as diffusion and probably turbulences influence the OH profile much more. The rise is slower and exponential functions enable the fitting of the complete profile. Depending on the size of the photolysed volume, either mono- or biexponential decays will be used to fit the experimental traces as good as possible. Decays of up to 100 s^{-1} can be measured in this configuration. Even though faster decays can be measured in the OLC configuration, a major drawback of the OLC is that the entire FAGE cells must be rotated by 90° from their quantification configuration, making switching from quantification to reactivity mode slow and tedious. The NDC does not require this rotation, and therefore a faster change is possible, an important issue during field campaigns

2. Intercomparative measurements during CompOH

OH reactivity measurements have become systematic during field campaigns since the measurement of OH total loss helps to increase the understading of the HOx chemistry. To date, almost 30 field campaigns with measurements of OH reactivity were reported in different environments. Total OH reactivity in urban areas such as Tokyo (Yoshino et al., 2006, 2012), New York (Ren et al., 2003), Mexico City (Shirley et al., 2006) or Paris (Dolgorouky et al., 2012) was measured in range from 10 to 200 s^{-1}. In these environments, OH reactivity was dominated by the reactivity of species emitted from anthropogenic sources such NO_2, alkenes and aromatic species. Measurements were also conducted in coastal areas (Lee et al., 2009) and in environments dominated by the emission of Biogenic Volatile Organic Compounds (BVOC) (Carlo et al., 2004; Nölscher et al., 2012; Lou et al., 2010; Whalley et al., 2011). As already discussed in the Chapter 1, OH reactivity measurement can be compared to calculated OH reactivities. Calculated OH reactivities are obtained by summing product of the concentration times the bimolecular rate coefficients of each reactant (e.g. NO_2, CO, VOC) with OH. In many cases, it was observed that the calculated OH reactivity was smaller than the measured OH reactivity indicating that a portion of reactive species reacting with OH were not measured. The difference between the measured reactivity and the calculated one is called missing reactivity. Depending on the conditions and also on the availability of supporting VOC measurements (GC, PTR-MS), it was shown that up to 90% of the measured OH reactivity was not explained. In most works, the unknown reactivity is attributed to secondary oxidation products such as Oxygenated Volatile Organic Compounds (OVOC) and also primary emitted products such as undetected monoterpenes (Carlo et al., 2004; Lee et al., 2009; Nölscher et al., 2012; Yoshino et al., 2012).

Up to date, OH reactivity measurements were made using 3 different methods described in Chapter 1 and none of these methods were intercompared. During the second part of the CompOH campaign, an intercomparative measurement took place between 2 CRM instruments and 1 flash photolysis method. Unfortunately, measurements from the LSCE-CRM were only available for the last three days of the campaign and only for one day and a half for the UL-OH reactivity. In the following parts, we present the preliminary results of the OH reactivity intercomparative measurements.

2.1. Experimental conditions

Three instruments were intercompared. The two CRM (MPI-CRM and LSCE-CRM) characteristics can be found in the Table 4 in the Chapter 1. A detailed description of the UL-OH reactivity system during CompOH is given in the following paragraphs. The two CRM instruments are very similar and were described in recent studies (Dolgorouky et al., 2012; Nölscher et al., 2012). The CRM technique is very different from the flash photolysis method. First, the total OH reactivity is determined indirectly by measuring the concentration of a reagent (pyrrole) in different environments (with and without artificially added OH radicals and in zero air and in ambient air) using mass spectrometry. In the flash photolysis method the OH decay is measured directly by LIF. In Table 2 is summarized the performances of the three OH reactivity techniques that were intercompared during CompOH.
The flash photolysis technique has a better limit of detection than the CRM however the CRM has larger dynamic range since they can measure OH reactivity up to 300 s^{-1}.

Table 2. Performances of the 3 OH reactivity techniques during CompOH

Groups	Method	LOD / s^{-1} (2σ)	k'_{max} / s^{-1}	time res. / s	Uncertainty (1σ)
MPI, Mainz	CRM/PTR-MS	3-4	300	10-60	16-20 %
LSCE, Paris	CRM/PTR-MS	3	-	120	20 %
University of Lille	Flash photolysis/LIF	0.6	100	30-120	15 %

2.1.1. UL-OH reactivity

During CompOH the ninety-degree configuration was preferred as we changed from the quantification mode to the OH reactivity mode in the middle of the campaign. Installing the OH reactivity system in the OLC is time consuming since the FAGE cells need to be set horizontally. On July 6th the FAGE cells were moved inside the container and the photolysis cell was installed on top of the FAGE cells. A 10 m long 3/8" Teflon line was installed on a mast on top of the container to sample ambient air with a rate of approximately 12 L/min. 9.5 L/min were pumped through the FAGE cells and ~2.5 L/min were sampled by an additional diaphragm pump set at the end of the photolysis cell in order to increase the refreshing time. The pressure in the cell was lower (P~725 Torr) than atmospheric pressure due to a restriction of the flow through the Teflon line. The pressure in the FAGE cells was equal to 1.72 Torr. OH was produced from the photolysis of ambient O_3 with a 266 nm laser expanded beam (dia~20 mm) with a frequency of 2 Hz (Quantel Brilliant B). The laser beam was aligned to be in the middle of the photolysis cell. The laser energy was of 10 mJ which corresponded to an energy density of 0.9 mJ/cm^2. The photolysis laser energy was observed to be stable and measured using a photodiode (Hamamatsu, S1722) before entering the photolysis cell. OH decays were measured at 308 nm with the 5 kHz SIRAH laser. The choice was made that neither O_3 nor H_2O was added to the ambient air sampled. This method has the advantage that no dilution of the air sampled is made which eased the data analysis. For zero air measurements, synthetic dry air (99.9 %, Air Liquide) was used in which a O_3 concentration of 65 ppb (using an ozone generator, Ansyco) and ~3000 ppm of H_2O (using a bubbler) were added. On Figure 3 is represented the OH decay from air zero for an accumulation of 60 photolysis laser shots.

The OH reactivity time resolution was set to be of 30 s meaning that each OH decays were accumulated over 60 photolysis laser shots. As O_3 varied from approximately 10 to 50 ppb during the measurement and no O_3 was added to the sampled flow the signal to noise ratio (S/N) varied as function of the ambient O_3 concentration. To obtain the OH reactivity data a Labview based program was developed to fit the decays, taking into account the signal to noise variations. Before fitting each OH decay, the signal to noise ratio was checked and compared to a chosen empirical value (typically 2). First, we selected a time range from 0.03 to 0.05 s, representative of the maximum signal level, and we calculated the signal mean divided by the standard deviation. If the mean divided by the standard deviation was higher than 2, the OH decay was fitted and the next OH decay was analyzed. However, if the S/N

was lower than 2, we added the present OH decay with the following one. The S/N test was run again and if S/N>2 the signal was fitted. In these conditions, when the reactivity was high and/or the O_3 concentration was low, the time resolution was lowered since 2 to 3 decays were needed to be added in order to fulfil the criterion.

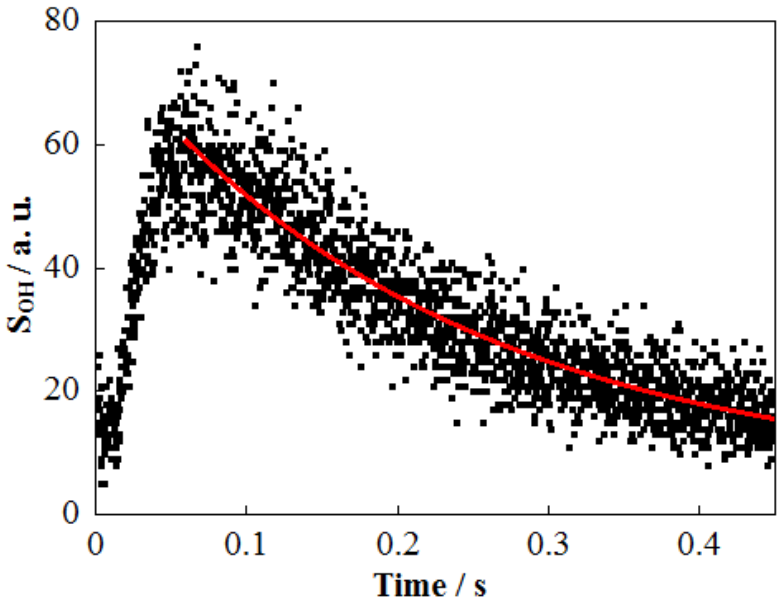

Figure 3. OH decay in zero air, k' = 4.4 ± 0.2 s^{-1}
$[O_3]$=65 ppb, $[H_2O]$~3000 ppm, [OH]~7 × 10^8 cm^{-3}
The solid line represents in a single exponential decays. Fit starts at t=0.06 s

This represents a drawback of sampling the ambient air (i.e. no O_3 or H_2O addition) alone which counterbalance the advantage of the non-dilution. In order to improve the system, we recently installed a new ozone generator based on a Hg lamp flow tube (UVP, 97-0067-02) which has the advantage to provide high O_3 concentration with a very low flow. However, this instrument was not yet available during CompOH and using the O_3 diluter (Ansyco) high flows would have been needed to increase the O_3 concentration.

Zero air measurement was made three times on the 9th and on the 10th at the beginning, in the middle and at the end of the measurement. On Figure 4 is a representation of a typical zero air measurement during CompOH. Zero air decay measurements were carried out in the same pressure conditions as ambient measurement i.e. P~725 Torr.

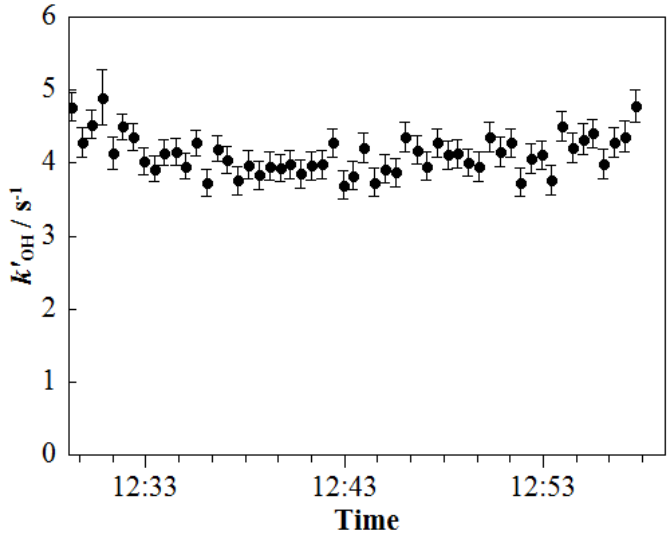

Figure 4. Example of a zero air measurement during CompOH
Error bars are 1σ fit error on the decay rate *k'*

The average of the zero air decay rate over the entire campaign was found to be 4.8 ± 0.6 s^{-1}. The minimum OH reactivity variation that can be measured with the UL-OH reactivity system is obtained from the standard deviation of the mean of zero air decay rates. From the example given on Figure 4, we obtained a mean of 4.1 s^{-1} and a standard deviation of 0.3 s^{-1}. So, we estimate our limit of detection to be of 0.6 s^{-1} at 2σ uncertainty. The main contribution for the zero decay rate comes from OH losses via physical diffusion through the photolysis cell volume. The cylinder purity was given as 99.9 % and the water was ultrapure (Milli-Q). In order to know the impact of the impurity in the zero air decay measurement, we estimated the concentration these impurity species would need to be assuming the impurity react at the same rate of:

- isoprene (k=1.1 × 10^{-10} cm^3/s) (Atkinson et al., 2006), [impurity] = 1.5 ppb
- methane (k=6.0 × 10-15 cm^3/s) (Atkinson et al., 2006), [impurity] = 25 ppm

The accuracy of the OH decay rates was obtained by measuring the rate coefficient of the reaction between OH and CO (R 4). The reaction was studied under pseudo first order conditions i.e. [CO]>>[OH]. Pseudo-first order rates were measured for different concentration of CO and the second order rate coefficient was obtained from the pseudo-first order plot (see Figure 5).

$$k' = k_{OH+CO}[CO] + k_{zero\ air} \qquad \text{Eq. 1}$$

A 0.1% CO diluted in N_2 flow was mixed with zero air with O_3 and H_2O. Flow rates were controlled using calibrated mass flow controllers. On the left panel of the Figure 5 is represented the OH decays rates for the different CO concentrations used for calibrating the UL-OH reactivity system. On the right panel a pseudo first order plot is represented where the pseudo first order rate coefficients *k'* are plotted as function of the CO concentrations. From a linear regression analysis (Eq. 1) we obtained the second-order rate coefficient which is in good agreement with the recommended IUPAC value within our pressure conditions (k_{OH+CO}=2.26 × 10^{-13} cm^{-3} s^{-1}, (Atkinson et al., 2004)). The intercept of 5.2 s^{-1} represents the air zero decay.

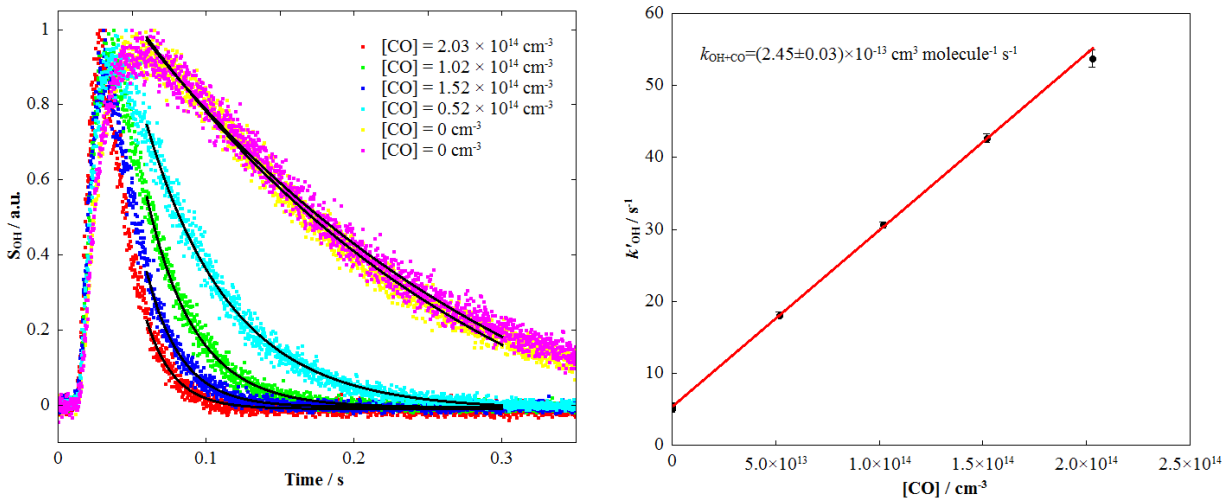

Figure 5. Plots of the OH decays for different CO concentrations (left) and pseudo-first order plot of the CO+OH reaction (right)
P=725 Torr, errors bars are 1σ
Left – Solid lines represent single exponential decays, Right – Solid line represents linear regression

2.1.2. Measurement details

During the first part of the campaign, the OH reactivity was continuously measured by the MPI-CRM. The observations showed that the total OH reactivity was very low with an average of 3.6±2.3 s^{-1} over the first 5 days of the campaign. The 3 instruments measured simultaneously only for 1 day and a half for different reasons. While the MPI-CRM was running continuously, the LSCE-CRM got important technical problems and only measured from the 8th up to the 10th. For the UL-OH reactivity, electronic problems occurred with the photolysis laser. Fortunately, we were able to replace the broken components however we were able to measure only for 1 days and a half (the 9th afternoon and the 10th). The original plan, additional to ambient measurements, was to inject known VOC mixtures in the three

different apparatus and compare the measured OH reactivity. However, due to the numerous technical problems of the UL-OH reactivity and the LSCE-CRM these experiments could not be realised. Instead, on the last afternoon of the campaign, the three sampling lines were joined together and artificial OH reactivity was generated from cigarette smoke, car exhaust, grass or melon were made in order to test the instruments on a larger range of reactivities and the measurement compared. In the end, only 9 hours of simultaneous ambient measurement are available. Intensive VOC measurements along with NOx, CO and O_3 were made during this time periods. In Table 3 is summarized the mean and standard deviation of the ancillary measurement between the 9th and the 10th of July. In addition, we assumed that the CH_4 concentration was constant and equal to 1.8 ppm.
(http://www.ncdc.noaa.gov/oa/climate/gases.html).

Table 3. Mean and standard deviations of NO, NO_2, O_3, CO and VOCs between the 9th and the 10th of July

Species	mean ± SD	Species	mean ± SD
NO / ppbv	2 ± 7	benzene / pptv	113 ± 52
NO_2 / ppbv	5 ± 4	ethylbenzene / pptv	265 ± 225
O_3 / ppbv	31 ± 10	heptane / pptv	66 ± 84
CO / ppbv	110 ± 25	octane / pptv	72 ± 78
ethane / pptv	725 ± 434	toluene / pptv	940 ± 1133
ethylene / pptv	729 ± 522	1,3,5-TMB / pptv	107 ± 119
propane / pptv	351 ± 484	1,2,4-TMB / pptv	200 ± 251
propene / pptv	194 ± 126	1,2,3-TMB / pptv	47 ± 59
n-butane / pptv	292 ± 193	m,p-xylene / pptv	582 ± 647
i-butane / pptv	316 ± 303	o-xylene / pptv	195 ± 214
acetylene / pptv	218 ± 163	isoprene / pptv	15 ± 15
1,3-butadiene / pptv	345 ± 350		

2.2. Results and discussion

On Figure 6 is represented the measurement of the total OH reactivity by the three different instruments along with the measurement of CO, O_3 and NOx for the complete intercomparison. The analysis of the results is split into two parts:

(i) ambient measurement from the 9th midday up to the 10th midday,

(ii) forced OH reactivity measurement on the afternoon of July10th.

All the data were averaged or interpolated to 5 min. For the ambient measurements, the calculated OH reactivity was determined using the concentration of each individual measurement and the bimolecular rate coefficients given in Table 4.

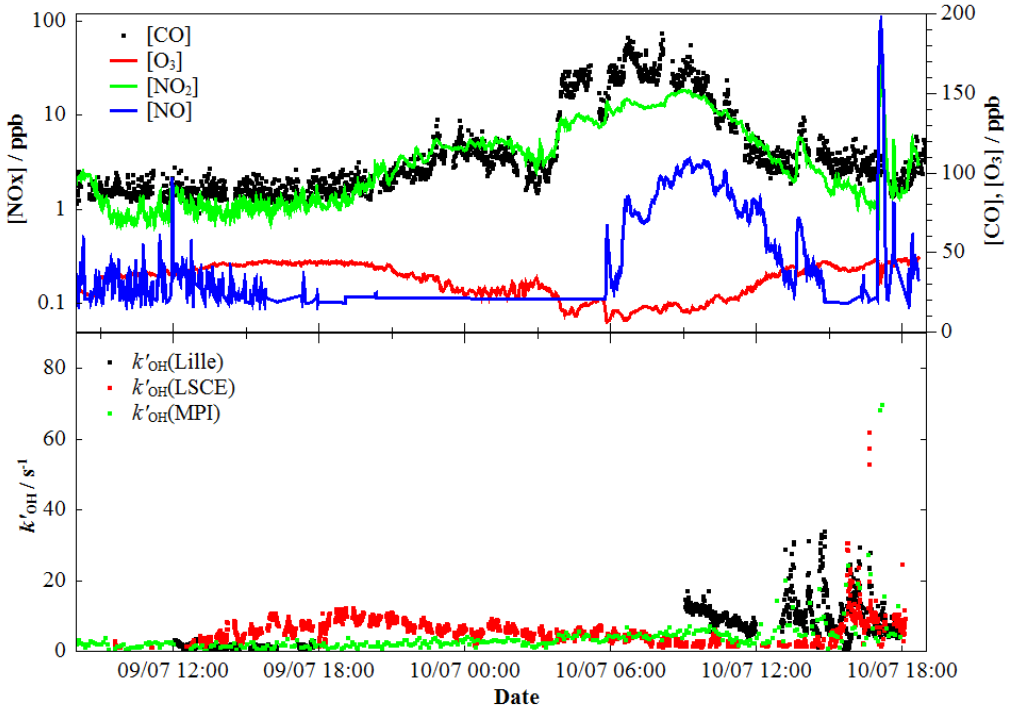

Figure 6. OH reactivity measurement between the 9th and the 10th.
Top panel – Ancillary measurements: CO (black dots), O_3 (red line) NO (blue line) and NO_2 (green line)
Bottom panel – OH reactivity measurements: UL-OH reactivity (black dots),

2.2.1. Ambient measurements

A close up of the ambient measurement is given in Figure 7. On the 9th afternoon, the NOx concentration was very low with concentration of NO and NO_2 lower than 1 ppb. The CO concentration was of 100 ppb. The O_3 concentration reached a maximum of approximately 45 ppb. During this first period (from 12:00 to 18:00), the measurement by the Lille and the MPI instruments are similar with the measurement of a steady OH reactivity of k'_{OH}(MPI) =1.62 ± 0.74 s^{-1} and k'_{OH}(Lille) =1.47 ± 0.34 s^{-1} in agreement with the calculated OH reactivity k'_{OH} (calculated) = 1.43 ± 0.21 s^{-1}. During this period, the OH reactivity was dominated by CO, CH4 and NOx and accounted for almost 75% of the total OH reactivity as can be seen on Figure 8. The percentage of missing OH reactivity during this measurement period was of 4 % for Lille and 13 % for Mainz. On the other hand, the LSCE instruments displayed a very different profile with a maximum reactivity of approximately 10 s^{-1} around 4 pm and a mean of k'_{OH}(LSCE) = 5.40 ± 2.10 s^{-1} (74 % of missing reactivity). The strong disagreement of the

LSCE measurement was afterwards related to the temperature inside the container however no corrections of the data were given at the time of writing this manuscript.

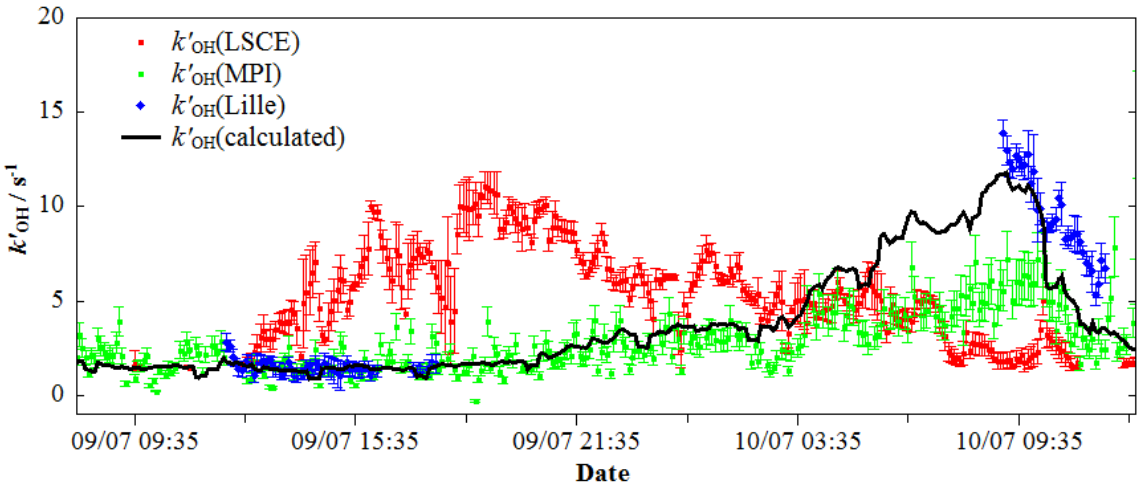

Figure 7. Close up of the ambient measurement by the three instruments
OH reactivity measurements from LSCE (red dots), MPI (green dots) and Lille (blue dots)
The solid line represents the calculated OH reactivity

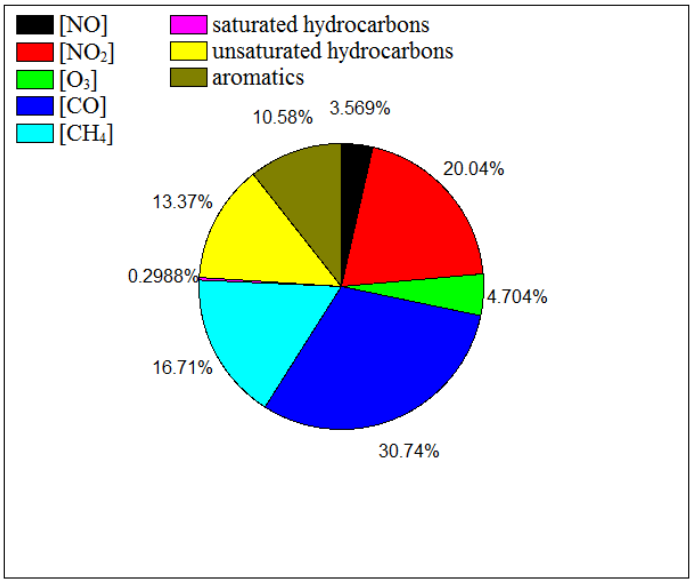

Figure 8. Pie chart of the contribution of the different measured species to OH reactivity. from 12:00 to 18:00 on July 9th.

During the night a pollution plume from Paris was observed with a sharp increase of the CO and NO_2 concentrations around 3 am on the 10th. The UL-OH reactivity instrument was not measuring. The LSCE and the MPI instruments measured extremely different profiles. The LSCE-CRM measured a decrease of the reactivity whereas the MPI-CRM observed a slow increase in agreement with the calculated OH reactivity. On the morning measurement of the

10th, all three instruments were measuring but none of them were measuring the same OH reactivity. The calculated OH reactivity showed that OH reactivity was dominated in decreasing order by the NOx, the aromatic hydrocarbons, NO, the unsaturated species and CO (Figure 9). Comparison with different instruments that both CRM underestimated the OH reactivity (the MPI-CRM underestimated by a factor of 0.6, the LSCE-CRM by a factor of 2.2) whereas the UL-OH reactivity overestimated the OH reactivity by 24%. During this period, the NO concentration was 1.98 ± 0.78 ppb. It is well known that the OH reactivity methods suffer from a NO interference mainly due to the recycling of OH via the reaction of HO_2 with NO which tends in both methods to underestimate the OH reactivity. The MPI-CRM data are the only data corrected for the NO interference: during the morning measurement period, the raw data were multiplied on average by a factor of 2.3 in order to obtain the final data. No correction on the OH reactivity data as function of the NO concentration was given for the LSCE-CRM and the UL-OH reactivity. From laboratory measurements it was found for the LSCE-CRM found that at a concentration of 5 ppb the total OH reactivity needed to be multiplied by a factor 1.13 (Dolgorouky et al., 2012). However, the NO concentration was only of 2 ppb meaning that the correction would be less than 10%. For the UL-OH reactivity, the dependence of the decay rate measurement as function of the NO concentration was not yet performed. Nevertheless, the Lille instrument was inspired from the Tokyo OH reactivity instrument in which a correction of less than 5 % was estimated for a NO concentration of 20 ppb.

Definitive conclusions are difficult to draw as the data are still preliminary and some corrections are needed for the LSCE-CRM. However, from these results, we observed that during an unpolluted event the MPI-CRM and the UL-OH reactivity were in agreement within their respective errors whereas during the moderated pollution event on the morning of the 10th, they have shown a disagreement. Even though the MPI-CRM OH reactivity data were corrected for the NO concentration, the OH reactivity data were lower than the calculated OH reactivity. The NO correction on the OH reactivity measurement using the UL-OH reactivity instrument will be performed in the near future.

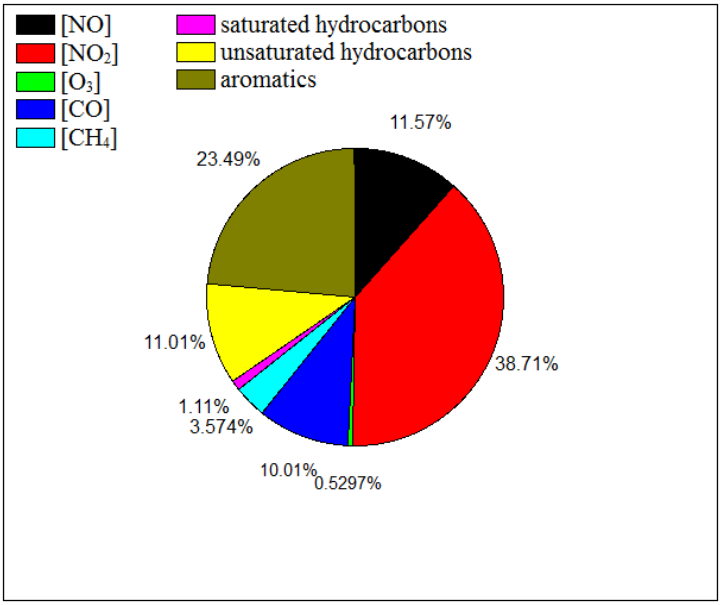

Figure 9. Pie chart of the contribution of the different measured species to OH reactivity from 9:00 to 12:00 on July 10th.

Table 4. Bimolecular rate coefficients of the different organic and inorganic species measured during CompOH.
The rate coefficients are given at T=298K and P=10^5 Pa. For the OH reactivity calculation, ambient pressure and temperature were used (Atkinson and Arey, 2003).

Species	rate coefficients	Species	rate coefficients
Inorganic		- *Unsaturated hydrocarbons*	
NO	1.8×10^{-11}	ethylene	9.1×10^{-12}
NO_2	1.1×10^{-11}	propene	3.0×10^{-11}
O_3	7.3×10^{-14}	acetylene	1.0×10^{-12}
CO	2.2×10^{-13}	1,3-butadiene	2.9×10^{-12}
		isoprene	1.0×10^{-10}
Organic			
- *Aromatics*		- *Saturated hydrocarbons*	
benzene	1.2×10^{-12}	methane	6.4×10^{-15}
ethylbenzene	7.0×10^{-12}	ethane	2.4×10^{-13}
toluene	5.6×10^{-12}	propane	1.1×10^{-12}
1,3,5-TMB	5.7×10^{-13}	i-butane	5.0×10^{-13}
1,2,4-TMB	3.3×10^{-13}	n-butane	2.4×10^{-12}
1,2,3-TMB	3.3×10^{-13}	heptane	4.4×10^{-13}
m,p-xylene	1.1×10^{-11}	octane	7.1×10^{-13}
o-xylene	1.7×10^{-12}		

2.2.2. Forced measurements

For the last measurement period in the afternoon of the 10th, the 3 sampling lines were joined together (see Figure 10) and artificial OH reactivity was produced from melon, grass, cigarette smoke, cola, onion and car exhaust.

Figure 10. Photograph of the experiment performed on July 10th during CompOH

The aim of this experiment was to generate a higher reactivity range than the ambient reactivity. No ancillary measurements were performed during this period and so only the profile and absolute reactivities can be looked at. The OH reactivity measurement displayed spikes due to the presence of for example grass at the entrance of the sampling line. Generally, we observed a relative good agreement between the three instruments. However, the MPI-CRM observed much higher OH reactivity than the two other instruments especially the UL-OH reactivity set-up. The main reason is that when reactants were placed in front of the line a puff containing high concentration of VOC was sampled. Due to the high VOC concentration, the OH generated inside the photolysis cell reacted very rapidly and in consequence it was not possible to record any OH decays as the signal to noise ratio was too low. This shows one limitation of the UL-OH reactivity system in the configuration such as used during CompOH when only ambient O_3 is used to generate OH radicals. Ideally, by adding a constant high O_3 concentration (60 to 100 ppb) through the photolysis cell, the signal will become less dependent on the ambient O_3 concentration. When car exhaust was sampled we can observed that MPI-CRM measured negative reactivity due to the high NO concentration (data not corrected). During this experiment, the UL-OH reactivity did not measure any significant

reactivity because of the too high reactant concentration released from the car exhaust. The problem of this experiment was the high variation of the reactivity which limits the data interpretation.

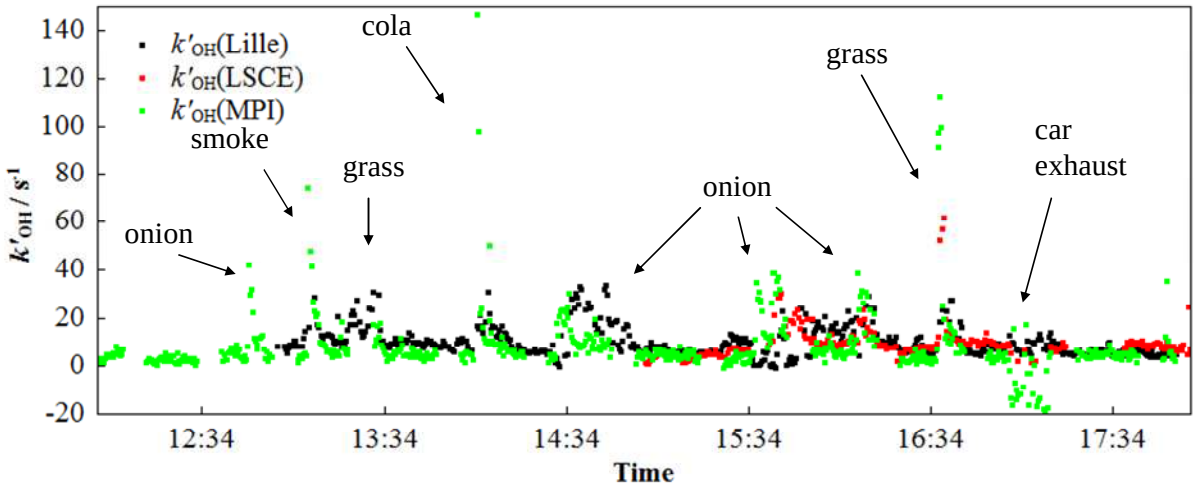

Figure 11. OH reactivity measurement on July 10th afternoon.
Lille (black dots), LSCE (Red dots), MPI(green dots)

We have presented the first intercomparative measurements between three instruments that measure OH reactivity. Due to technical problems, only a small data set can be used for the analysis. Preliminary conclusions show that under non-polluted conditions the flash photolysis and the CRM technique show very good agreement. However, under a moderated pollution event, we observed that, compared to the calculated OH reactivity, the CRM instruments were underestimating the OH reactivity by a factor from 0.6 to 2.2 indicating that the applied NO correction was not sufficient. This first attempt to intercompare the CRM with the flash photolysis technique was a relative success. It showed the need to undergo intercomparison in a similar fashion to the comparison made for HOx quantification in more controlled conditions. Intercomparative measurement could be performed in atmospheric chambers such as the SAPHIR chamber where conditions can be controlled and varied over large ranges. The impact of NO on the measurement of OH reactivity is one of the main issue and need to be investigated for every instrument.

2.2.3. Correlation plots

An additional to analyze and compare the OH reactivity measurement during the intercomparison is to plot one measurement versus another measurement. Figure 12 presents a scatter plot where the OH reactivity measurement data points from the MPI-CRM were plotted as function of the UL-FAGE OH reactivity data points. For the correlation plot, the data were averaged to 5 min. Since large variations were observed on the 10th afternoon during the non-ambient measurement, the data were excluded from the scatter plots. Only were included the data from the 9th afternoon and the 10th morning. During this period, both apparatus measured 70 simultaneous points. By applying a linear regression to the data points, we obtained a slope equal to 0.41 ± 0.02, an intercept of 0.82 ± 0.17 s^{-1} and a coefficient of determination r^2 = 0.80. These results indicate that most of the variations were observed by the two instruments however the quantitative agreement is poor. The UL-OH reactivity system measured 60 % higher OH reactivity than the MPI-CRM instrument. As already discussed previously, the most likely explanation would be that one or the two instrument are poorly characterized for the well-known NO interference.

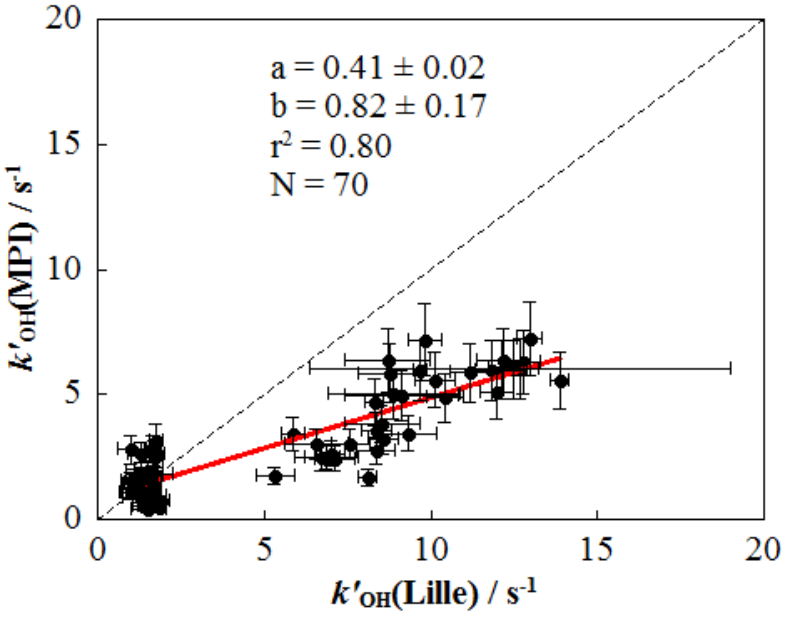

Figure 12. Scatter plots of the OH reactivity measurement by the MPI-CRM vs. the UL-FAGE OH reactivity system. Data were averaged to 5 min. Errors are given at 1σ. The solid line corresponds to a linear regression, y = ax+b.

3. Study of the reaction between NO_2* and H_2O

In this work, we took advantage of the high sensitivity of the FAGE technique to study the controversial reaction between NO_2* and H_2O as a source of OH radicals.
Indeed, a new potential source of atmospheric OH was recently proposed through the reaction of electronically excited NO_2 by visible light with H_2O via the following mechanism

$$NO_2 + h\nu\ (\lambda > 420\ nm) \rightarrow NO_2^* \quad (R\ 6)$$
$$NO_2^* + H_2O \rightarrow OH + HONO \quad (R\ 7)$$

The electronically excited NO_2 can also be deactivated through collisions with other molecules

$$NO_2^* + H_2O \rightarrow NO_2 + H_2O \quad (R\ 8)$$
$$NO_2^* + N_2 \rightarrow NO_2 + N_2 \quad (R\ 9)$$
$$NO_2^* + O_2 \rightarrow NO_2 + O_2 \quad (R\ 10)$$

Li et al. (Li et al., 2008) have studied the reaction at low pressure by exciting NO_2 in the 560-640 nm range in the presence of water vapour and using in-situ laser induced fluorescence to follow the OH formation. They have reported a rate constant for the reaction (R 7) of 1.7×10^{-13} cm^3 s^{-1} and shown that the OH generated had a linear dependence with respect to energy flux which excluded a multi-photon absorption process. The upper limit, defined as k_7/k_8 (i.e. ratio between reactive quenching and collisional quenching), obtained in their work was 1×10^{-3}.
In a previous study, Crowley and Carl (Crowley and Carl, 1997) observed an OH formation below 450 nm from a 2-photons absorption by NO_2 leading to $O(^1D)$ formation followed by the reaction with H_2O. Nevertheless, they did not observe OH formation at 532 nm, where the 2-photon process is not sufficiently energetic to form $O(^1D)$, and they established an upper limit equal to 7×10^{-5}, more than one order of magnitude lower than the one reported by Li et al (Li et al., 2008).
Wennberg and Dabdub (Wennberg and Dabdub, 2008) performed a model accounting for the result from Li et al. (Li et al., 2008) under polluted urban conditions. Even though this reaction has a low yield (1×10^{-4}), i.e. fraction of NO_2* that reacts with H_2O rather than being quenched (reactions [(R 8)-(R 10)]) to NO_2, a significant increase in percentage of O_3 concentration up to 40 % was calculated.

The disagreement between the two studies and the possible major impact of this reaction on atmospheric chemistry lead to a new study by Carr et al. (Carr et al., 2009). They failed to observe OH formation from the excited NO_2 reaction with H_2O using an unfocused laser excitation. The upper limit calculated from their study was 6×10^{-5} at the 2σ level, in good agreement with Crowley et al. (Crowley and Carl, 1997). They concluded that the OH formation observed by Li et al. (Li et al., 2008) could have been generated from a multi-photon process even though this possibility was ruled out by Li et al. (Li et al., 2008). They highlighted that the dependence of OH signal on laser fluence although linear had a negative intercept which was in contradiction with a single photon absorption process. Li et al. (Li et al., 2009) gave an answer to this comment, they mentioned that the negative intercept was likely due to an electronic offset and that the energy fluence used was higher in their study.

To conclude on whether this reaction is relevant on atmospheric chemistry, we studied the reaction using a laser photolysis cell coupled to FAGE (Fluorescence Assay Detection by Gas Expansion) cells for the detection of OH radicals using an unfocused and a focused excitation beam. The high sensitivity of the FAGE permits to detect lower OH concentrations than in the previous studies. Here are only presented highlights of the results obtained from the study of the excited NO_2 reaction with H_2O, more details can be found in Amedro et al. (Amedro et al., 2011).

A photolysis flow tube was coupled to the FAGE cell in the 90° configuration in order to follow OH decays. Gas was pumped continuously from the laser photolysis cell (held at 11 Torr in He) through a small aperture (1 mm) into the FAGE detection cells (1.5 Torr) at a flow rate of 300 ccm STP. The excitation beam is generated by a dye laser (Quantel TDL50, Rhodamine 590), pumped by a frequency doubled YAG laser (Quantel YG 781C) and had a repetition rate of 2 Hz. For the excitation of NO_2, the dye laser beam has been used directly at 565 nm with pulse energies of 9 to 15 mJ $pulse^{-1}$, while for the relative calibration measurements a doubling crystal was introduced into the laser beam and O_3 was photolysed at 282.5 nm in the presence of H_2O with pulse energies of 3 mJ $pulse^{-1}$

$$O_3 + h\nu \rightarrow O(^1D) + O_2 \qquad \text{(R 11)}$$
$$O(^1D) + H_2O \rightarrow 2OH \qquad \text{(R 12)}$$

The low yield of OH formation from the reaction (R 7) along with the low time resolution, due to the separation between radical generation and detection in our system obliged the experimental conditions to be chosen carefully in order to achieve the detection of OH. The

measurements were made at low pressure (11 Torr Helium) and with a maximum NO_2 concentration set to 2×10^{14} cm^{-3} in order to diminish the rate of the strongly dependent reaction of OH with NO_2 and be able to follow the OH decay rate through the reaction with NO_2.

Figure 13 shows the OH signals from the calibration with O_3 at 282.5 nm and from the reaction of excited NO_2 with H_2O at 565 nm under unfocused conditions (upper graph a) and under focused conditions (lower graph b).

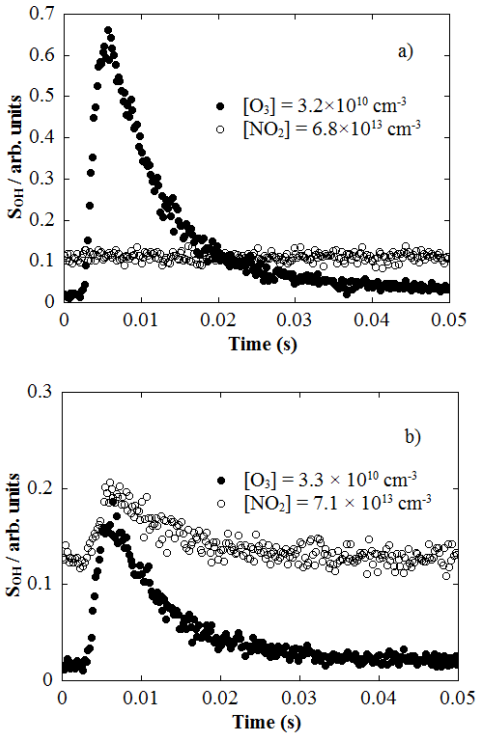

Figure 13. Formation of OH radicals from O_3 (closed symbols, 3 mJ at 282.5 nm excitation) and NO_2 (open symbols, 15 mJ at 565 nm excitation): graph (a) unfocused excitation laser and graph (b) focused laser.

We can clearly see that under unfocused conditions no OH formation was observed from the excited NO_2 reaction with H_2O even though the sensitivity was 3-4 times higher than in focused conditions, due to the bigger distance between the beam and the nozzle, involving mores losses by diffusion out of the probing volume. This is a clear indication that the single-photon absorption process used to explain the formation of OH from the excited NO_2 reaction with H_2O can be ruled out as the same laser power being used, the same OH concentration should be produced in both configurations, and should be even better seen in the unfocused condition where the sensitivity is higher. From the measurements under unfocused conditions, and using the calibration factor from the O_3 calibration, the upper limit obtained was 8×10^{-6}

at the 1σ level, in agreement with the results from Carr et al. (Carr et al., 2009) and Crowley et al. (Crowley and Carl, 1997).

From the measurements under focused conditions and using the O_3 photolysis calibration, the upper limit calculated was 1×10^{-3} in good agreement with Li et al. (Li et al., 2008). It can be seen on Figure 14, showing the dependence of the OH-signal seems to be linear with laser fluence, that the linear regression does not pass through the origin and shows a negative intercept. It is interesting to remark that the same observations were made by Li et al. (Li et al., 2008) and they explained it as an electronic offset. In our experiment, we do not observe any electronic offset, this is understandable as the generation and the detection are physically separated and also time delayed (Δt ~ 2 ms). The dashed line in Figure 14 represents a squared dependence of the OH-signal as function of the excitation beam, involving a 2 photon absorption by the same NO_2. It can be seen that such dependence can not be excluded; however, our energy range is too small to draw any further conclusions.

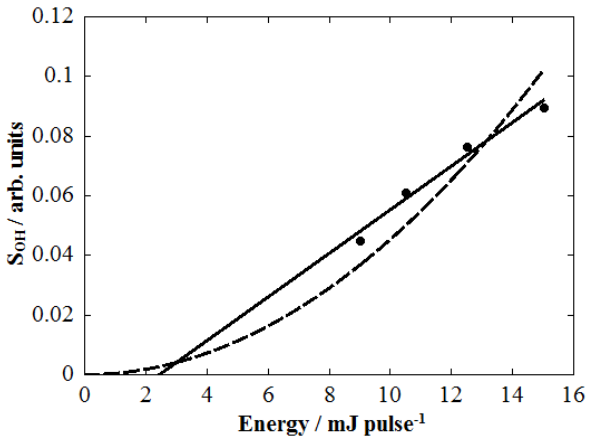

Figure 14. Intensity of the OH fluorescence signal as a function of the photolysis energy: full line linear regression, dashed line squared dependence of OH-signal as function of photolysis energy.

Figure 15 shows the dependence of the OH signal as function of the NO_2 concentration and it can be observed that the linear regression does not pass through the origin even though no OH was observed in the absence of NO_2. Li et al. (Li et al., 2008) proposed a mechanism involving two excited NO_2* that could explained the OH(v=1) they observed in their work

$$NO_2^* + H_2O \rightarrow NO_2 + H_2O^* \quad \text{(R 13)}$$

$$NO_2^* + H_2O \rightarrow OH(v'' \geq 1) + HONO \quad \text{(R 14)}$$

As this mechanism would involved two excited NO_2*, the OH signal should exhibit a squared dependence on the reactant concentration, [NO_2], as well as on the laser fluence as pointed out by Carr et al. (Carr et al., 2009). In our experiment, the reactant concentration decreased rapidly due to diffusion out of the very small photolysis volume, thus information about the mechanism from the Figure 15 are difficult to deduce reliably.

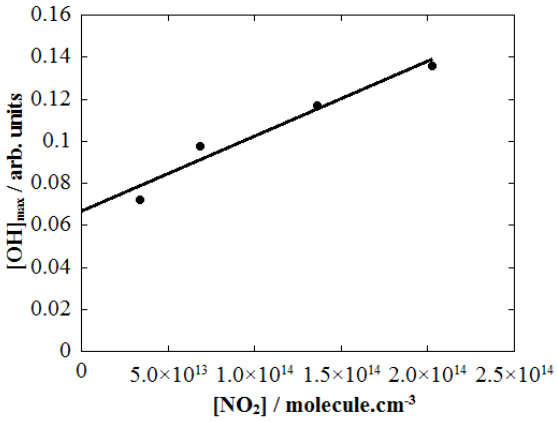

Figure 15. Intensity of the OH signal as function of NO_2 concentration: full line linear regression

In this work, we have shown that the OH formation from the NO_2 excited reaction with H_2O at 565 nm was not originated from a single absorption process. Nevertheless, due to the experimental conditions, conclusive information about the mechanism can not be drawn. The compelling experiment in this work is that we observed OH radicals with a similar yield to Li et al. (Li et al., 2008) when using a focused excitation beam, but we did not observe any OH when using an unfocused beam. The OH yield for the reaction (R 7) calculated from our study was 8×10^{-6} more than one order of magnitude lower than the one obtained from Li et al. (Li et al., 2008). In consequence, from our results, this reaction does not play any significant role under atmospheric conditions.

Conclusion

In this chapter, we described the OH reactivity technique that was developed at the University of Lille. Based on the flash photolysis method, we described the different tests that were conducted to understand the physical effects that affect the OH decay profile. By expanding the laser beam, we were able to obtain single exponential decays which are easier to analyze. Two different configurations were tested. The Online Configuration (OLC) was found to be less affected by physical effects compared to the Ninety Degree Configuration (NDC). Also, the range of reactivity measured is larger in the OLC than in the NDC. However, the NDC is more appropriate when the FAGE was deployed on the field since the FAGE cells do not need to be turned.

The UL-OH reactivity system was deployed for the first time during CompOH where it was intercompared with two other instruments based on the CRM technique. The results showed a good agreement under very low NO conditions whereas discrepancies were observed under high NO concentration. The need to perform other intercomparative measurements under more controlled conditions was shown.

Also, we demonstrated that the high sensitivity of the UL-OH reactivity instrument could be adapted for kinetic measurements with the study of the NO_2* with H_2O reaction. We have shown that the OH formation from the NO_2 excited reaction with H_2O at 565 nm was not originated from a single absorption process. In consequence, from our results, we concluded that this reaction does not play any significant role under atmospheric conditions.

4. References

Amedro, D., Miyazaki, K., Parker, A., Schoemaecker, C. and Fittschen, C.: Atmospheric and kinetic studies of OH and HO2 by the FAGE technique, Journal of Environmental Sciences, 24(1), 78–86, doi:10.1016/S1001-0742(11)60723-7, 2012.

Amedro, D., Parker, A. E., Schoemaecker, C. and Fittschen, C.: Direct observation of OH radicals after 565 nm multi-photon excitation of NO2 in the presence of H2O, Chemical Physics Letters, 513(1–3), 12–16, doi:10.1016/j.cplett.2011.07.062, 2011.

Atkinson, R. and Arey, J.: Atmospheric Degradation of Volatile Organic Compounds, Chem. Rev., 103(12), 4605–4638, doi:10.1021/cr0206420, 2003.

Atkinson, R., Baulch, D. L., Cox, R. A., Crowley, J. N., Hampson, R. F., Hynes, R. G., Jenkin, M. E., Rossi, M. J. and Troe, J.: Evaluated kinetic and photochemical data for atmospheric chemistry: Volume I - gas phase reactions of Ox, HOx, NOx and SOx species, Atmos. Chem. Phys., 4(6), 1461–1738, doi:10.5194/acp-4-1461-2004, 2004.

Atkinson, R., Baulch, D. L., Cox, R. A., Crowley, J. N., Hampson, R. F., Hynes, R. G., Jenkin, M. E., Rossi, M. J., Troe, J. and IUPAC Subcommittee: Evaluated kinetic and photochemical data for atmospheric chemistry: Volume II – gas phase reactions of organic species, Atmos. Chem. Phys., 6(11), 3625–4055, doi:10.5194/acp-6-3625-2006, 2006.

Carlo, P. D., Brune, W. H., Martinez, M., Harder, H., Lesher, R., Ren, X., Thornberry, T., Carroll, M. A., Young, V., Shepson, P. B., Riemer, D., et al.: Missing OH Reactivity in a Forest: Evidence for Unknown Reactive Biogenic VOCs, Science, 304(5671), 722–725, doi:10.1126/science.1094392, 2004.

Carr, S., Heard, D. E. and Blitz, M. A.: Comment on “Atmospheric Hydroxyl Radical Production from Electronically Excited NO2 and H2O”, Science, 324(5925), 336b–336b, doi:10.1126/science.1166669, 2009.

Crowley, J. N. and Carl, S. A.: OH Formation in the Photoexcitation of NO2 beyond the Dissociation Threshold in the Presence of Water Vapor, J. Phys. Chem. A, 101(23), 4178–4184, doi:10.1021/jp970319e, 1997.

Dolgorouky, C., Gros, V., Sarda-Esteve, R., Sinha, V., Williams, J., Marchand, N., Sauvage, S., Poulain, L., Sciare, J. and Bonsang, B.: Total OH reactivity measurements in Paris during the 2010 MEGAPOLI winter campaign, Atmospheric Chemistry and Physics Discussions, 12(4), 10937–10994, doi:10.5194/acpd-12-10937-2012, 2012.

Lee, J., Young, J., Read, K., Hamilton, J., Hopkins, J., Lewis, A., Bandy, B., Davey, J., Edwards, P., Ingham, T., Self, D., et al.: Measurement and calculation of OH reactivity at a United Kingdom coastal site, Journal of Atmospheric Chemistry, 64(1), 53–76, doi:10.1007/s10874-010-9171-0, 2009.

Li, S., Matthews, J. and Sinha, A.: Atmospheric Hydroxyl Radical Production from Electronically Excited NO2 and H2O, Science, 319(5870), 1657–1660, doi:10.1126/science.1151443, 2008.

Li, S., Matthews, J. and Sinha, A.: Response to Comment on "Atmospheric Hydroxyl Radical Production from Electronically Excited NO2 and H2O", Science, 324(5925), 336c–336c, doi:10.1126/science.1166877, 2009.

Lou, S., Holland, F., Rohrer, F., Lu, K., Bohn, B., Brauers, T., Chang, C. C., Fuchs, H., Häseler, R., Kita, K., Kondo, Y., et al.: Atmospheric OH reactivities in the Pearl River Delta – China in summer 2006: measurement and model results, Atmos. Chem. Phys., 10(22), 11243–11260, doi:10.5194/acp-10-11243-2010, 2010.

Nölscher, A. C., Williams, J., Sinha, V., Custer, T., Song, W., Johnson, A. M., Axinte, R., Bozem, H., Fischer, H., Pouvesle, N., Phillips, G., et al.: Summertime total OH reactivity measurements from boreal forest during HUMPPA-COPEC 2010, Atmos. Chem. Phys., 12(17), 8257–8270, doi:10.5194/acp-12-8257-2012, 2012.

Ren, X., Harder, H., Martinez, M., Lesher, R. L., Oliger, A., Shirley, T., Adams, J., Simpas, J. B. and Brune, W. H.: HOx concentrations and OH reactivity observations in New York City during PMTACS-NY2001, Atmospheric Environment, 37(26), 3627–3637, doi:10.1016/S1352-2310(03)00460-6, 2003.

Sadanaga, Y., Yoshino, A., Watanabe, K., Yoshioka, A., Wakazono, Y., Kanaya, Y. and Kajii, Y.: Development of a measurement system of OH reactivity in the atmosphere by using a laser-induced pump and probe technique, Review of Scientific Instruments, 75(8), 2648–2655, doi:doi:10.1063/1.1775311, 2004.

Wennberg, P. O. and Dabdub, D.: ATMOSPHERIC CHEMISTRY: Rethinking Ozone Production, Science, 319(5870), 1624–1625, doi:10.1126/science.1155747, 2008.

Whalley, L. K., Edwards, P. M., Furneaux, K. L., Goddard, A., Ingham, T., Evans, M. J., Stone, D., Hopkins, J. R., Jones, C. E., Karunaharan, A., Lee, J. D., et al.: Quantifying the magnitude of a missing hydroxyl radical source in a tropical rainforest, Atmos. Chem. Phys., 11(14), 7223–7233, doi:10.5194/acp-11-7223-2011, 2011.

Yoshino, A., Nakashima, Y., Miyazaki, K., Kato, S., Suthawaree, J., Shimo, N., Matsunaga, S., Chatani, S., Apel, E., Greenberg, J., Guenther, A., et al.: Air quality diagnosis from comprehensive observations of total OH reactivity and reactive trace species in urban central Tokyo, Atmospheric Environment, 49(0), 51–59, doi:10.1016/j.atmosenv.2011.12.029, 2012.

Yoshino, A., Sadanaga, Y., Watanabe, K., Kato, S., Miyakawa, Y., Matsumoto, J. and Kajii, Y.: Measurement of total OH reactivity by laser-induced pump and probe technique—comprehensive observations in the urban atmosphere of Tokyo, Atmospheric Environment, 40(40), 7869–7881, doi:10.1016/j.atmosenv.2006.07.023, 2006.

Thesis summary

From this thesis work, we have shown that the UL-FAGE is suitable for the ambient measurements of OH and HO_2 radicals. The UL-FAGE was designed following the numerous improvements that were made over the last 20 years. The instrument is now fully automated and can be deployed on the field much more easily than at the beginning of this thesis. The purchase of the measuring container along with the knowledge we have learnt through the different field measurements will be useful for the future campaigns.

In Chapter 1, from the review of the different techniques that measures OH and HO_2, we put the development of the UL-FAGE in perspective. Measurements of OH radicals using the FAGE technique have been very successful. The CIMS technique is the only other available technique that owns the sensitivity and time resolution for the measurement of OH. Recently, Mao et al. (Mao et al., 2012) showed that their instruments based on the FAGE technique was suffering of an unknown interference. They observed that the OH was produced internally within the FAGE cells. For HO_2, the FAGE technique was up to recently thought to be the most sensitive and selective technique. However, Fuchs et al. (Fuchs et al., 2011) showed that detection of certain RO_2 species were corrupting the HO_2 measurement using FAGE. These newly discovered interferences for the measurement of OH and HO_2 cast doubt on the selectivity of the FAGE technique.

Each part of the UL-FAGE was described in Chapter 2. The calibration procedure was explained. The LOD for OH and HO_2 was found to be of 4×10^5 and 5×10^6 cm^{-3} respectively for one minute integration time. The strong H_2O dependence of the sensitivity using the calibration source could not be reproduced during ambient measurements. Interferences were observed for O_3 and acetone. Results have shown that these interferences were negligible in most of environments. However, we observed that the O_3 interference, contrary to acetone, was independent of the laser power. This indicates that OH is produced internally from an unknown dark reaction i.e. non-photolytic.

In Chapter 3, we presented the intercomparative measurement with the FZJ-LIF in the SAPHIR chamber in 2010. The results have shown an excellent agreement for the OH measurement over a wide range of concentrations and conditions. From the exchange of the calibration source, we concluded that a great part of the difference measured between the two instruments was due to the calibration. For HO_2, the correlation was found to be very good however the FZJ-LIF measured on average 50 % more than the UL-FAGE. Both instruments suffered from the RO_2 interference with different magnitudes.

Two ambient measurements in which the UL-FAGE was deployed were presented in Chapter 4. During CompOH, the UL-FAGE was intercompared with the LATMOS-CIMS. The correlation was good but non-linear. The explanations for this have not been found yet. In a second part, we reported the first direct measurement of OH and HO_2 radicals indoor. Concentrations up to 1×10^6 cm^{-3} and 2.5×10^7 cm^{-3} were measured for OH and HO_2 respectively. We observed that the formation of OH was linked with the HONO concentration and the photolysis rate intensities even though most of the UV light spectra is cut out by the windows.

In the last chapter, attention was given to the measurement of OH reactivity. We presented the apparatus that was adapted from the FAGE system to measure OH reactivity. The UL-OH reactivity was deployed during the CompOH intercomparative measurement. Agreement was observed between the UL-OH reactivity system and the MPI-CRM instrument under low NO condition. However, strong disagreement was observed under moderately high NO concentration. The UL-OH reactivity system was also used for the study of the reaction between NO_2* and H_2O as a new potential OH source. From our measurement, we concluded that this reaction has no impact on the tropospheric chemistry.

Abstract

HOx(=OH+HO_2) radicals play a central role in the degradation of hydrocarbons in the troposphere. Reaction of OH with hydrocarbons leads in the presence of NOx to the formation of secondary pollutants such as O_3. Due to its high reactivity, the concentration of OH radicals (<0.1ppt) and its lifetime are very low (<1s). In order to validate atmospheric chemistry models, the development of highly sensitive instruments for the measurement of OH and HO_2 is needed. An instrument based on the FAGE technique (Fluorescence Assay by Gas Expansion) was developed at the University of Lille for the simultaneous measurement of HOx radicals. The limit of detection for OH and HO_2 is of 4×10^5 cm^{-3} and 5×10^6 cm^{-3} respectively for 1 min integration time, appropriate for ambient measurements. The instrument was deployed in 4 field campaigns in different environments: simulation chamber, rural, suburban and indoor. The Lille FAGE was validated during 2 intercomparative measurements in an atmospheric chamber and in ambient air. In parallel, the FAGE set-up was adapted for the measurement of the OH reactivity. OH reactivity is the measure of the total loss of OH radicals that includes the reaction of all chemical species with OH. Ambient air is sampled through a photolysis cell where OH is artificially produced and it decays from the reaction with reactants present in ambient air is recorded by LIF in the FAGE. The OH reactivity system was deployed during an intercomparative measurement and used for the study of the reaction between NO_2* and H_2O as a source of OH.

Keywords: HOx radicals, FAGE, Intercomparative measurement, OH reactivity

Résumé

Les radicaux HOx (=OH+HO_2) jouent un rôle central dans la dégradation des hydrocarbures dans la troposphère. La réaction d'OH avec les hydrocarbures mène en présence de NOx à la formation de polluants secondaires comme l'ozone. Du fait de sa réactivité élevée, la concentration en OH (<0.1 ppt) ainsi que son temps de vie (<1 s) sont faibles. Pour valider les modèles de chimie atmosphérique, le développement d'appareils capable de mesurer ces très faibles concentrations est nécessaire. Un appareil basé sur la technique FAGE (Fluorescence Assay by Gas Expansion) a été développé à l'Université de Lille pour la mesure simultanée des radicaux HOx. La limite de détection atteinte est de 4×10^5 cm^{-3} pour OH and et 5×10^6 cm^{-3} pour HO_2 pour un temps de mesure de 1 min. L'appareil a été utilisé dans 4 campagnes de mesure dans différents environnements : en chambre de simulation, en milieu rural, en milieu urbain et à l'intérieur d'une classe. Le FAGE de Lille a été validé grâce à 2 intercomparaisons en chambre de simulation et en air ambiant. En parallèle, le FAGE a été adapté pour la mesure de la réactivité d'OH. La réactivité d'OH est l'inverse du temps de vie. L'air ambiant est échantillonné au travers d'une cellule de photolyse dans laquelle OH est produit. La décroissance d'OH mesurée est due à la réaction de OH avec les réactifs présents dans l'air ambiant. L'appareil de mesure de la réactivité d'OH a participé à une campagne de mesure où il a été intercomparé. De plus, la réaction entre NO_2* et H_2O comme nouvelle source potentielle d'OH a été étudiée.

Mots clés: radicaux HOx, FAGE, intercomparaison, réactivité OH